

TECHNICAL REPORT GL-87-14

# SEISMIC STABILITY EVALUATION OF FOLSOM DAM AND RESERVOIR PROJECT

## Report 1 SUMMARY REPORT

by

M. E. Hynes-Griffin

Geotechnical Laboratory

DEPARTMENT OF THE ARMY  
Waterways Experiment Station, Corps of Engineers  
PO Box 631, Vicksburg, Mississippi 39180-0631

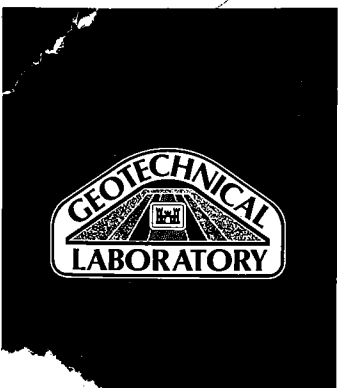
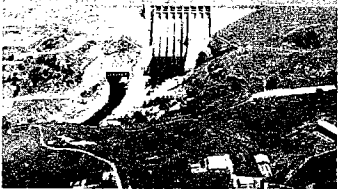


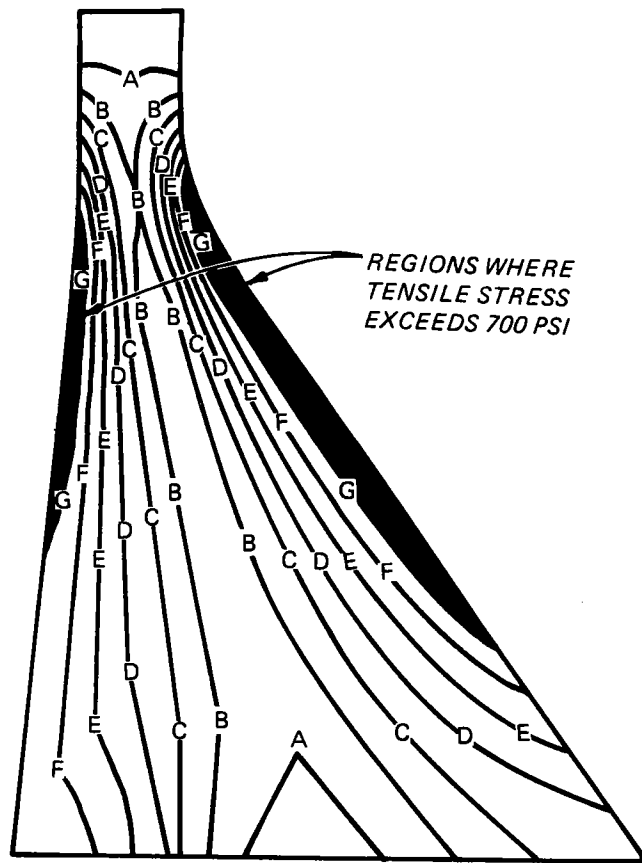
August 1987  
Draft Report

Prepared for US Army Engineer District, Sacramento  
Sacramento, California



US Army Corps  
of Engineers





CONTOUR VALUES: A = 100 PSI  
 B = 200 PSI  
 C = 300 PSI  
 D = 400 PSI  
 E = 500 PSI  
 F = 600 PSI

Figure 127. Contours of Maximum Principal Stresses Corresponding to Case 6 of Table 4

Unclassified  
SECURITY CLASSIFICATION OF THIS PAGE

REPORT DOCUMENTATION PAGE				Form Approved OMB No. 0704-0188	
1a. REPORT SECURITY CLASSIFICATION <u>Unclassified</u>			1b. RESTRICTIVE MARKINGS		
2a. SECURITY CLASSIFICATION AUTHORITY			3. DISTRIBUTION/AVAILABILITY OF REPORT		
2b. DECLASSIFICATION/DOWNGRADING SCHEDULE					
4. PERFORMING ORGANIZATION REPORT NUMBER(S) Technical Report GL-87-14			5. MONITORING ORGANIZATION REPORT NUMBER(S)		
6a. NAME OF PERFORMING ORGANIZATION USAEWES Geotechnical Laboratory		6b. OFFICE SYMBOL (if applicable) WESGH	7a. NAME OF MONITORING ORGANIZATION		
6c. ADDRESS (City, State, and ZIP Code)  PO Box 631 Vicksburg, MS 39180-0631			7b. ADDRESS (City, State, and ZIP Code)		
8a. NAME OF FUNDING/SPONSORING ORGANIZATION US Army Engineer District, Sacramento		8b. OFFICE SYMBOL (if applicable) SPKED	9. PROCUREMENT INSTRUMENT IDENTIFICATION NUMBER		
8c. ADDRESS (City, State, and ZIP Code)  650 Capitol Mall Sacramento, CA 95814			10. SOURCE OF FUNDING NUMBERS		
			PROGRAM ELEMENT NO.	PROJECT NO.	TASK NO.
11. TITLE (Include Security Classification)  Seismic Stability Evaluation of Folsom Dam and Reservoir Project; Report 1: Summary Report					
12. PERSONAL AUTHOR(S) Hynes-Griffin, Mary E.					
13a. TYPE OF REPORT Draft report		13b. TIME COVERED FROM _____ TO _____		14. DATE OF REPORT (Year, Month, Day) August 1987	
15. PAGE COUNT					
16. SUPPLEMENTARY NOTATION					
17. COSATI CODES			18. SUBJECT TERMS (Continue on reverse if necessary and identify by block number)  Folsom Dam (CA) Earthquakes and hydraulic structures Dam safety		
FIELD	GROUP	SUB-GROUP			
19. ABSTRACT (Continue on reverse if necessary and identify by block number)  The man-made water retaining structures at the Folsom Dam and Reservoir Project, located on the American River about 20 miles upstream of the the City of Sacramento, CA, have been evaluated for their seismic safety in the event of a Magnitude 6.5 earthquake occurring on the East Branch of the Bear Mountains Fault Zone at a distance of about 15 km. The evaluation process involved extensive review of construction records, field and laboratory investigations, and analytical studies. It has been determined that all man-made water retaining structures will perform satisfactorily except for Mormon Island Auxiliary Dam. Remedial or hazard-mitigating action is recommended.					
20. DISTRIBUTION/AVAILABILITY OF ABSTRACT <input type="checkbox"/> UNCLASSIFIED/UNLIMITED <input type="checkbox"/> SAME AS RPT. <input type="checkbox"/> DTIC USERS			21. ABSTRACT SECURITY CLASSIFICATION <u>Unclassified</u>		
22a. NAME OF RESPONSIBLE INDIVIDUAL			22b. TELEPHONE (Include Area Code)		22c. OFFICE SYMBOL

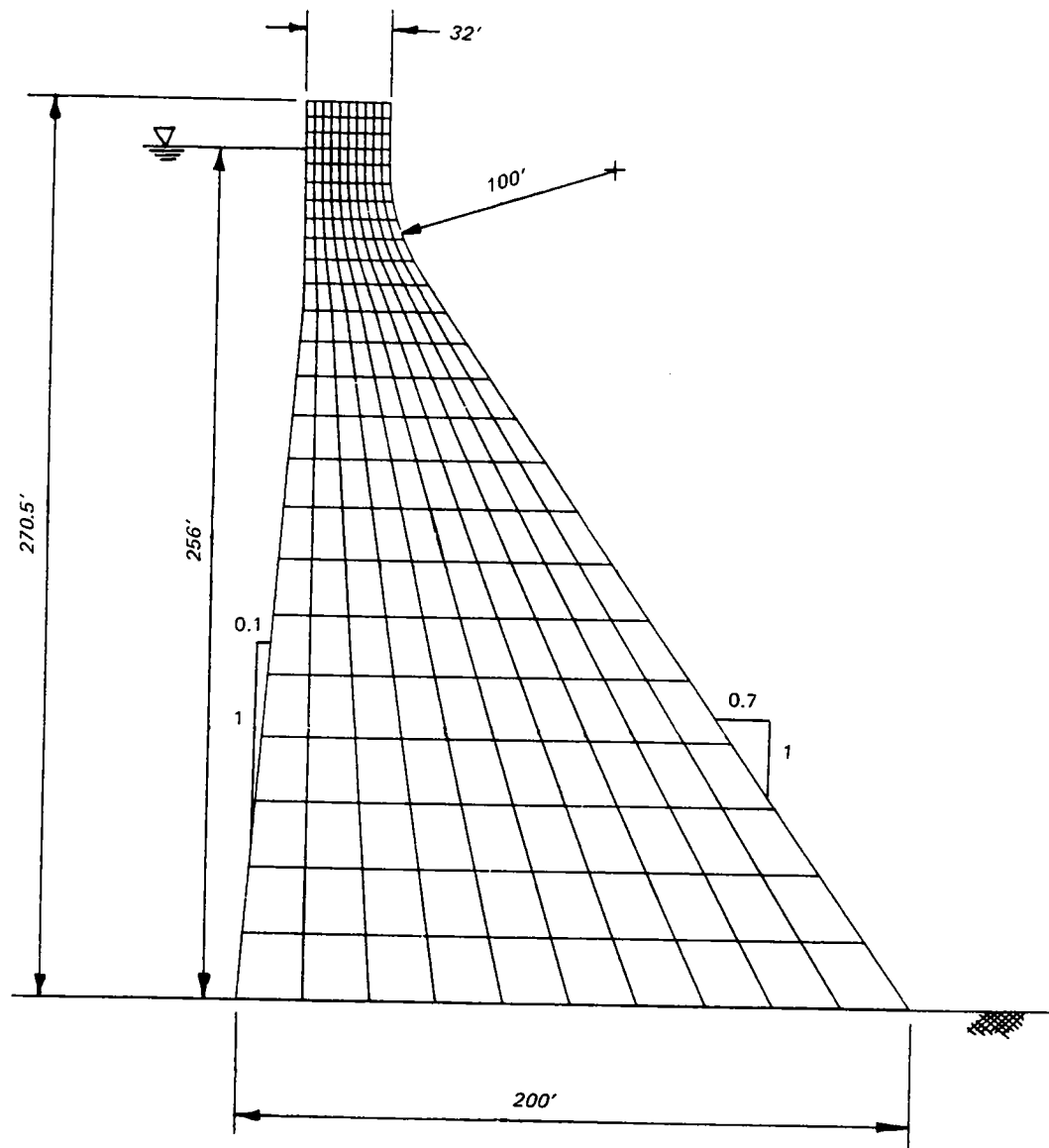


Figure 126. Finite Element Mesh of Nonoverflow Section

## PREFACE

The US Army Engineer Waterways Experiment Station (WES) was authorized to conduct this study by the US Army Engineer District, Sacramento (SPK), by Intra-Army Order for Reimbursable Services Nos. SPKED-F-82-2, SPKED-F-82-11, SPKED -F-82-34, SPKED-F-83-15, SPKED-F-83-17, SPKED-F-84-14, and SPKED-D-85-12. This report is one in a series of reports which document the seismic stability evaluations of the man-made water retaining structures of the Folsom Dam and Reservoir Project, located on the American River, in California. The Reports in this series are as follows:

- Report 1: Summary Report
- Report 2: Interface Report
- Report 3: Concrete Gravity Dam Report
- Report 4: Mormon Island Auxiliary Dam Report
- Report 5: Dike 5 Report
- Report 6: Wing Dams Report
- Report 7: Upstream Retaining Wall Report

The work in these reports is a joint endeavor between SPK and WES. Messrs. John W. White and John S. Nickell, of Civil Design Section 'A', Civil Design Branch, Engineering Division (SPKED-D) at SPK were the overall SPK project coordinators, and contributed to the evaluation of the concrete gravity dam. Messrs. Gil Avila and Matthew G. Allen, of the Soil Design Section, Engineering Division Geotechnical Branch, (SPKED-F) at SPK, made critical geotechnical contributions to field and laboratory investigations. Support was also provided by the South Pacific Division Laboratory. The WES Principal Investigator and Research Team Leader was Ms. Mary Ellen Hynes-Griffin, of the Earthquake Engineering and Geophysics Division (WESGH), Geotechnical Laboratory (GL), WES. Primary Engineers on the WES team were Messrs. Ronald E. Wahl and David W. Sykora, both of WESGH, Messrs. Vincent P. Chiarito, R. Stephen Wright and Robert L. Hall of the Structures Laboratory (SL) at WES, and Mr. Takashi Tsuchida, on temporary assignment to WES from the Port and Harbour Research Institute, Yokosuka, Japan. Geophysical support was provided by Mr. Jose Llopis, WESGH. Additional engineering support was provided by Messrs. Richard S. Olsen, Joseph P. Koester, and Richard H. Ledbetter, all of WESGH, and Ms. Wipawi Vanadit-Ellis of the Soil Mechanics Division (WESGE), GL, WES. Large-scale laboratory investigations were conducted by

$F_{PES}$  = Post-earthquake safety factor against sliding

$F_{STA}$  = Initial safety factor against sliding

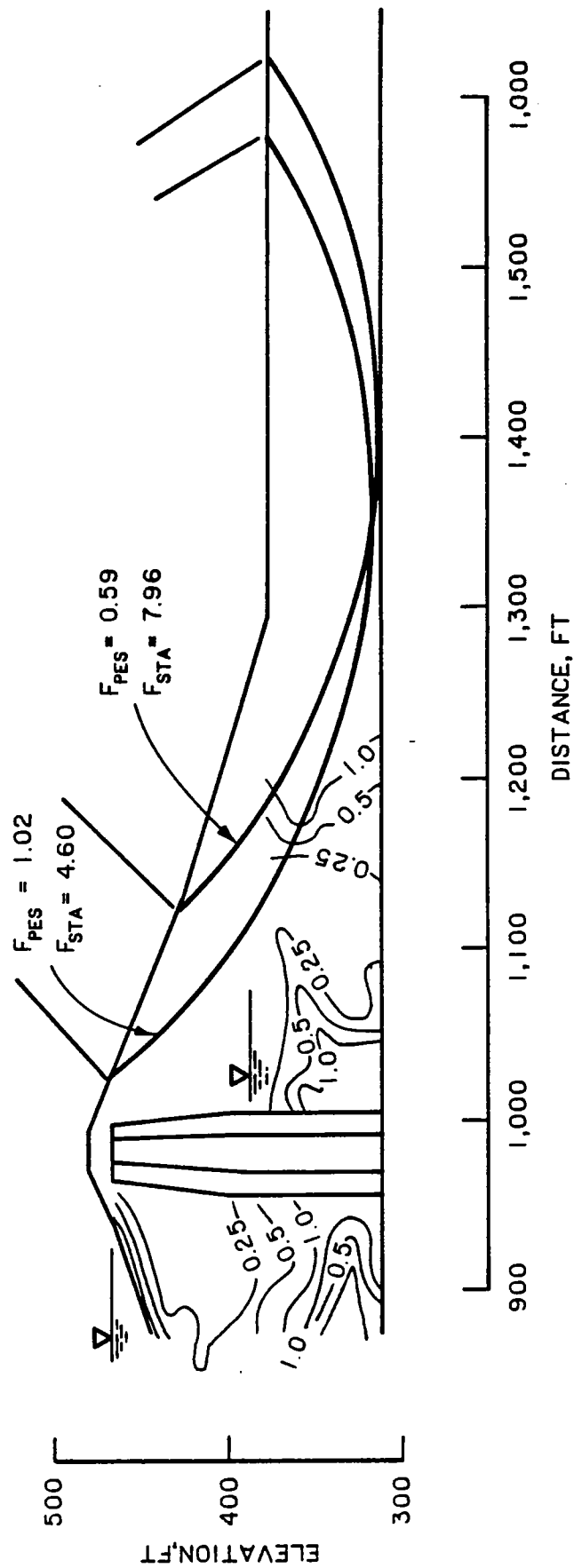


Figure 119. Post-earthquake slope stability for Mormon Island Auxiliary Dam, downstream slope

# CONTENTS

	<u>Page</u>
PREFACE . . . . .	1
SUMMARY OF STABILITY EVALUATION . . . . .	5
PART I: INTRODUCTION . . . . .	7
PART II: DIKE 5 STUDIES . . . . .	9
Dike 5 Description . . . . .	9
Field and Laboratory Investigations . . . . .	9
Liquefaction Potential Evaluation . . . . .	10
Permanent Deformation Estimates . . . . .	12
Stability Evaluation . . . . .	13
PART III: WING DAM STUDIES . . . . .	14
Wing Dam Description . . . . .	14
Field Investigations . . . . .	15
Liquefaction Potential Evaluation of Core Material . . . . .	16
Liquefaction Potential Evaluation of Shells . . . . .	16
Estimates of Cyclic Strength . . . . .	17
Static Finite Element Analyses . . . . .	21
Dynamic Finite Element Analyses and Liquefaction Potential Evaluation . . . . .	22
Post-Earthquake Slope Stability . . . . .	23
Permanent Deformation Estimates . . . . .	25
Stability Evaluation . . . . .	26
PART IV: INTERFACE STUDIES . . . . .	28
Interface Description and Approach for Safety Assessment . . . . .	28
Review of Construction Records . . . . .	28
Field and Laboratory Investigations . . . . .	29
Liquefaction Potential Evaluation . . . . .	29
Stability Evaluation . . . . .	30
PART V: RETAINING WALL STUDIES . . . . .	31
Retaining Wall Description . . . . .	31
Yield Acceleration Analyses . . . . .	32
Permanent Deformation Estimates . . . . .	35
Makdisi-Seed Calculations . . . . .	36
Sarma-Ambrayeses Calculations . . . . .	37
Modified Richards-Elms Calculations . . . . .	38
Post-Earthquake Stability Studies . . . . .	39
Stability Evaluation . . . . .	39
PART VI: MORMON ISLAND AUXILIARY DAM STUDIES . . . . .	40
Mormon Island Auxiliary Dam Description . . . . .	40
Field Investigations . . . . .	41
SPT Results in Zones 3 and 4 . . . . .	41
Geophysical Tests . . . . .	42
Test Pits in Foundation Gravels . . . . .	42

$F_{PES}$  = Post-earthquake safety factor against sliding

$F_{STA}$  = Initial safety factor against sliding

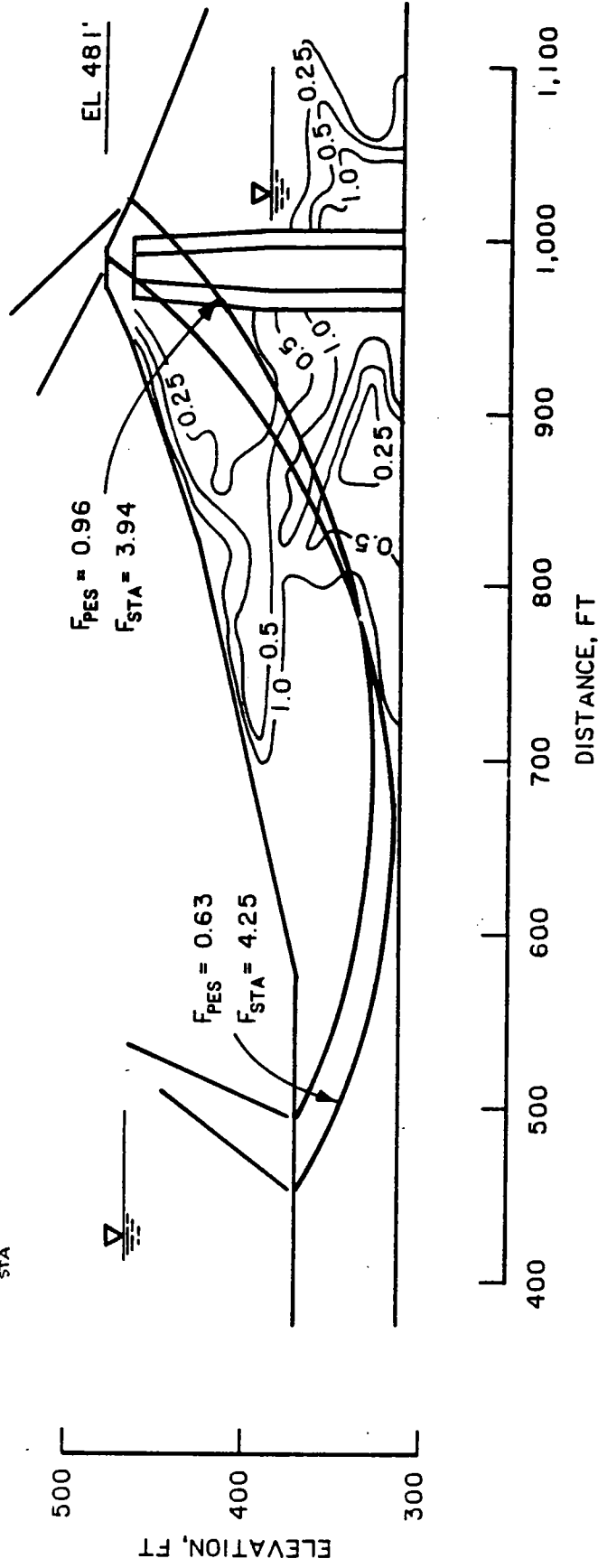


Figure 118. Post-earthquake slope stability of Mormon Island Auxiliary Dam, upstream slope

## SUMMARY OF STABILITY EVALUATION

The Folsom Dam and Reservoir Project is located on the American River, 20 miles upstream of the City of Sacramento, California. Based on geological and seismological investigations in the region, the seismic threat was determined to be an earthquake of Local Magnitude 6.5, at a distance of 15 km, on the East Branch of the Bear Mountains Fault Zone. The rock outcrop ground motion parameters used in this evaluation were a peak acceleration of 0.35 g, a peak velocity of 20 cm/sec, and a duration of ground motion above 0.05 g of 16 sec. The conclusions of this report concerning the earthquake safety of key features of the project are:

A. Dike 5 and all other dikes are safe from liquefaction and excessive deformation when subjected to the design earthquake motions and should perform well in the event of an earthquake. Permanent deformations are expected to be less than 0.5 meter.

B. The compacted core materials in the Wing Dams, in the vicinity of the Wing Dam and Concrete Dam Interface and at Mormon Island Auxiliary Dam are not susceptible to liquefaction and will retain most of their static shear strength during and immediately after an earthquake.

C. The shells and filter zones of the Wing Dams are expected to remain stable during and after the earthquake, but they may develop 15 to 30 percent excess pore pressures on the upstream side. Permanent deformation of the downstream shells should be less than 0.5 meter. The portion of Mormon Island Auxiliary Dam founded on rock is expected to perform similarly.

D. Analyses of Retaining Wall B show that the wall may slide, but earthquake-induced sliding is expected to be limited to less than 5 feet. This corresponds to a drop in crest height of less than 2 ft which can safely be tolerated in the embankment. In a worst-case scenario in which the retaining wall was assumed to be destroyed it was determined that the embankment slopes would be stable in the post-earthquake condition.

E. Mormon Island Auxiliary Dam will not be stable in the event of the design earthquake. Extensive liquefaction is expected in the dredged gravel foundation which underlies the upstream and downstream shells over an 800-ft long section of the dam. The undisturbed gravel foundation, which underlies the shells over an 1100-ft length of the dam, is still under study. Both upstream and downstream slopes founded on dredged gravel are expected to

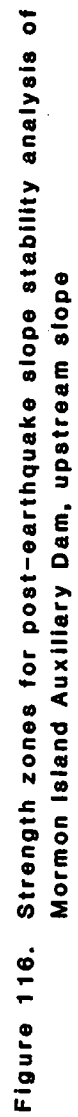


SEISMIC STABILITY EVALUATION OF FOLSOM DAM  
AND RESERVOIR PROJECT  
Report 1: Summary Report

PART I: INTRODUCTION

1. This report summarizes the investigations and results of a seismic stability evaluation of the man-made water-retaining structures at the Folsom Dam and Reservoir Project, located on the American River, about 20 miles upstream of the City of Sacramento, California. This seismic safety evaluation was performed as a cooperative effort between the US Army Engineer Waterways Experiment Station (WES) and the US Army Engineer District, Sacramento (SPK). Professors H. Bolton Seed, Anil K. Chopra and Bruce A. Bolt of the University of California, Berkeley, Professor Clarence R. Allen of the California Institute of Technology, and Professor Ralph B. Peck, Professor Emeritus of the University of Illinois, Urbana, served as Technical Specialists for the study. The Folsom project was designed and built by the Corps of Engineers in the period 1948 to 1956, and is now owned and operated by the US Bureau of Reclamation. The reservoir has a storage capacity of 1 million acre-ft at gross pool and includes approximately 4.5 miles of man-made water retaining structures that have a crest elevation of 480.5 ft above sea level. At gross pool, Elevation 466 ft, there is 14.5 ft of freeboard. This pool level was selected for the safety evaluation, based on a review of operation procedures and hydrologic records for the reservoir which show that the pool typically reaches Elevation 466 ft about 10% of the time during the month of June, and considerably less than 10% of the time during the other months of the year. Under normal operating conditions, the pool is not allowed to exceed Elevation 466 ft. Hydrologic records show that emergency situations which would cause the pool to exceed Elevation 466 ft are extremely rare events. A location map and plan of the project are shown in Figures 1 and 2.

2. A seismological study for the project was performed by Tierra Engineering, Inc. (1983). The seismic threat was determined to be an earthquake of Local Magnitude 6.5, at a distance of about 15 km, on the East Branch of the Bear Mountains Fault Zone. The peak acceleration at the site was determined to be 0.35g, the peak velocity 20 cm/sec and the bracketed duration (greater than 0.05 g) 16 sec. Two accelerograms that match these specified



## PART II: DIKE 5 STUDIES

### Dike 5 Description

4. Figure 2 shows a plan of the 8 dikes, which have a total length of 11,655 ft. Dike 5 is the largest of these compacted earthfill saddle dikes, all founded on weathered rock. As the largest, Dike 5 is more likely to have water against its upstream slope and have saturated zones than the other dikes, which are typically dry. Since all the dikes are essentially homogeneous in section, composed of compacted saprolite, Dike 5 is typical of the sections for all the other dikes. Consequently, Dike 5 was selected for study to represent the most critical case for all the dikes. Dike 5 has a crest length of 1920 ft and has a maximum height of 110 ft near Station 180+00. The portion of the embankment whose foundation is above Elevation 450 ft is founded on the Mehrten Formation, which consists of cobbles and gravel in a somewhat cemented clayey matrix. This formation was not considered to be susceptible to liquefaction due to the clay matrix, the cementation, the age, and the fact that it is unlikely to be saturated even with the maximum pool level. It was not investigated further.

5. Below Elevation 450 ft, Dike 5 is founded on weathered quartz diorite granite. The embankment is constructed of compacted decomposed granite scraped from the saprolite exposures in Borrow Area No. 2 (see Figure 2) and suitable fine-grained materials from the American River channel. The decomposed granite and the American River materials generally classify as Silty Sand (SM) according to the Unified Soil Classification System (USCS). The construction specifications required that the central portion of the embankment section, Zone C, contain the finer soils (to the maximum extent practicable) and receive more compactive effort than the upstream and downstream areas, Zone D. Seepage is controlled by a downstream drainage blanket. A plan of Dike 5 is given in Figure 5, and a typical section is shown in Figure 6.

### Field and Laboratory Investigations

6. Undisturbed sampling with a Denison sampler and Standard Penetration Tests (SPT) with trip hammer equipment were performed by WES near

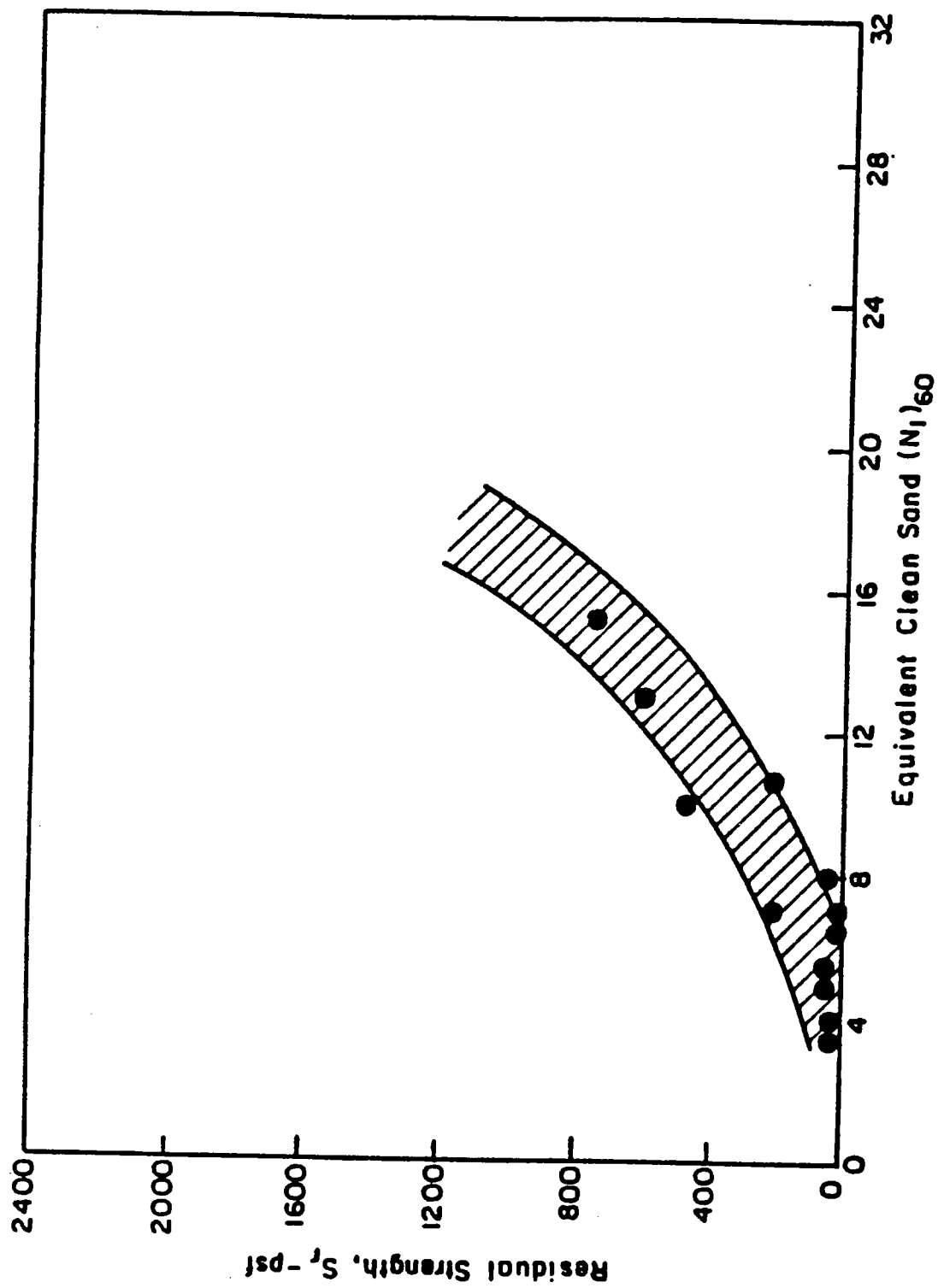


Figure 115. Tentative Relationship Between Residual Strength and SPT N-values for Sands (after Seed, 1984)

the input data for the column analyses. The stresses computed from both accelerograms, referred to as Accelerogram A and Accelerogram B, were very similar for the centerline column, as shown in Figure 12. Accelerogram A resulted in somewhat higher stresses than Accelerogram B for the upstream slope column, as shown in Figure 13.

9. The 1983 and 1984 cyclic strength charts from Seed's work are shown in Figure 14a and 14b. Figure 14a shows the 1983 plot of cyclic strength versus normalized blowcounts,  $N_1$ , for various earthquake magnitudes. This chart was developed from data for relatively clean sands and shows that for  $M = 6.5$  events, the cyclic loading resistance is about 20 percent higher, for any value of  $N_1$ , than for  $M = 7.5$  earthquakes. Figure 14b provides data for silty sands with different fines contents, expressing the cyclic stress ratio causing liquefaction (based on observations of liquefaction in the field), for a confining pressure of about 1 tsf and for earthquakes with  $M = 7.5$ , as a function of the  $N_1$ -value of a soil corrected to a 60 percent energy level,  $(N_1)_{60}$ . The cyclic stress ratios from Seed's charts are interpreted to correspond to development of 100% residual excess pore pressure. Using the results presented in Figure 14b, the required field blowcounts for safety factors of one were calculated from the SHAKE results on the basis of the following:

- a. The fines content of the silty sands in Dike 5 can be considered to be about 15 percent for Zone D and 20 percent for Zone C.
  - b. The cyclic stress ratio required to cause liquefaction for  $M = 6 \frac{1}{2}$  earthquakes is about 20 percent higher than that required for  $M = 7 \frac{1}{2}$  events.
  - c. The blowcounts measured with a trip hammer are about 30 percent lower than those corresponding to the  $(N_1)_{60}$  values shown in Figure 14b (Seed et al., 1984).
- and
- d. Appropriate corrections must be applied to the cyclic stress ratios determined from Figure 14b to allow for overburden pressures greater than 1 tsf at depths greater than about 20 ft.

The factor  $K_\sigma$  was used to reduce the cyclic stress ratios for higher confining stresses in accordance with the relationship shown in Figure 15a from Seed and Harder (1985). The factor  $C_N$  for a relative density of 60 to 80 percent shown in Figure 15b was used to normalize blowcounts to a confining stress of 1 tsf. Values of the SPT blowcount,  $N$ , (as measured in the field with trip hammer equipment) required to provide a factor of safety of one against liquefaction ( $r_u = 100\%$ ) determined on these bases are plotted in Figure 16 for the centerline and Figure 17 for the upstream slope. The measured field blowcounts are

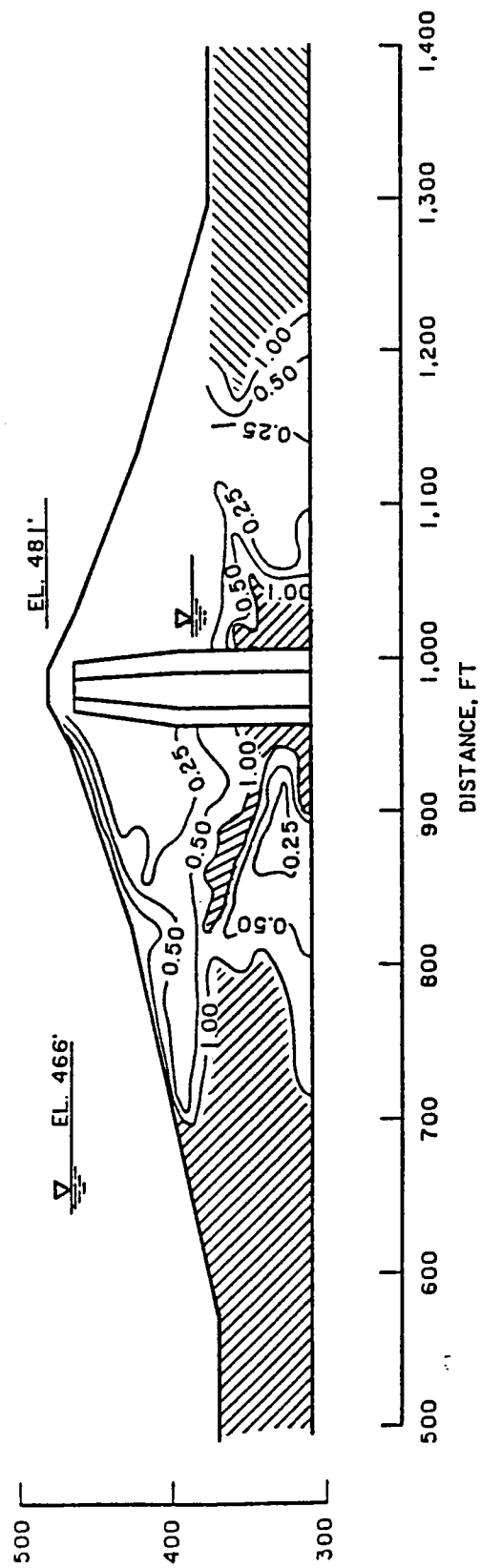


Figure 114. Contours of residual excess pore pressure ratio,  $R_u$  (%),  
for Mormon Island Auxiliary Dam.

fundamental periods of the dam are computed from the response spectra for the accelerograms, shown in Figure 4. The parameters listed in Table 1 were determined by following the maximum acceleration and fundamental period calculations procedure.

14. These parameters were used to enter the Makdisi-Seed charts for dynamic response and displacement shown in Figure 23. From these charts, the displacements plotted in Figures 24 and 25 were computed for upstream and downstream sliding surfaces. The displacements computed by this approach ranged from 0.05 to 0.35 m, quite similar to those computed by the Sarma-Ambraseys method.

#### Stability Evaluation

15. The liquefaction potential analyses showed that significant excess pore pressures will not develop as a result of the design earthquake. The permanent deformation analyses showed that earthquake-induced deformations are expected to be less than 0.5 m. Based on the method of construction, the materials involved, the field and laboratory investigations, and the liquefaction and permanent deformation analyses, it was concluded that Dike 5 will perform well during and immediately after the design earthquake. Since the other dikes are founded on weathered rock, were constructed of the same materials and in the same manner as Dike 5, and since they are typically dry and would not be saturated at the time of an earthquake, it was further concluded that all the dikes are expected to perform well during and immediately after the design earthquake.

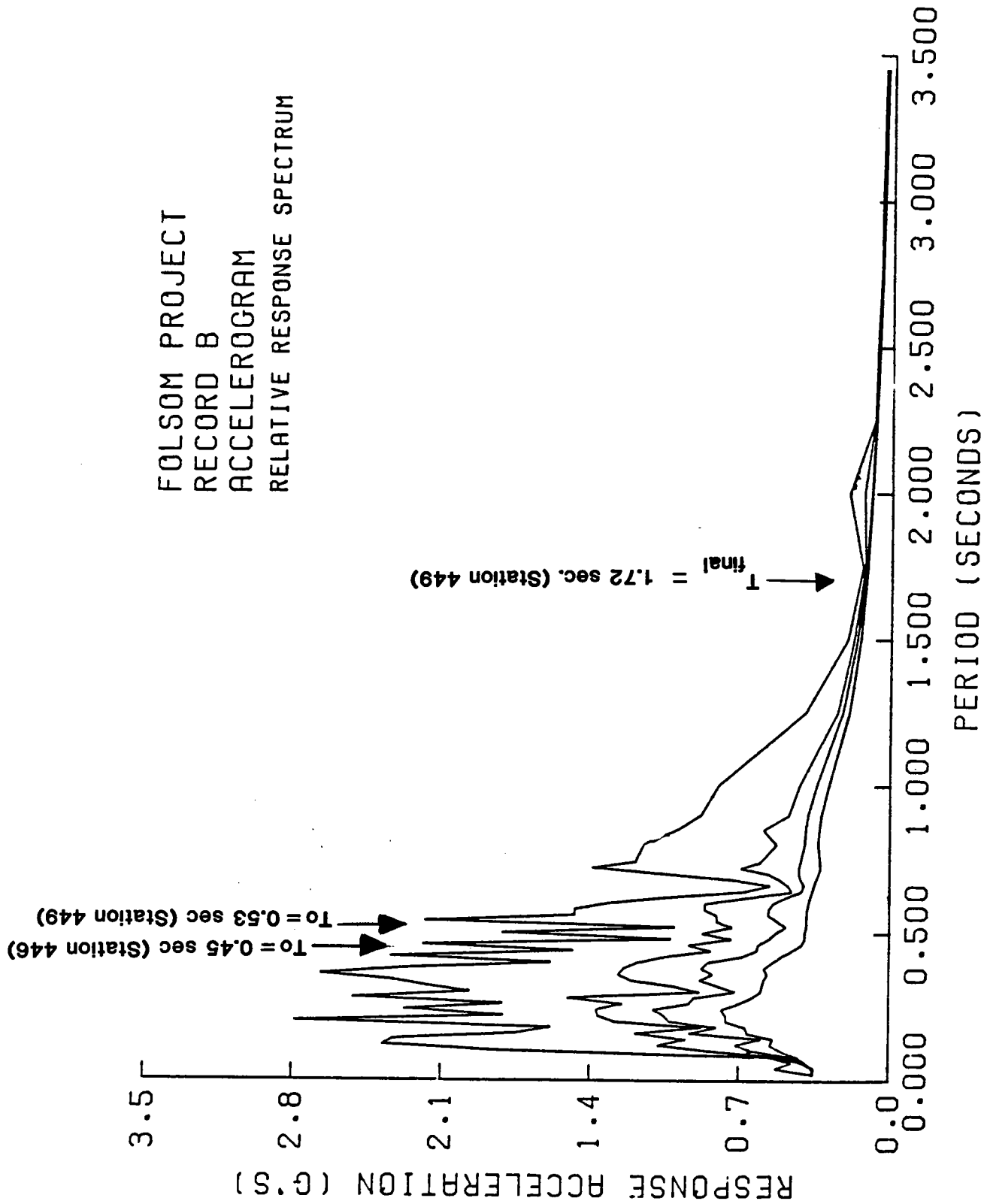


## Field Investigations

18. Undisturbed sampling with a Denison sampler and SPT borings with trip hammer equipment were performed at 5-ft intervals at the centerline to sample core material, and near the downstream edge of the crest to sample filter and core material at two locations on the Right Wing Dam, near Stations 235 and 270, and one location on the Left Wing Dam, near Station 303. Figure 26 shows the locations of the field investigations. SPT borings are denoted SS and undisturbed borings are denoted US. Steel cased borings, shown as SCB in Figure 26, were drilled with Odex equipment in the downstream gravel shells. The Odex system consists of a downhole pneumatic hammer with an expanding bit that pulls a steel casing behind the bit. When the casing is in place, the bit can be retracted and withdrawn through the casing. The steel casing used in these investigations had an inside diameter (ID) of 5 in. The Odex system was selected for installation of cased holes for subsurface geophysical testing because it did not require grouting of the gravels, the disturbance to the gravels was relatively minor, and several holes could be installed within a single work day. Unfortunately, this system does not provide satisfactory samples of the subsurface materials.

19. The US, SS, and SCB borings were drilled in pairs for geophysical crosshole testing. Test pits, shown as TP in Figure 26, were excavated in the downstream gravel shells at these locations to determine in situ densities and obtain disturbed samples for laboratory testing. Pairs of undisturbed and SPT borings were also drilled in core material at the interface area near Stations 285 and 299.

20. Typically, the SPT blowcounts in the core material exceeded 40 blows per ft. There were two low blowcounts, 18 at 30 ft and 24 at 60 ft, observed at Station 235 in the existing embankment material, but index tests later showed higher fines content in these samples. Shear wave velocities in the core ranged from about 900 to 1000 fps in the top 20 ft, to about 1100 to 1600 fps at depth. The average dry density from record samples of core material was 127 pcf, and the total unit weight was estimated to be 142 pcf. Shear wave velocities in the shell ranged from 850 fps near the surface of the slope, to 1350 fps at depth. Large-scale in situ density tests on the gravel shell and transition material showed average dry densities of 136 pcf for the Right Wing Dam and 133 pcf for the Left Wing Dam.



CURVE FOR 0.2.5 AND 10 PERCENT DAMPING

Figure 112. Initial and Final fundamental periods for Mormon Island Auxiliary Dam compared with response spectra for Accelerogram B

- b. Calculate initial effective stresses in the shells with static finite element analyses.
- c. Calculate earthquake-induced dynamic shear stresses from dynamic finite element analyses.
- d. Compute safety factors against liquefaction from Steps a, b and c above.

Each of these steps is described below.

Estimates of cyclic strength

23. Cyclic strength of the shell gravels of the Wing Dams was estimated from in situ and laboratory tests performed on gravels from the shells and foundation of Mormon Island Auxiliary Dam. These gravels are representative of Zone B, the transition zone in the Right Wing Dam, and Zone E, the shells of the Left Wing Dam. The shells of Mormon Island Auxiliary Dam are constructed of material from the same borrow pit as the shells of the Left Wing Dam and in much the same manner, except lift thicknesses at Mormon Island were 18 in. and at the Wing Dams, 24 in. From construction records and photographs, the thin, loose rockfill, Zone A material, appears to be widely graded with some fines. In these analyses, the Zone A material is assumed to have the same cyclic loading characteristics as the Zone B gravels.

24. The results of in situ Becker Hammer Tests (BHT) conducted in the shells at Mormon Island Auxiliary Dam were used to estimate cyclic strength of shell gravels for the Wing Dams by translation of the Becker blowcounts, NB, into equivalent SPT blowcounts (Harder et al., 1986), followed by application of Seed's empirical procedure. The Becker Hammer field investigations and cyclic strength determinations are described in more detail in the section of this report on Mormon Island Auxiliary Dam. The equivalent  $(N_1)_{60}$  values for the Becker blowcounts in shell gravels averaged 23 blows per ft. The fines content observed in the test pits ranged from 1 to 12% with an average of 5%. The test pits reached a maximum depth of 11 ft in the Right Wing Dam, 20 ft in the Left Wing Dam, and 19 ft at Mormon Island Auxiliary Dam. Samples from the Becker soundings at depths of 0 to 40 ft in shell material had fines contents that ranged from 10 to 28% with an average of 15%. Cyclic strengths for the shell gravel were obtained from Seed's 1984 chart with an assumed average fines content of about 8%. This resulted in a cyclic stress ratio of 0.35 required to generate 100% excess pore pressure in 8 cycles (representative of

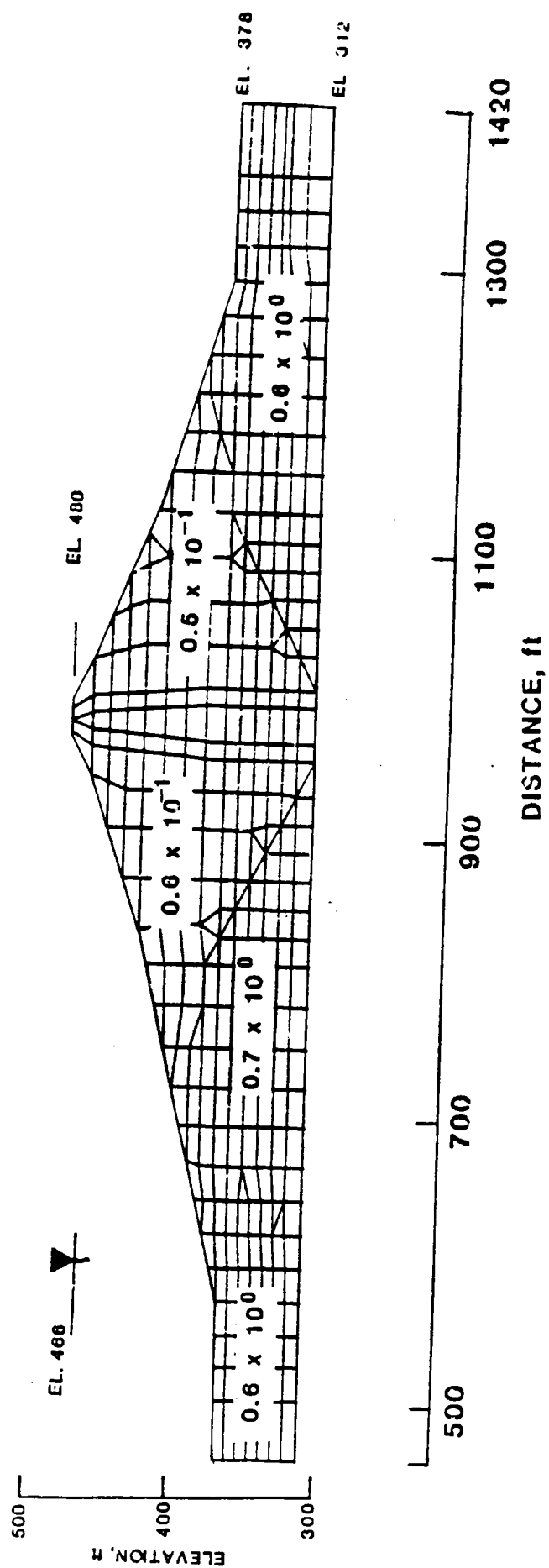


Figure 111. Effective shear strains in percent computed with FLUSH and Accelerogram B for Mormon Island Auxiliary Dam

$$\left( \frac{\tau_c}{\sigma_v} \right)_{\substack{\sigma \neq 1 \\ \alpha \neq 0}} = K_\sigma K_\alpha \left( \frac{\tau_c}{\sigma_v} \right)_{\substack{\sigma=1 \\ \alpha=0}} \quad (3)$$

28. A computed safety factor of 1.0 against liquefaction,  $FS_L$ , corresponds to a residual excess pore pressure ratio,  $R_u$ , of 100 percent. As values of  $FS_L$  increase, the corresponding values of  $R_u$  decrease. This relationship was roughly estimated from the laboratory data. Values of  $FS_L$  less than 1.0 are interpreted as the development of  $R_u = 100\%$  during the earthquake, rather than towards the end of the earthquake.

29. To demonstrate that the laboratory gradation and density are representative of actual field conditions, they are compared with the gradations and in situ density tests from Test Pits 1, 2, 3 and 4 in Figures 44 through 47. The laboratory gradation generally falls within the observed gradation ranges shown in Figure 44 for the Right Wing Dam and Figure 46 for the Left Wing Dam. In situ dry density was observed to change with variations in gradation. The in situ dry densities from the test pit data are plotted versus the corresponding uniformity coefficient ( $C_u$ ) from the individual in situ density test gradations in Figure 45 for the Right Wing Dam and Figure 47 for the Left Wing Dam. Maximum and minimum densities were estimated from laboratory tests for several gradations with different values of  $C_u$ . Compaction molds of 18 and 36 in. diameter were used in these tests for gradations with maximum particle sizes of 3 and 6 in., respectively. Both vibratory and impact compaction methods were used for maximum laboratory density. It was found that the laboratory compaction results underestimated maximum dry density, since a few in situ dry densities exceeded the laboratory maximum estimates. More representative values of maximum dry density were estimated as the envelope of all laboratory and in situ results. Figure 45 indicates that the average relative density of the Right Wing Dam gravel shell material (Zone B) is about 65 percent. Figure 47 indicates that the average relative density of the Left Wing Dam gravel shell (Zone E) is about 60 percent. The average relative density of the Mormon Island Auxiliary Dam shell gravel is about 70 percent. The laboratory target dry density of 134 pcf was selected to model relative densities observed in the gravel shells of both

FUNDAMENTAL PERIOD = 1.72 sec.

Note: Accelerations are in g's

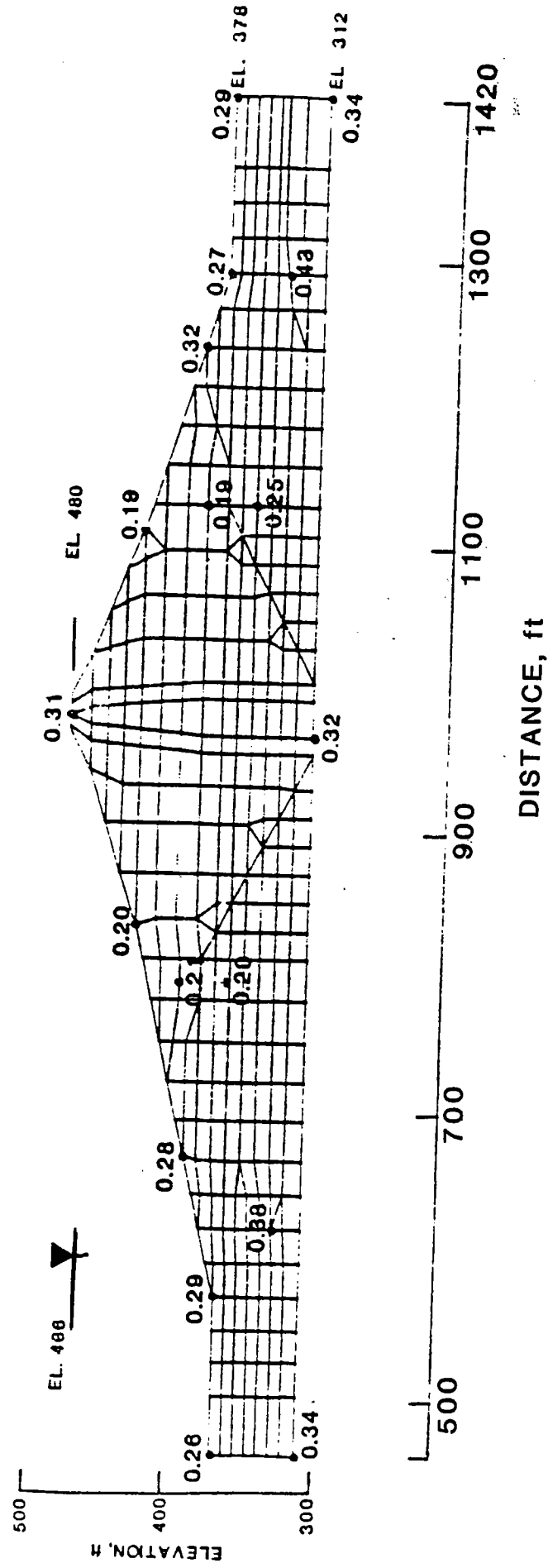


Figure 110. Maximum accelerations computed with FLUSH and Accelerogram B for selected nodal points, Mormon Island Auxiliary Dam

32. Evan's work (1987) also indicated that relative pore pressure development behavior for isotropically consolidated specimens can be observed in test results that are not corrected for membrane compliance effects. Cyclic stress levels before the failure level (observed or extrapolated to 100% in the membrane compliance affected test) at 8 cycles can be associated with lower excess pore water pressures. These lower cyclic stress levels are normalized by the failure level to yield safety factors and are plotted with their corresponding residual excess pore pressure ratios in Figure 52. Laboratory test results on anisotropically consolidated specimens not corrected for membrane compliance effects indicate higher residual excess pore water pressures at a given factor of safety against liquefaction than isotropically consolidated test results. Evan's work (1987) shows that these higher pore pressures are not observed in anisotropically consolidated test results that are corrected for membrane compliance effects.

#### Static finite element analyses

33. Static finite element analyses were performed to determine the pre-earthquake vertical effective stresses and the initial static shear stresses on horizontal planes throughout the dam. This information was used to calculate values of  $\alpha$ , the ratio of initial horizontal shear stress to initial effective vertical stress, so that the appropriate cyclic strength can be associated with each element. The mesh was developed from a composite of several cross sections along the axes of the Right and Left Wing Dams. The tallest upstream slope occurs near Station 283 near the wrap-around of the Right Wing Dam with the Concrete Gravity Dam. Only this section has been analyzed. The field section and the idealized analysis section are shown in Figure 53, and the finite element mesh used for both the static and dynamic finite element analyses is shown in Figure 54.

34. The static analysis was performed with the program FEADAM, which models construction of the dam with successive layers and uses a hyperbolic stress-strain curve. Input parameters were estimated from field (shear wave velocity and in situ density) and laboratory (drained and undrained triaxial shear) tests. Table 2 lists the FEADAM hyperbolic input parameters for the Wing Dam analyses.

35. Figure 55 shows the computed contours of initial vertical effective stress, Figure 56 shows the computed contours of initial static shear stress on horizontal planes, and Figure 57 shows contours of  $\alpha$ .

$$\tau_{\text{FLUSH}} = 0.65 \cdot \tau_{\text{MAX}}$$

UNITS ARE IN ksf

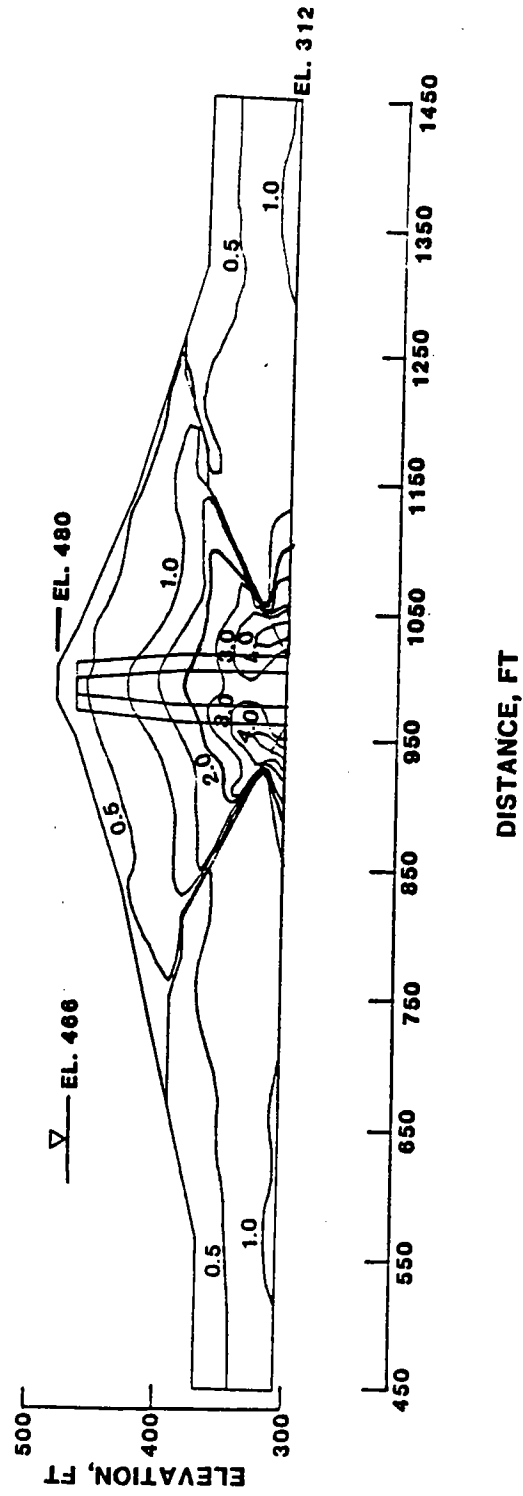


Figure 109. Contours of average dynamic shear stress,  $\tau_{\text{FLUSH}}$ , computed with FLUSH and Accelerogram B for Mormon Island Auxiliary Dam

stress of 1 tsf) and a relative density of 70 percent. Since the Right Wing Dam Zone B gravel actually has a lower relative density, about 65 percent, the available cyclic strength can be estimated by proportionally adjusting the value 0.35 to  $(0.65/0.70) \times 0.35 = 0.325$ . This will result in an 8 percent reduction in the safety factor values shown in Figure 62. With this adjustment, the safety factors against liquefaction for the Right Wing Dam gravels are typically greater than or equal to 1.4.

40. For the Left Wing Dam gravels ( $D_r \approx 60\%$ ), a similar adjustment needs to be made to the available cyclic strength,  $(0.60/0.70) \times 0.35 = 0.30$ . This results in a 17 percent reduction of the safety factors against liquefaction shown in Figure 62. For the Left Wing Dam, all the safety factors against liquefaction are typically greater than or equal to 1.3.

41. The initial fundamental period of the Wing Dam section analyzed was estimated to be 0.28 sec from Sarma's approximation (Sarma, 1979). Figure 63 shows that the initial fundamental period of the dam falls well within the high energy portion of the response spectrum of Accelerogram B. This means that the section selected for analysis will undergo significant earthquake loading in the numerical dynamic response analysis with Accelerogram B as the input ground motion. Hence, the analysis section and Accelerogram B are well suited for the seismic safety evaluation of the Left and Right Wing Dams.

42. During earthquake shaking, the embankment materials undergo shear straining. Consequently, the shear modulus is reduced in the manner indicated in Figure 59. The fundamental period of the dam increases as the shear modulus decreases. The fundamental period of the idealized 2-dimensional section after the earthquake was 0.83 sec, determined from the FLUSH output. Both the initial and post-earthquake fundamental periods are shown on response spectra for Accelerogram B in Figure 63.

#### Post-Earthquake Slope Stability

43. The post-earthquake slope stability of the shells was determined by: (a) mapping the distribution of excess pore water pressures in the upstream shell of the dams based on the relationship between factor of safety against liquefaction and excess pore water pressure given in Figure 52 (the higher  $R_u$  values for  $\alpha > 0$  were used in these calculations), and (b) computing factors of safety against sliding with effective stress slope stability

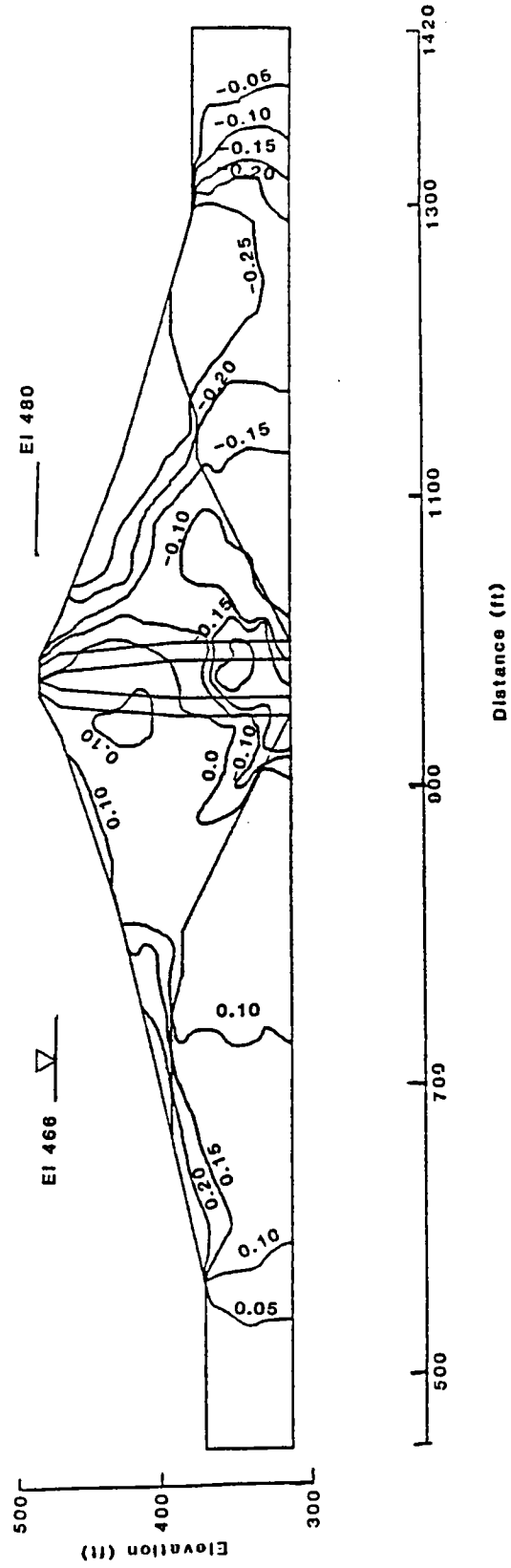


Figure 108. Contours of Alpha Ratio.

corresponds to a factor of safety against liquefaction of about 1.3. This corresponds to a relative density of about 50 percent. For the deeper circle shown in Figure 65b, the factor of safety against a slide is estimated to be about 1.45 for the Right Wing Dam (relative density of 65%) and 1.40 for the Left Wing Dam (relative density of 60%).

46. These studies indicate that the safety factor against sliding for the Wing Dams immediately after the earthquake is above unity, and the most critical surfaces are relatively shallow and do not cross the core of the dam to daylight on the downstream slope. Consequently, the Wing Dams are expected to perform well in this failure mode.

#### Permanent Deformation Estimates

47. Excess pore water pressures will not develop in the downstream shell of the Wing Dams because they are not saturated. A conservative permanent deformation analysis was performed to estimate an upper bound on Newmark-type deformations that could develop during sliding. In these analyses, yield accelerations were computed for the upstream slope with a pool elevation of 466 ft, and with a 20% reduction in strength of the materials in the shells and in the core. The program used was ARCEQS, based on Sarma's method. The upstream slope at Station 285 with the pool at Elevation 466 ft was analyzed rather than a downstream slope since it would represent the lowest possible yield acceleration for any downstream slope. For symmetrical upstream and downstream slopes, the yield acceleration,  $k_y$ , of a fully submerged upstream slope is less than that of the downstream slope, and the ratio of the two yield accelerations is approximately equal to the ratio of buoyant unit weight,  $\gamma_b$ , to total unit weight,  $\gamma_t$ , a value of about 0.5 to 0.6. For the Wing Dams, the effect of submergence more seriously reduces computed values of yield acceleration than the relatively small difference in slope angle (generally 1 V on 2.25 H for the upstream slopes and 1 V on 2.0 H for the downstream slopes). As seen in the section on Dike 5, where the slope angles are 1 V to 3.25 H upstream and 1 V to 2.25 H downstream, the largest permanent deformations are generally computed for upstream surfaces. For Station 285, a yield acceleration of 0.18g was computed for a deep circular surface passing through the core and the upstream shell. Yield accelerations for other surfaces ranged from 0.9 to 0.29.

Note: Units are in ksf

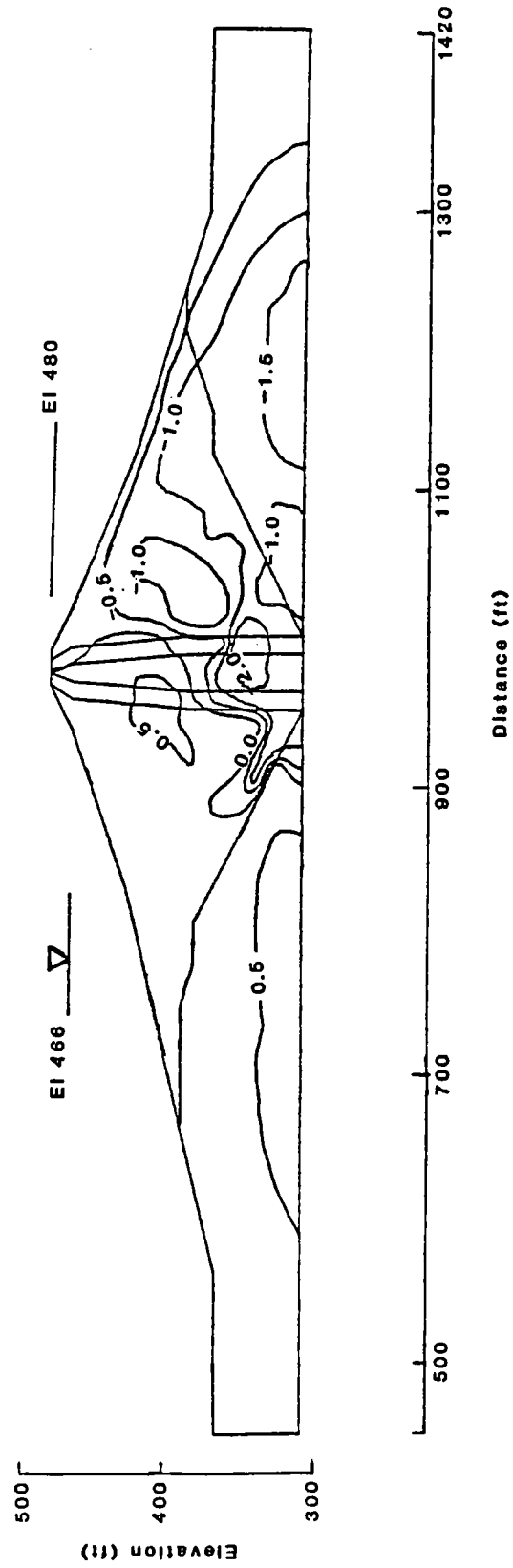


Figure 107. Contours of static shear stresses on horizontal planes.

deformation analyses, it was concluded that the Wing Dams will perform well during and immediately after the design earthquake.

Note: Units are in ksf

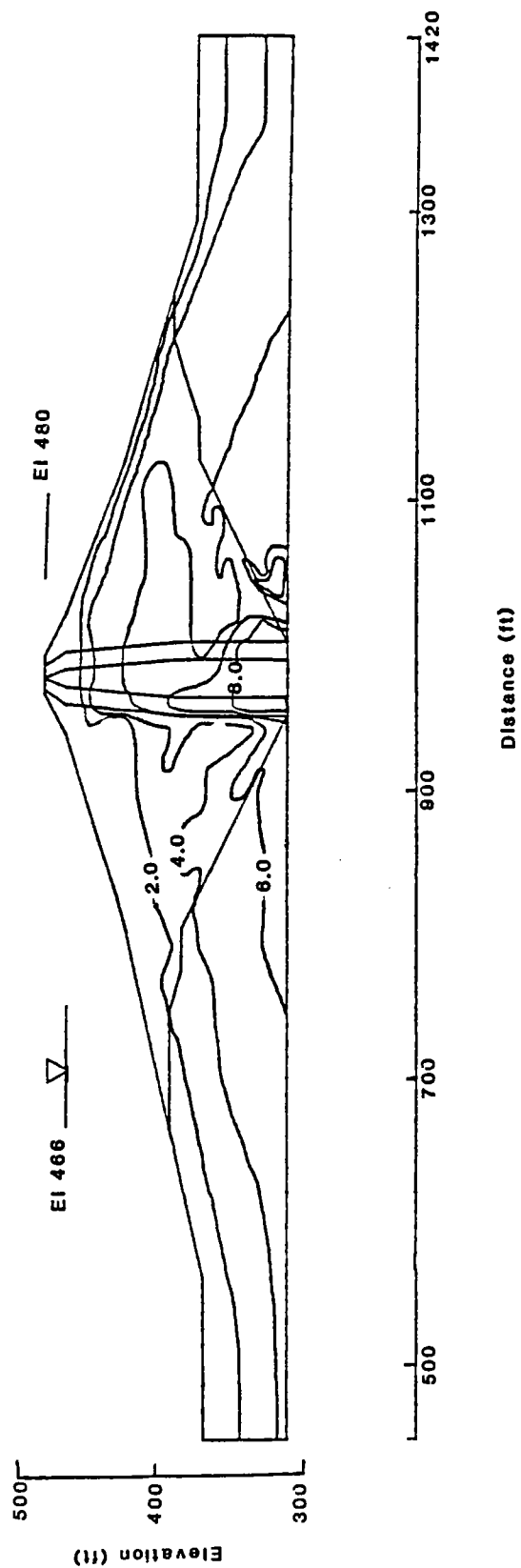


Figure 106. Contours of horizontal effective stress.

subsurface conditions, specifically, the geometry of concrete pours and excavated bedrock trenches at the bases of the enveloped monoliths. Construction photographs also showed actual construction procedures, which were compared to construction specifications for concurrence. In particular, these photographs showed equipment and procedures used in the compaction of core material, including material adjacent to the concrete gravity dam.

55. Following review of this information, there was some concern about the adequacy of compaction in areas inaccessible to large equipment. These areas were primarily located at the bases of the enveloped concrete monoliths. Figure 69 is a photograph from construction dated 6 August 1953. It shows a 25-ft wide trench at the downstream bases of concrete monoliths 1, 3, 4, and 6. Interviews with construction inspection personnel verified that inaccessible areas were carefully compacted with hand-held equipment.

#### Field and Laboratory Investigations

56. To examine core material placed in contact with the end monoliths at higher elevations, pairs of undisturbed and SPT borings were drilled at either end of the concrete gravity dam. Figure 26 shows the locations of these borings in plan and the sampled depths. Laboratory efforts were aimed at index testing. The logs, index test results, and blowcounts for the SPT borings are shown in Figures 70 through 73. The estimated  $N_1$  values typically averaged about 30 blows per ft, and the index tests showed that the core materials were slightly plastic, with an average fines content of 20 to 25 percent passing the No. 200 sieve.

#### Liquefaction Potential Evaluation

57. For non-plastic soils, an estimated value of  $(N_1)_{60}$  of about 20 to 23 is required at this location. The dynamic finite element results from Figure 61 were used to estimate required values of  $(N_1)_{60}$ . Although there are occasional measured values of  $(N_1)_{60}$  less than or equal to the required value, it was concluded that in general, the core materials at this location were adequately compacted. In consideration of the decomposed nature of saprolite, the method of placement, the fines content, the plasticity of the fines, the measured blowcounts, and the typically unsaturated condition of the core

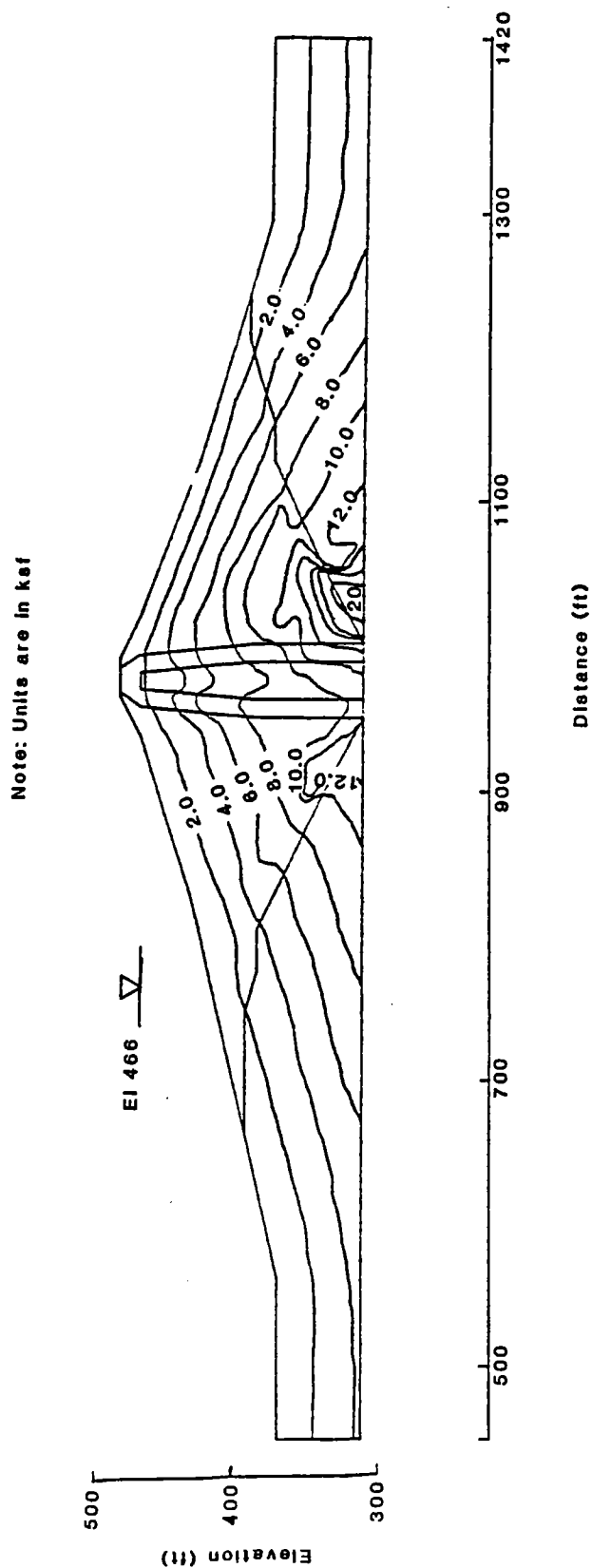


Figure 105. Contours of vertical effective stress.

## PART V: RETAINING WALL STUDIES

### Retaining Wall Description

59. Three retaining walls were constructed in the wrap-around area parallel to the river. Downstream retaining walls were constructed on both the Right and Left wrap-around areas. Upstream, only the Right wrap-around area required a retaining wall, denoted Retaining Wall B in Figure 26. Failure of the downstream walls would not result in immediate, catastrophic loss of the reservoir, consequently they did not receive further study. The upstream wall is of concern since the embankment shell is saturated and the intake ports for the powerhouse are located riverward of the wall, and could be blocked if the wall and embankment slid due to the design earthquake. The seismic safety evaluation of the wall was aimed at determining whether the integrity of the embankment wrap-around was threatened if the wall were to fail. If excessive sliding were to occur, the freeboard could be lost and the reservoir contents could escape, leading to catastrophic failure of the dam.

60. Retaining Wall B is 406 ft in length, and the crest of the wall is controlled by its intersection with the slope of the Right Wing Dam envelopment. Detailed plans and sections of Retaining Wall B are shown in Figures 74 and 75. The wall's maximum height is 82 ft near wall axis Station 0+29, and its lowest height is 27 ft at wall axis Station 4+35. Part III of this report contains descriptions of the materials which form the backfill behind the wall, specifically the Zone A rockfill, the Zone B gravel and the Zone C core. Figure 76 is a construction photograph dated 16 April 1954 which shows the completed wall with Zone A backfill in place. This photograph shows that a two-lane construction road exists at the base of the riverward face of the wall. Thus, the wall can undergo at least 20 ft of horizontal displacement without falling into the river channel.

61. Horizontal displacements on the order of 20 ft or more, along with a deep-seated sliding failure surface through the embankment fill would seriously threaten the integrity of the envelopment area and reduce the crest elevation to the pool level. It is estimated that 10 ft of horizontal displacement could safely be tolerated since this corresponds roughly to a 5 ft reduction in crest height, leaving a freeboard of about 10 ft, and since a

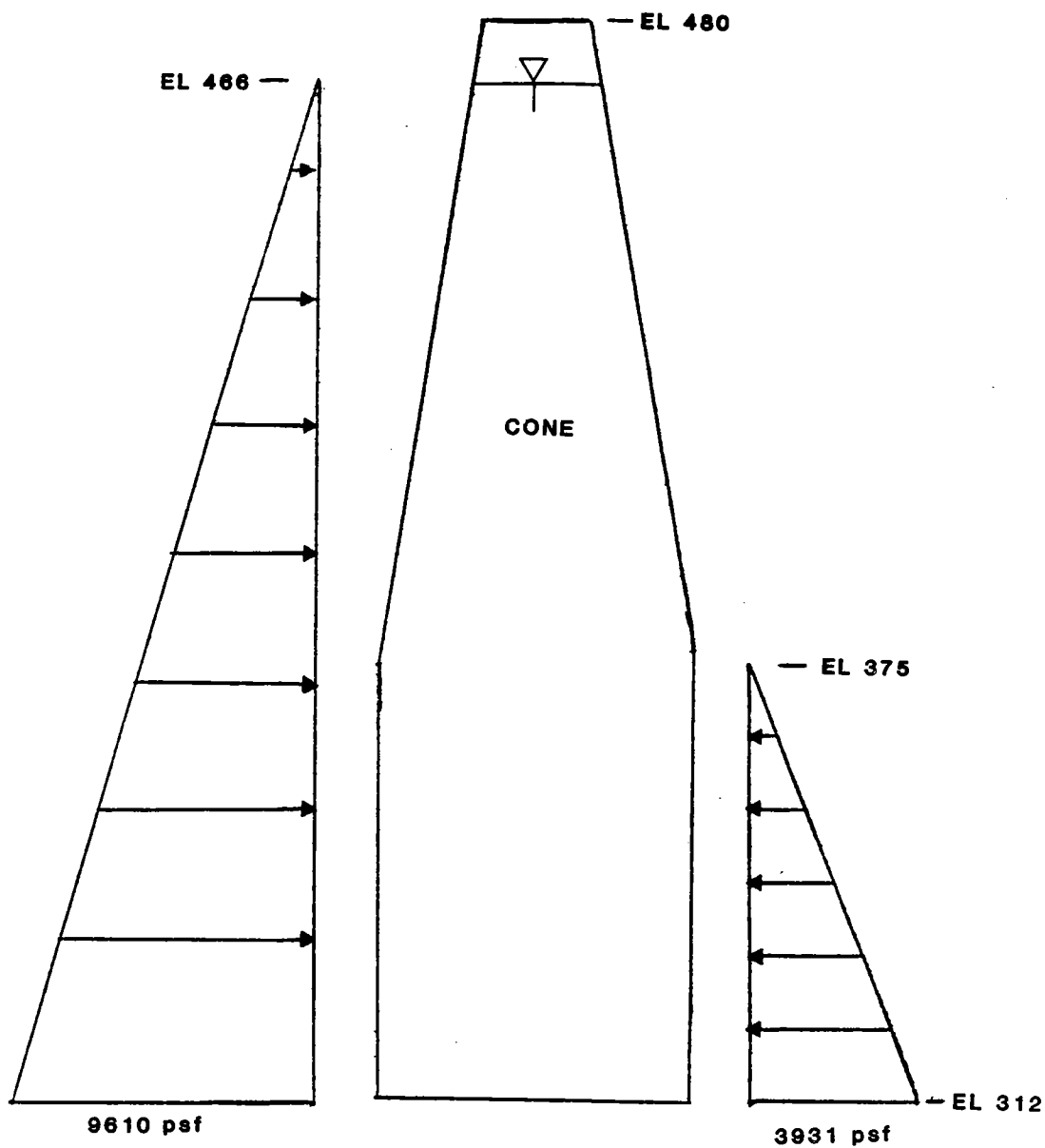


**Figure 104. Hydrostatic pressure distribution acting on impervious core of Mormon Island Dam for static finite element analysis.**

friction angle at the base of the wall was conservatively estimated as 30 degrees.

65. A homogeneous backfill with a total unit weight of 152 pcf was used in the Mononobe-Okabe calculations. The problem was solved as if the wall and backfill were not submerged. Then the resulting yield acceleration,  $k_y^*$ , was multiplied by the ratio of buoyant unit weight to total unit weight to determine  $k_y$ , the yield acceleration that accounts for the effect of submergence. In this way, horizontal loads are computed with the total unit weight of the backfill but effective or buoyant unit weight controls the vertical stresses and hence shear strength along the critical sliding surface. The ratio of buoyant unit weight to total unit weight is 0.6 for the Zone A and gravel transition backfill.

66. In the Mononobe-Okabe procedure, there is a condition that  $\psi$ , the arctan of the horizontal seismic coefficient, must be less than or equal to the friction angle,  $\phi$ , minus the slope angle,  $i$ . Values larger than this correspond to a non-equilibrium condition, and backfill material would fail by raveling and sliding until the slope angle  $i$  was reduced to the limiting value of  $\phi - \psi$ . Over the range of backfill strengths investigated, the condition that  $\psi$  be less than or equal to  $\phi - i$  was maintained for all computed yield accelerations without changing the slope angle  $i$ .

67. The backfill strengths were selected to correspond to excess pore pressure levels uniformly distributed throughout the backfill. With no excess pore pressure,  $r_u = 0$ , the effective friction angle of the Zone B gravel and that assumed for the Zone A rockfill is  $43^\circ$ , as presented earlier in Part III. The simple p-q diagram construction shown in Figure 79 was used to determine that backfill friction angles of  $43^\circ$ ,  $37.9^\circ$ ,  $33.1^\circ$  and  $29.9^\circ$  correspond to excess pore pressure levels of 0%, 10%, 20% and 25%, respectively. These strengths were used to determine the yield accelerations listed in Table 3.

68. It was estimated in the Wing Dam studies that the upstream shell of the Right Wing Dam may develop an average  $R_u$  about equal to or slightly less than 24 percent. The minimum yield acceleration was  $k_y = 0.025g$ , computed for section A-A with an excess pore pressure field of 25 percent ( $\phi = 29.9^\circ$ ). The corresponding failure surface is inclined at an angle of  $34^\circ$  which intercepts the core as shown in Figure 80a. The minimum yield acceleration computer for section C-C was 0.034 for the excess pore pressure field of 25 percent. This failure surface is inclined at  $34.5^\circ$  and also intercepts the core, as shown in

381 ELEMENTS  
399 NODAL POINTS

NOTE: ALL ELEMENTS BELOW LINE ARE SUBMERGED

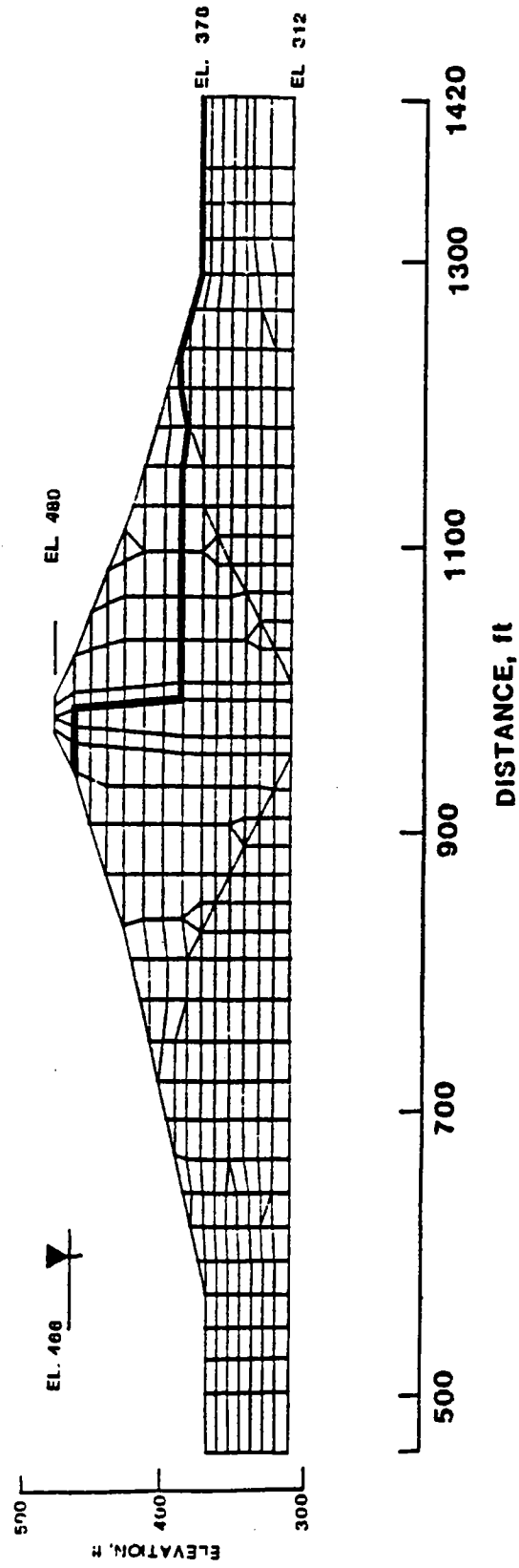


Figure 103. Finite element mesh of representative section of Mormon Island Auxiliary Dam.

31.1° and  $c = 0$ . This failure surface is inclined at 34° and intercepts the core. A more representative, yet conservative UTEXAS2 analysis of section A-A with a shell strength of  $\phi = 29.9^\circ$  and  $c = 0$ , and a core strength of  $\phi = 0$  and  $c = 4000$  psf (less than half the measured laboratory R-strength), resulted in a yield acceleration of 0.073g and a failure surface that does not intercept the core, but is confined to the upstream shell.

72. A degree of conservatism is called for in the analysis of Retaining Wall B due to a lack of well-documented case histories of submerged retaining walls subjected to seismic loading, variability in Newmark-type displacement calculations, and uncertainties in the material properties of the embankment fill, particularly Zone A, which construction records show is a rockfill with considerable fines dumped in 12-ft lifts. In view of these uncertainties, and to determine an upper bound for Newmark-type displacement of the wall and backfill, the displacement calculations were carried out with  $k_y = 0.025g$ , with the understanding that the actual displacements in the field should be less than the computed values.

#### Permanent Deformation Estimates

73. Earthquake-induced permanent displacements were estimated with three methods: Makdisi-Seed, Sarma-Ambraseys and modified Richards-Elms. The Makdisi-Seed and Sarma-Ambraseys methods explicitly include embankment amplification effects in the displacement calculations. The modified Richards-Elms approach is more approximate with regard to ground motion amplification, but due to the modifications developed by Whitman and Liao (1985) it quantitatively accounts for the many uncertainties in Newmark displacement calculations such as theoretical deficiencies in the sliding-block model, the random nature of earthquake ground motions, uncertainty in parameters characterizing the backfill, wall and foundation, and other, poorly understood deficiencies of the simple sliding block model. Each of these methods was applied to the retaining wall problem to estimate the range of earthquake-induced displacements consistent with the conservatively computed minimum yield acceleration of 0.025g. As discussed earlier, the wall and wrap-around backfill should be able to easily tolerate displacements of about 10 ft.

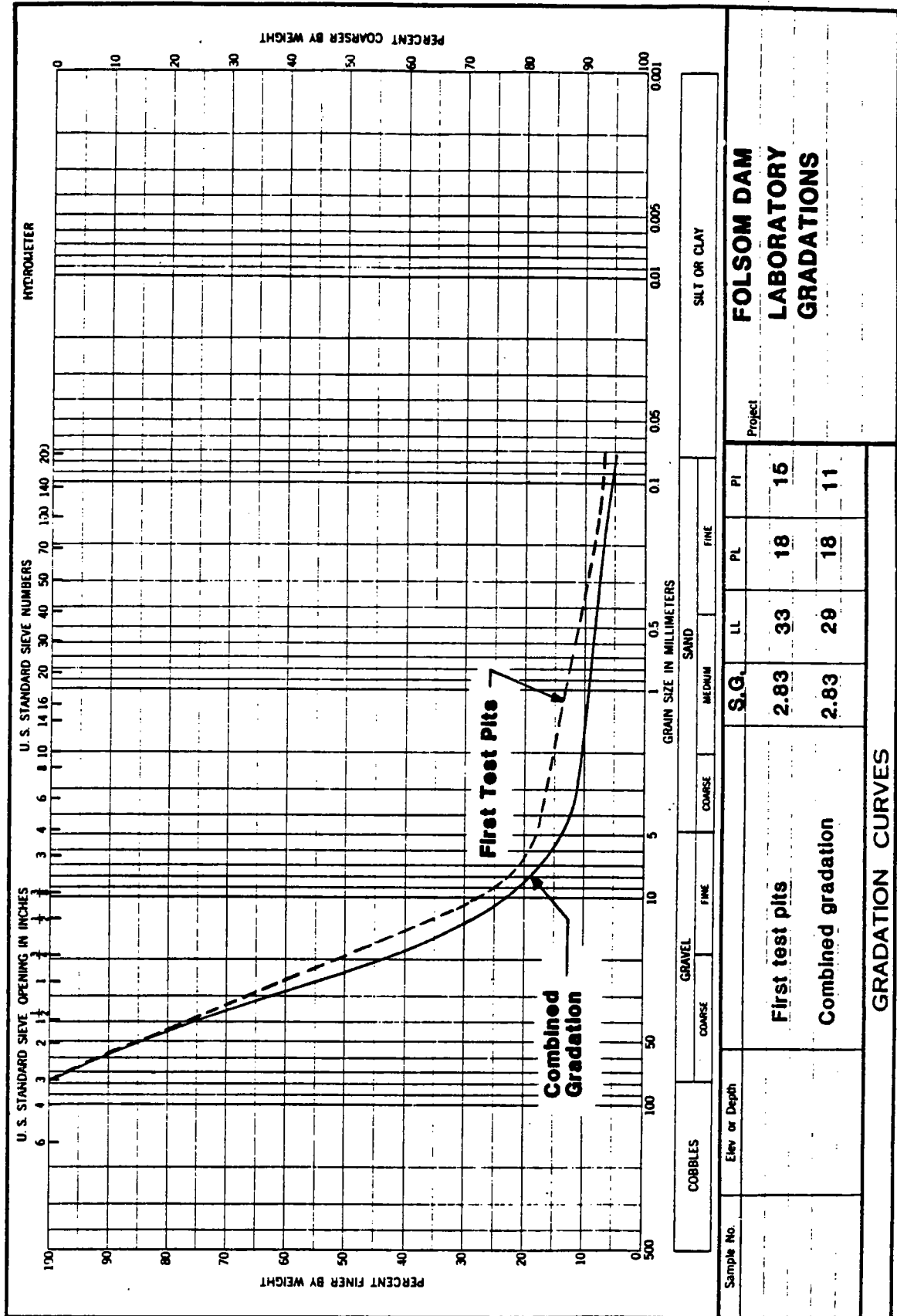


Figure 102. Folsom gravel gradations used in laboratory testing.

$0.025/0.80 = 0.03$ . The corresponding upper-bound displacement is 7.2 ft. With the compounded conservatism of lower-bound yield acceleration and upper-bound seismic coefficient and displacement values, it is expected from this application of the Makdisi-Seed procedure that movement along the failure surface will occur, but be limited to less than 7 ft.

#### Sarma-Ambraseys calculations

77. This procedure involves the following parameters:

- a. The yield acceleration,  $k_y$  (fixed at 0.025)
- b. The fundamental period of the system,  $T_o$
- c. The amplification factor  $a$ , from which the maximum earthquake seismic coefficient ( $A$ , defined as the maximum embankment acceleration averaged over the sliding mass) is determined as  $A = a \times \text{peak bedrock acceleration}$ .
- d. The ratio  $y/h$  as defined above. For this case,  $y/h = 1.0$ .

Values of amplification factor  $a$  were computed with SEISCOE for both earthquake records A and B for a range of fundamental periods,  $T_o = 0.1$  to 4 sec., and are shown in Figure 20 for several values of  $y/h$ . The maximum value of  $a$  from Figure 20 is 2.25 for  $y/h = 1.0$ , and occurs over the range  $T_o = 0.20$  to 0.25 sec. The fundamental period of the Wing Dam section computed with FLUSH was 0.83 sec. At  $T_o = 0.83$  sec, the amplification factor  $a$  is 1.0. The fundamental period of the concrete gravity dam, including foundation stiffness and the presence of the reservoir, is approximately 0.3 sec, and the corresponding amplification factor is approximately 1.75. The maximum value of  $a = 2.25$  was used for the displacement calculations.

78. Newmark displacement charts were calculated for earthquake records A and B for several values of  $k_y/A$ , and are shown in Figure 19. For  $k_y = 0.025$  and  $A = 2.25 \times 0.35 = 0.79$ ,  $k_y/A = 0.32$ . The corresponding chart displacement,  $U_c$ , is 91 cm (3 ft) for record A and 36 cm (1.2 ft) for record B. The field displacement,  $U_f$  is calculated as  $\alpha \times a \times U_c$ . The factor  $\alpha$  is a term from the solution to the equations of motion for relative displacement of the sliding block (see Hynes-Griffin and Franklin, 1984), and is a function of the inclination of the sliding surface ( $34^\circ$ ) and the friction angle of the backfill ( $29.9^\circ$ ). The factor  $\alpha$  is equal to  $\cos(34^\circ - 29.9^\circ)/\cos(29.9^\circ) = 1.15$ . The resulting field displacement for record A is  $U_f = 1.15 \times 2.25 \times 91 \text{ cm} = 235 \text{ cm}$  (7.7 ft), and for record B,  $U_f = 1.15 \times 2.25 \times 36 \text{ cm} = 93 \text{ cm}$  (3 ft). As seen with the Dike 5 permanent displacement calculations, the

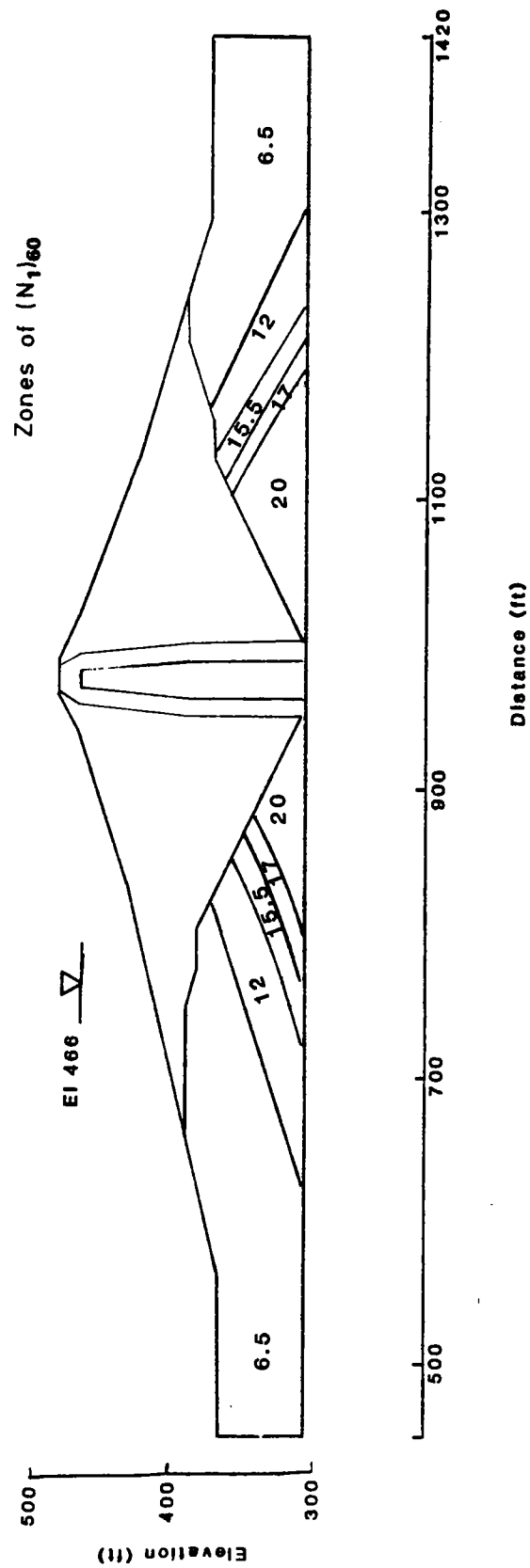


Figure 101. Zones of  $(N_1)_{60}$  for foundation gravels, at Mormon Island Auxiliary Dam estimated from Becker Hammer soundings and computed vertical effective stresses from static finite element analyses.

### Post-Earthquake Stability Studies

80. A study was made of the consequences of complete wall failure by investigating two worst-case scenarios. In one case, the wall is assumed to have toppled, and the backfill slope is still approximately 1 vertical to 2 horizontal but the shell strength is reduced to a residual value of 1800 psf (based on an estimated  $(N_1)_{60}$  of 19 for the envelopment shell from adjusted Becker data, and a corresponding residual strength from Seed (1986) shown in Figure 115). In this extreme case, the slope has a factor of safety of 1.12 against post-earthquake sliding. In the other case, the retaining wall and all of Zone A are assumed to be lost, leaving the gravel transition Zone B exposed at a slope of 1 vertical on 1.5 horizontal, with a residual strength of 1800 psf. In this extreme case, the factor of safety against post-earthquake sliding was 1.07. Since the safety factors against liquefaction typically exceed 1.4 in the Right Wing Dam, the post-earthquake stability of the wrap-around slope will be greater than that for the residual conditions listed above, and the deformations associated with development of soil strength will be considerably less than those needed for residual conditions.

### Stability Evaluation

81. The Makdisi-Seed, Sarma-Ambraseys and modified Richards-Elms approaches all gave earthquake-induced permanent displacement estimates of Retaining Wall B and Right Wing envelopment fill of less than 10 ft. These Newmark sliding-block analyses indicate that some damage to the wall is expected but the deformations will be limited. Worst-case scenario investigations show the slopes will be stable even with total failure of the wall. Catastrophic loss of the reservoir is not expected as a result of the damage to the upstream retaining wall and envelopment fill.

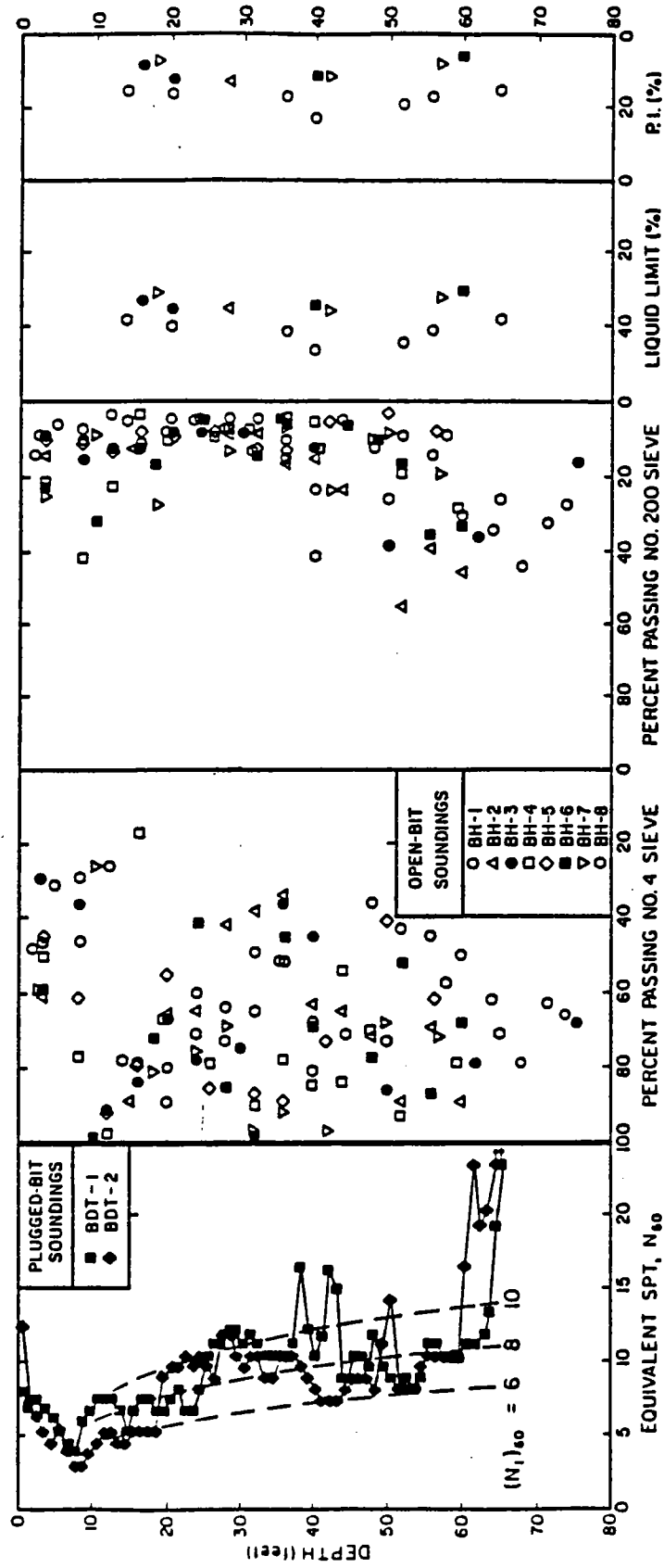


Figure 100C. Equivalent SPT Blowcounts and Classification Test Data from Soundings performed in the Downstream

Flat Area, Mormon Island Auxiliary Dam (from Harder, 1986).

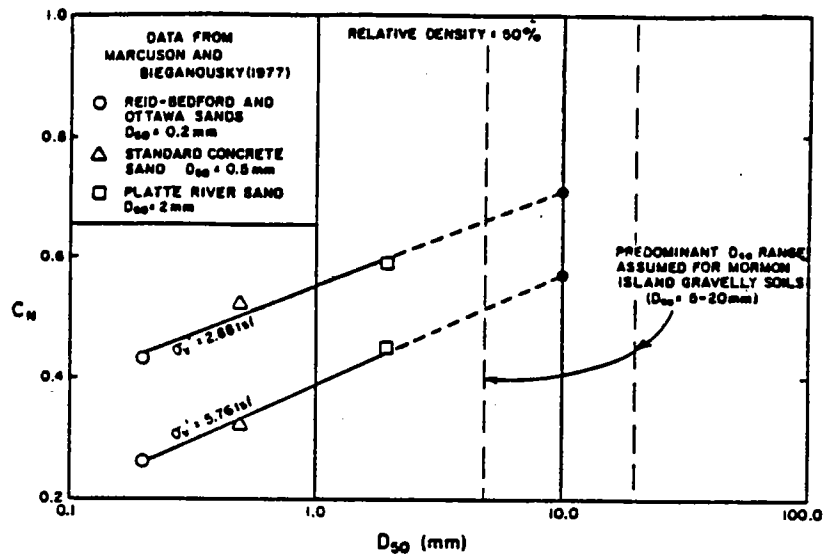
the dam vary according to the foundation conditions, with the flattest slopes in the vicinity of the dredged tailings. The downstream slopes of the dam vary between 1 vertical to 2 horizontal and 1 vertical to 3.5 horizontal, and the upstream slopes vary between 1 vertical to 2 horizontal and 1 vertical to 4.5 horizontal.

### Field Investigations

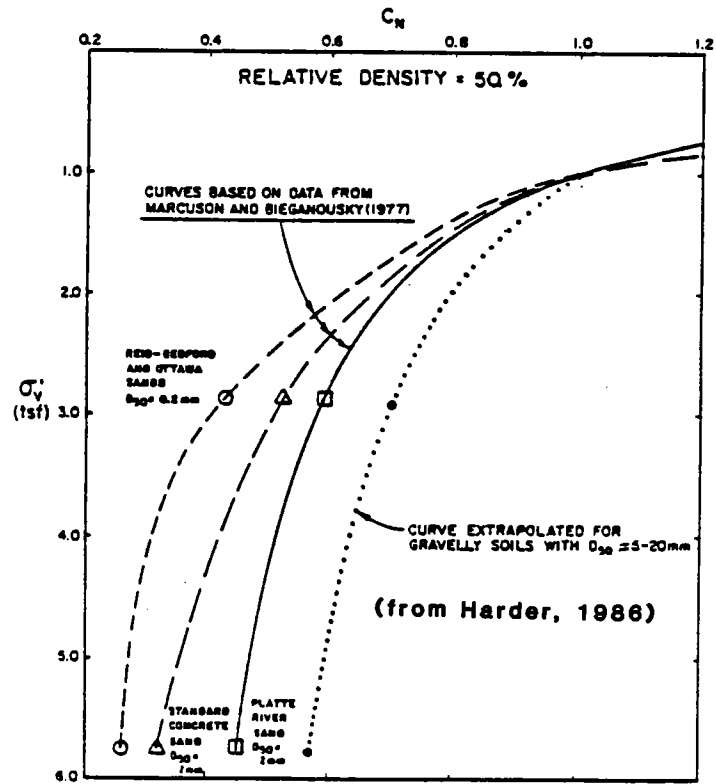
85. Field investigations were concentrated at the tallest section of the dam where the dredged tailings form the foundation for the shells. Field investigation of the shell and foundation tailings was confined to the downstream area. It is assumed that the information observed downstream is also representative of the material upstream of the core of the dam. The program included SPT and undisturbed sampling of the core, geophysical tests, test pits and shafts to obtain disturbed samples and determine in situ density, and Becker Hammer testing. With the exception of limited surface geophysical testing, the undisturbed alluvium was excluded from the investigations. The locations of the various field investigations are shown in Figures 85, 86 and 87. The results of these investigations are discussed below.

#### SPT results in Zones 3 and 4

86. Two pairs of holes were drilled in the vicinity of Station 449+75. Each pair consisted of an undisturbed hole, denoted US in Figure 85, spaced 10 ft along the dam axis from a SPT hole, denoted SS in Figure 85. Borings US-6 and SS-6 were drilled through the Zone 4 core materials at the dam centerline and borings US-7 and SS-7 were drilled at the downstream edge of the dam, mainly through Zone 3 compacted decomposed granite. SPT samples were obtained with trip hammer equipment and drilling fluid, and undisturbed samples were obtained with a Denison sampler. The blowcounts are shown in Figure 88. Record samples show the core is a mixture of clay, sand, and gravel. The average core gradation has about 7 percent gravel, 57 percent sand, and 36 percent plastic fines. The average plasticity index is 20 and the average liquid limit is 40. Record samples of the Zone 3 decomposed granite show an average gradation of 7 percent gravel, 73 percent sand, and 20 percent silty fines with no to low plasticity, typically a liquid limit (LL) of 28 and a plasticity index (PI) of 4.



(a)



(b)

Figure 100. Relationship between  $C_N$  Correction and Overburden Pressure.

90. The test pits reached a maximum depth of about 8 ft in the dredged tailings. The materials were oven-dried to determine in situ dry densities. Several of the observed gradations were reconstructed in the laboratory to determine maximum and minimum dry densities. Since no well established procedure exists to determine these values for gravels, both impact and vibratory loads were applied to samples in a range of mold sizes from 11 in. to 36 in. in diameter. The laboratory estimates of maximum and minimum density are shown in Figure 92. Since several of the measured in situ dry densities exceeded the laboratory maximum values, the maximum dry density was estimated as an envelope of all the data. The relationship between maximum and minimum dry densities and gradation, expressed by the uniformity coefficient,  $C_u$ , is shown in Figure 92. It is estimated that the in situ relative density is about 35 percent. Specific gravity tests were performed on the plus-No. 4 and minus-No. 4 fractions. Both fractions had an average value of  $G_s$  equal to 2.83.

91. The average fines content of the foundation gravel was 6 percent (LL = 33, and PI = 15) for the first test pit series and 5 percent (LL = 29, and PI = 11) for the second. Due to the method of deposition of dredged tailings and the observations from construction, it is known that the fines content increases significantly with depth. Further evidence of this was provided by the Becker Hammer samples discussed later in this section.

#### Test pits in downstream shell

92. A shaft approximately 15-ft deep was excavated in the downstream shell to measure in situ densities and gradations of the Zone 1 gravel. The range of these gradations is shown in Figure 93. The average of the foundation gradations was almost identical to the average of the shell gradations. This combined average gradation, scalped to a maximum particle size of 3 in. was used in subsequent laboratory tests. The test results indicate the in situ relative density of the shell gravel is approximately 70 percent, as shown in Figure 94. The fines were found to be somewhat plastic, with average plasticity index of 11 and liquid limit of 28. The average fines content was about 5 percent. Both the plus-No. 4 and the minus-No. 4 fractions had an average  $G_s$  equal to 2.83.

#### Becker Hammer tests

93. A detailed description of the Becker Hammer investigations is given by Allen (1984). Summary details are described in this section. Figures 85

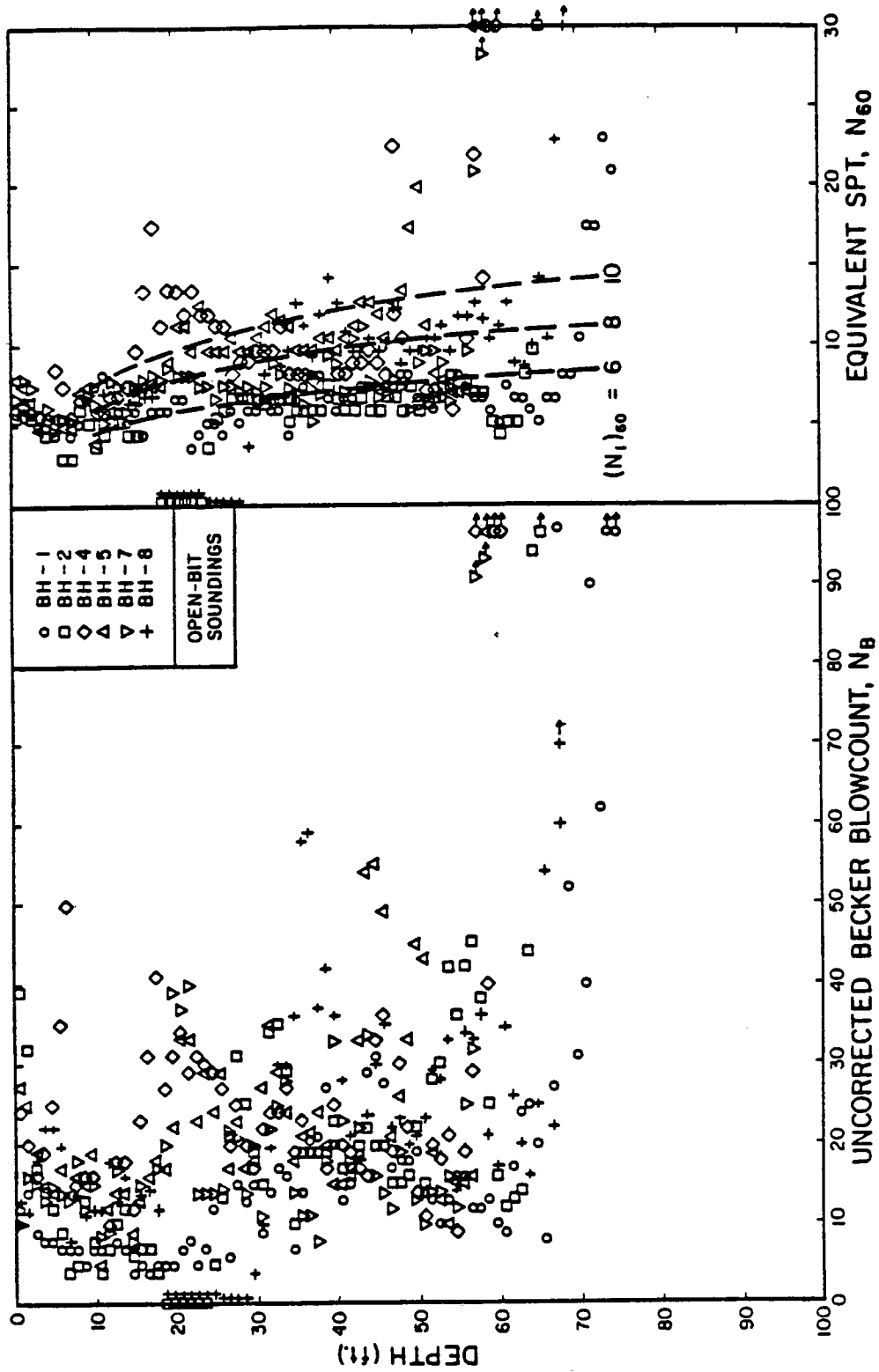


Figure 99. Uncorrected Becker and Equivalent SPT Blowcounts for Soundings BH- 1, 2, 4, 5, 7, and 8 performed in the Downstream Flat Area, Mormon Island Auxiliary Dam (from Harder, 1986).

representative of the dredged tailings beyond the upstream and downstream toes of the dam. Beneath the dam, an increase in  $(N_1)_{60}$  with depth was observed in the foundation gravels (see Figures 95 and 96). It is estimated that the foundation gravels have densified under the embankment load. The effect was most pronounced in the closed-bit sounding, BDT-3. In an effort to best represent the field conditions, this strength increase was included in the characterization of the foundation gravels beneath the embankment shells. The higher foundation blowcounts observed in BDT-3 were extrapolated to other locations beneath the shells by consideration of the vertical effective stress contours from the static finite element analyses. Table 4 lists the estimated  $(N_1)_{60}$  values and Figure 101 shows the assumed distribution of  $(N_1)_{60}$  values throughout the foundation gravels.

#### Liquefaction Potential Evaluation of Zone 4 Core and Zone 3 Filter Materials

98. Due to the plasticity of the fines, the high fines content, the method of material placement, and the high degree of compaction of Zone 4, this material was considered not to be susceptible to liquefaction and no significant excess pore pressures are expected to develop in the core. The Zone 3 decomposed granite filter is also well compacted and has a large fines content. It was concluded from the studies on the Wing Dams and Dike 5 that this material would also not be susceptible to liquefaction, and no significant excess pore pressures are expected to develop.

#### Liquefaction Potential Evaluation of Shell and Foundation Gravels

99. The steps to evaluate liquefaction susceptibility and post-earthquake slope stability described in the Wing Dam Studies were also used to evaluate the seismic stability of Mormon Island Auxiliary Dam. As mentioned earlier, the shells of Mormon Island Auxiliary Dam were compacted in 18-inch lifts and are denser than the Right and Left Wing Dam shells which were compacted in 2 foot lifts.

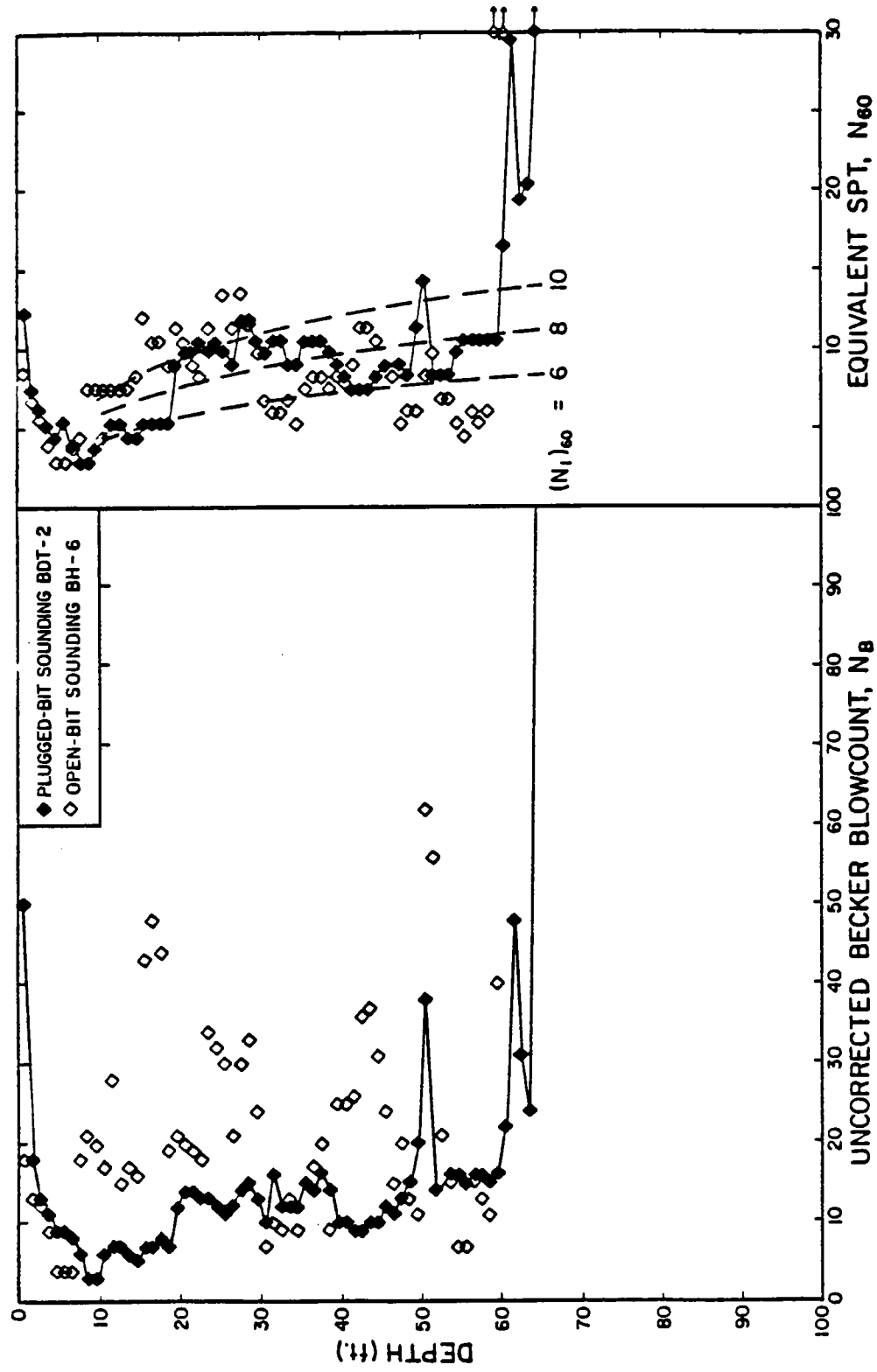


Figure 98. Uncorrected Becker and Equivalent SPT Blowcounts for Soundings BH-6 and BDT-2 performed in the Downstream Flat Area, Mormon Island Auxiliary Dam (from Harder, 1986).

shell gravels with  $\alpha$  equal to zero. The pore pressure curve for  $\alpha = 0$  shown in Figure 52 was used to estimate  $R_u$  for the foundation gravels.

104. Consolidated undrained triaxial compression tests on laboratory specimens compacted to a relative density of 40 percent show that the foundation gravel has an effective friction angle of about 41 degrees before and after cyclic loading.

#### Static finite element analyses

105. FEADAM was used to calculate the initial effective stresses in the foundation and shells of Mormon Island Auxiliary Dam. In these analyses, the foundation was first formed in layers to develop a level ground foundation for the shells, but the excavated portion was not included, resulting in a notched geometry. The embankment was then built up in layers to fill the excavation and complete the dam. This simulated construction sequence improved the accuracy of the computed stresses. The mesh is shown in Figure 103, and the hyperbolic input parameters are shown in Table 7. The reservoir and tailwater loads are applied as nodal forces against the core. These loads are shown schematically in Figure 104. The computed vertical effective stress contours are shown in Figure 105, the horizontal effective stress contours are shown in Figure 106, the initial static shear stresses on horizontal planes are shown in Figure 107, and the  $\alpha$  contours are shown in Figure 108.

#### Dynamic finite element analyses

106. The same mesh from the static finite element analyses was used in the dynamic finite element analysis with the program FLUSH and Accelerogram B. Preliminary SHAKE analyses indicated that Accelerogram B resulted in about the same to slightly higher dynamic stresses than Accelerogram A. The distribution of shear wave velocities in the section was discussed earlier, and the zones are shown in Figure 89. To develop appropriate input ground motions, Accelerogram B, a rock outcrop record, was input to SHAKE to compute corresponding bedrock ground motions at the base of a free field soil column taken from the first column of elements in the finite element mesh. As with the Wing Dams, the average sand modulus degradation curve was used. Figure 109 shows contours of computed maximum cyclic shear stresses on horizontal planes multiplied by 0.65. The computed accelerations for several points in the section are shown in Figure 110. The computed shear strain levels are shown in Figure 111.

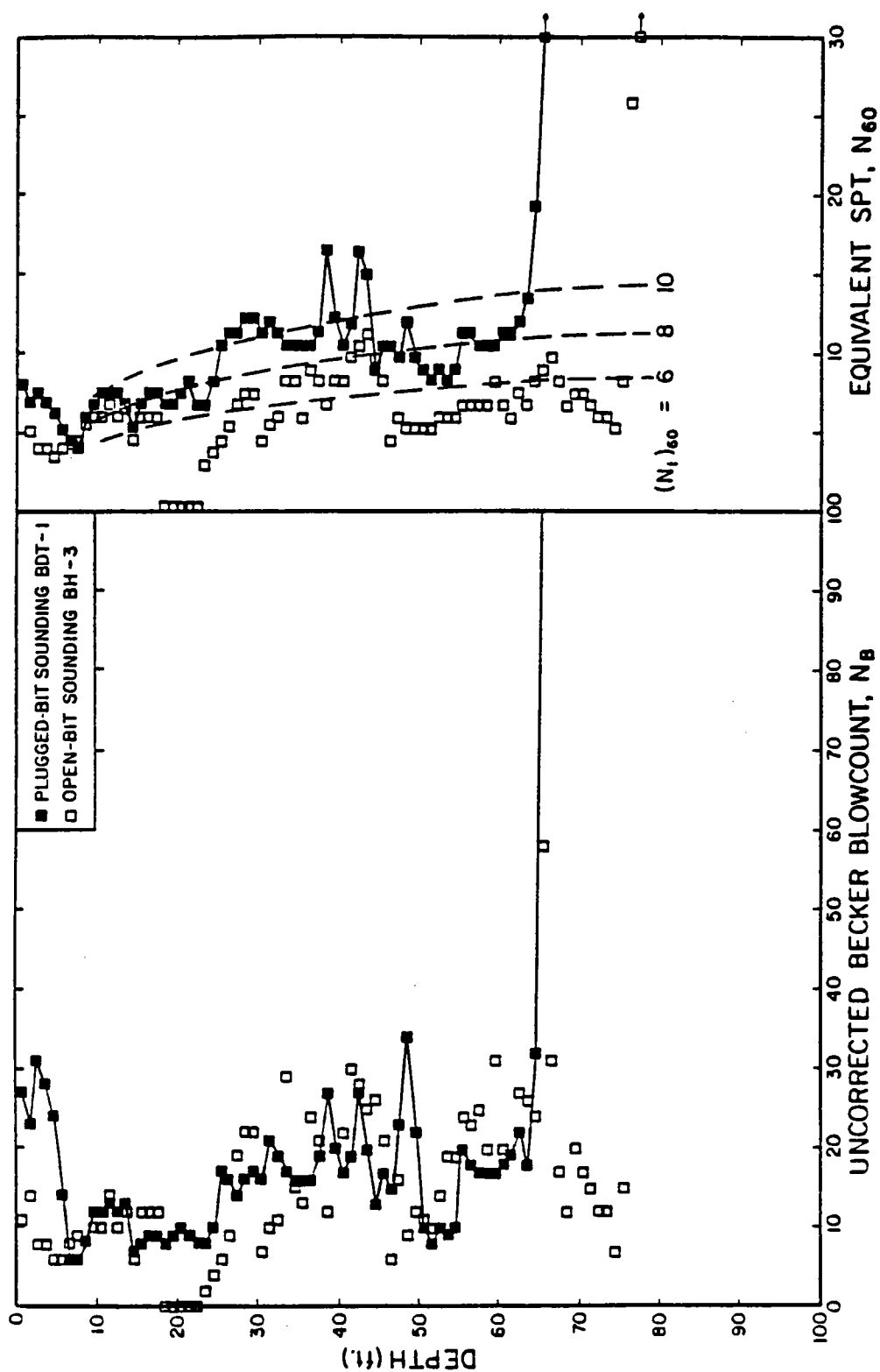


Figure 97. Uncorrected Becker and Equivalent SPT Blowcounts for Soundings BH-3 and BDT-1 performed in the Downstream Flat area, Mormon Island Auxiliary Dam (from Harder, 1986).

## Post-Earthquake Slope Stability

111. The safety factor contours from Figure 113 were associated with corresponding residual excess pore water pressure ratios,  $R_u$ , from Figure 52. Contours of estimated residual excess pore pressure ratios are shown in Figure 114. The residual strength of the liquefied soils was estimated from  $(N_1)_{60}$  values from Seed's chart (Seed, 1986) shown in Figure 115. For the portions of the embankment with safety factors against liquefaction greater than 1.0, the residual excess pore pressures were used to estimate the available effective strength. The section was zoned with the strength parameters shown in Figures 116 and 117 for post-earthquake slope stability analyses with UTEXAS2.

112. Both upstream and downstream failure surfaces were investigated. No cracks were incorporated in the computations. Since several surfaces have safety factors against sliding less than one for both upstream and downstream slopes, the objective in the search was to find the approximate location of potential failure surfaces with safety factors against sliding equal to unity, and thus estimate the volume of material involved in initial post-earthquake sliding.

113. Figure 118 shows two post-earthquake failure surfaces computed for the upstream slope. The safety factors against sliding ( $F_{PES}$ ) are 0.96 and 0.63. Surfaces passing through materials above and downstream of the surface with  $F_{PES} = 0.96$  have safety factors against sliding of less than one. Surfaces that are deeper and involve materials further downstream of the surface with  $F_{PES} = 0.96$  have safety factors against sliding greater than one. The surface with  $F_{PES} = 0.96$  deeply cuts into the core and exits approximately at the pool elevation on the downstream slope. For general information purposes, static safety factors against sliding before the earthquake ( $F_{STA}$ ) for the same surfaces are also shown.

114. Figure 119 shows similar information for the downstream slope. Surfaces that intercept material upstream of the post-earthquake sliding surface marked  $F_{PES} = 1.02$  have safety factors against sliding greater than one. Surfaces that pass through materials shallower and downstream of the surfaces marked  $F_{PES} = 1.02$  have safety factors less than one. The static (pre-earthquake) safety factors are also shown. The critical surface,  $F_{PES} = 1.02$ ,

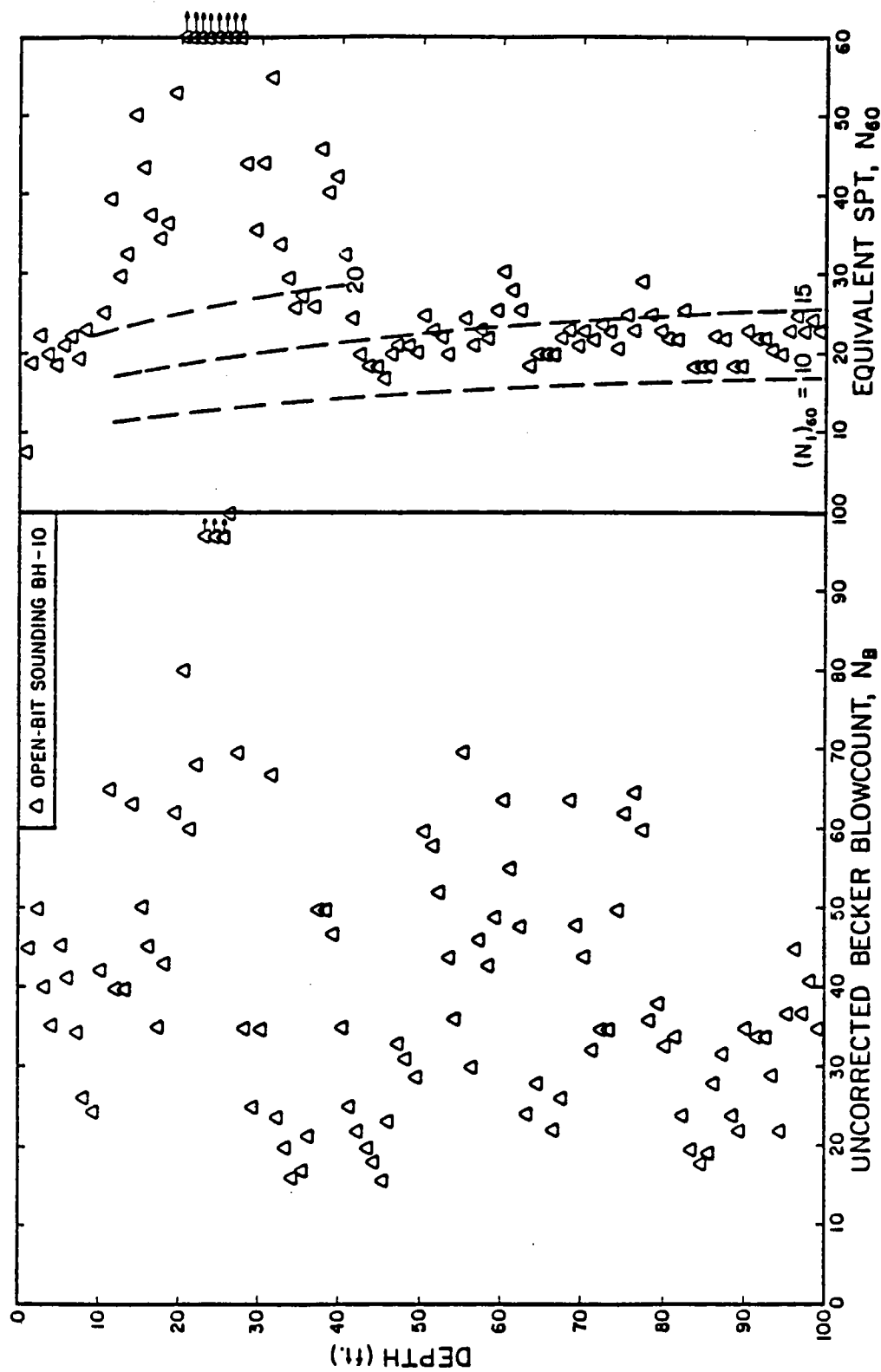


Figure 96. Uncorrected Becker and Equivalent SPT Blowcounts for Sounding BH-10 performed through downstream slope, Mormon Island Auxiliary Dam (from Harder, 1986).

## Stability Evaluation

118. Mormon Island Auxiliary Dam is 4820 ft long. From the right end of the dam to Station 439, and from Station 458 to the left end of the dam, the embankment dam is founded on rock. From similarity to the Wing Dams, it is expected that these portions of Mormon Island Auxiliary Dam founded on rock will perform well during and immediately after the earthquake. Although some excess pore pressures may develop in saturated portions of the shells, they do not pose a stability problem, and permanent deformations are expected to be tolerable, less than 0.5 m.

119. From Station 446 to Station 454, the channel alluvium has been dredged for its gold content, and this dredged material forms the foundation for the upstream and downstream shells of the dam. Extensive liquefaction and slope instability is expected in this portion of the dam and foundation. Catastrophic loss of the reservoir is expected. Remedial or hazard-mitigating measures should be enacted immediately.

120. No analysis has been made of the portion of the dam with shells founded on undisturbed alluvium. Initial fundamental periods for these sections are estimated to range from 0.25 to 0.4 sec. This range brackets the peak of the response spectra for Accelerogram B. Further field investigation and analysis is necessary to determine whether the remedial work needs to include the undisturbed alluvium in addition to the dredged tailings. As of this writing, SPK has initiated this additional field work and complementary laboratory work as part of the remedial action design process.

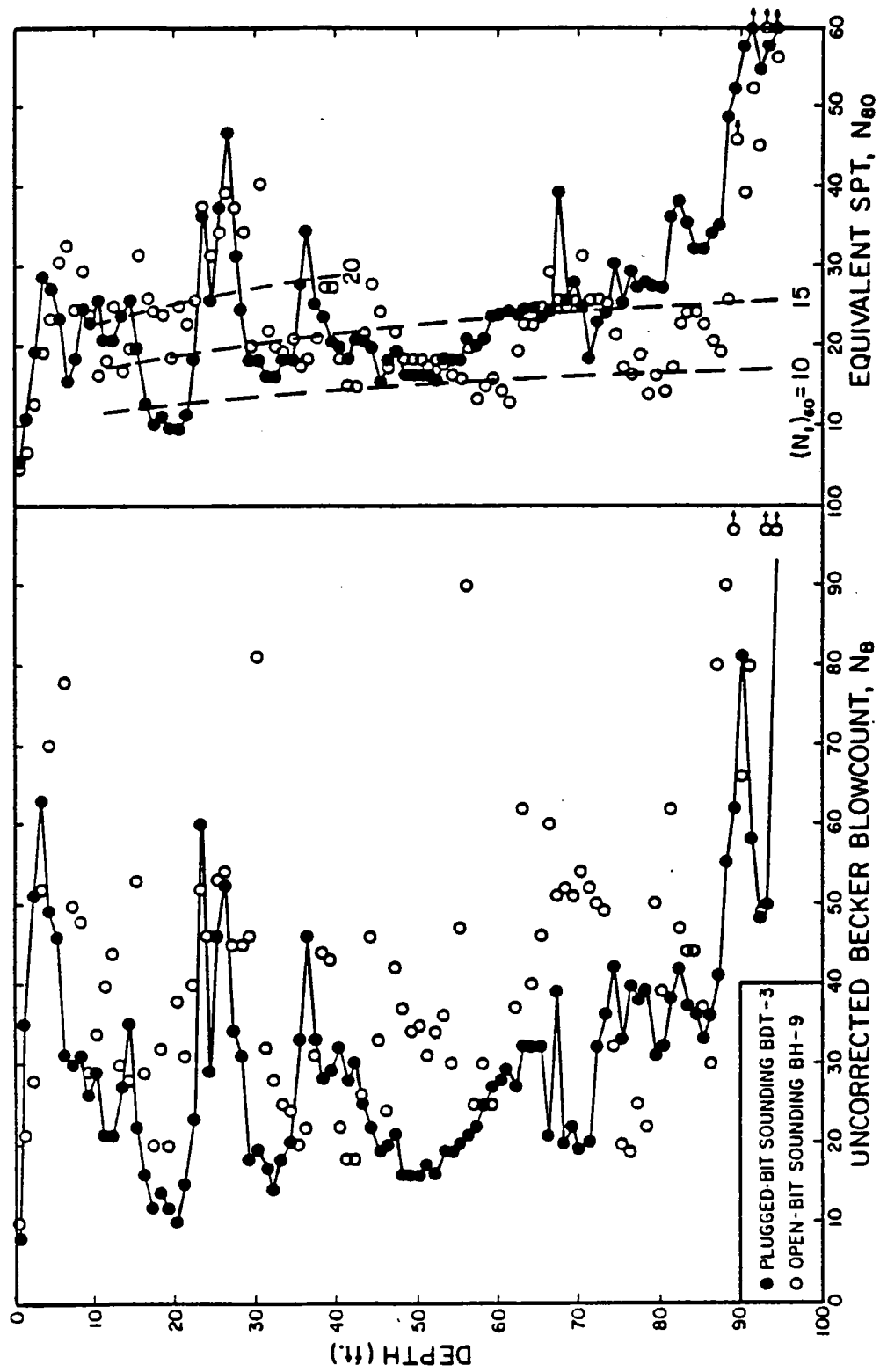


Figure 95. Uncorrected Becker and Equivalent SPT Blowcounts for Soundings BH-9 and BDT-3 performed through Downstream Slope, Mormon Island Auxiliary Dam (from Harder, 1986).

lean and rich concrete are in very good condition and the aggregate is of very good quality. Specimens for laboratory testing were selected from these cores. A limited large-scale coring program was also carried out on the crest and downstream face and in the galleries to obtain 12-in. diameter specimens for laboratory strength testing.

124. Six NX-size core holes were drilled 20 ft into the foundation rock from locations within the foundation grouting gallery. These locations are shown in Figures 124 and 125. Table 9 lists the length of concrete and rock obtained from these holes, as well as average core recovery and average Rock Quality Designation (RQD). Inspection of the rock cores showed that the granodiorite rock is only slightly weathered near the surface, and is generally unweathered below the top few feet of rock. Rock core recovery was typically 100 percent, with a low of 91 percent in one hole. Average RQD for the cores indicate that the intensity of fracturing in the rock decreases (and RQD increases) in going from the right abutment to the left abutment. Average RQD values ranged from 36 (poor rock quality) to 96 (excellent rock quality).

125. Goodman Jack tests were performed in the NX holes to determine in situ moduli at depth intervals of 2, 10 and 20 ft from the top of rock. Modulus of deformation and modulus of elasticity were calculated from the field measurements. The measured modulus of deformation ranges from 0.2 to  $3.9 \text{ psi} \times 10^6$ , and averages about  $1.65 \text{ psi} \times 10^6$ . The measured modulus of elasticity ranges from 0.6 to  $7.5 \text{ psi} \times 10^6$ , and averages about  $2.1 \text{ psi} \times 10^6$ . The modulus of elasticity of the rock was also estimated from the geophysical data obtained at several locations along the embankment dams (Sharp and Curro, 1987). Based on the geophysical data obtained at this site and measured compression-wave velocities at other similar sites, and published results of modulus, unit weight, and Poisson's ratio, the compatible set of rock properties listed in Table 10 was determined. The geophysical test results and reasoning indicate the modulus of elasticity of the rock ranges from 5.8 to  $11.0 \text{ psi} \times 10^6$ , with a best estimate value of  $7.9 \text{ psi} \times 10^6$ . These values are consistent with the in situ borehole jack measurements, since the geophysical tests involve a higher loading rate and lower strain levels than the Goodman Jack tests.

126. Static and dynamic laboratory tests were performed on 6- and 12-in. diameter samples of rich and lean concrete (summarized in Raphael, 1987). It was observed in the laboratory that 90 percent of the concrete

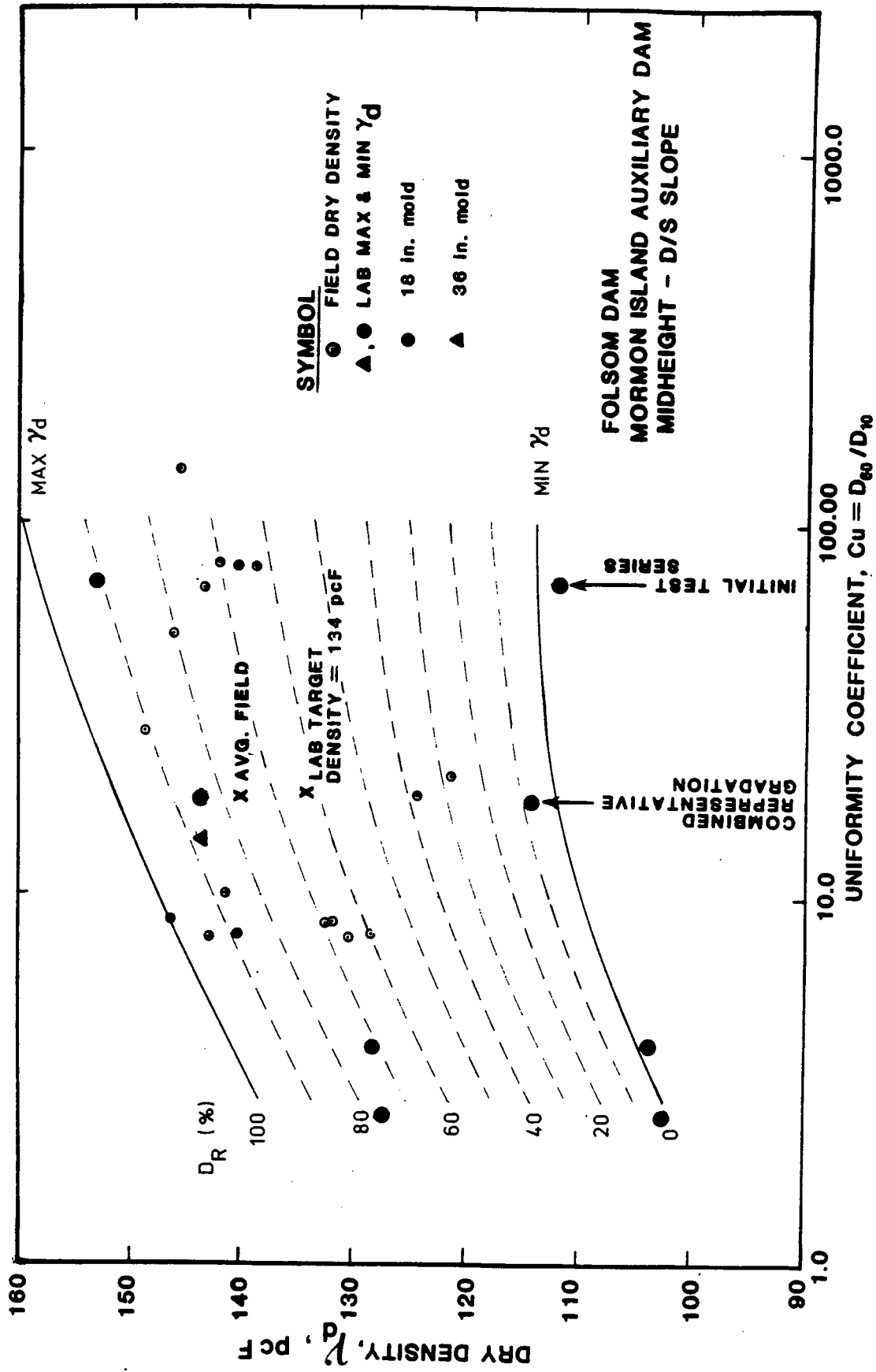


Figure 94. FIELD MEASURED DRY DENSITIES AND UNIFORMITY COEFFICIENTS FROM TEST  
 SHAFT IN EMBANKMENT GRAVEL AT MORMON ISLAND DAM

predominant modes of vibration and to accurately evaluate the stresses throughout the monolith. Since the critical tensile stresses in the dam result entirely from the dynamic effects of the earthquake loading, the modulus of elasticity for the concrete used in the analyses corresponds to the dynamic value,  $5.9 \times 10^6$  psi. Poisson's ratio is taken as the average of the static and dynamic values, 0.19. The response analyses were conducted with the three sets of rock properties shown in Table 10 to assess the sensitivity of the results to the foundation stiffness.

130. Energy dissipation in the dam and foundation materials is represented by hysteretic damping with damping factor  $\eta$ . A constant hysteretic damping factor  $\eta_s = 0.1$  for the dam concrete and  $\eta_F = 0.1$  for the foundation rock are assumed (Fenves and Chopra, 1984).

131. The absorptive nature of the reservoir bottom is characterized by the wave reflection coefficient  $\alpha$ . It is difficult to determine exact values of  $\alpha$ , since the bottom materials generally are composed of variable layers of exposed rock, alluvium, and other sediments. For analysis of proposed or recently impounded reservoirs, where sedimentation is slight,  $\alpha = 0.90$  or 1.0 is recommended. For older dams where reservoir bottom deposits are more substantial,  $\alpha = 0.75$  or 0.90 is perhaps more appropriate (Fenves and Chopra, 1986). Since Folsom Dam was completed in 1956, it is likely that a value of  $\alpha$  no greater than 0.90 is justified. However, given the uncertainty in the values of  $\alpha$ , analyses using both  $\alpha = 0.90$  and 0.99 were conducted.

#### Earthquake ground motions

132. The two horizontal accelerograms provided by Bolt and Seed (1983) for the seismic safety evaluation and designated elsewhere in this report as Record A and Record B are designated in this section as EQ1H and EQ2H, respectively. The accelerograms are shown in Figure 3 and the response spectra are shown in Figure 4. The peak acceleration of these records is 0.35 g which occurs at 6.12 sec in EQ1H and at 1.92 sec in EQ2H. Two vertical accelerograms, EQ1V and EQ2V, were generated from the corresponding horizontal record by increasing the frequency content by a factor of 1.5 and by multiplying the amplitudes by 0.6.

133. Because the monolith geometry and static loading is nonsymmetric, the static and earthquake-induced stresses on the upstream and downstream faces are not equal. In one case, the earthquake-induced forces are directed downstream in order to calculate the principal stresses in the dam. In the

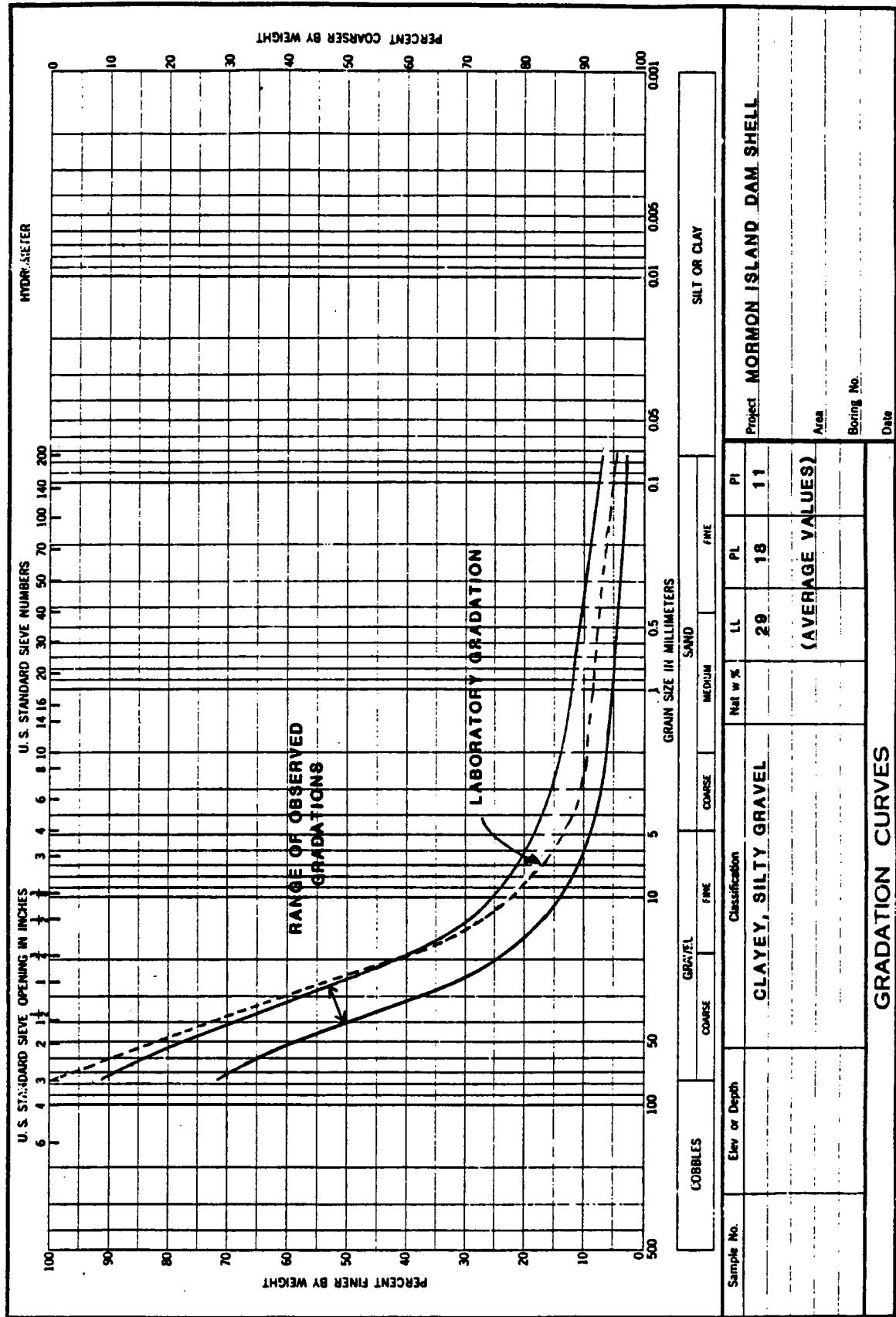


**Figure 93. Range of gradations observed in test shaft in downstream Mormon Island Auxiliary Dam shell. Laboratory gradation shown for comparison.**

137. It is worthy to note that for all analyses, the latest time of occurrence of the maximum principal tensile stress is 6.23 sec. It is clear from this result that the 10.24 sec duration of the response history is satisfactory. For these relatively stiff structures, the peak response is expected to occur slightly later than the maximum ground acceleration which, for the horizontal record of EQ1, occurs at 6.12 sec. Since the horizontal accelerations produce greater seismic effects than the vertical, the result that the maximum stresses occur at 6.23 sec is consistent.

#### Analysis results

138. As indicated previously, a total of eight sets of ground motions result when the different combinations of directions are considered for both earthquakes. To assess the critical ground motion, analyses were made for each set of foundation rock properties shown in Table 10. In these analyses, the material properties of the concrete were an elastic modulus of  $5.9 \times 10^6$  psi, a Poisson's ratio of 0.19 and a unit weight of 158 pcf. The reservoir bottom reflectivity was taken as 0.90 and the hysteretic damping factors for the dam and foundation rock were 0.10. The results of these analyses are summarized in Table 11 which shows the maximum principal tensile stresses on the upstream and downstream faces. As shown in Table 11, the absolute maximum stresses (identified by asterisks) for each foundation condition arise on the downstream face. For the low foundation modulus, earthquake EQ1, directions H-V, produce a maximum tensile stress of 633 psi. For the intermediate and high moduli, the critical ground motion is EQ2, directions -HV, and the maximum stresses are 727 psi and 916 psi, respectively. On the basis of these findings, EQ1H-V is used for further study for the low modulus foundation, and EQ2-HV is employed for the average and high moduli.

139. Table 12 presents the maximum stresses which result for the two reservoir bottom reflectivity values  $\alpha = 0.90$  and 0.99, for each foundation modulus. Note that  $\alpha = 0.99$  corresponds to essentially a totally reflective reservoir bottom. For comparison, the maximum stresses for  $\alpha = 0.90$  from Table 11 are included in Table 12. The results in Table 12 show that the greatest principal stress occurs for the case in which the foundation modulus and reservoir bottom reflection coefficient are the largest. In recognition of the age of the Folsom reservoir and the likelihood of substantive sedimentation, the appropriate results to consider are those in which  $\alpha = 0.90$ . For the average foundation modulus (Case 3), Table 12 shows a maximum principal

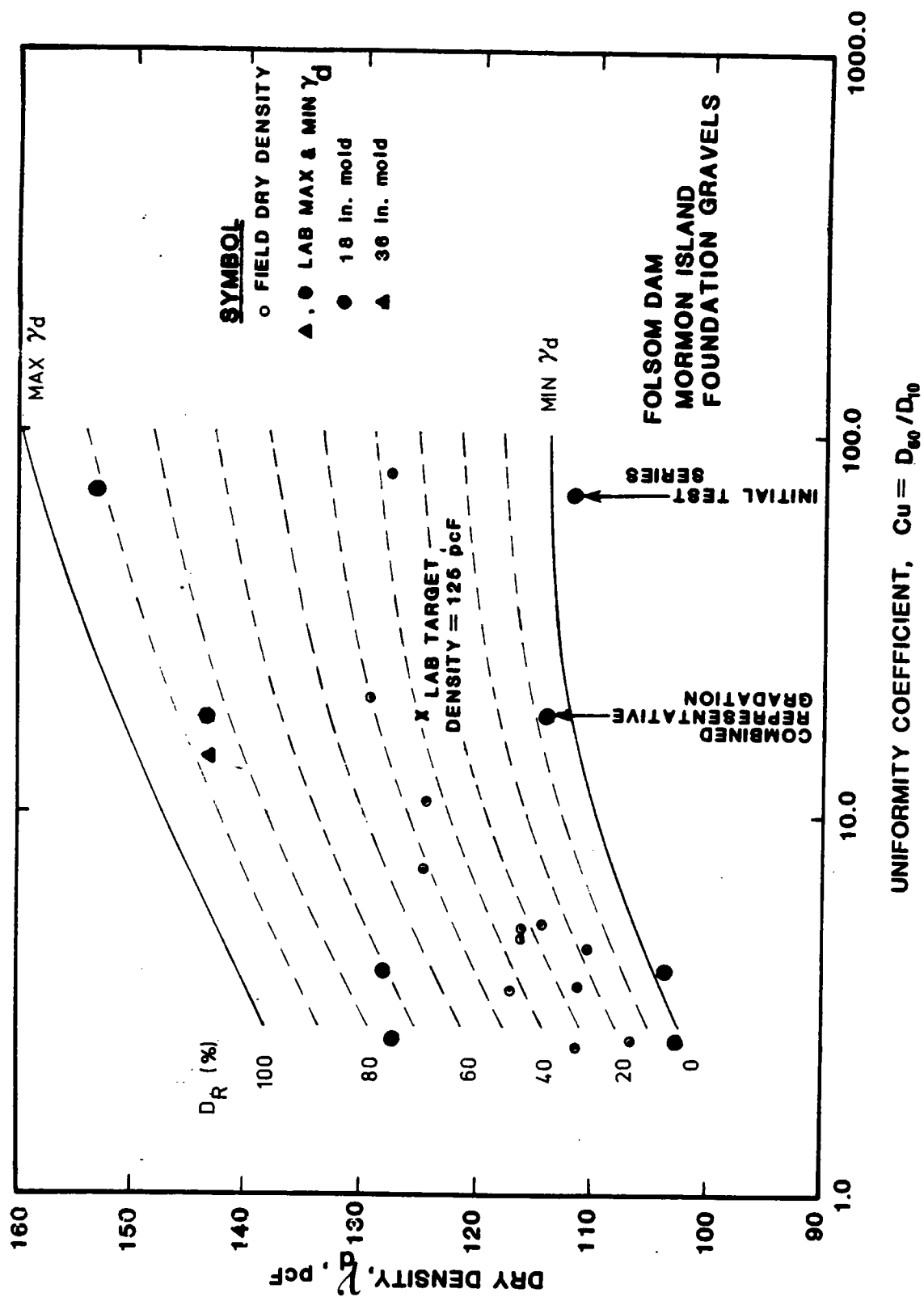


Figure 92. FIELD MEASURED DRY DENSITIES AND UNIFORMITY COEFFICIENTS FROM TEST PITS IN FOUNDATION GRAVELS AT MORMON ISLAND DAM

tensile stress. As indicated earlier, these stresses occur at a location of 73.8 feet down from the crest. Following the procedure of Mlakar (1986) and employing the results of a recent probabilistic study of sliding blocks on soil and rock sites (Lin and Whitman, 1986), the expected permanent displacement of the cracked upper portion of the monolith is 6.3 inches, 1 percent of the width of the monolith at the crack elevation. The conclusion is that even if the monolith cracks completely through the section, the permanent displacements are small, and the dam will remain stable.

#### Stability Evaluation

143. The analytical studies show that for the range of parameters most likely to represent the conditions of the dam, foundation, and reservoir, the computed earthquake-induced stresses in the monolith approach the apparent tensile strength of the concrete when the gravity dam is subjected to the design earthquakes. Even under the most unfavorable conditions, the analyses indicate that if cracking occurs, it will be limited in extent and depth of penetration. In the remote possibility of complete cracking through the monolith at the location of the maximum principal tensile stresses, a sliding block analysis indicates a small permanent displacement of the cracked upper portion of the dam. Based upon these findings, it is concluded that the Concrete Gravity Dam will maintain its structural integrity during and after the design earthquake.

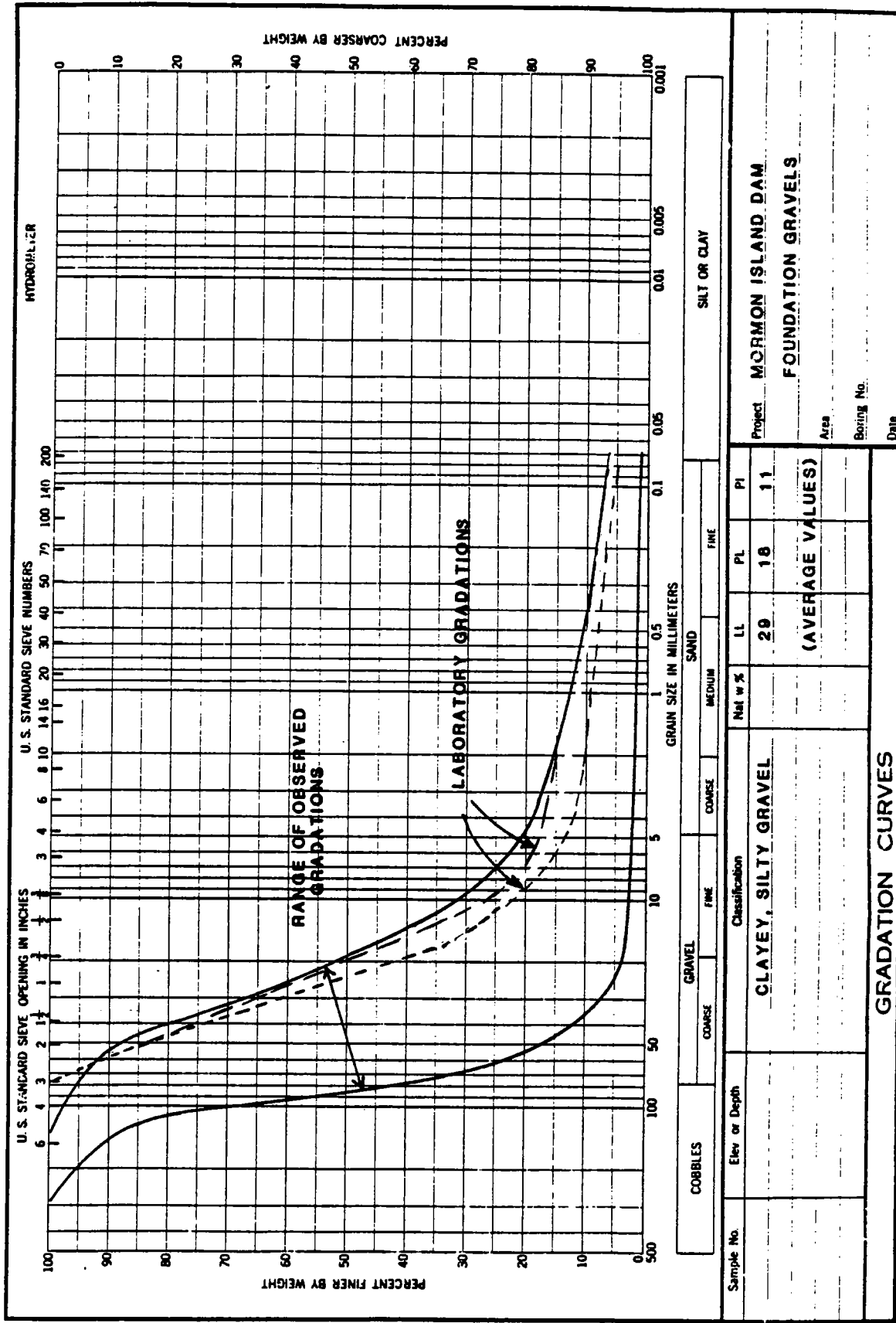


Figure 91. Range of gradations observed in second test pit series, dredged gravel foundation at Mormon Island Auxiliary Dam. Laboratory gradations shown for comparison

- g. Analyses of the Concrete Gravity Dam show that if cracking occurs at all, it will be limited in extent and depth of penetration. In the remote possibility of complete cracking through the dam at the location of the maximum principal tensile stresses, a sliding block analysis indicates a small permanent displacement of the cracked upper portion of the dam. Based upon these findings, it is concluded that the Concrete Gravity Dam will maintain its structural integrity during and after the design earthquake.

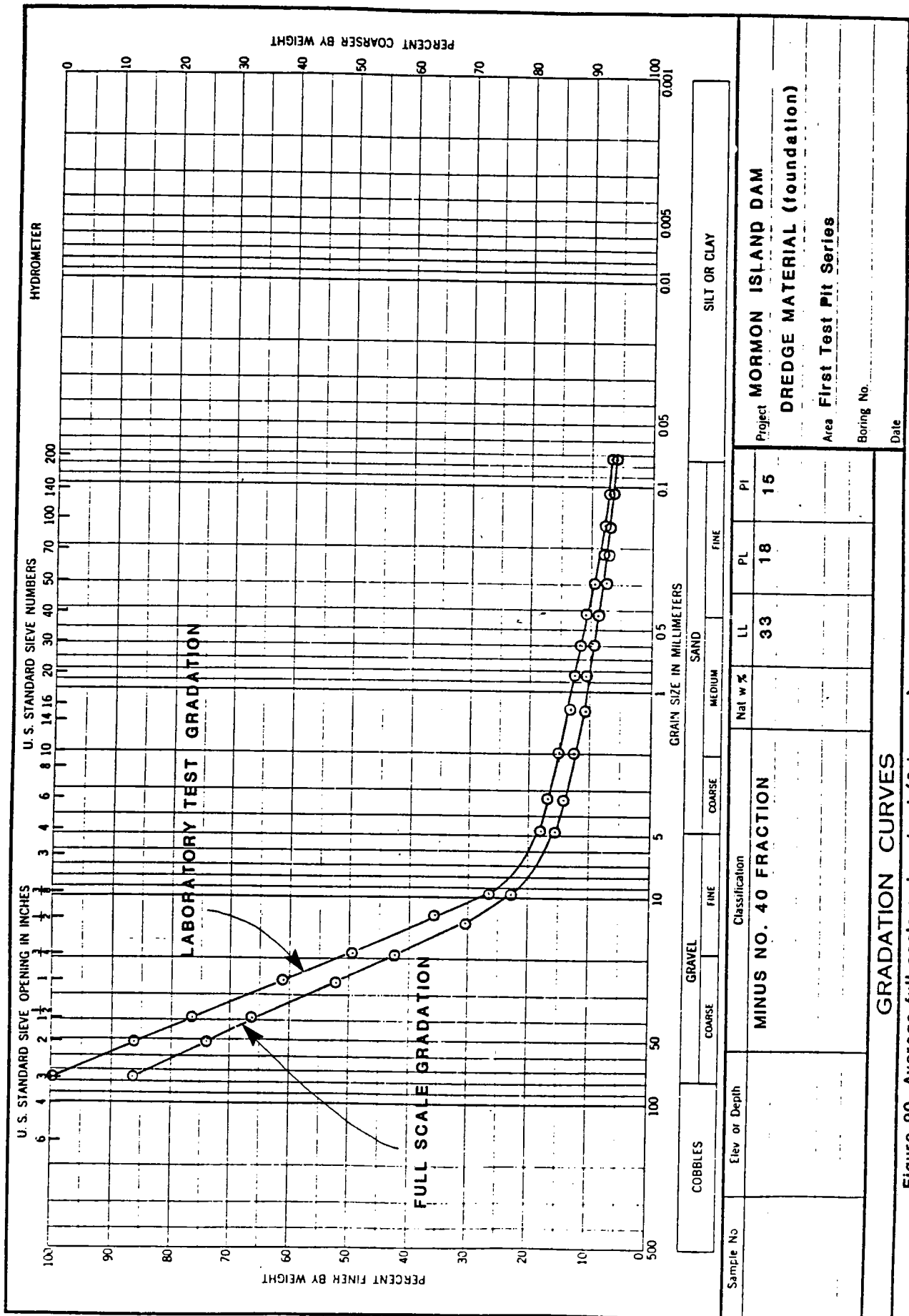





Figure 90. Average full scale and scalped (3 in. max) gradations observed in first test pit series in dredged gravel foundation at Mormon Island Auxiliary Dam. Full scale gradation scalped to 3 in. maximum particle size used in laboratory tests.

- Hynes-Griffin, M. E., 1979. "Dynamic Analysis of Earth Embankments for the Richard B. Russell Dam and Lake Project." Design Memorandum, Richard B. Russell Dam and Lake. Volume IV, Earth Embankments, Appendix VIII. US Army Engineer District, Savannah, Georgia.
- Lin, J. S., and Whitman, R. V., 1986. "Earthquake Induced Displacements of Sliding Blocks," Journal of Geotechnical Engineering, American Society of Civil Engineers, Vol. 112, No. GT2, pp. 44-59.
- Makdisi, F. I., and Seed, H. B., 1979. "Simplified Procedure for Estimating Dam and Embankment Earthquake-Induced Deformations." Journal of the Geotechnical Engineering Division, American Society of Civil Engineers. Vol 104, No. GT7, pp 849-867.
- Mlakar, P. F., 1986. "Nonlinear Response of Concrete Gravity Dams to Strong Earthquake-Induced Ground Motion," for the US Army Engineer Waterways Experiment Station, Vicksburg, Mississippi, conducted under contract DACW39-85-M-4964.
- Newmark, N. M., 1965. "Effects of Earthquakes on Dams and Embankments," Geotechnique, Vol 15, No. 2, pp 139-160.
- Raphael, J. M., 1987. "Mass Concrete Properties for Seismic Evaluation of Engelbright Dam, Folsom Dam, and Pine Flat Dam," for the US Army Engineer District, Sacramento, California, conducted under contract DACW05-86-P-1049, Oct., 1986, revised, Jan., 1987.
- Sarma, S. K., 1979. "Response and Stability of Earth Dams During Strong Earthquakes." Miscellaneous Paper GL-79-13, US Army Engineer Waterways Experiment Station, CE, Vicksburg, Mississippi.
- Seed, H. B., 1979. "19th Rankin Lecture: Considerations in the Earthquake Resistant Design of Earth and Rockfill Dams," Geotechnique, Vol. 29, No. 3, pp. 215-263.
- Seed, H. B., 1986. "Design Problems in Soil Liquefaction," UCB/EERC Report No. 86/02, University of California, Berkeley, CA.
- Seed, H. B. and Harder, L. F., 1985. Personal Communication, University of California, Berkeley, California.
- Seed, H. B., and Idriss, I. M., 1970. "Soil Moduli and Damping Factors for Dynamic Response Analyses." Report No. EERC 70-10. Earthquake Engineering Research Center, University of California, Berkeley, California.
- Seed, H. B., Lee, K. L., Idriss, I. M., and Makdisi, F., 1973. "Analysis of the Slides in the San Fernando Dams during the Earthquake of Feb. 9, 1971." Report No. EERC 73-2. Earthquake Engineering Research Center, University of California, Berkeley, California.
- Seed, H. B. and Peacock, W. H. 1971. "Test Procedures for Measuring Soil Liquefaction Characteristics," Journal of the Soil Mechanics and Foundations Division, A.S.C.E., Vol 97, No. SM8. pp 1099-1119.
- Seed, H. B., Tokimatsu, K., Harder, L. F., and Chung, R. M., 1984. "The Influence of SPT Procedures in Soil Liquefaction Resistance Evaluations," UCB/EERC Report No. 84/15, University of California, Berkeley, CA.

# SHEAR WAVE VELOCITY DISTRIBUTION FOR MORMON ISLAND DAM

NOTE: VELOCITIES ARE IN fps

-  Embankment gravel
-  Dredged Gravel
-  Clay/Weathered Material

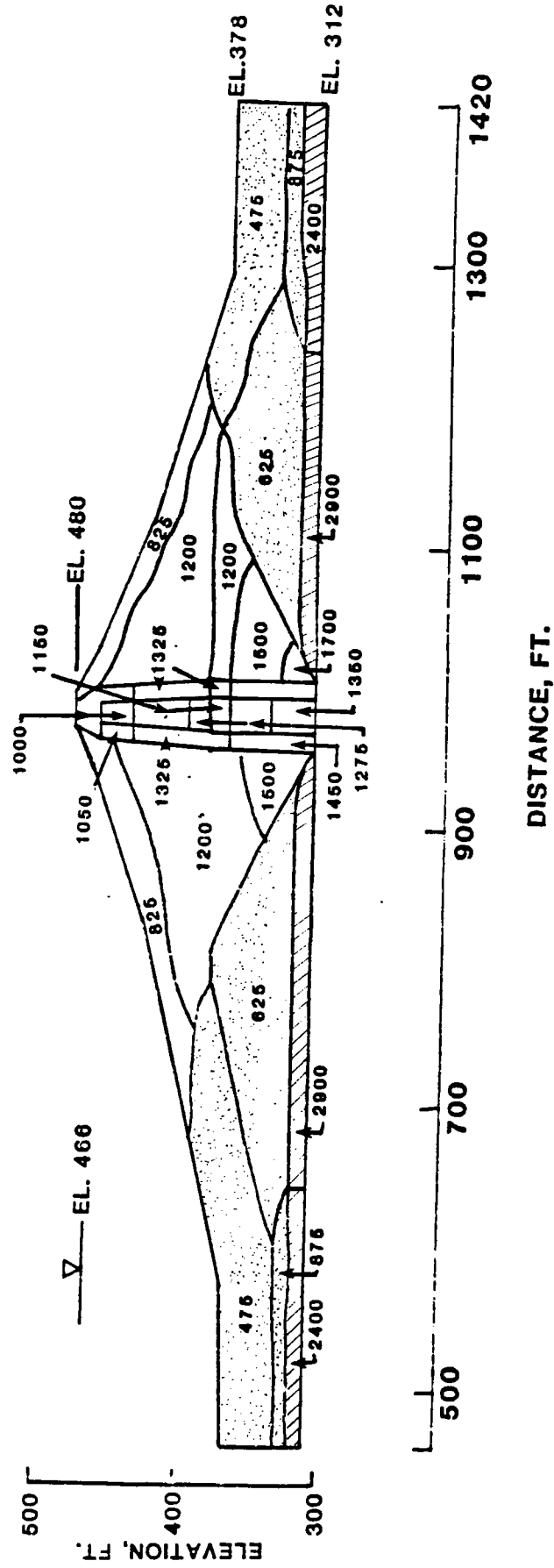


Figure 89. Shear wave velocity distribution for FLUSH analysis of Mormon Island Auxiliary Dam.

Table 1  
Parameter Values for Makdisi-Seed Fundamental Period  
Estimation Procedure

<u>Parameter</u>	<u>Record A</u>	<u>Record B</u>
Fundamental Period ( $T_0$ )	0.34 sec	0.32 sec
Maximum Crest Acceleration ( $a_{\max}$ )	1.27 g	1.11 g
Strain Compatible Damping ( $\lambda$ )	13.5%	12.6%
Strain Compatible Shear Modulus (G)	2249 ksf	2456 ksf
Strain Compatible Shear Wave Velocity ( $V_s$ )	790 fps	790 fps

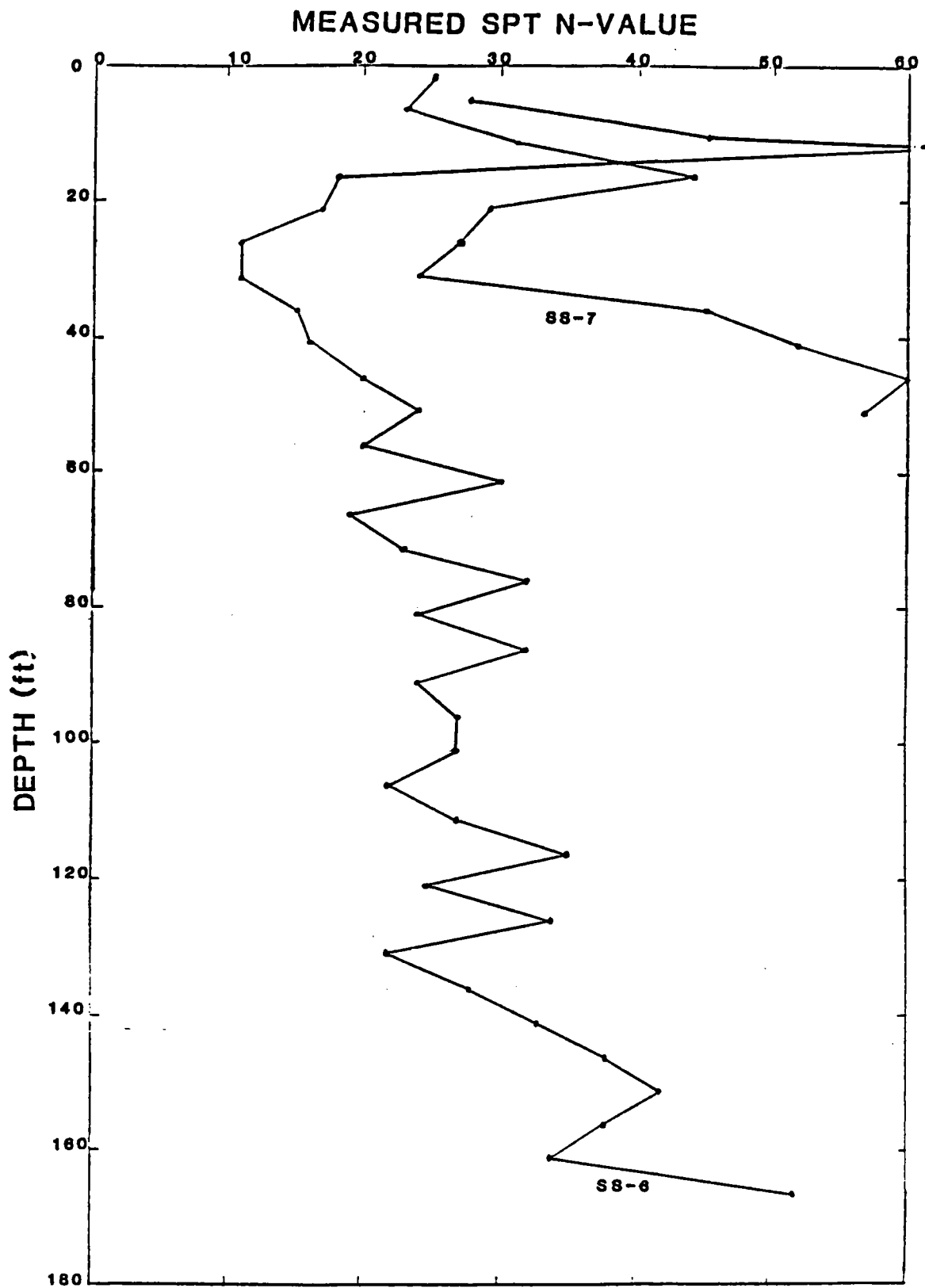


Figure 88. SPT blowcounts measured in core (Zone A, Boring SS-6) and filter (Zone 3, Boring SS-7) materials.

Table 3  
Summary of Yield Accelerations for Retaining Wall B

Residual Excess Pore Pressure $r_u$	Corresponding Effective Friction Angle of Backfill* $\phi'$ (°)	Yield Acceleration, $k_y$ (g)			
		Section A-A		Section C-C	
		Mononobe- Okabe	UTEXAS2**	Mononobe- Okabe	UTEXAS2**
0	43	0.15	0.13	0.15	0.16
10	37.9	0.10	0.11	0.11	0.125
20	33.1	0.05	0.08	0.06	0.09
25	29.9	0.025	0.06	0.03	0.065

\* For gravel shell,  $C = 0$

\*\* Core strengths are  $C = 0$ ,  $\phi' = 31.1^\circ$ .

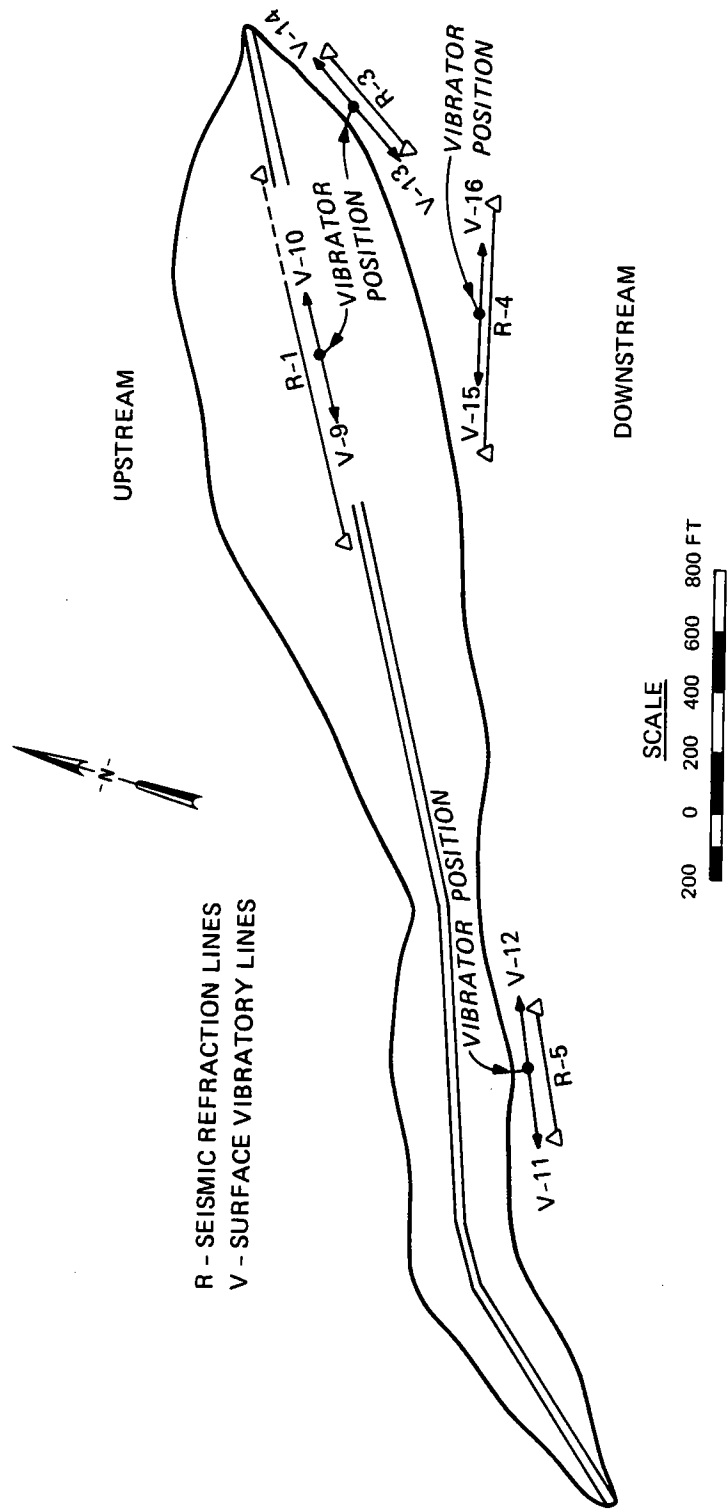


Figure 87. Plan of surface geophysical investigations at Mormon Island Auxiliary Dam

Table 5

## Stress-Controlled Cyclic Triaxial Tests (First Test Pit Gradation)

Test No.	Minor Effective Consolidation Stress $\sigma_{3c}$ (psi)	Consolidation		Dry Unit Weight After Consolidation $\gamma_{DC}$ (pcf)	Relative Density $D_R$ (%)	Cyclic Stress Ratio
	$K_c = \frac{\sigma_{VC}}{\sigma_{HC}}$	Stress Ratio	$\pm \sigma_{DC}$			
			$2 \sigma_{3c}$			
1	20	1.0		129.8	53.1	0.21
2	20	1.0		129.4	52.1	0.29
3	20	1.0		129.1	51.3	0.24
4	10	1.0		129.3	51.8	0.35
5	20	1.0		127.7	47.6	0.28

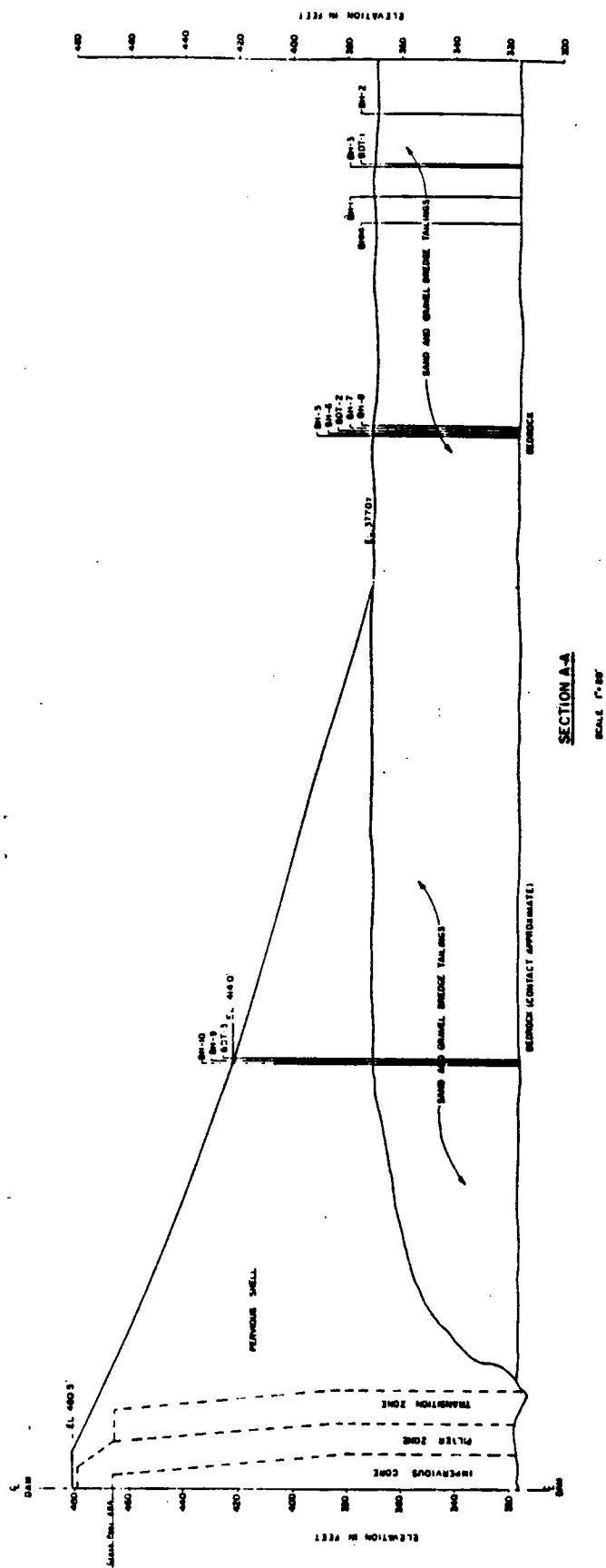


Figure 86. Section A-A of Mormon Island Auxiliary Dam (see Figure 85) showing materials sampled with Becker Hammer soundings.

Table 6 (Concluded)

Test No.	Minor Effective Consolidation Stress $\sigma_{3c}$ (psi)	Consolidation		Dry Unit Weight After Consolidation $\gamma_{DC}$ (pcf)	Relative Density $D_R$ (%)	Cyclic Stress Ratio $\frac{\pm \sigma_{DC}}{2 \sigma_{3c}}$
		Stress Ratio $K_c = \frac{\sigma_{VC}}{\sigma_{HC}}$				
16	40	2.0		131.3	56.9	0.45
17	80	1.0		134.4	64.5	0.25
18	20	1.5		127.6	47.3	0.50
19	20	1.5		127.5	47.1	0.35
20	80	1.5		129.0	51.0	0.25
21	80	1.5		130.3	54.4	0.29
22	40	1.5		135.2	66.4	0.50
23	40	1.5		137.4	71.6	0.65
24	40	2.0		137.6	72.0	0.99
25	20	2.0		135.0	66.0	0.99

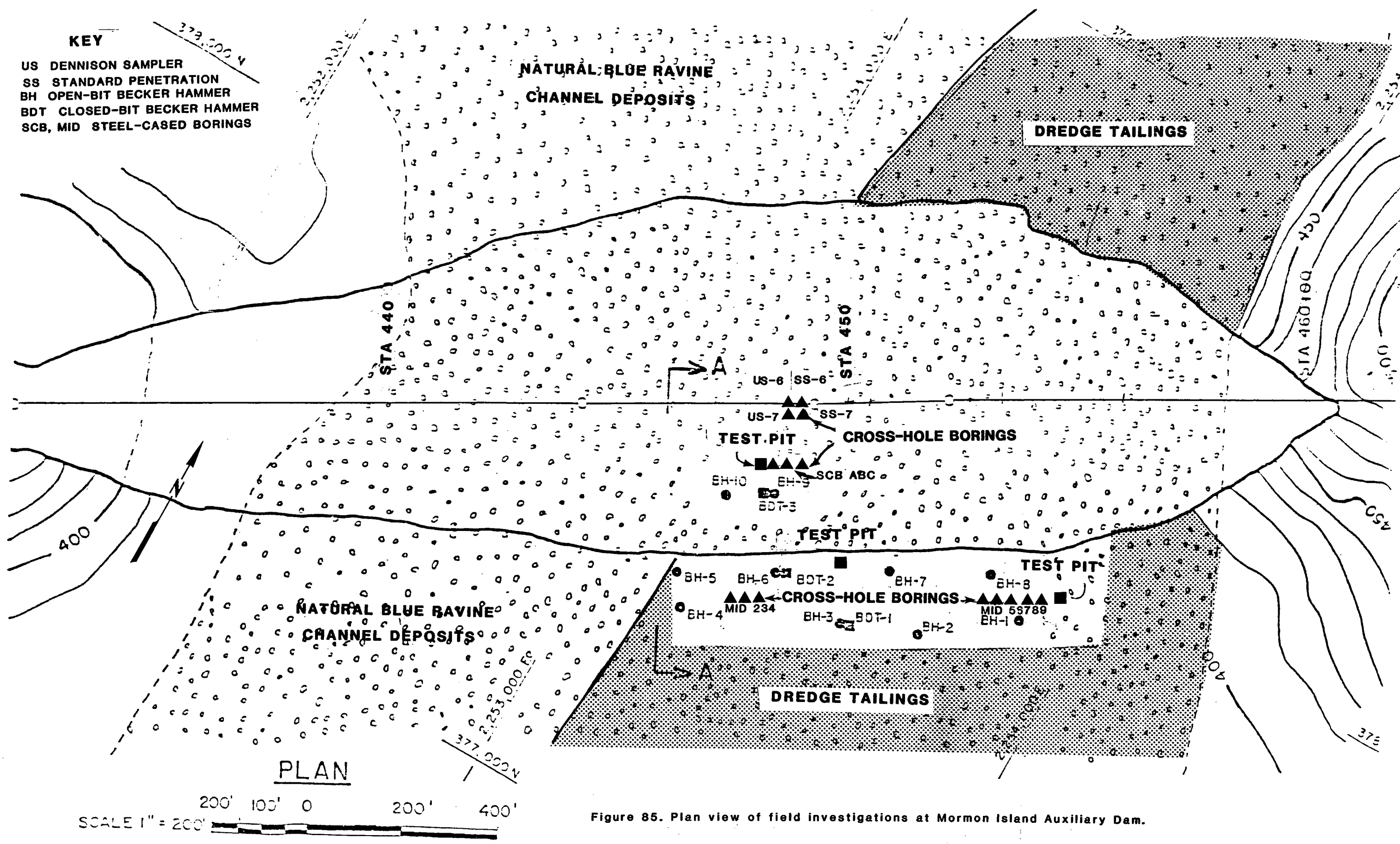


Figure 85. Plan view of field investigations at Mormon Island Auxiliary Dam.

Table 8  
Six-Inch Concrete Core Samples

<u>Core Hole</u> <sup>1</sup>	Depth (Feet)	Lengths of Core Samples One Foot or Greater
		(feet)
1C-1	7.0	2.1, 2.9
1C-2	6.1	2.0, 1.2, 1.2
1C-2A	2.0	2.0
1C-3	6.0	1.7, 1.3
1C-3A	3.4	1.3, 1.4
1C-4	6.4	1.9, 1.3, 1.3, 1.7
1C-5	7.0	1.8, 1.0, 2.3, 1.7
1C-5*	1.7	1.4
1C-5*A	3.6	1.6, 1.7
1C-6	6.4	1.9, 1.2, 1.8, 1.4
1C-7	10.8	1.5, 2.0, 1.1, 1.0
1C-8	8.7	2.3, 2.6, 2.0
1C-9	5.65	1.8, 1.5, 2.35
1C-10	8.4	1.8, 2.2, 1.0
1C-11	6.0	1.2, 1.8, 3.0
1C-12	7.5	1.7, 2.8, 3.0
1C-13	6.8	1.8, 3.2, 1.6
1C-14	6.9	1.8, 2.0, 3.1
1C-15	6.3	1.25, 1.75, 3.3
1C-16	12.8	1.2, 1.2, 1.7, 1.7, 1.0, 1.0, 1.0, 1.5, 1.5
1C-17	17.1	1.2, 2.5, 2.8, 1.4, 1.1, 1.3, 1.7, 2.7, 1.7
1C-18	10.8	1.8, 2.3, 2.5, 2.7, 1.4
1C-19	15.9	1.9, 1.4, 1.7, 1.8, 1.5, 1.6, 1.4, 1.8, 1.7
1C-20	9.0	1.9, 1.2, 1.0, 1.9, 2.0
1C-20A	8.4	1.7, 2.0, 2.4, 2.2
1C-20B	5.5	1.6, 1.5
1C-20C	4.1	1.0, 1.3, 1.6
1C-21	15.9	1.1, 1.2, 1.2, 1.4, 1.4, 1.4, 1.0, 1.0, 1.0, 1.4, 1.7, 1.2

Note

1. For hole locations refer to Figures 124 and 125.

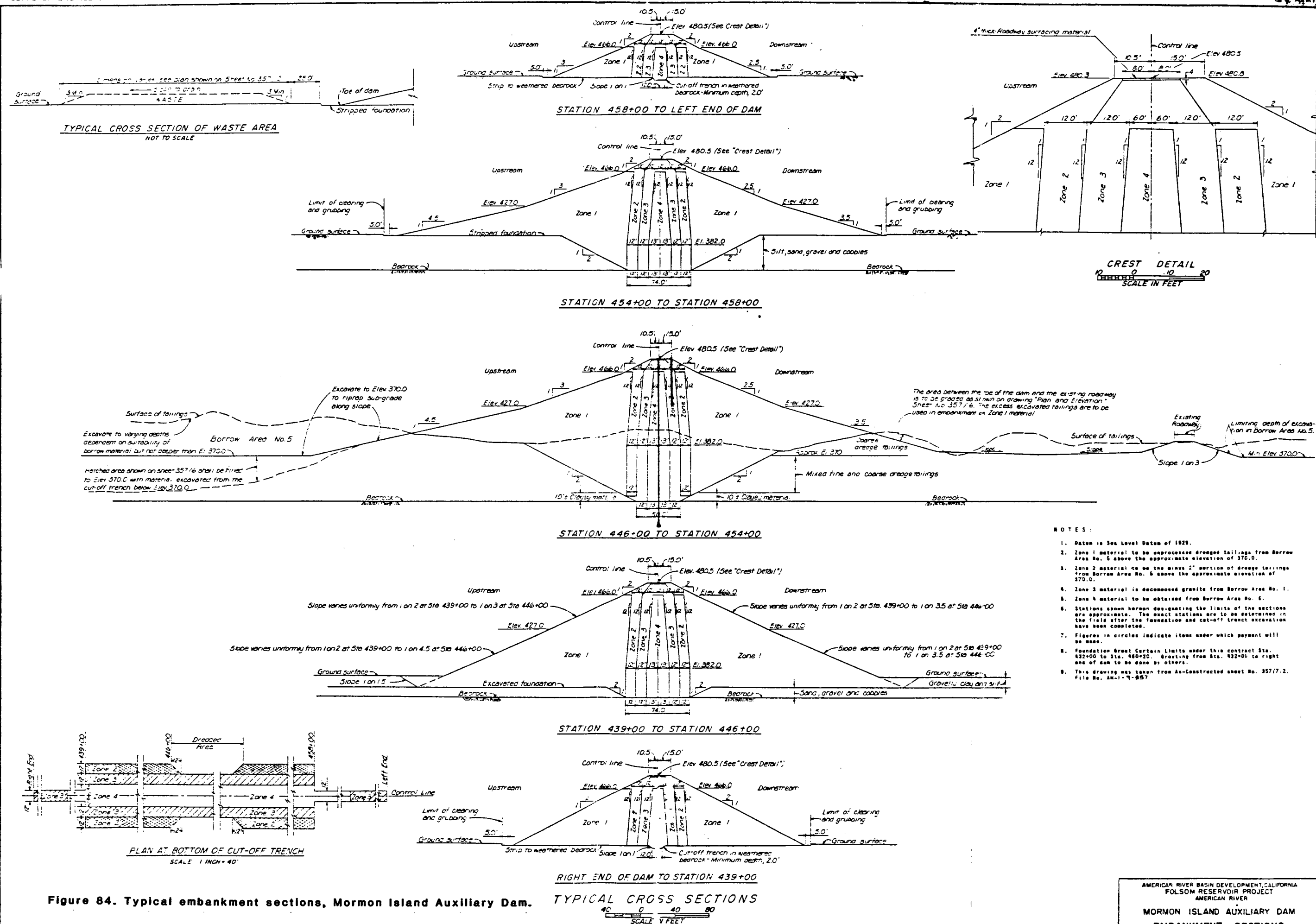
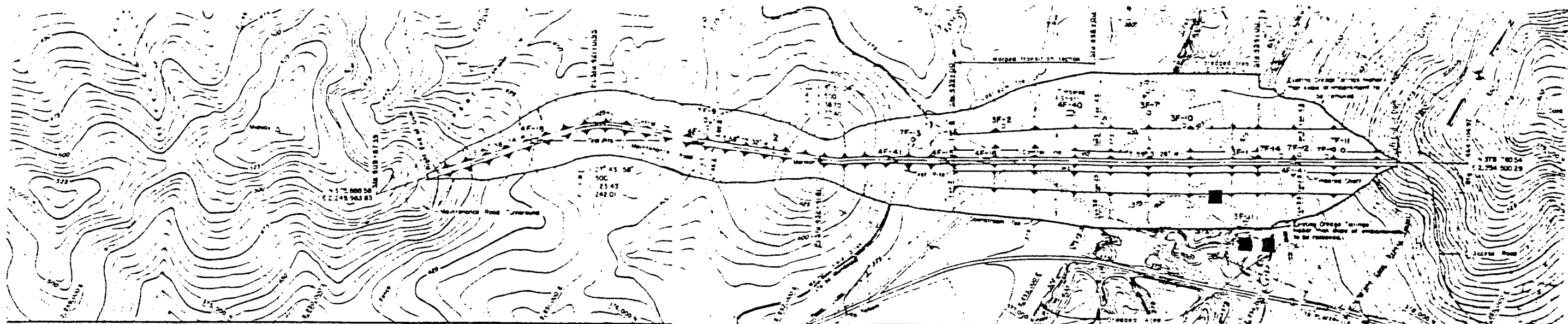


Figure 84. Typical embankment sections, Mormon Island Auxiliary Dam.

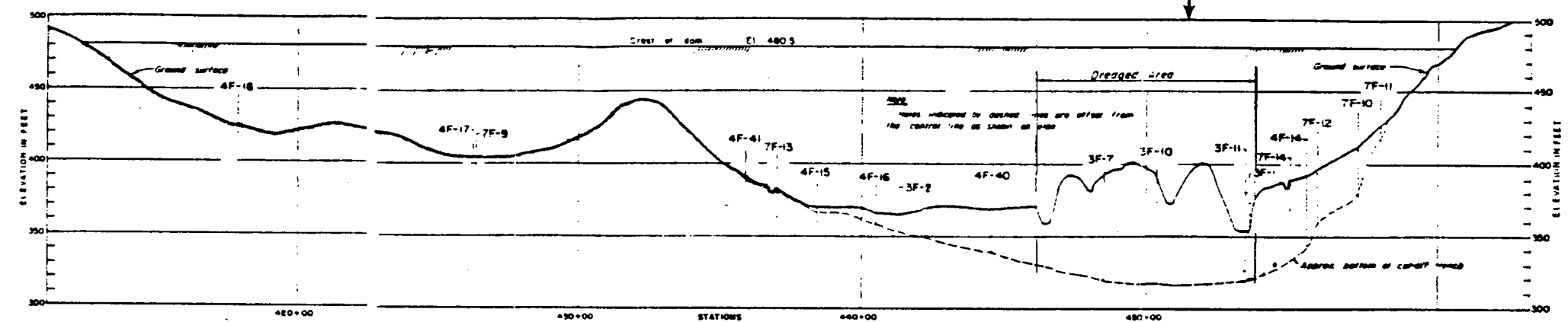
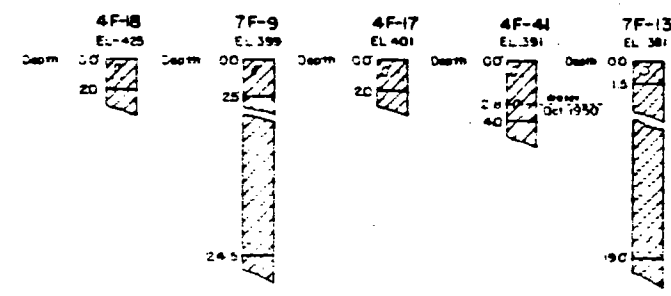
Table 10

Compression- Wave Velocity Vp (fps)	Poisson's Ratio $\nu$	Total Unit Weight $\gamma$ pcf	Young's Modulus E psi	Remarks
14,000	0.30	167	$5.8 \times 10^6$	Lower Bound
16,000	0.25	171	$7.9 \times 10^6$	Average
18,000	0.20	174	$1.1 \times 10^7$	Upper Bound

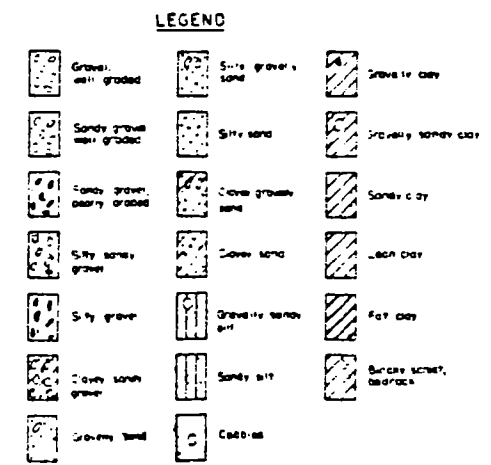
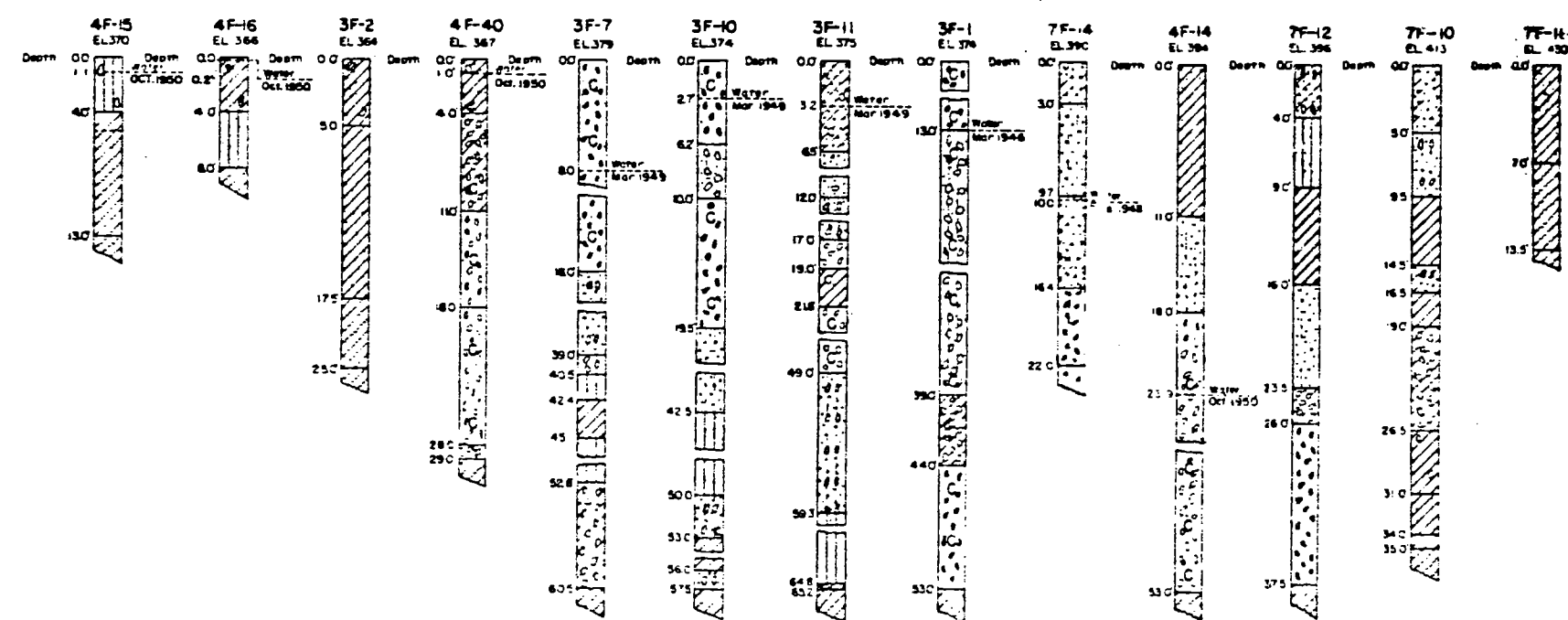


PLAN  
SCALE = 1" = 100'

ANALYSIS  
SECTION



PROFILE ON CONTROL LINE



- NOTES
1. Datum is Sea Level Datum of 1929.
  2. Elevations shown on logs are ground surface elevations.
  3. Laboratory classification shown for all materials, according to the Corps of Engineers' Uniform Soil Classification, except those shown in logs of holes 3F-1, 3F-2, 7F-13 and 7F-14, which are field classifications.
  4. Holes 3F-1 and 3F-2 were drilled with a 12" churn drill. Holes 3F-7, 3F-10 and 3F-11 were drilled with a 10" churn drill. Samples were taken with a power auger and push tube sampler, where possible.
  5. All 4F holes are open pits or shafts.
  6. All 7F holes were drilled with a Fanning drill rig using a 7" diameter rotary core drill.
  7. Typical embankment sections shown on Sheet No. 357/7.
  8. Limit of contractor's work areas including waste areas are shown on drawing Sheet No. 357/2.
  9. Slopes of warped transition vary uniformly from Station 439+00 to 446+00.
  10. The term 'gravel' under the classification system used for this drawing, applies to grain sizes larger than the No. 10 sieve.
  11. The term 'cobbles' includes material from 3" to 18" in size and the presence of some is indicated by the letter 'C' in the logs.
  12. This drawing was taken from As-Constructed sheet no. 357/3, File No. AM-1-7-357.

Figure 83. Plan and axial section of Mormon Island Auxiliary Dam.

Table 12  
Summary of Maximum Principal Stresses:

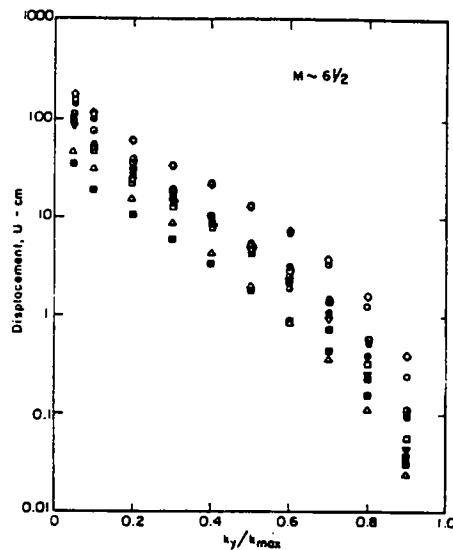
$$\eta_F = \eta_s = 0.10$$

<u>Case</u>	<u>Foundation Modulus (million psi)</u>	<u>Reservoir Bottom Reflectivity, <math>\alpha</math></u>	<u>Maximum Principal Stress (psi)</u>
1	5.8	0.90	633
2	5.8	0.99	656
3	7.9	0.90	727
4	7.9	0.99	804
5	11.0	0.90	916
6	11.0	0.99	974

Table 13  
Summary of Maximum Principal Stresses: EQ2-HV,

$$E_F = 11.0 \text{ million psi, and } \alpha = 0.99$$

<u>Case</u>	<u>Foundation Hysteretic Damping, <math>\eta_F</math></u>	<u>Dam Hysteretic Damping, <math>\eta_s</math></u>	<u>Maximum Principal Stress (psi)</u>
1	0.10	0.10	974
2	0.25	0.10	814
3	0.25	0.14	738
4	0.25	0.20	636



VARIAION OF PERMANENT DISPLACEMENT WITH  
YIELD ACCELERATION - MAGNITUDE 6-1/2  
EARTHQUAKE

Embankment Characteristics for Magnitude 6-1/2 Earthquake

Case #	Embankment Description	Height (ft.)	Base Acceleration (g)	$T_o^{(1)}$	$k_{max}^{(2)}$ (g)	Symbol
1	Example Case - slope = 2:1 - $k_{2max}$ = 60	150	0.2 (Caltech record)	0.8	(a) 0.31 (b) 0.12	● ■
2	Example Case - slope = 2:1 - $k_{2max}$ = 60	150	0.5 (Caltech record)	1.08	(a) 0.4 (b) 0.18	○ □
3	Example Case - slope = 2:1 - $k_{2max}$ = 80	150	0.5 (Lake Hughes record)	0.84	(a) 0.33 (b) 0.16	⊙ △
4	Example Case - slope = 2-1/2:1 - $k_{2max}$ = 80	150	0.5 (Caltech record)	0.95	(a) 0.49 (b) 0.22	○ ▽
5	Example Case - slope = 2:1 - $k_{2max}$ = 60	75	0.5 (Caltech record)	0.6	(a) 0.86 (b) 0.26	● ■

(1)  $T_o$  = Calculated first natural period of the embankment.

(2)  $k_{max}$  = Maximum value of time history of:

(a) crest acceleration

(b) average acceleration for sliding mass extending through full height of embankment.

Figure 82. Variation of permanent displacement with yield acceleration for  
Magnitude 6.5 earthquakes (from Makdisi and Seed, 1977).

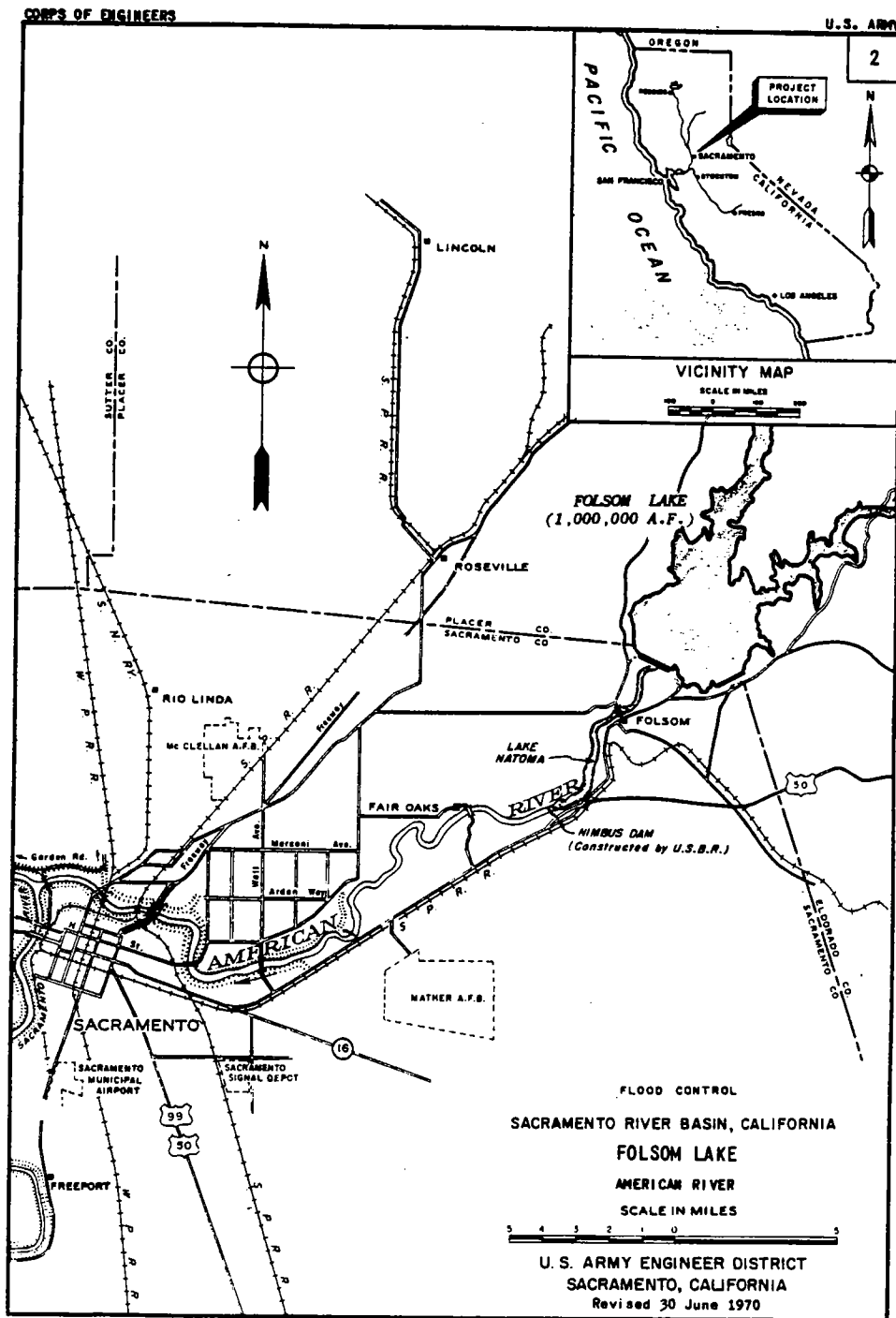
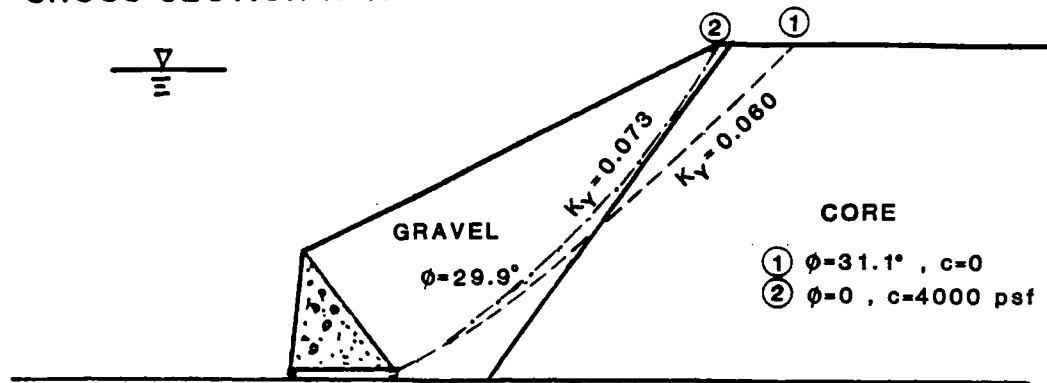


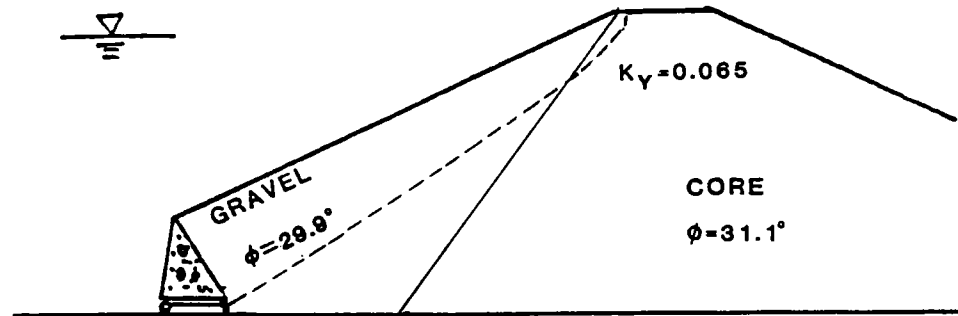
Figure 1. Location of Folsom Dam and Reservoir Project.

### CROSS SECTION A-A



(a)

### CROSS SECTION C-C



(b)

Figure 81. Locations of critical failure surfaces from UTEXAS2 calculations for sections A-A and C-C with  $r_u = 25\%$  in shell.

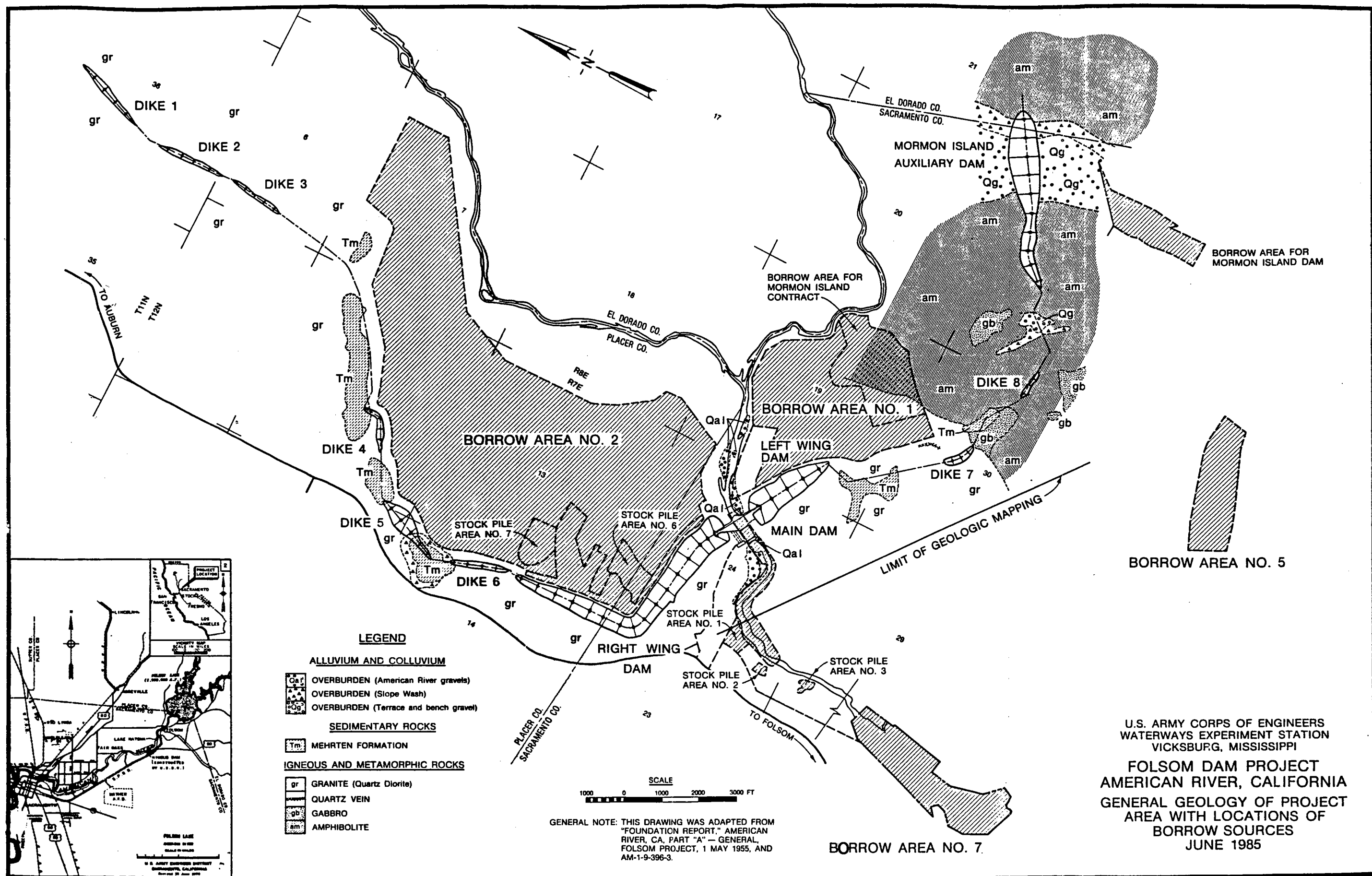
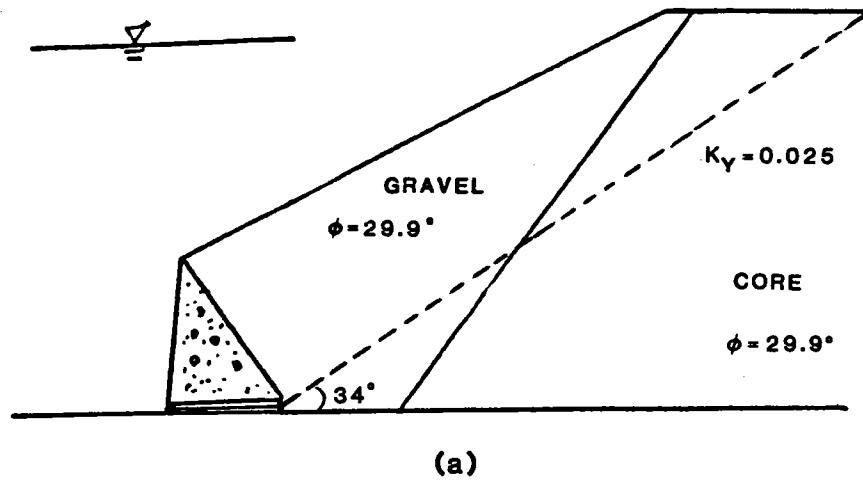


Figure 2. Plan of man-made retaining structures at Folsom Dam Project.

# CROSS SECTION A-A



# CROSS SECTION C-C

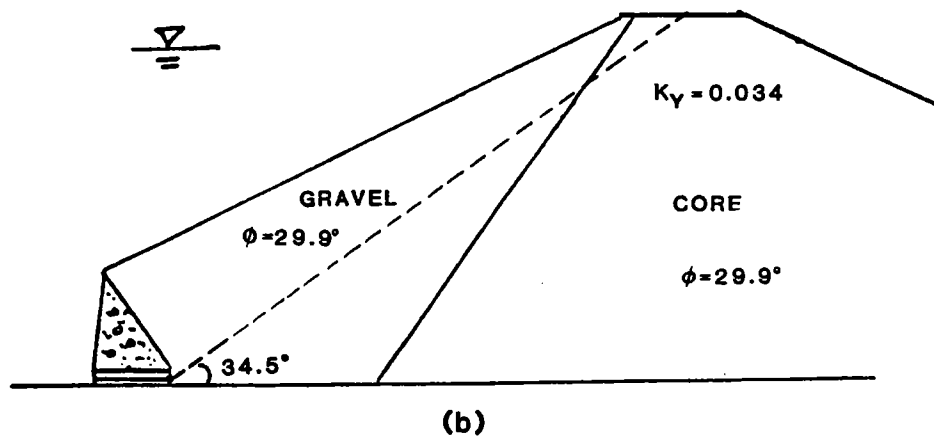


Figure 80. Locations of critical failure surfaces from Mononobe-Okabe calculations for sections A-A and C-C with  $r_u = 25\%$ .

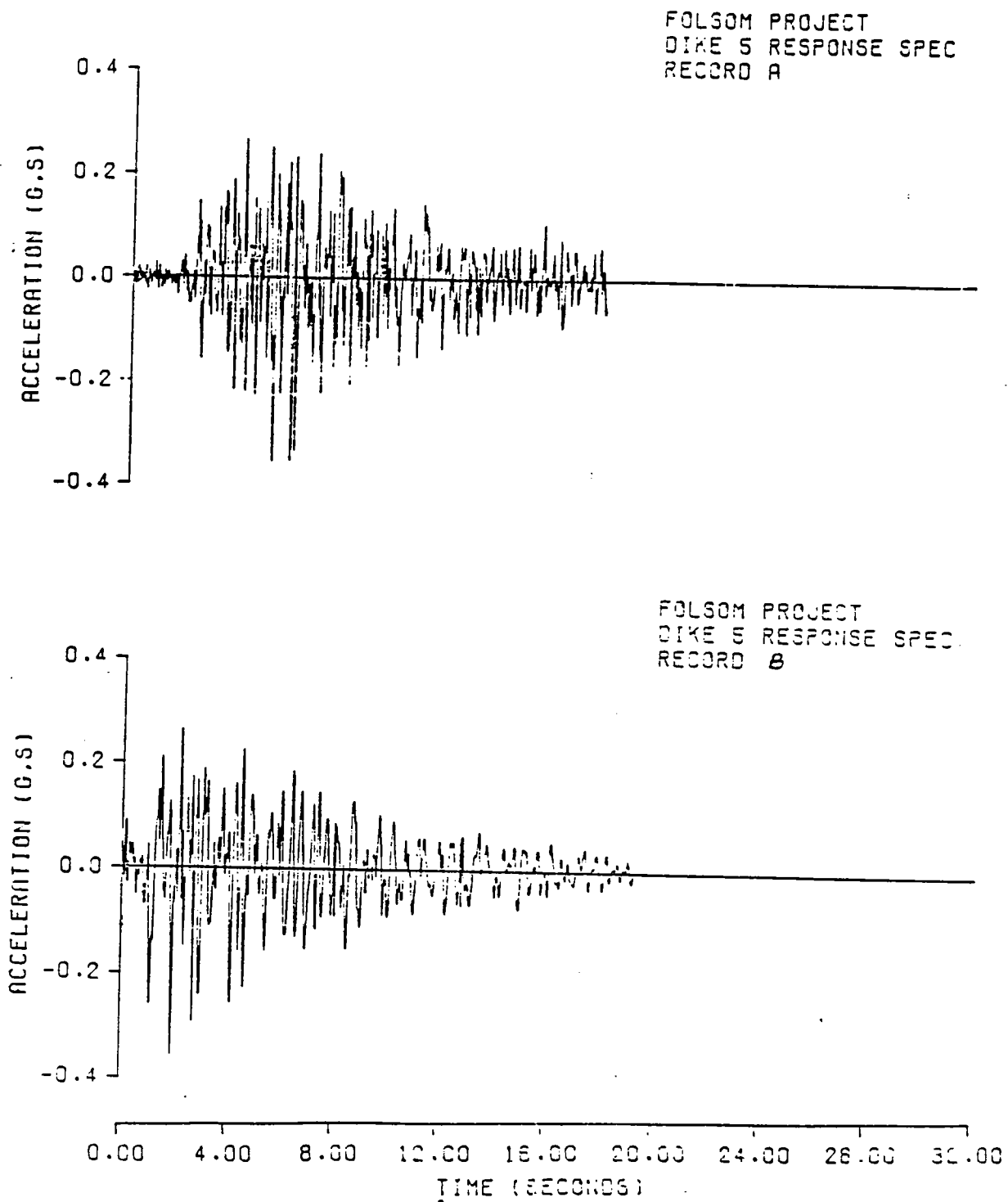


Figure 3. Acceleration histories used in the analysis

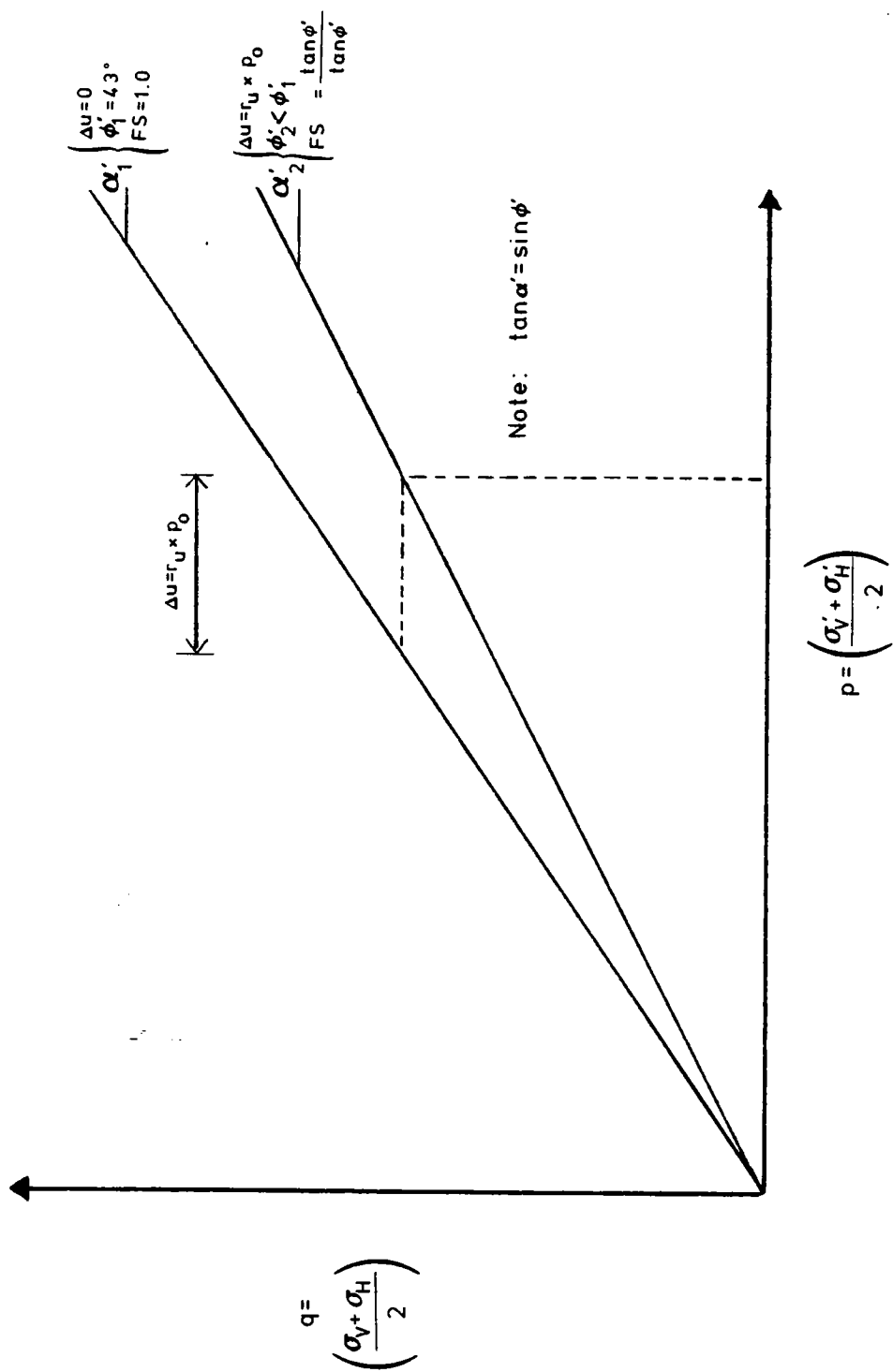
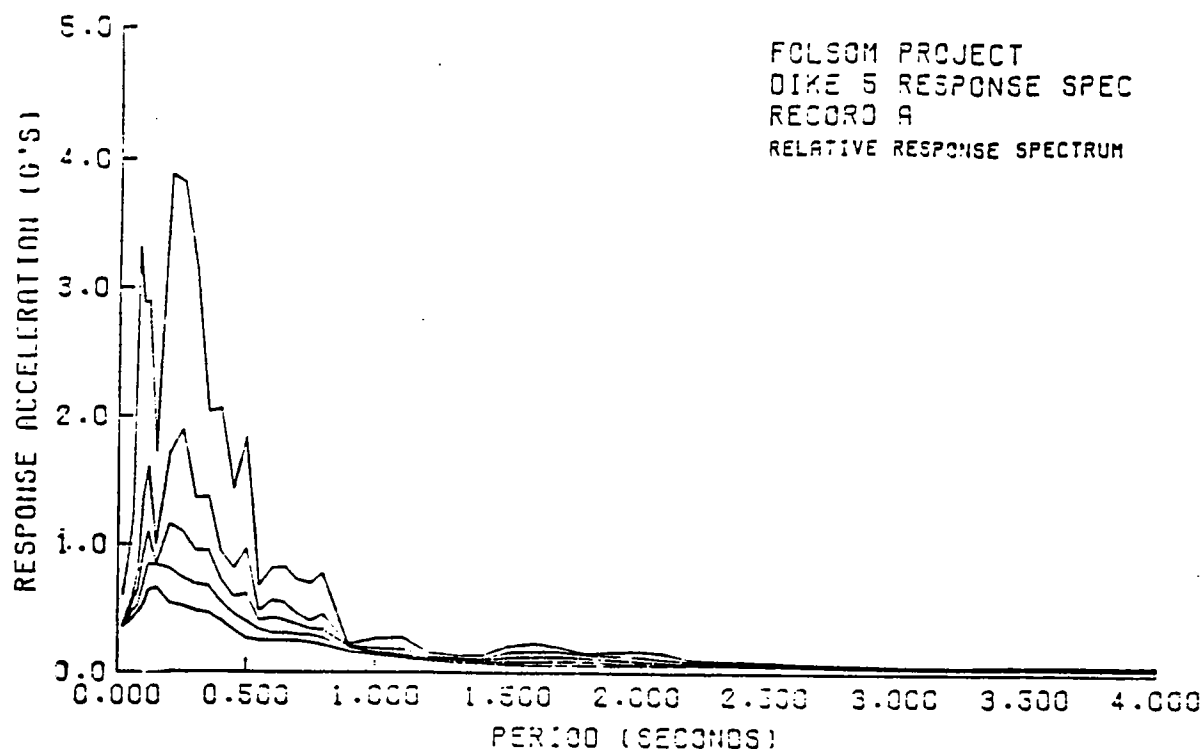
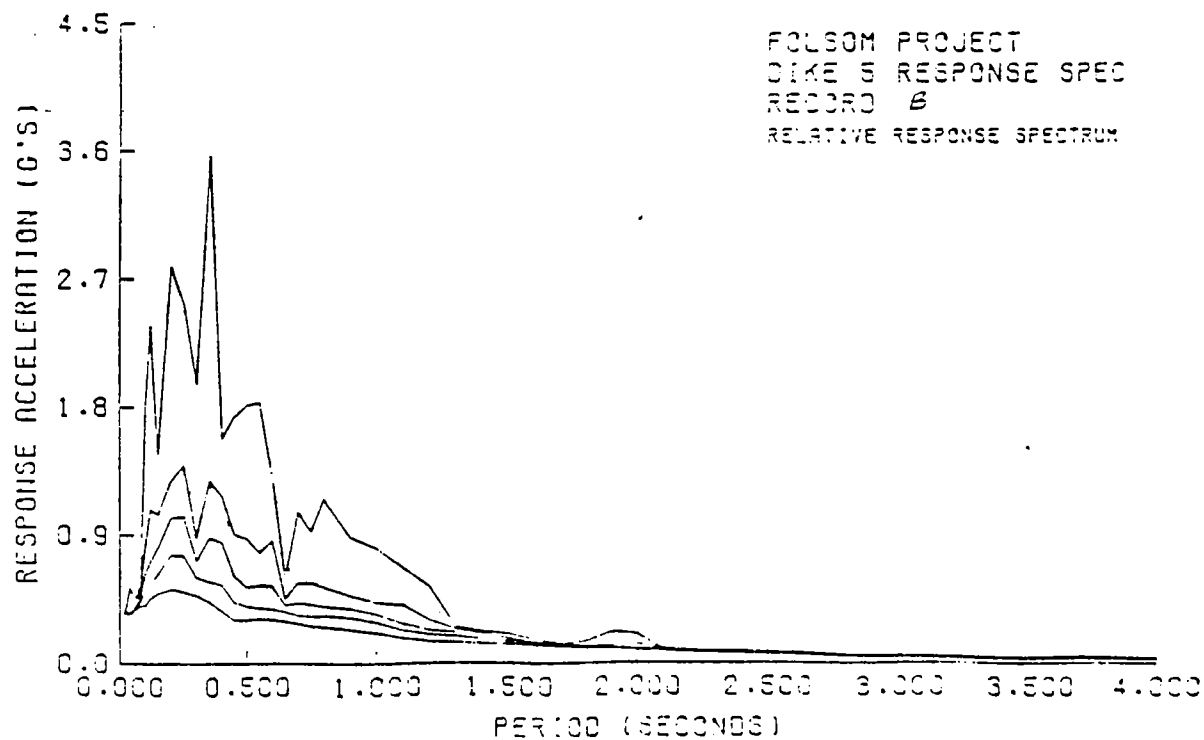


Figure 79. Procedure for estimating reduced friction angles corresponding to various levels of residual excess pore pressure

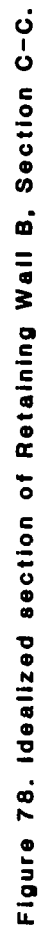


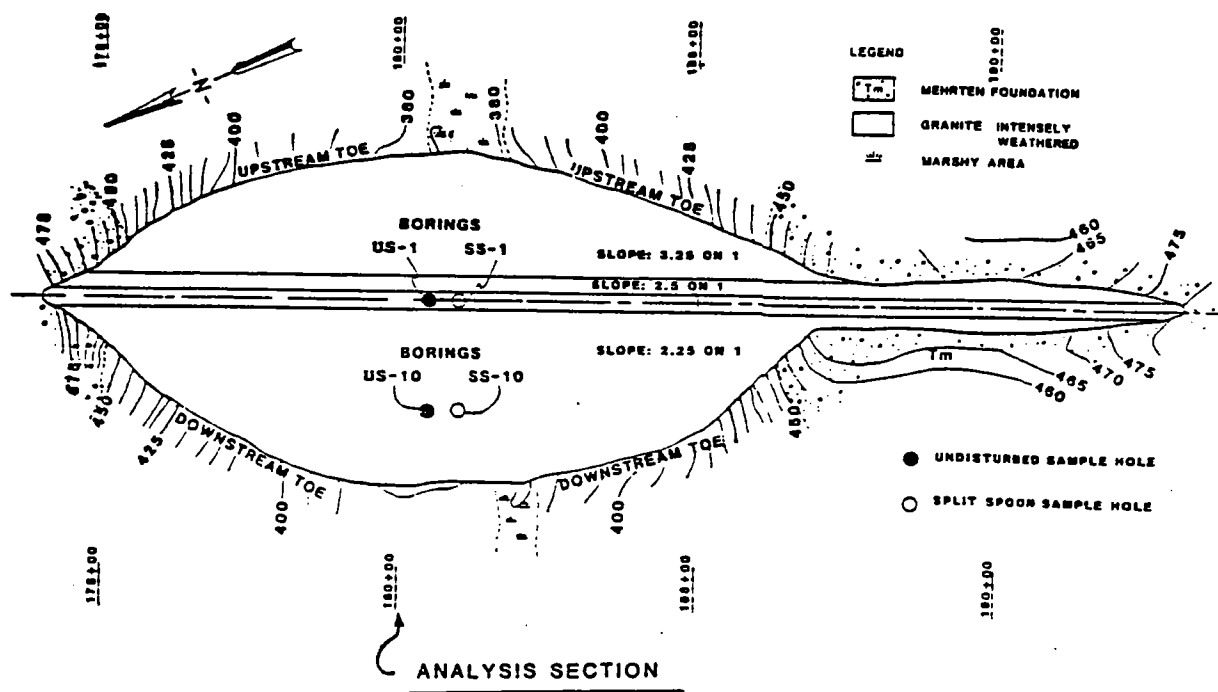
CURVE FOR 0.2, 5, 10 AND 20 PERCENT DAMPING



CURVE FOR 0.2, 5, 10 AND 20 PERCENT DAMPING

Figure 4. Response spectra of records A and B





PLAN VIEW OF DIKE 5

Figure 5. Plan view of Dike 5

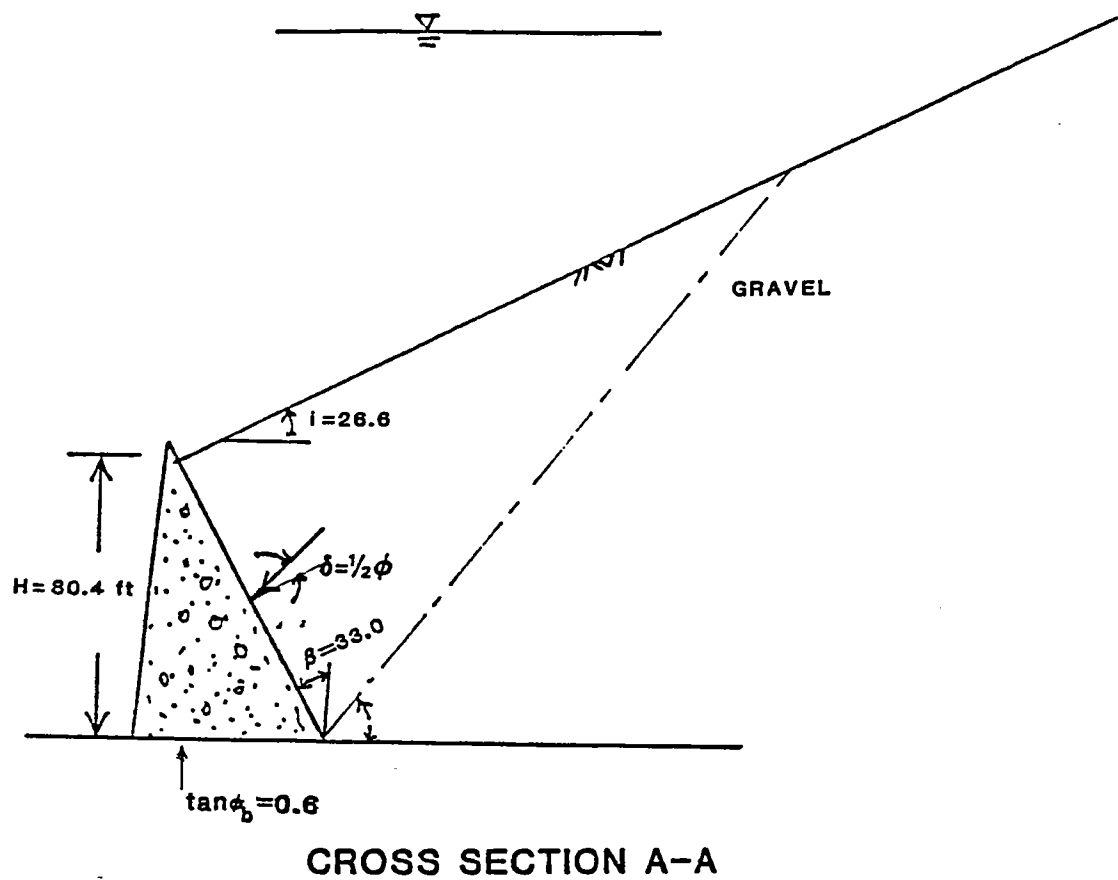
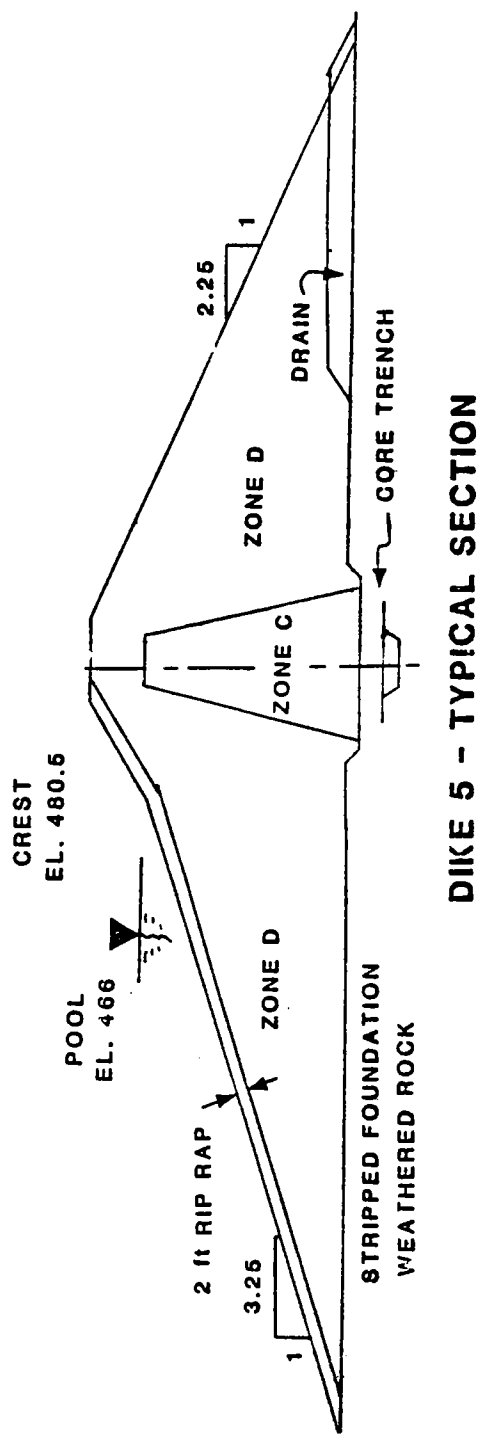


Figure 77. Idealized section of Retaining Wall B, Section A-A.



#### Material Descriptions

Zone C - Decomposed granite from Borrow Area No. 2 and suitable fine-grained material from American river channel

Zone D - Decomposed granite from Borrow Area No. 2 - practically the same as material in Zone C.

Figure 6. Cross-sectional view of Dike 5

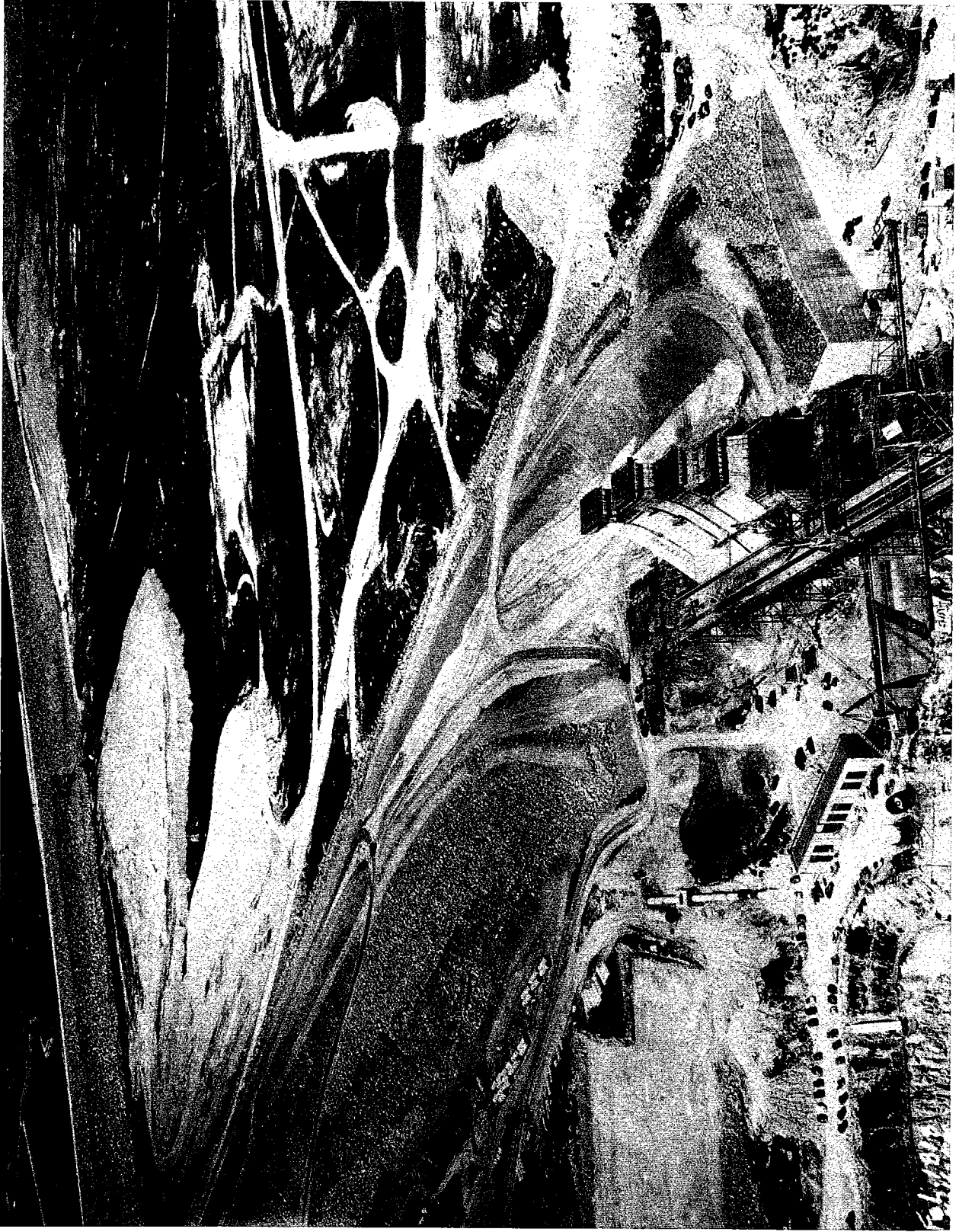
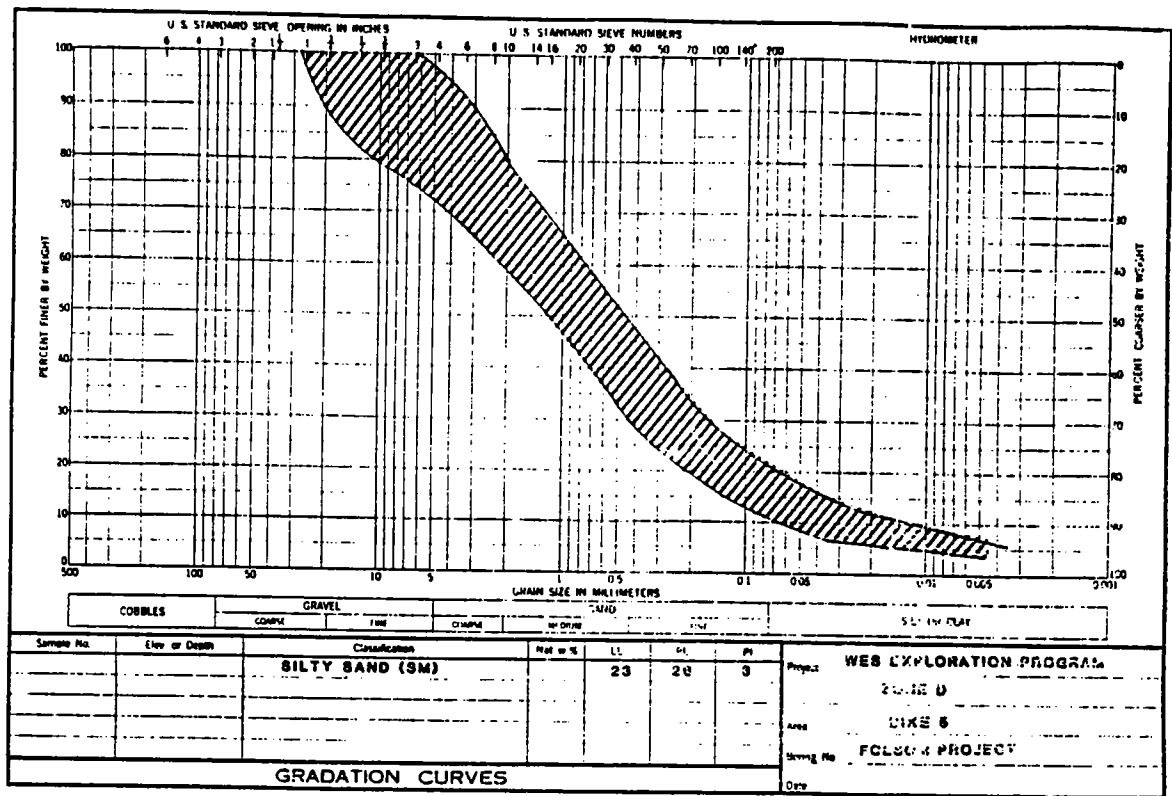
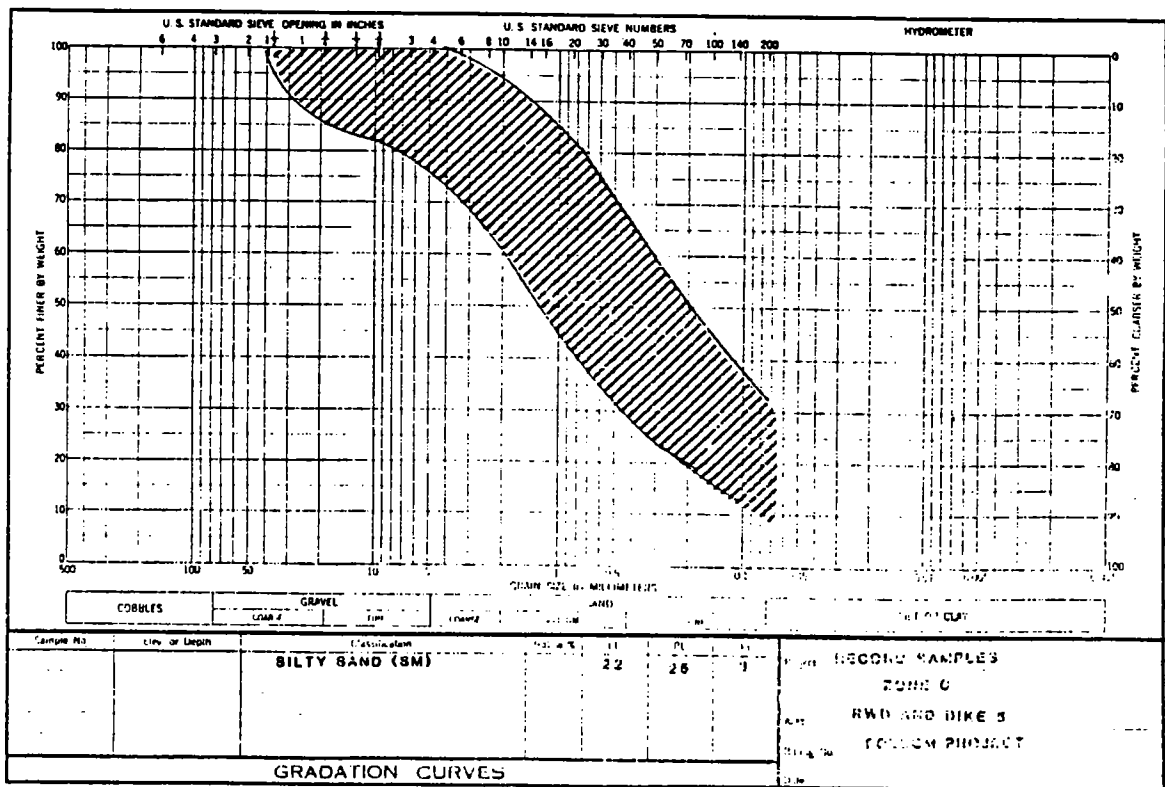


Figure 76. Construction photograph FOL. 1818, dated 4/16/54, showing construction of Right Wing Dam, concrete monoliths, and Retaining Wall B (completed)

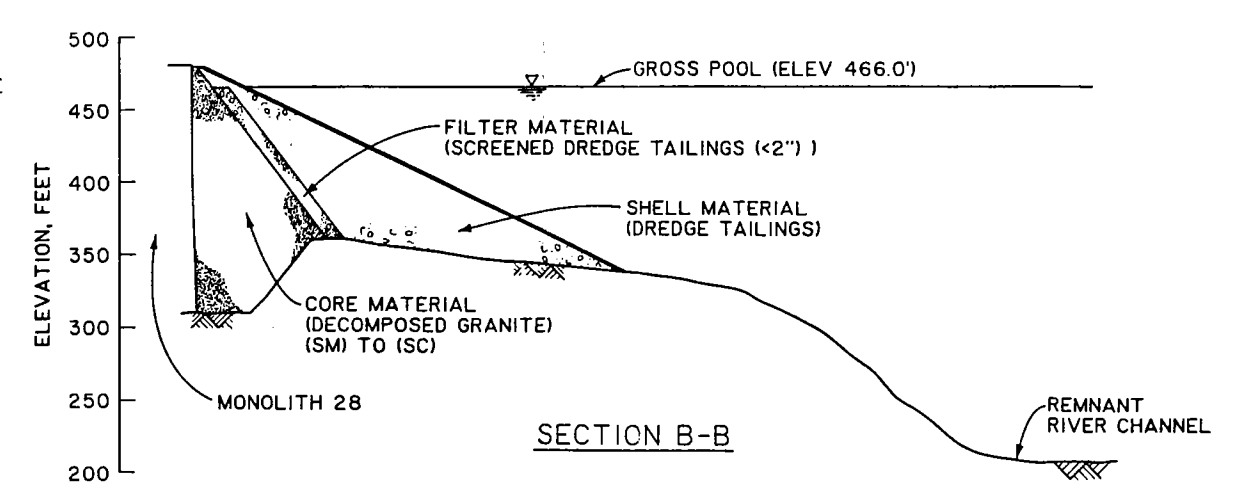
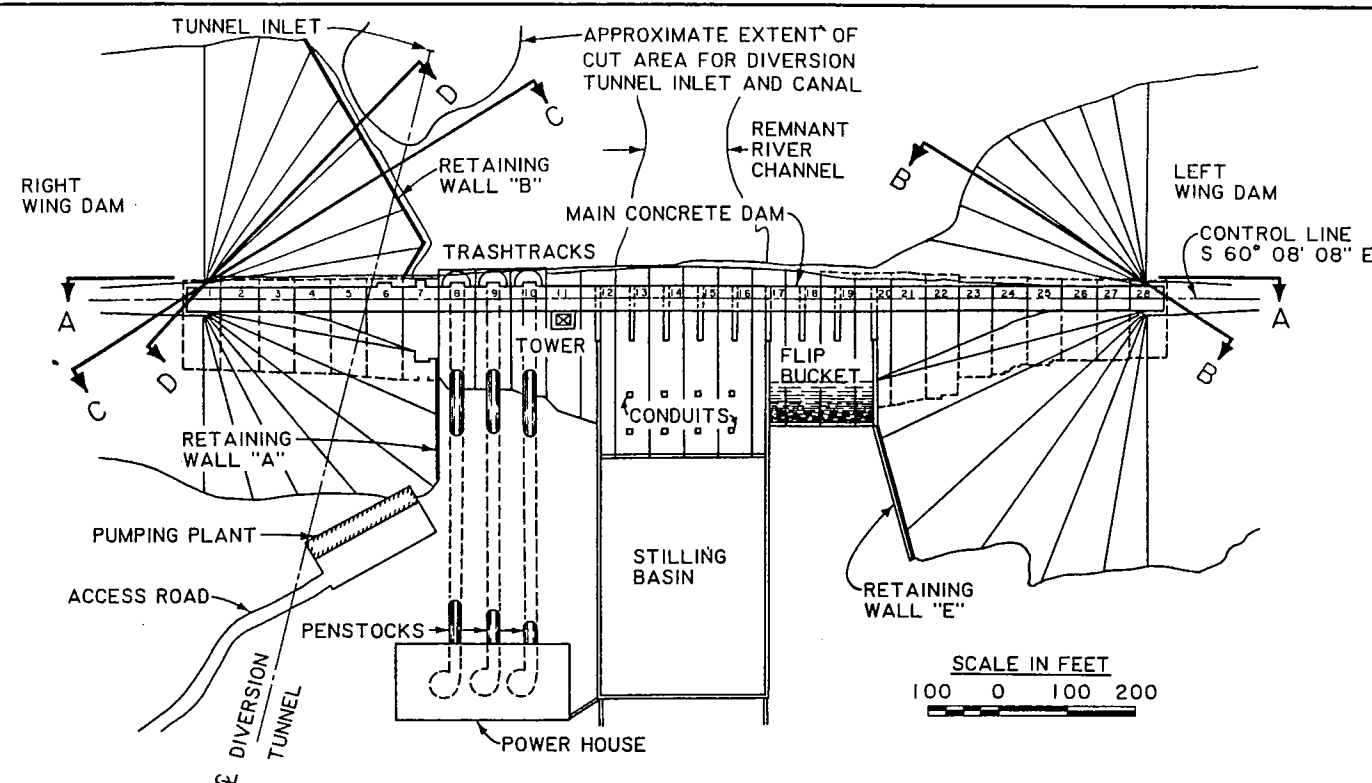


ENG FORM 2087



ENG FORM 2087

Figure 7. Gradation ranges for core and shell (Zones C and D), Dike 5



- NOTES:
1. PROJECTION OF RETAINING WALL "B" ON CROSS-SECTION RETAINING WALL "B" INTERSECTS MAIN DAM 30° FROM PERPENDICULAR DIRECTIONS (SEE PLATE G).
  2. CROSS-SECTIONS DEVELOPED FROM VARIOUS TOPOGRAPHIC MAPS DRAWN PRIOR TO DURING CONSTRUCTION AND CONSTRUCTION PHOTOGRAPHS

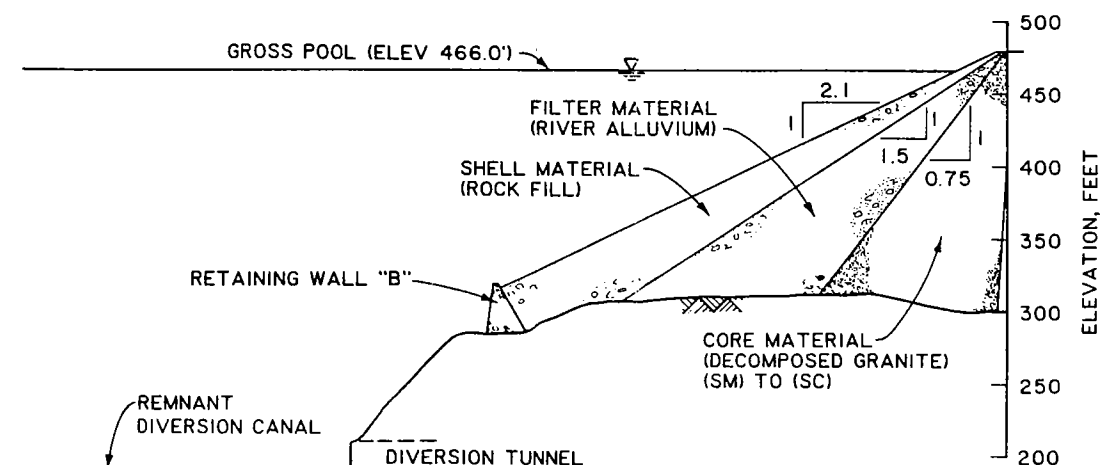
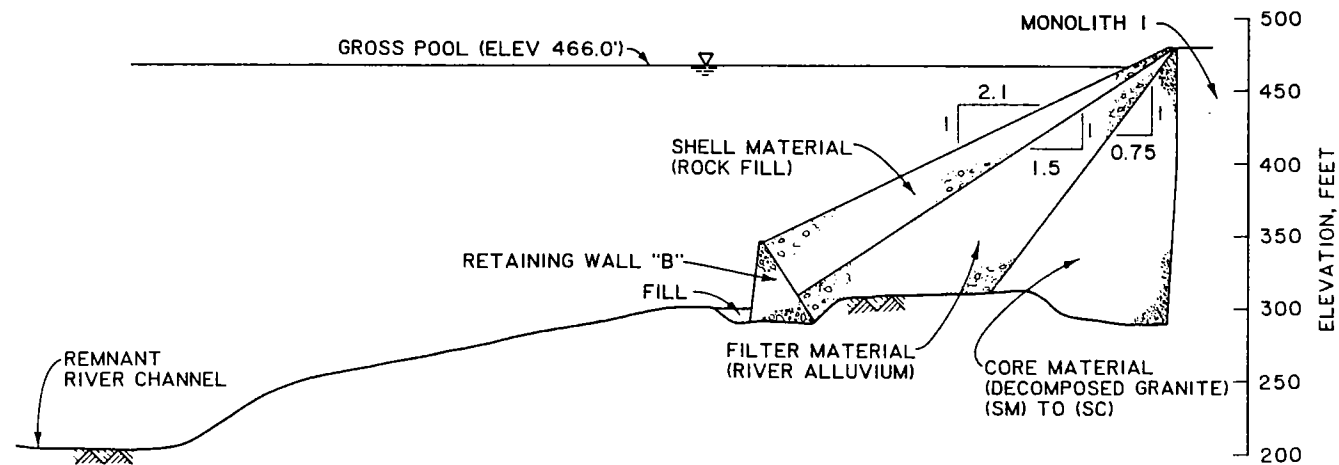
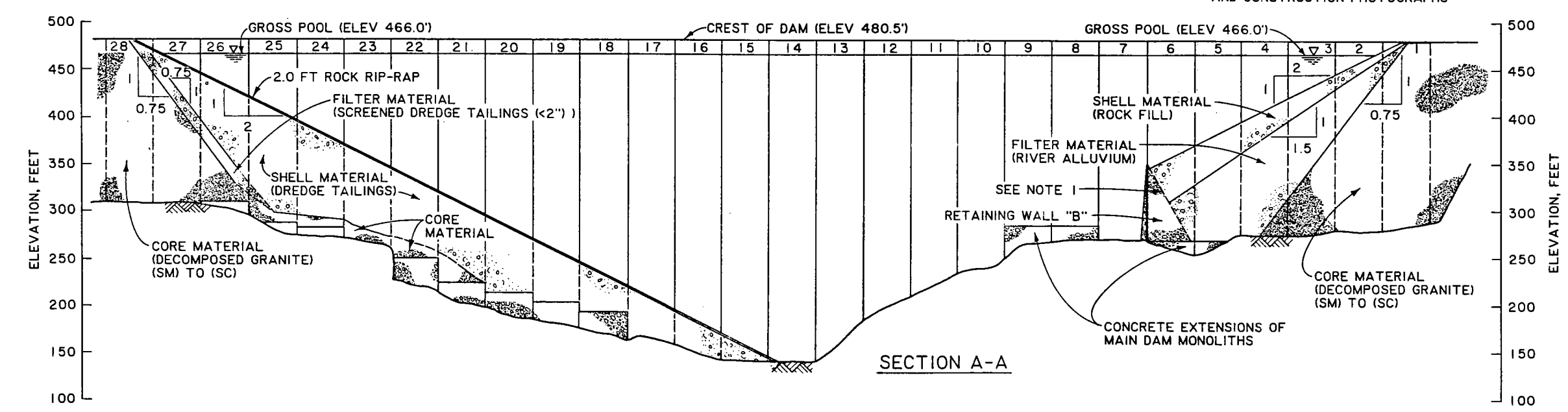


Figure 75. Plan and sections of upstream envelopment areas and Retaining Wall B

CROSS-SECTIONS ON UPSTREAM SIDE OF WING DAMS  
JUNE 1985

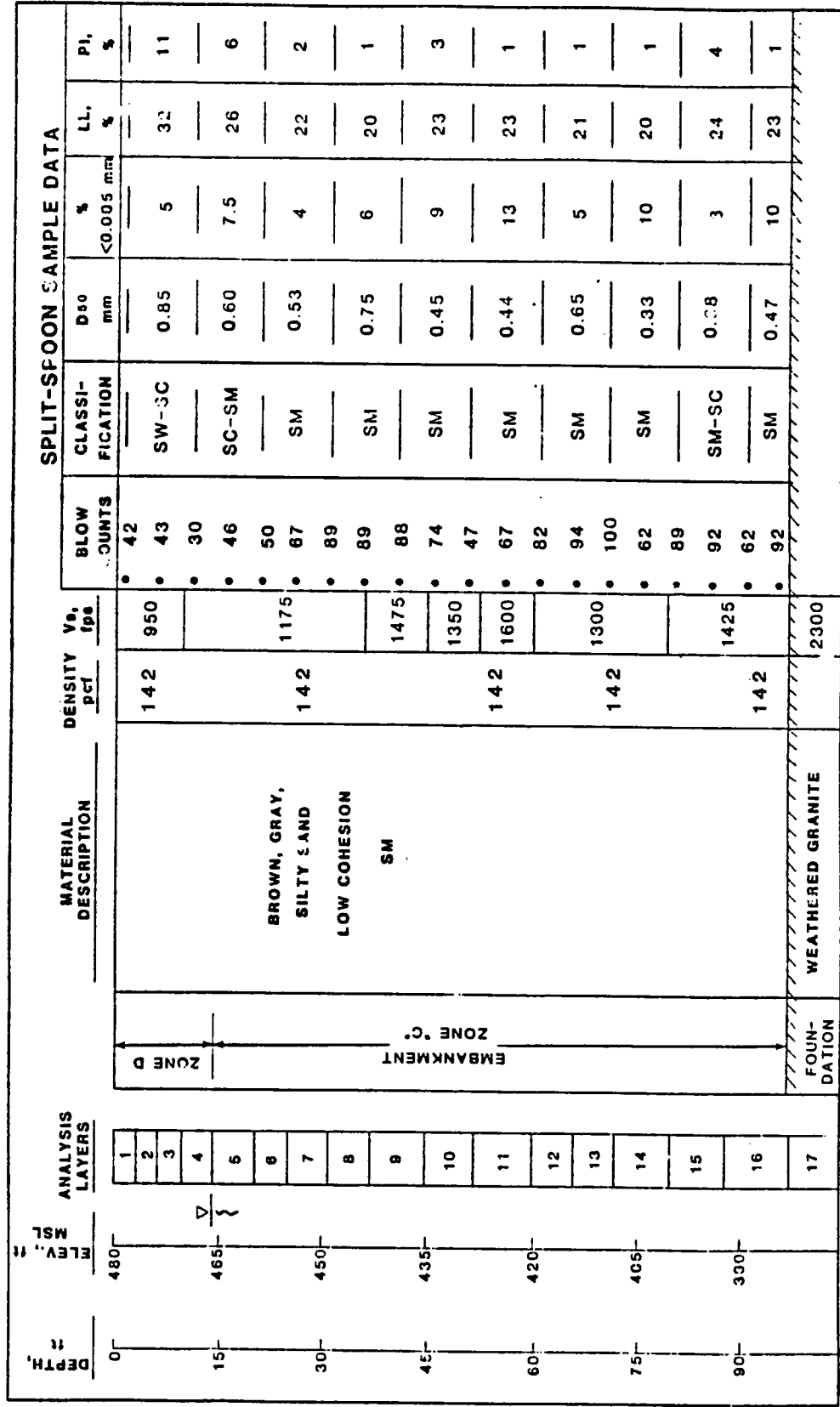
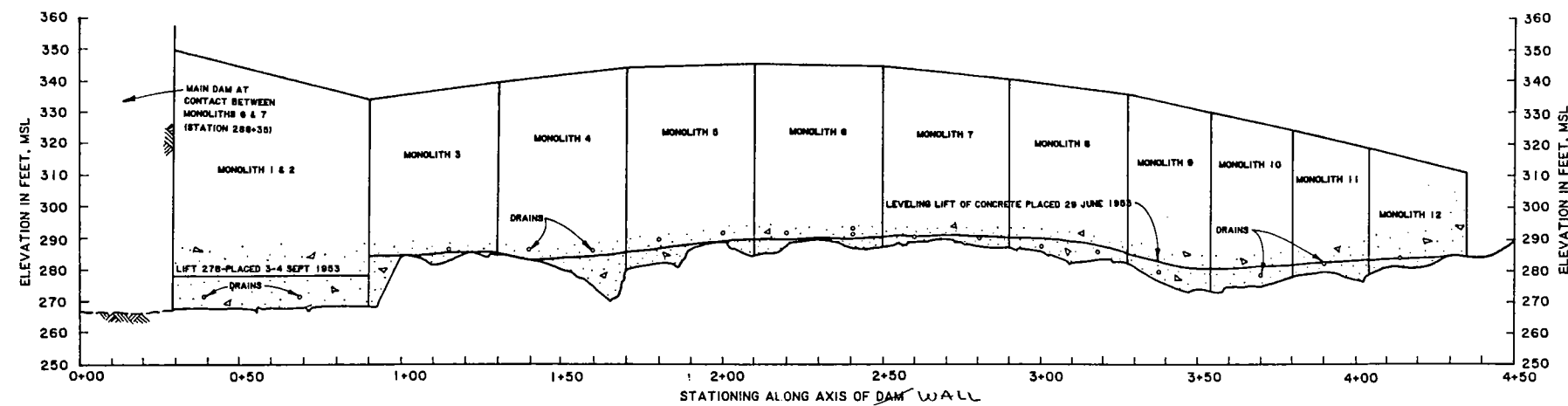
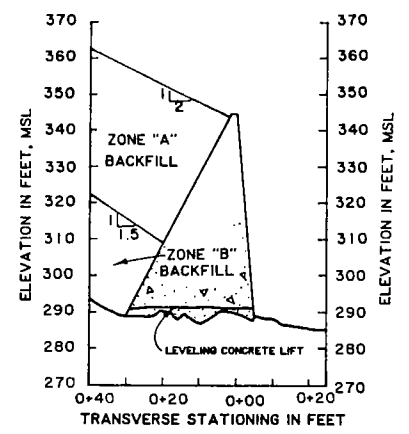


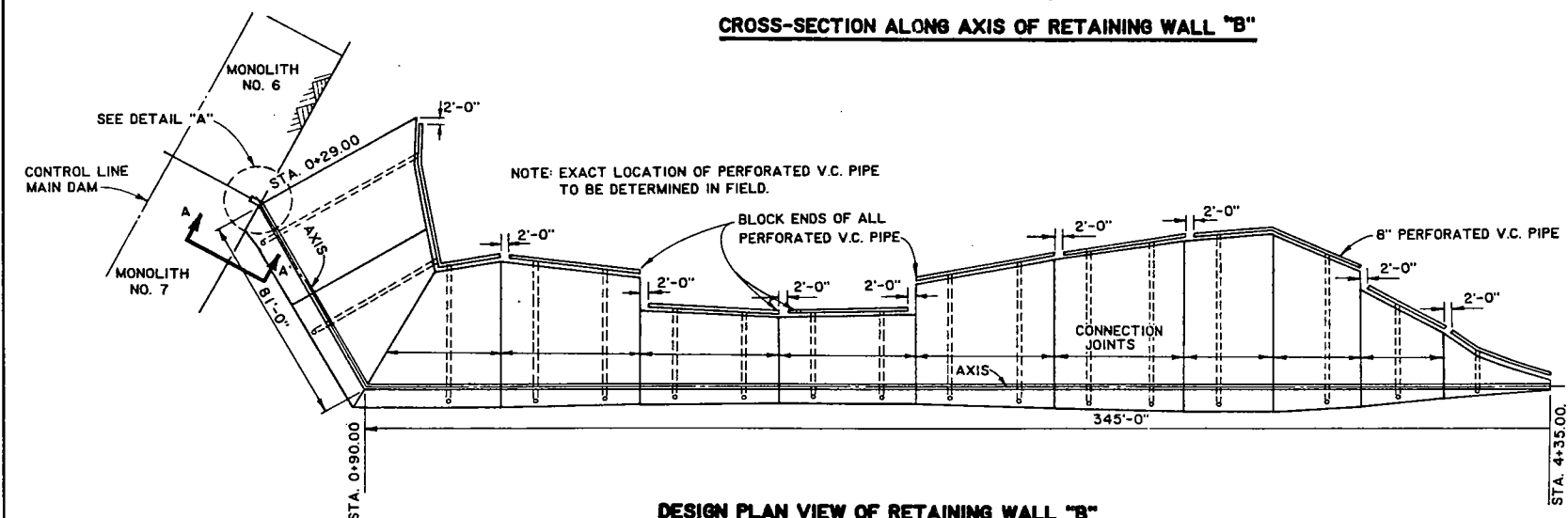
Figure 8. Centerline soil profile, Dike 5



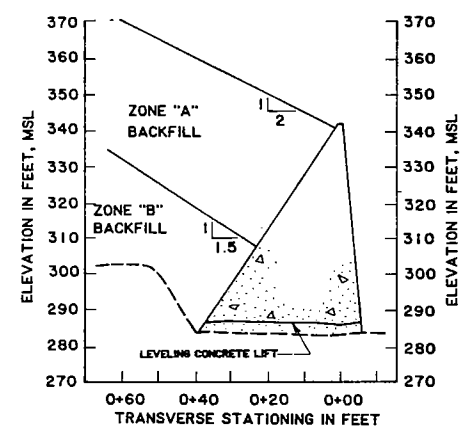
**CROSS-SECTION ALONG AXIS OF RETAINING WALL "B"**



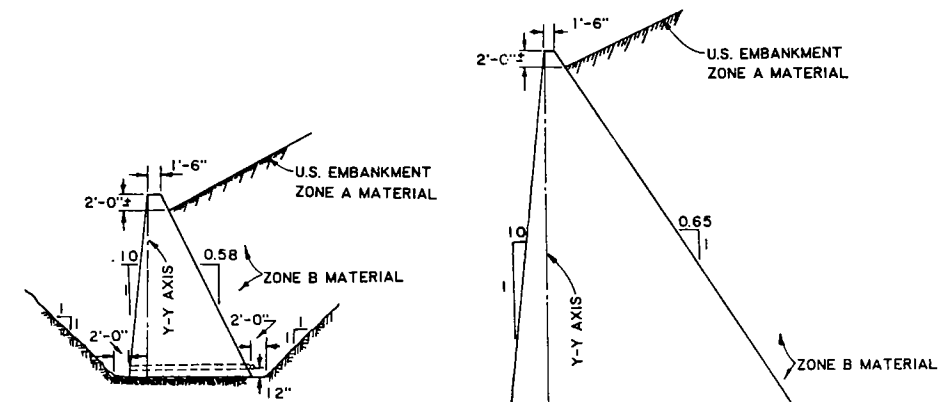
**TRANSVERSE CROSS-SECTION AT STATION 2+30**



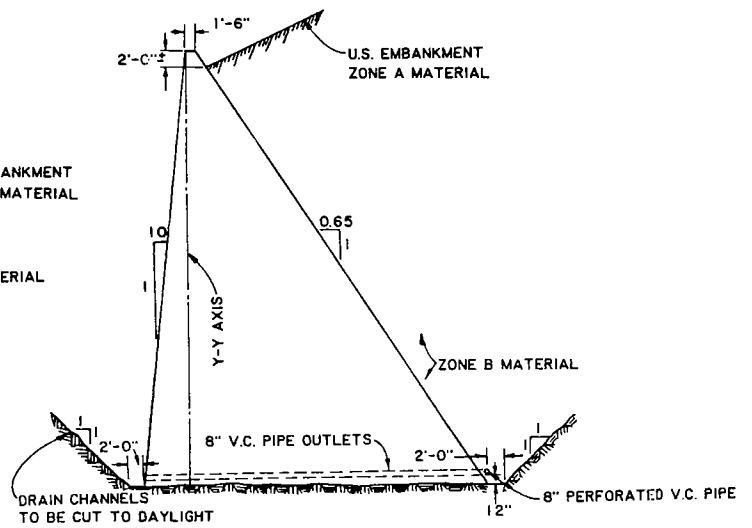
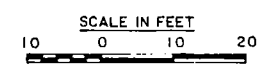
**DESIGN PLAN VIEW OF RETAINING WALL "B"**



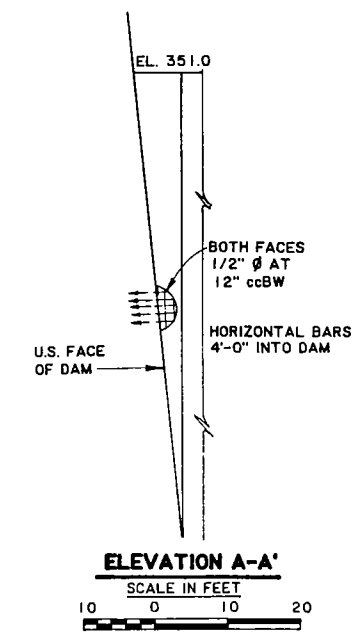
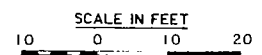
**TRANSVERSE CROSS-SECTION AT STATION 1+90**



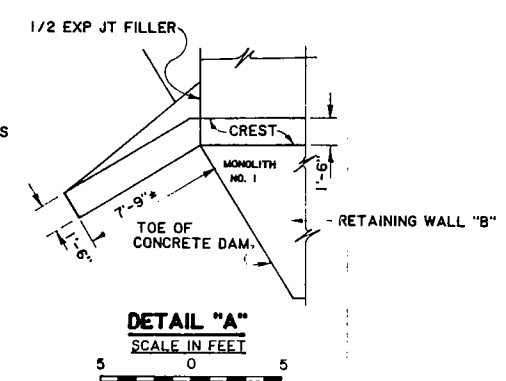
**TYPICAL SECTION WALL "B"**  
FOR HEIGHT OF WALL 5'-0" TO 50'-0"  
STA. 1+70.00 TO STA. 2+50.00 -  
STA. 3+80.00 TO STA. 4+35.00



**TYPICAL SECTION WALL "B"**  
FOR HEIGHT OF WALL 50'-0" TO 80'-0"  
STA. 0+29.00 TO STA. 1+70.00 - STA. 2+50.00 TO STA. 3+80.00



**ELEVATION A-A'**  
SCALE IN FEET  
10 0 10 20



**DETAIL "A"**  
SCALE IN FEET  
5 0 5

U.S. ARMY CORPS OF ENGINEERS  
WATERWAYS EXPERIMENT STATION  
VICKSBURG, MISSISSIPPI  
**FOLSOM DAM PROJECT**  
AMERICAN RIVER,  
CALIFORNIA  
DETAIL OF RETAINING  
WALL "B"  
JUNE 1985

**Figure 74. Plan and sections of Retaining Wall B**

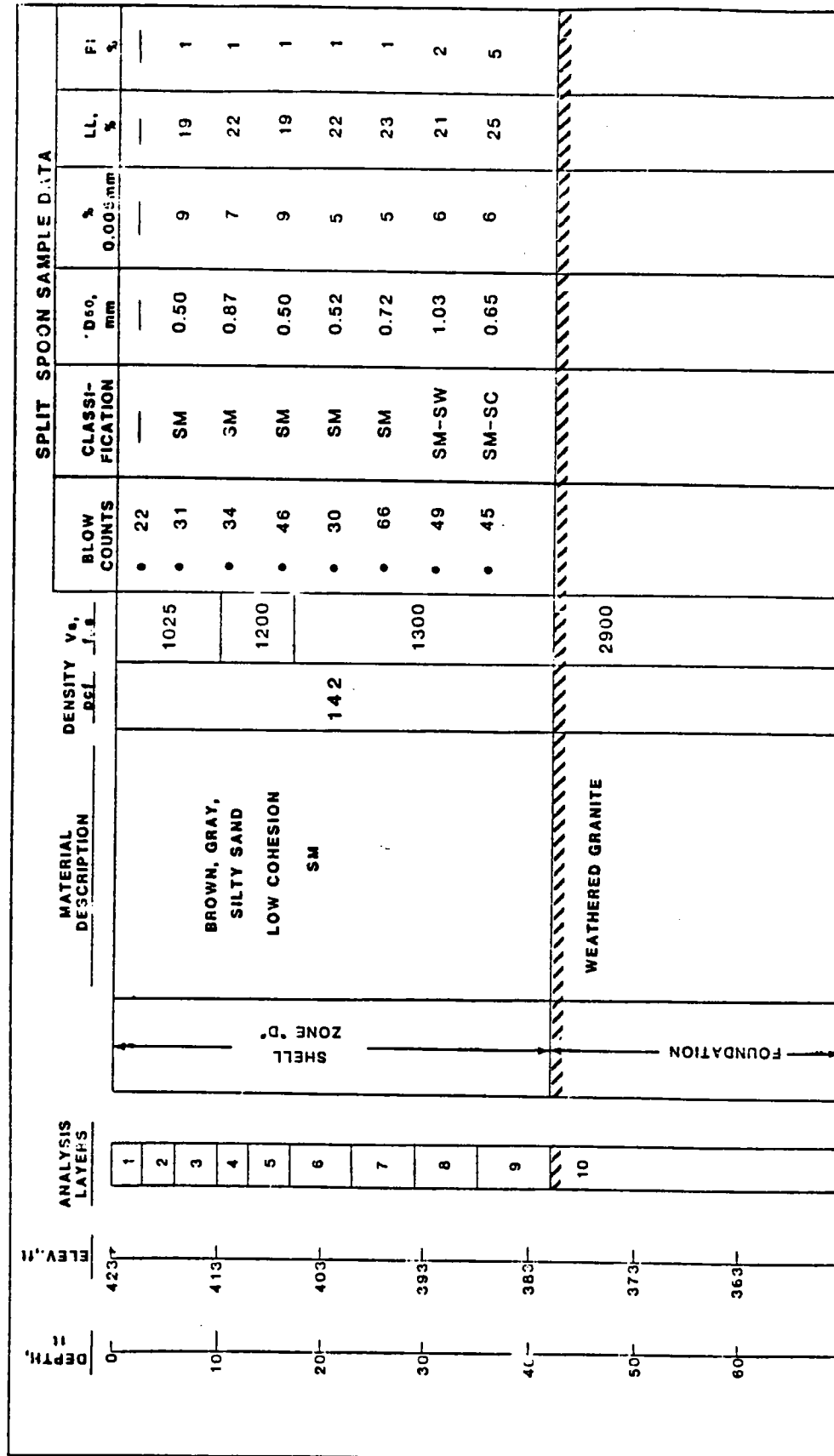


Figure 9. Upstream slope soil profile, Dike 5

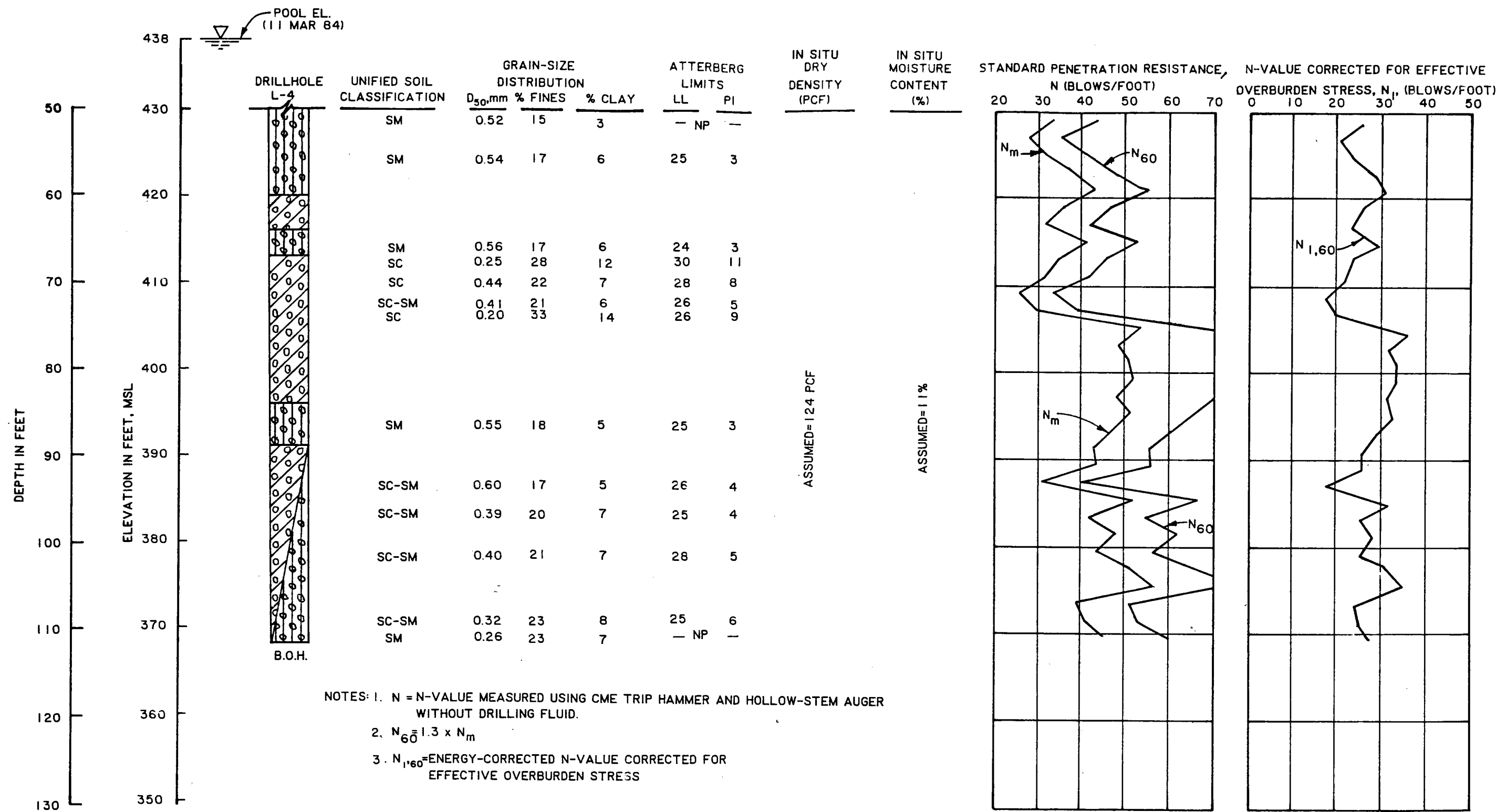


Figure 73. Summary of field and laboratory index data for Boring L-4, Left Wing Dam Interface area

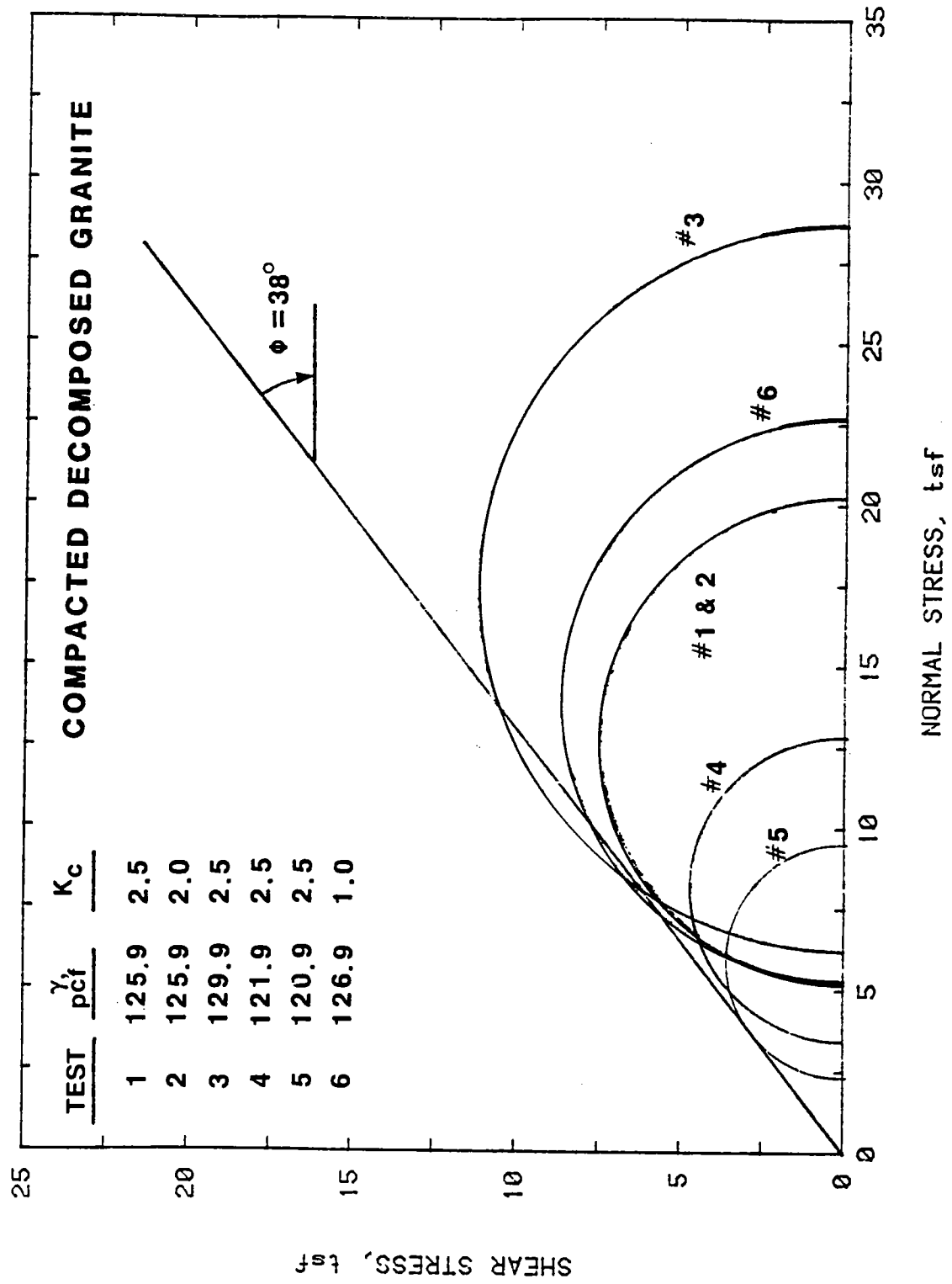


Figure 10. Effective stress strength envelope from R tests on compacted decomposed granite.

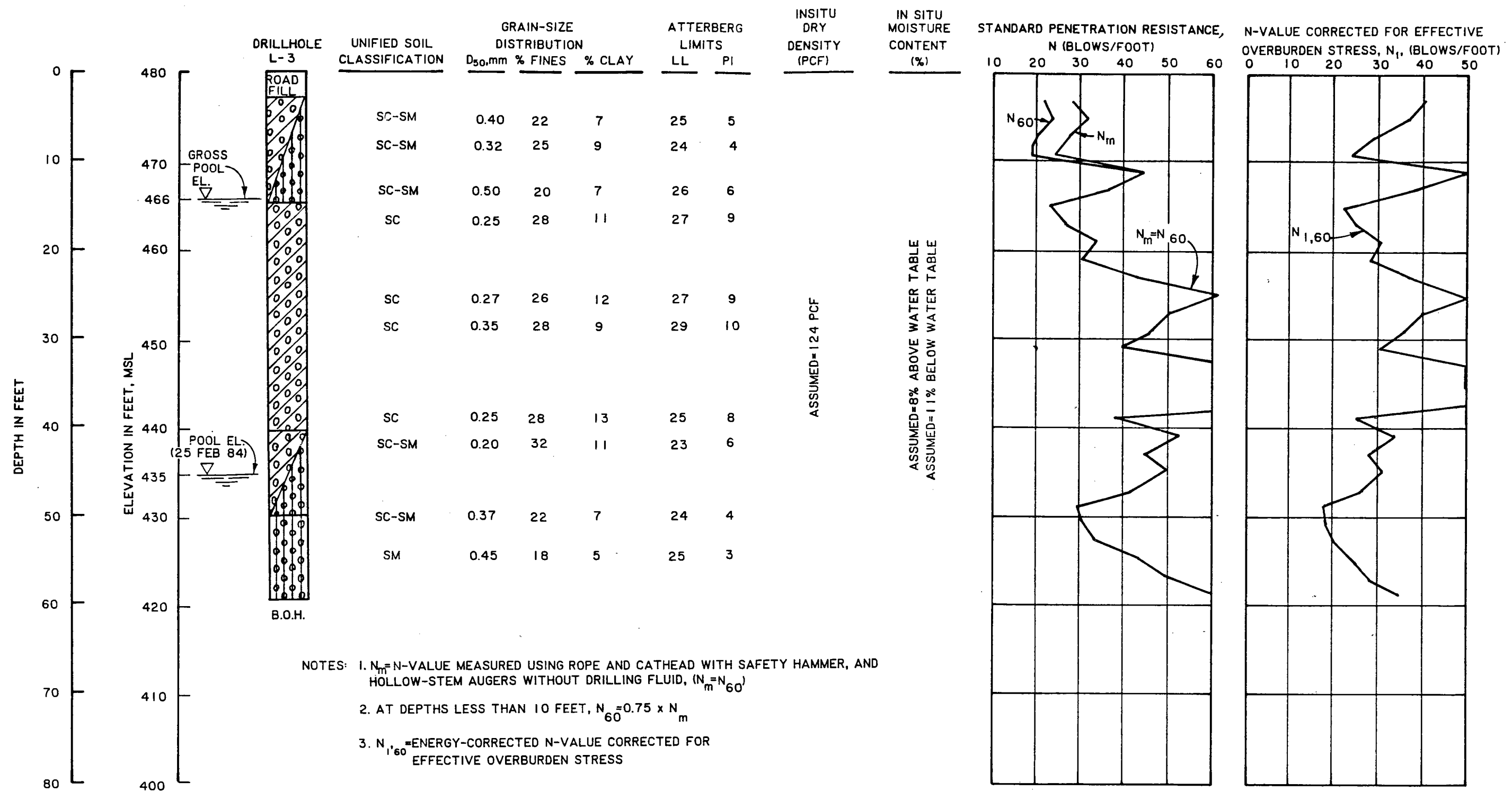


Figure 72. Summary of field and laboratory index data for Boring L-3, Left Wing Dam Interface area

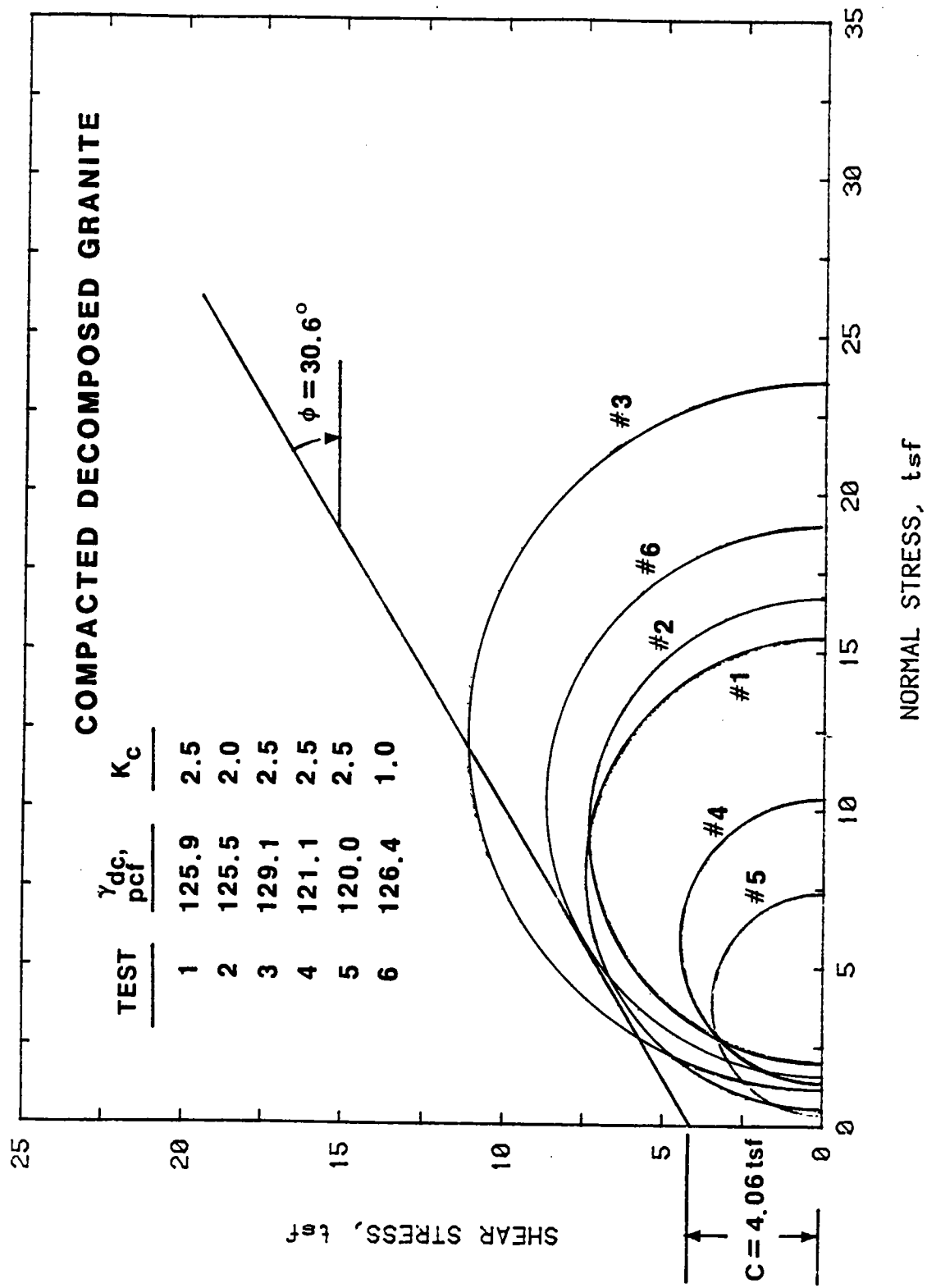


Figure 11. Total stress strength envelope from R tests on compacted decomposed granite.

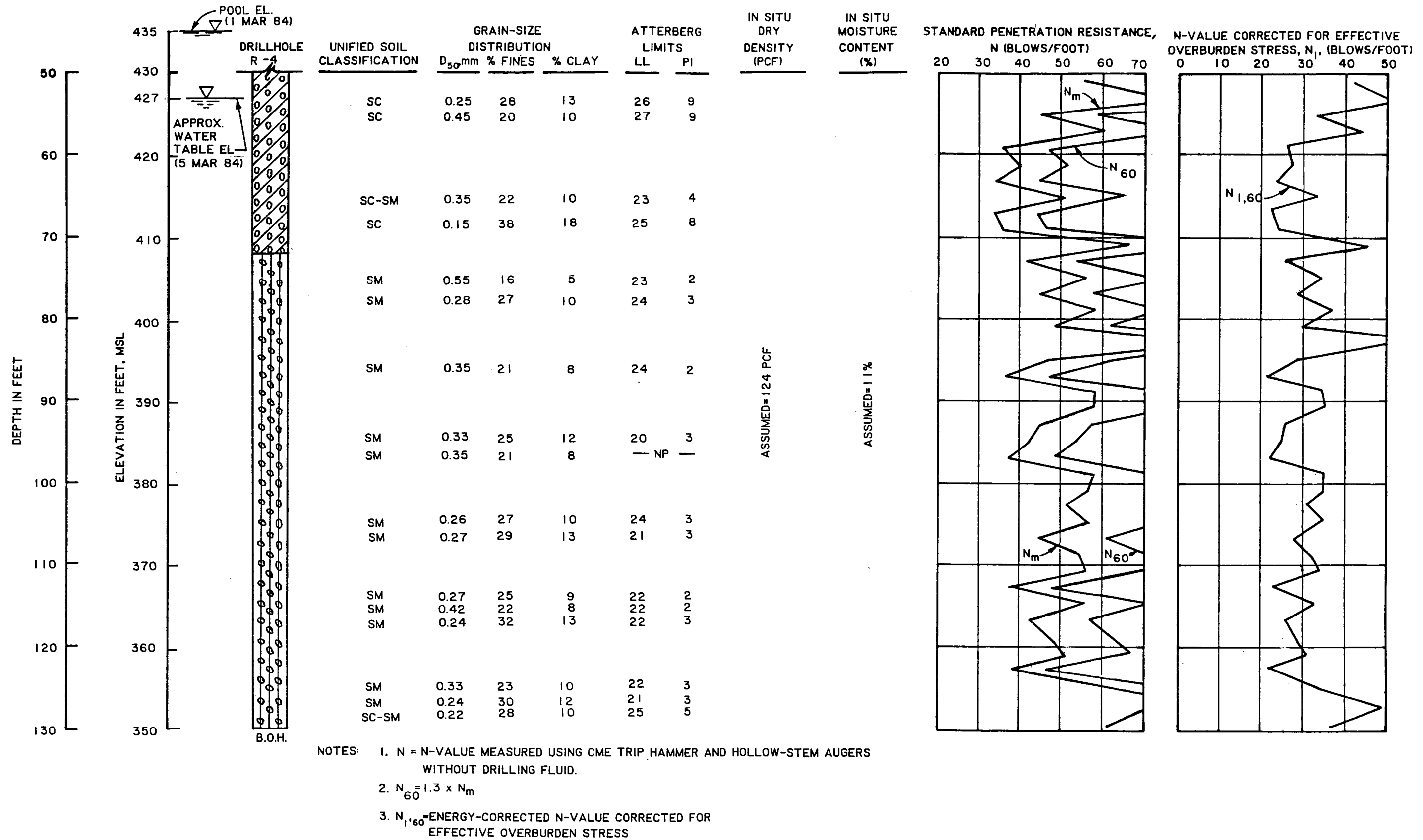


Figure 71. Summary of field and laboratory index data for Boring R-4, Right Wing Dam Interface area

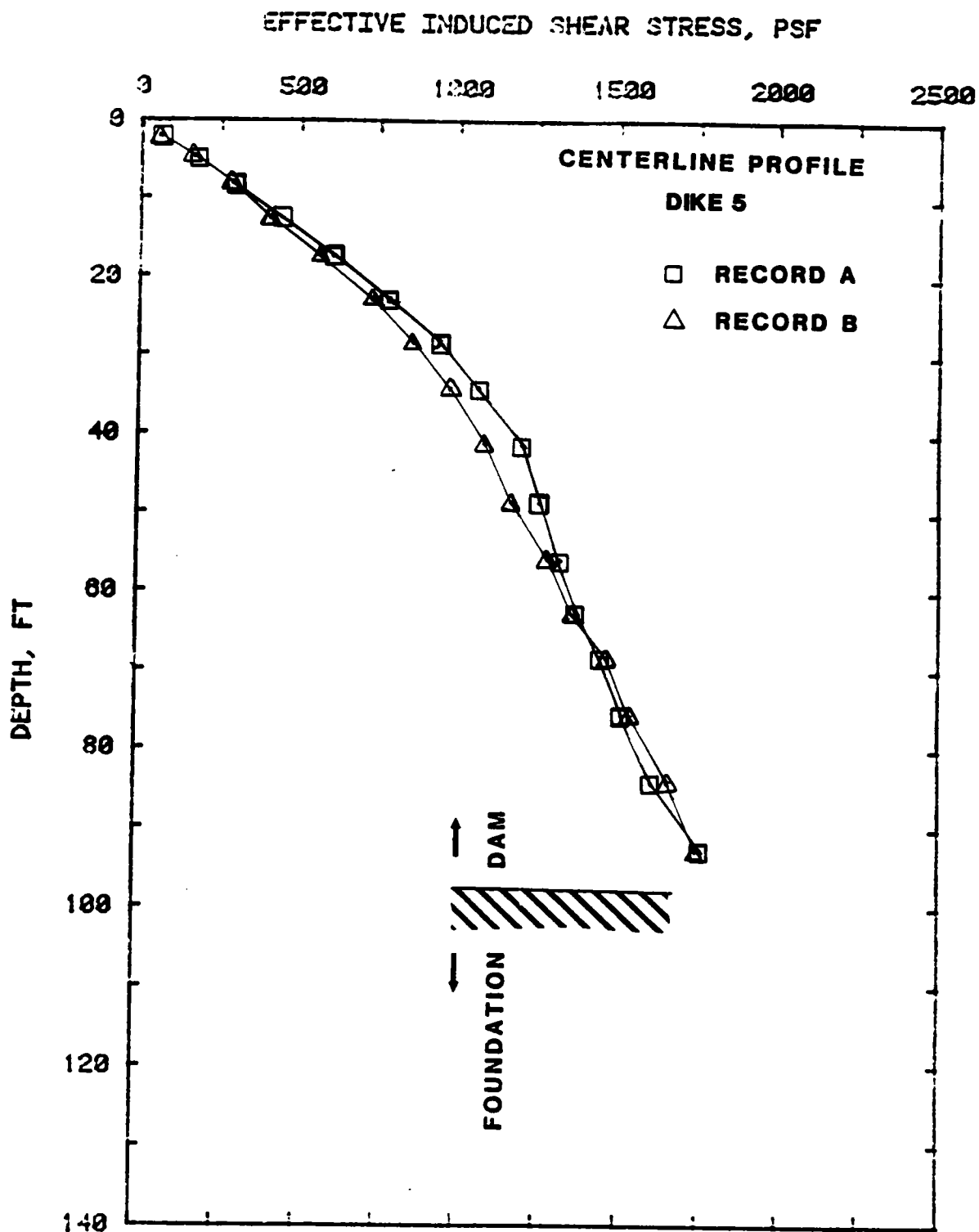


Figure 12. Effective dynamic shear stresses in centerline profile, Dike 5 induced by records A and B

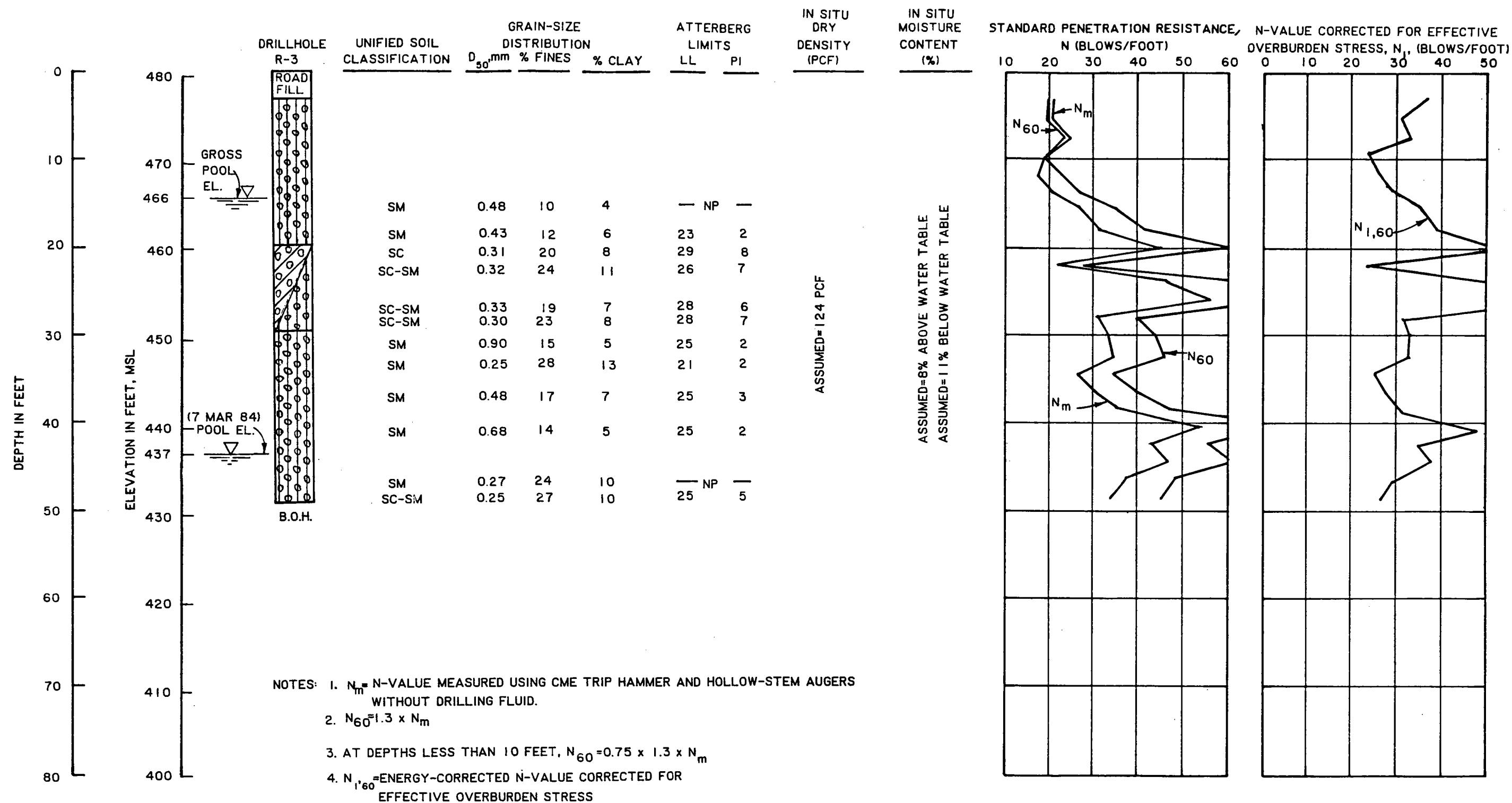


Figure 70. Summary of field and laboratory index data for Boring R-3, Right Wing Dam Interface area

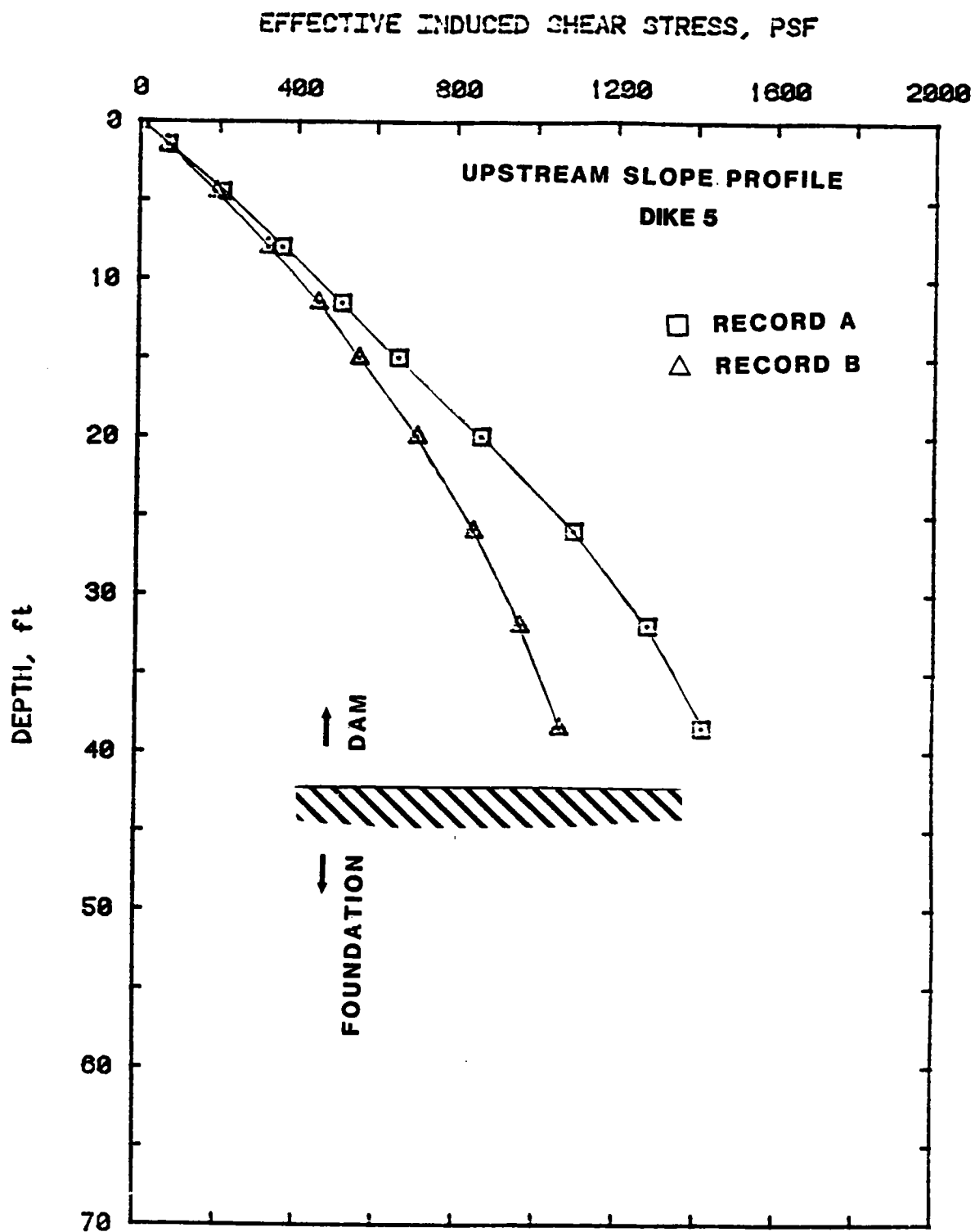


Figure 18. Effective dynamic shear stresses in upstream slope profile induced by records A and B, DiKE 5

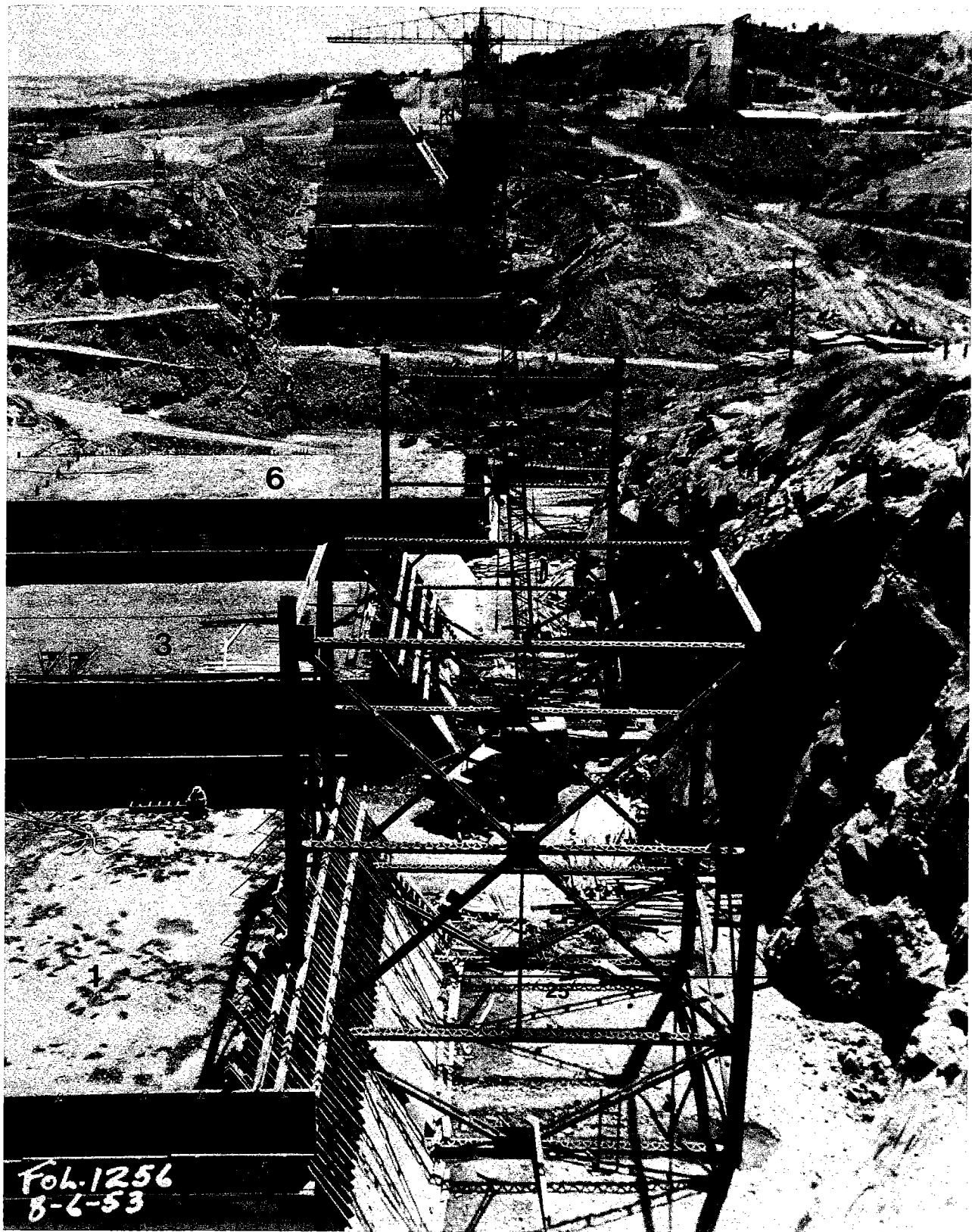


Figure 69. Construction photograph FOL. 1256, dated 8/6/53 showing geometry of rock trench at base of enveloped concrete monoliths, Right Wing Dam

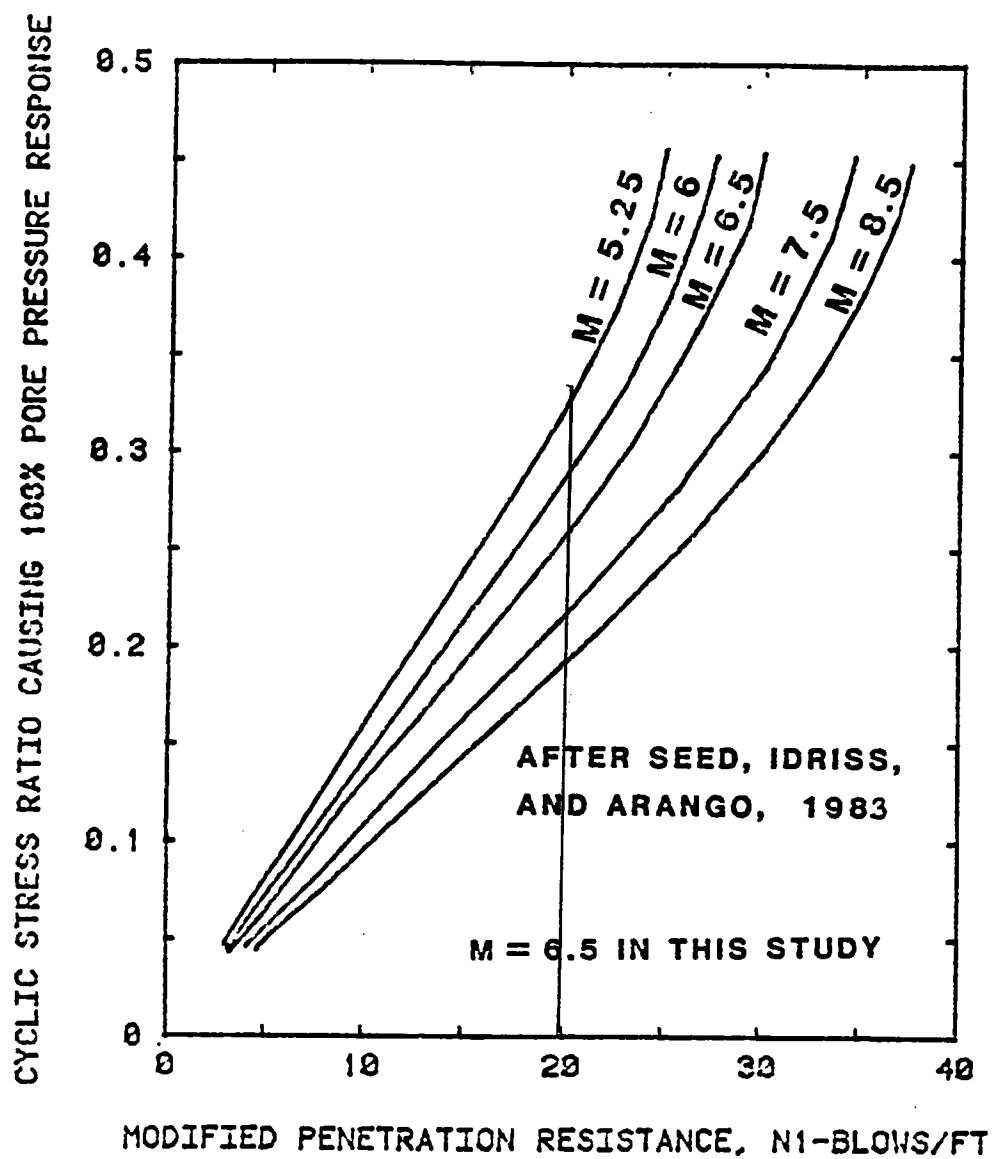
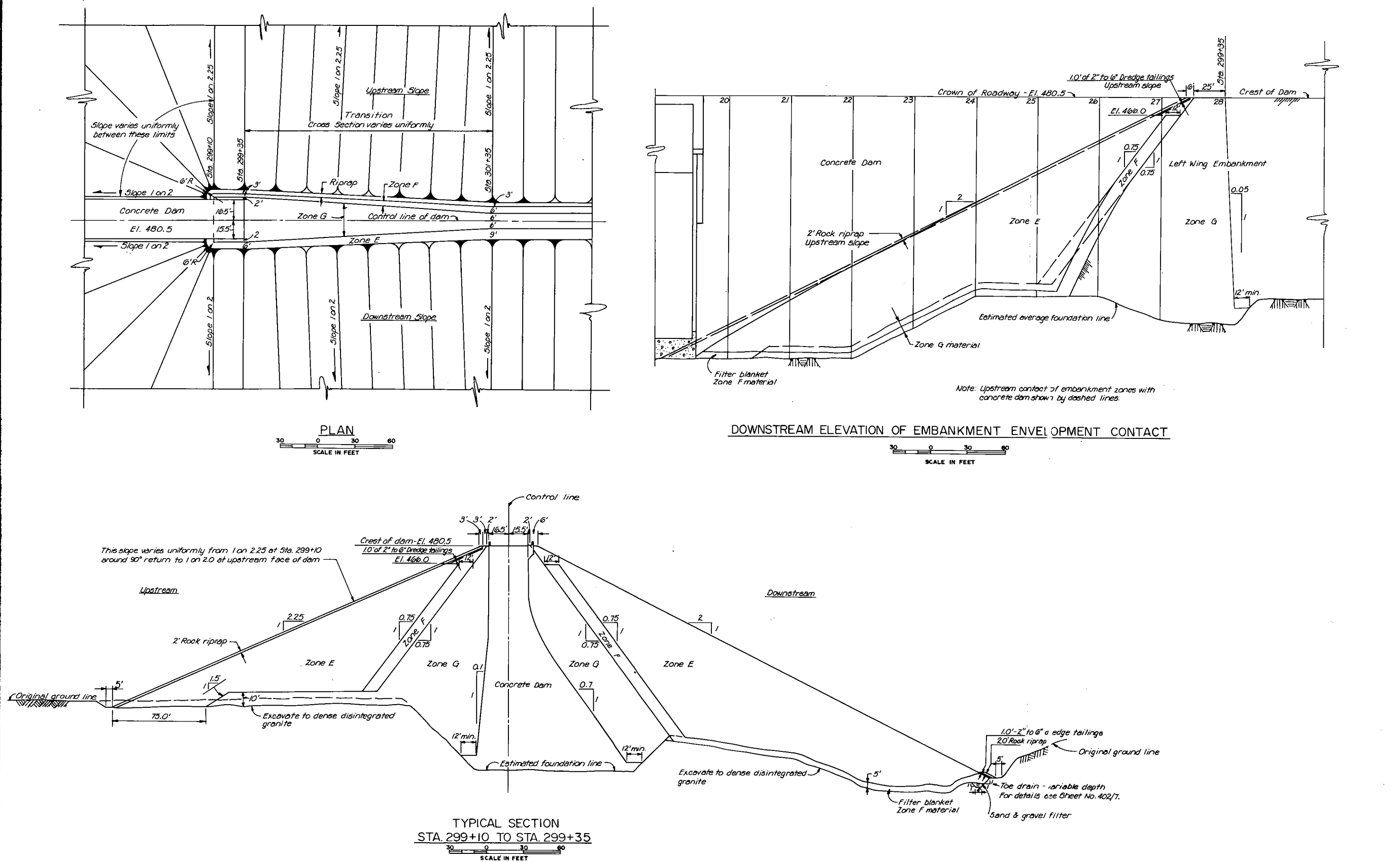


Figure 14a.  $N_1$  versus stress ratio causing liquefaction for different magnitude earthquakes



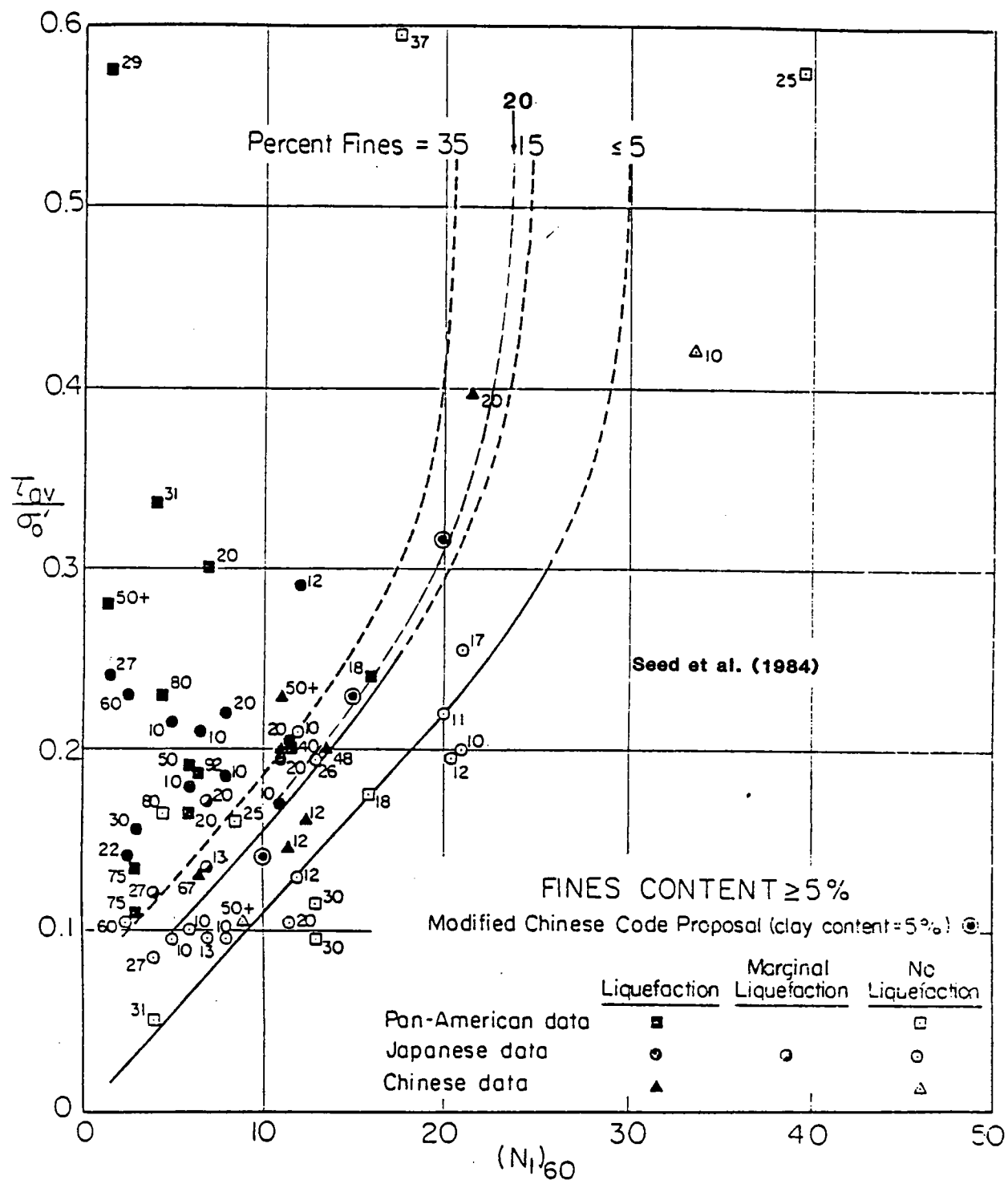
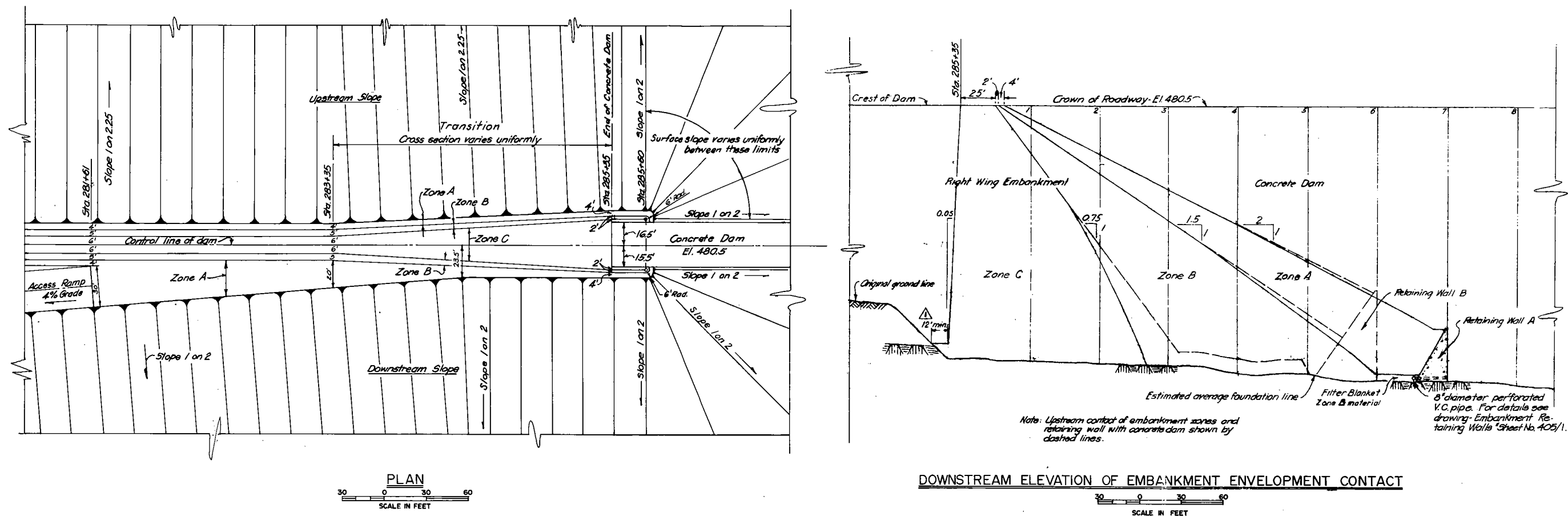


Figure 14b. Relationships between stress ratio causing liquefaction and  $(N_1)_{60}$ -values for silty sands for M=7-1/2 earthquakes (from Seed, Tokimatsu, Harder, and Chung, 1984).



**Figure 67. Plan and sections of Right Wing Dam Interface area.**

AMERICAN RIVER BASIN DEVELOPMENT, CALIFORNIA  
FOLSOM RESERVOIR PROJECT  
AMERICAN RIVER  
FOLSOM DAM  
RIGHT WING DAM  
ENVELOPMENT OF CONCRETE DAM

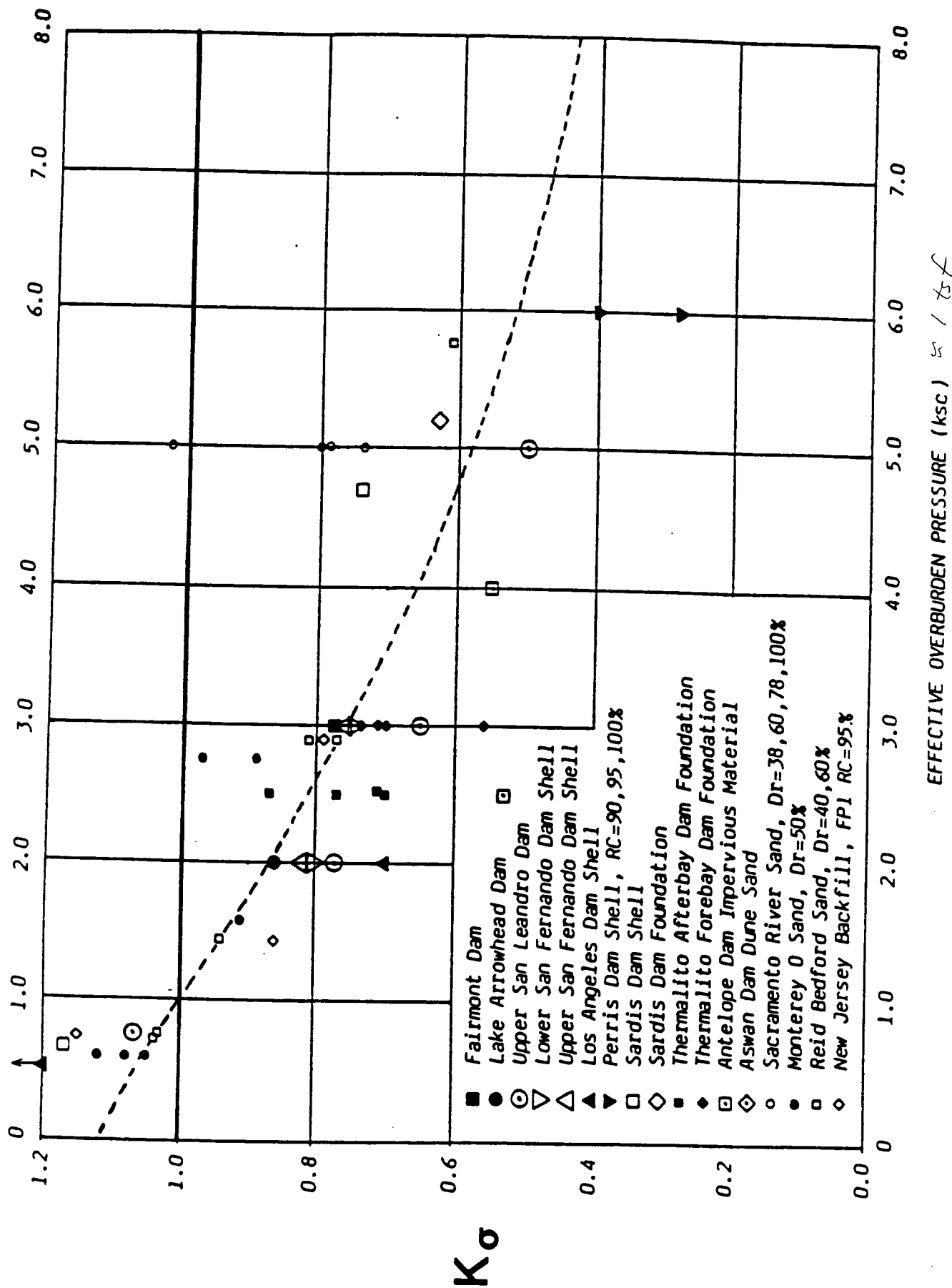


Figure 15a. Factor  $K_\sigma$  to adjust cyclic stress ratio required to cause 100% pore pressure response with changes in effective overburden pressure (from Seed, 1985)

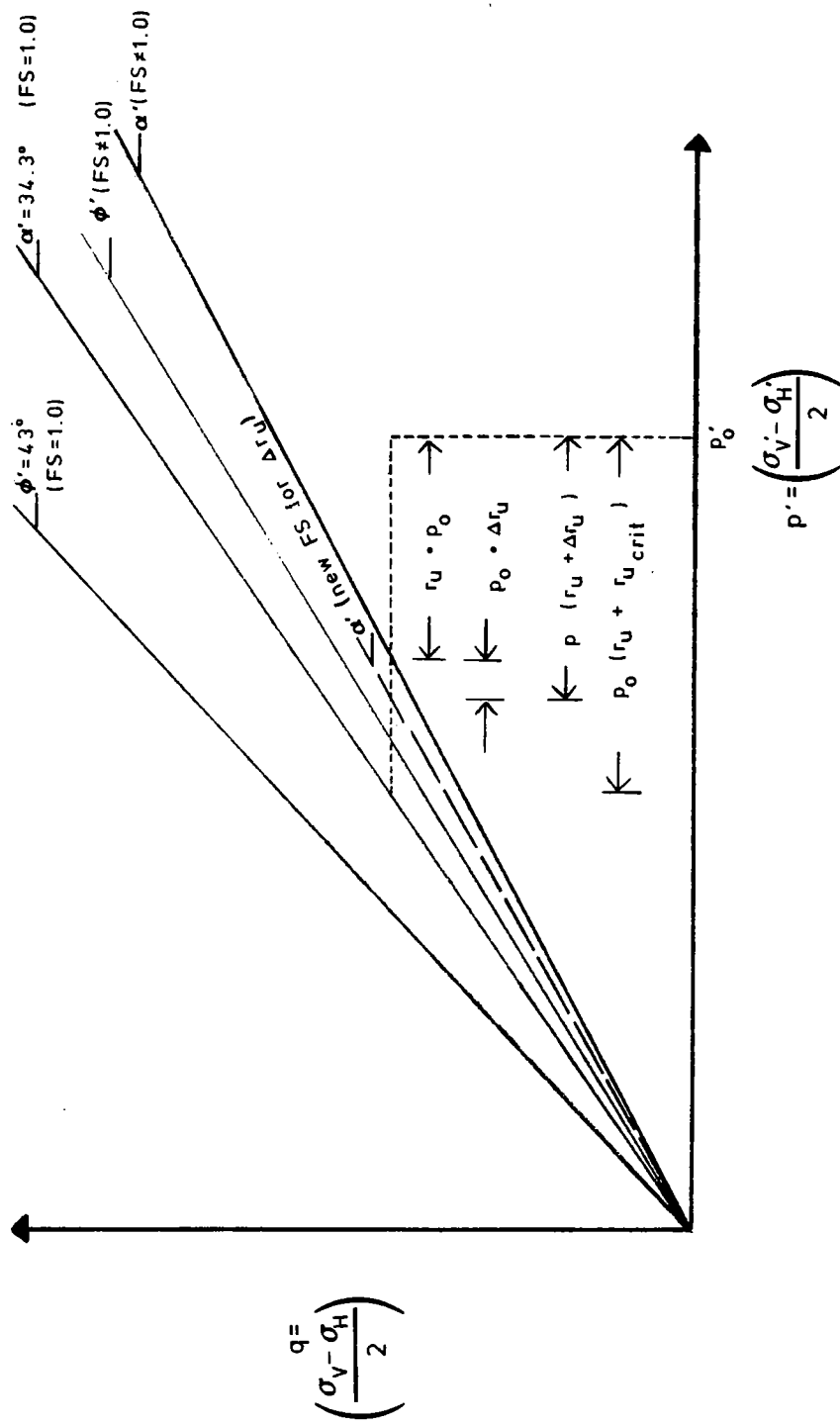


Figure 66. Construction on p-q diagram to estimate changes in factors of safety against sliding with increases in earthquake-induced residual excess pore pressures,  $r_u$

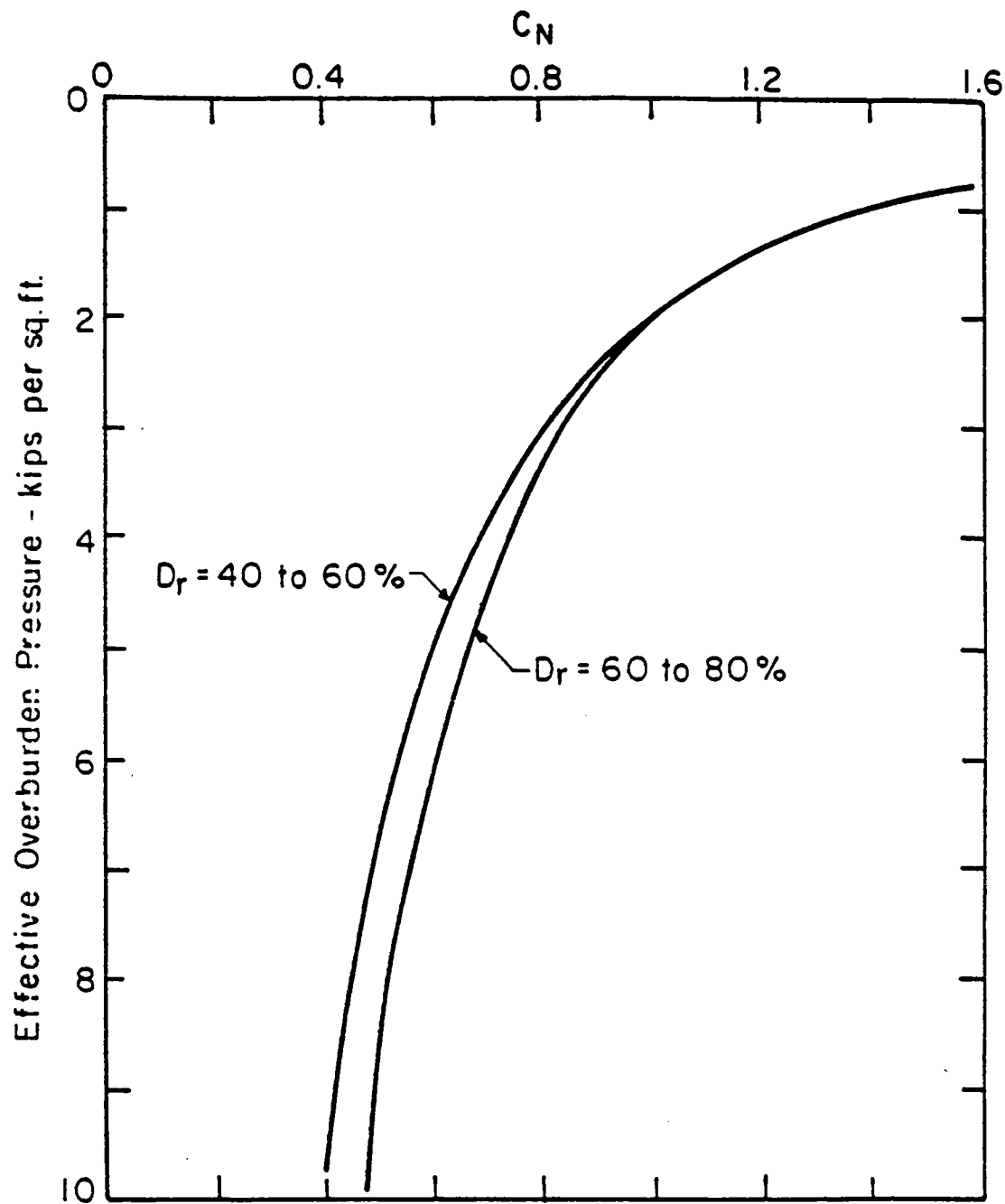


Figure 15b. Normalization factor  $C_N$  to adjust SPT blowcounts to a confining stress of 1 tsf (from Bleganousky and Marcuson, 1976)

# POST-EARTHQUAKE STABILITY ANALYSIS

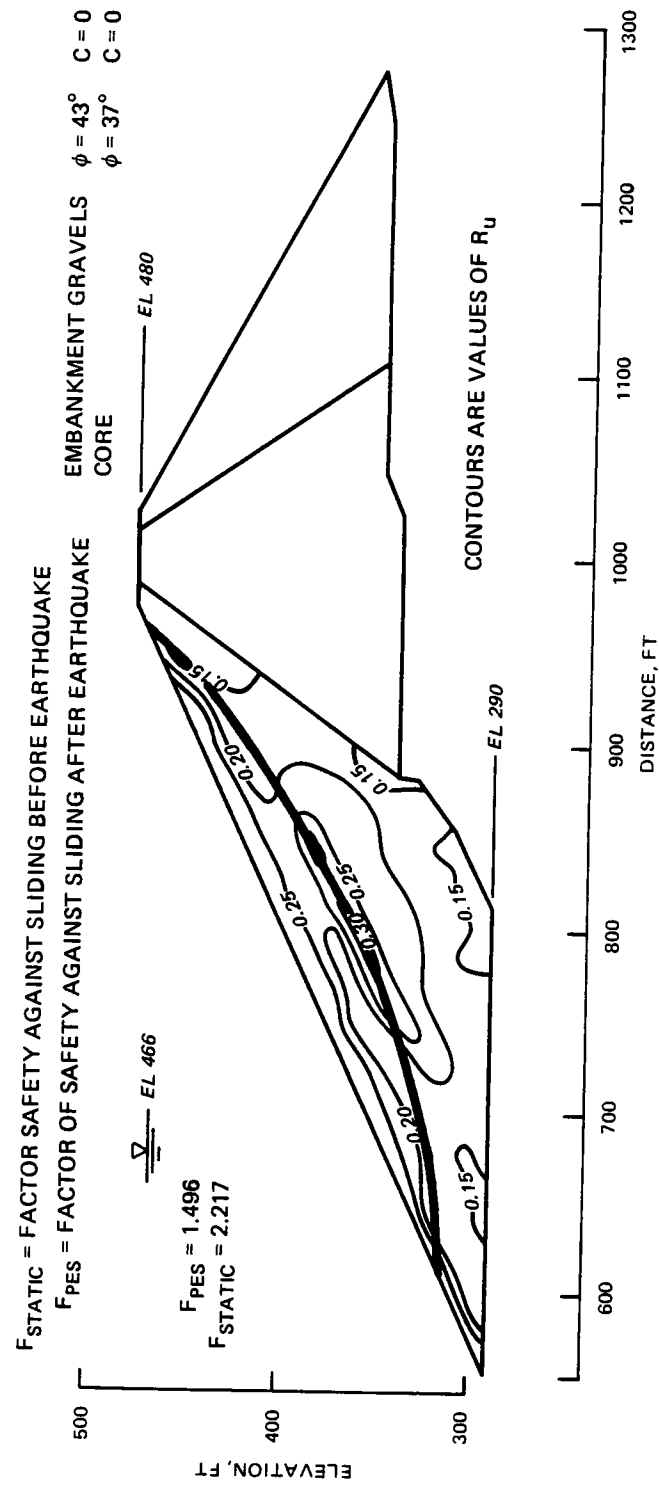


Figure 65b. Typical circular surface passing through zone of high earthquake-induced residual excess pore pressure

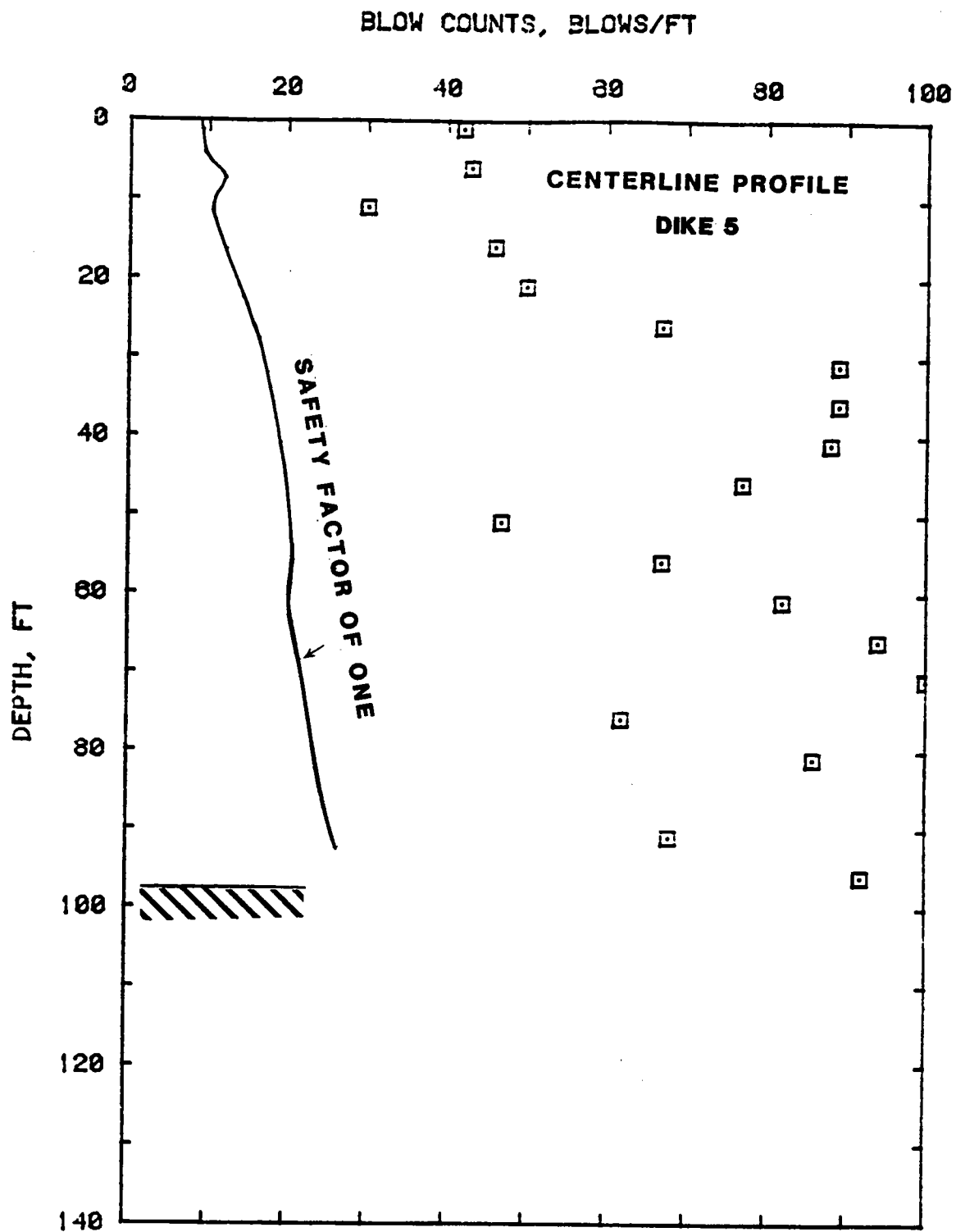


Figure 16. SPT blowcounts compared with blowcounts required for safety factor of one for centerline profile, Dike 5

# POST - EARTHQUAKE STABILITY ANALYSIS

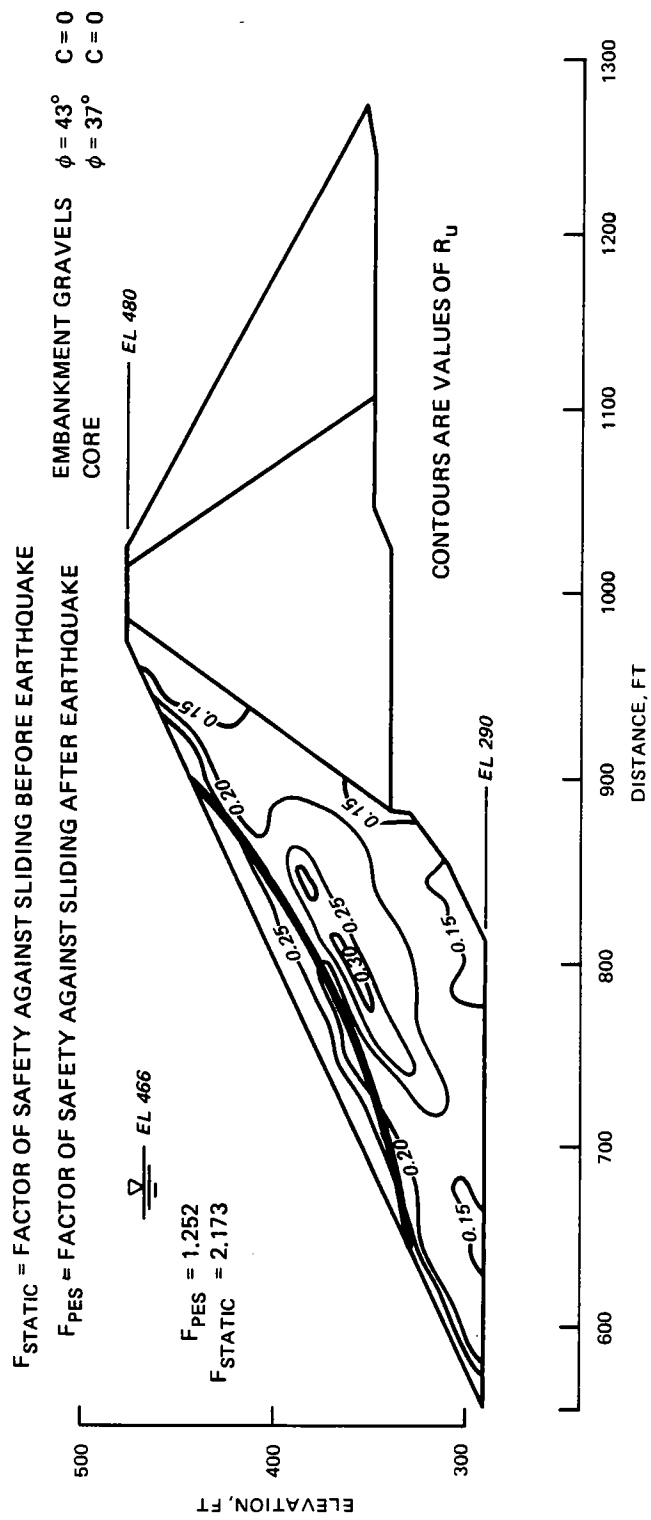


Figure 65a. Circular surface with minimum factor of safety against sliding, Wing Dam

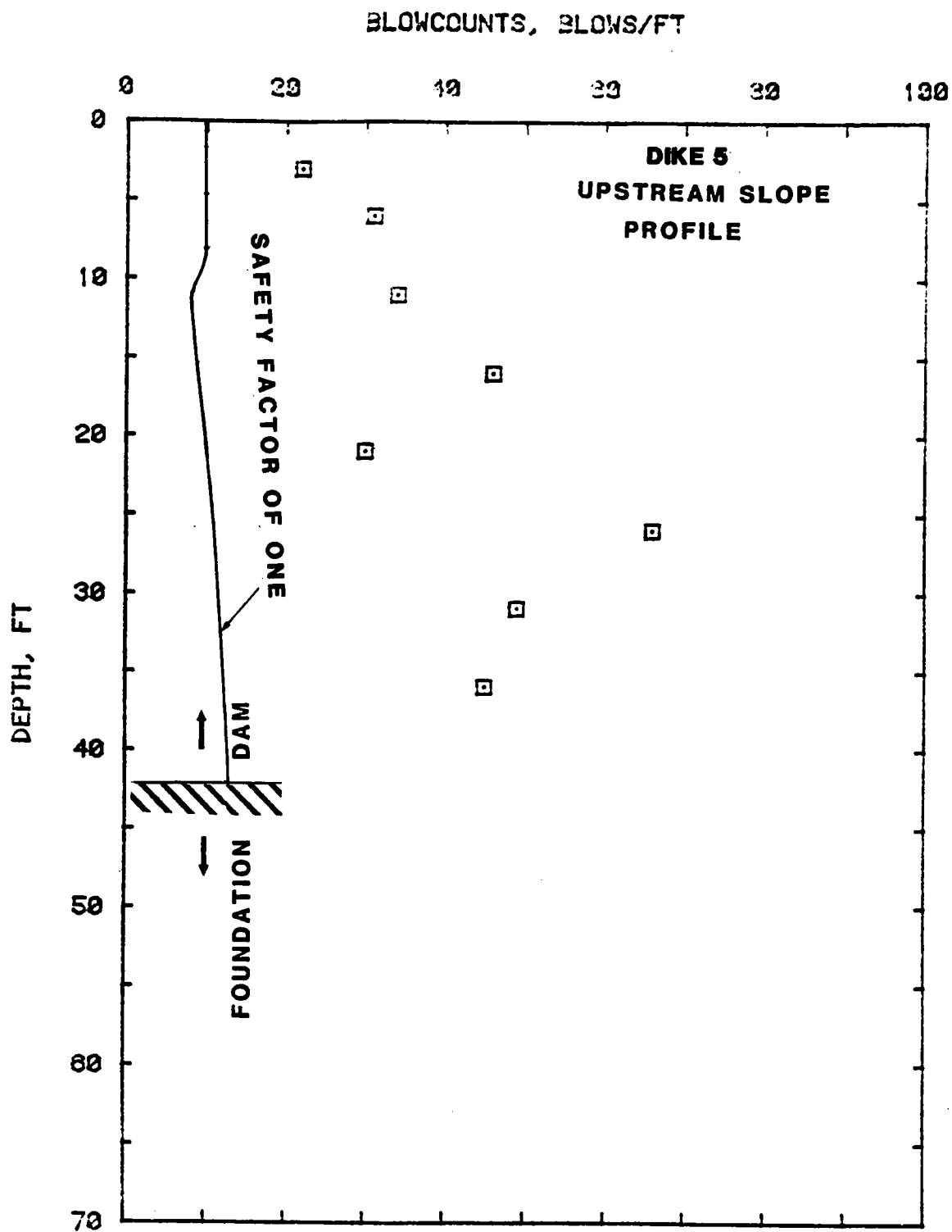


Figure 17. SPT blowcounts compared with blowcounts required for safety factor of one for upstream profile, **DiKE 5**

# CONTOURS OF RESIDUAL EXCESS PORE WATER PRESSURE RATIO

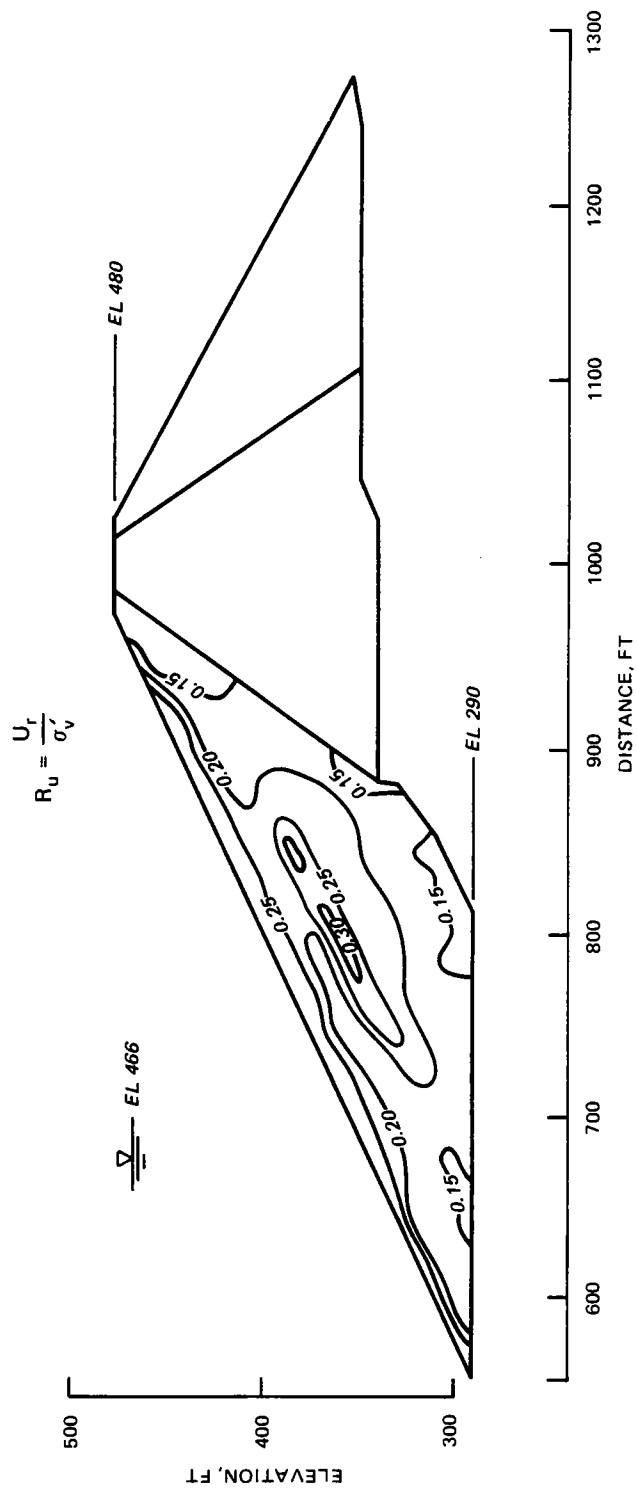
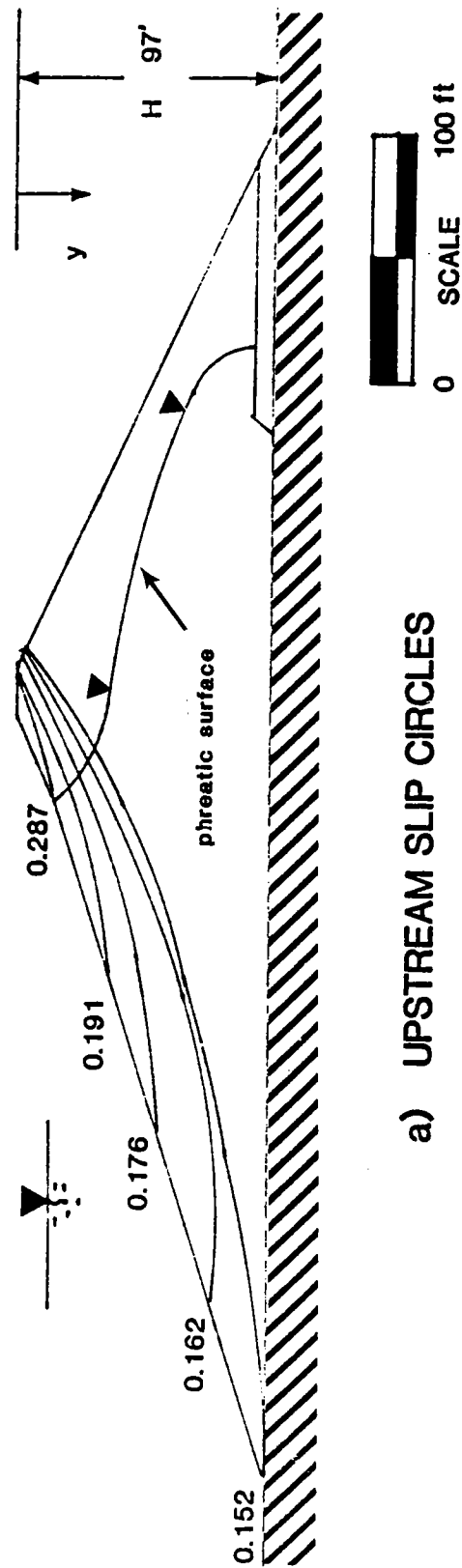
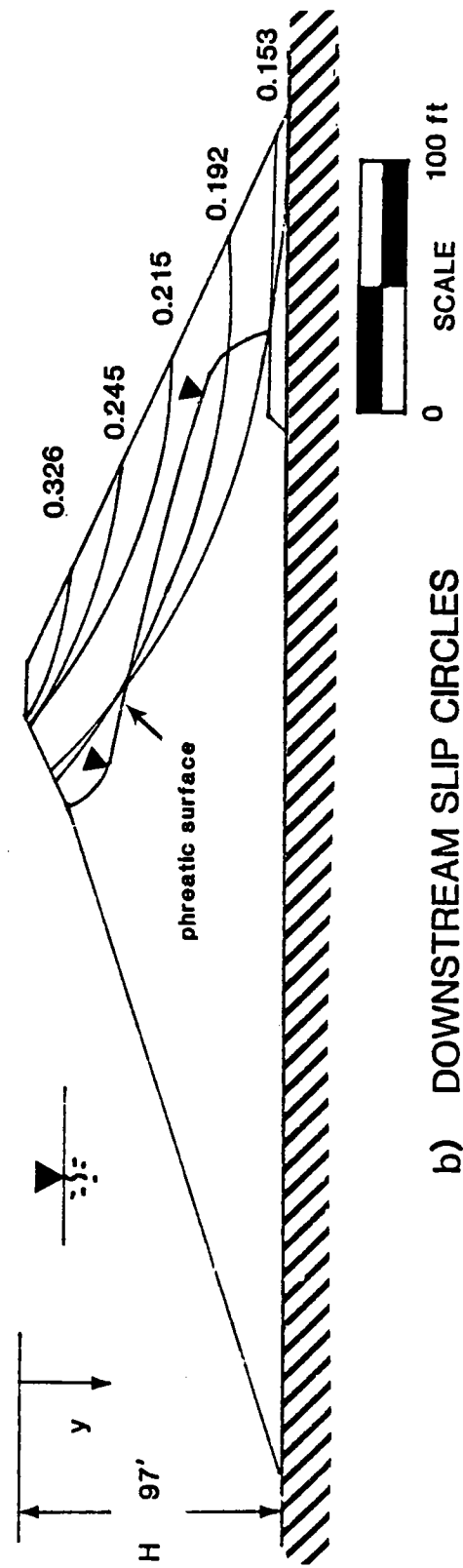


Figure 64. Earthquake-induced residual excess pore pressure field in upstream shell of Wing Dam



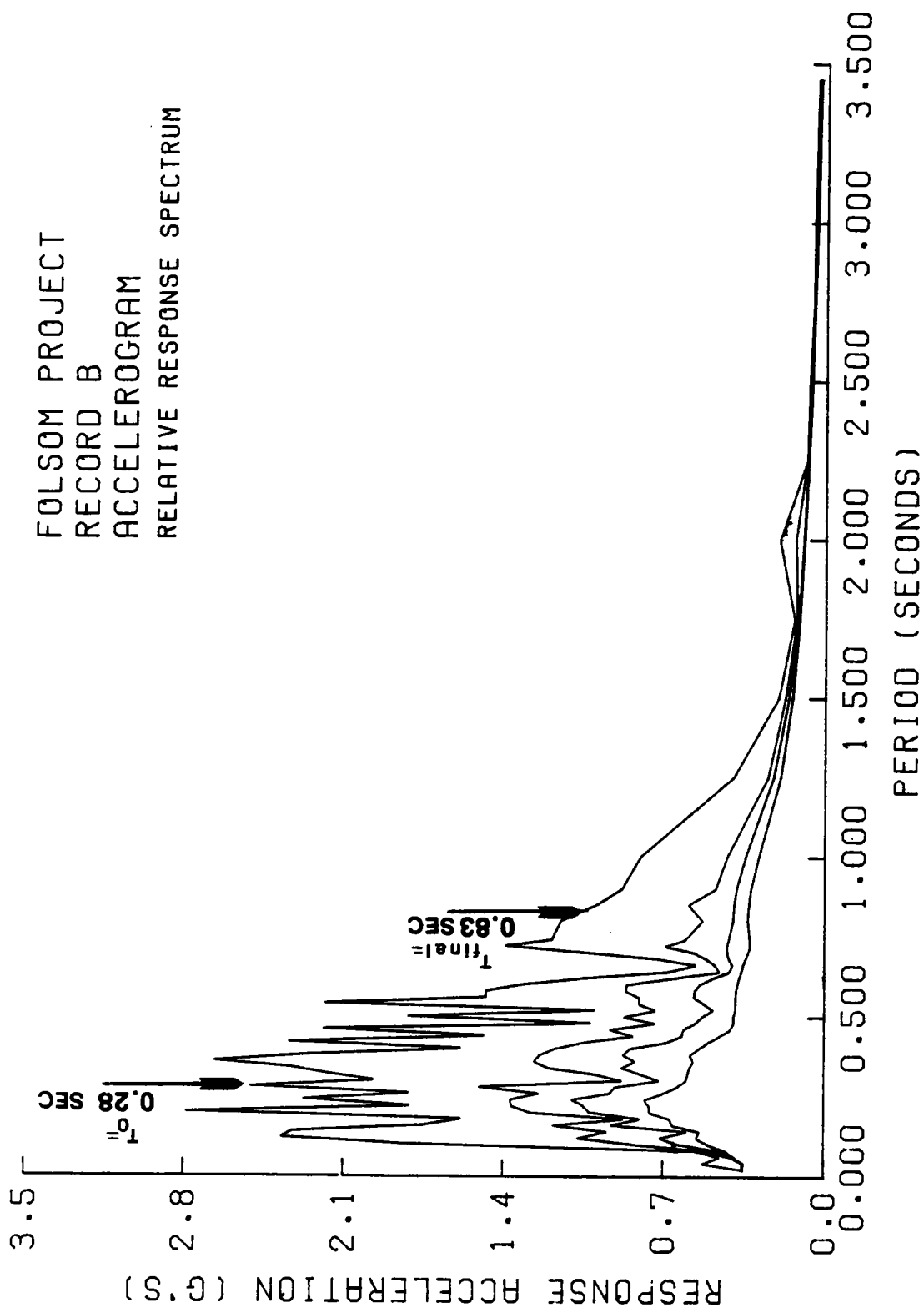
a) UPSTREAM SLIP CIRCLES



b) DOWNSTREAM SLIP CIRCLES

Figure 18. Cross-section of Dike 5 showing yield acceleration and slip circles as determined by ARCEQS

FOLSOM PROJECT  
RECORD B  
ACCELEROGRAM  
RELATIVE RESPONSE SPECTRUM



CURVE FOR 0.2, 5 AND 10 PERCENT DAMPING

Figure 63. Initial and post-earthquake fundamental periods for Wing Dam analysis section compared with Accelerogram B response spectra

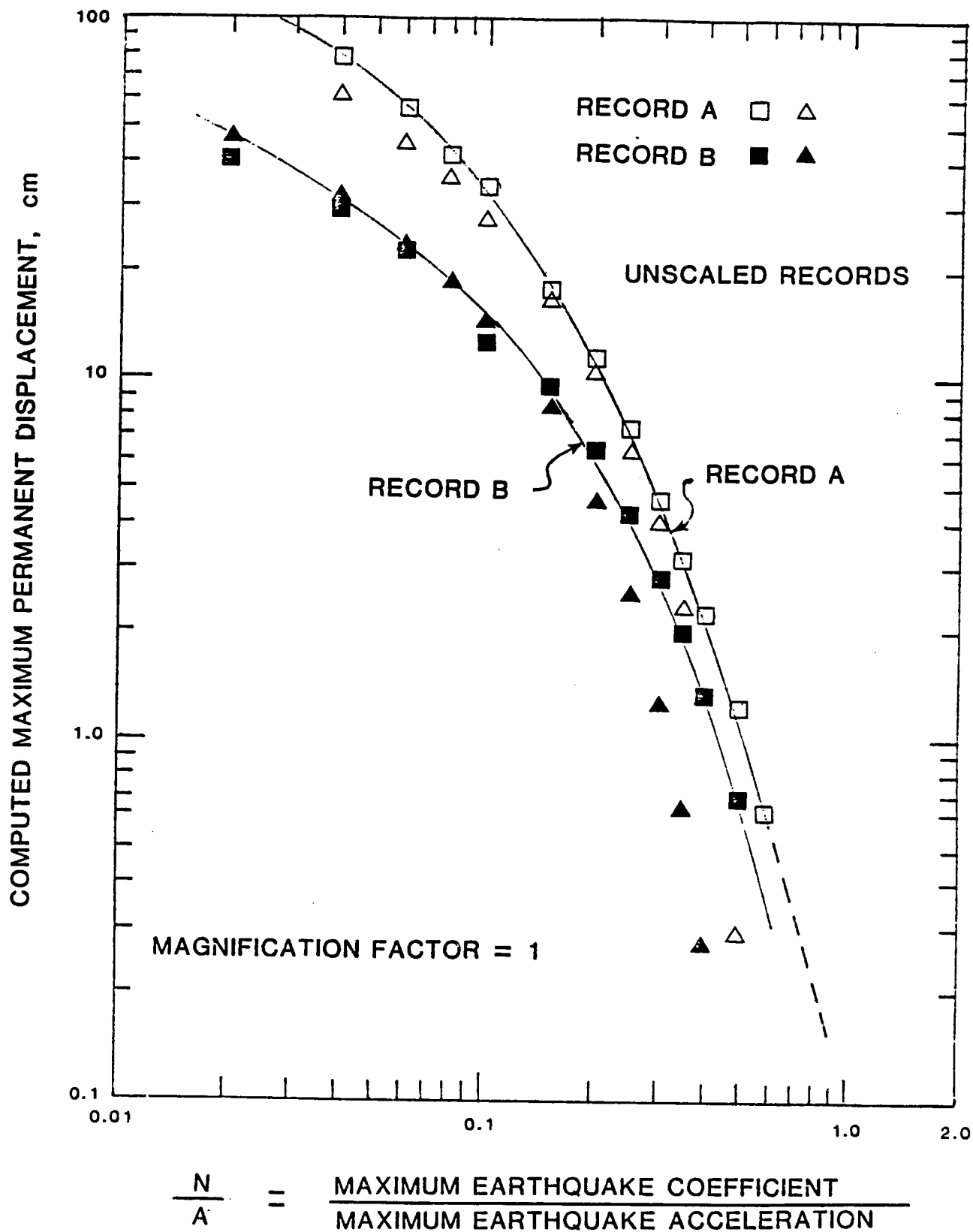


Figure 19. Sliding block analysis - computed permanent displacements for records A and B

# RIGHT WING DAM -- SAFETY FACTOR AGAINST LIQUEFACTION

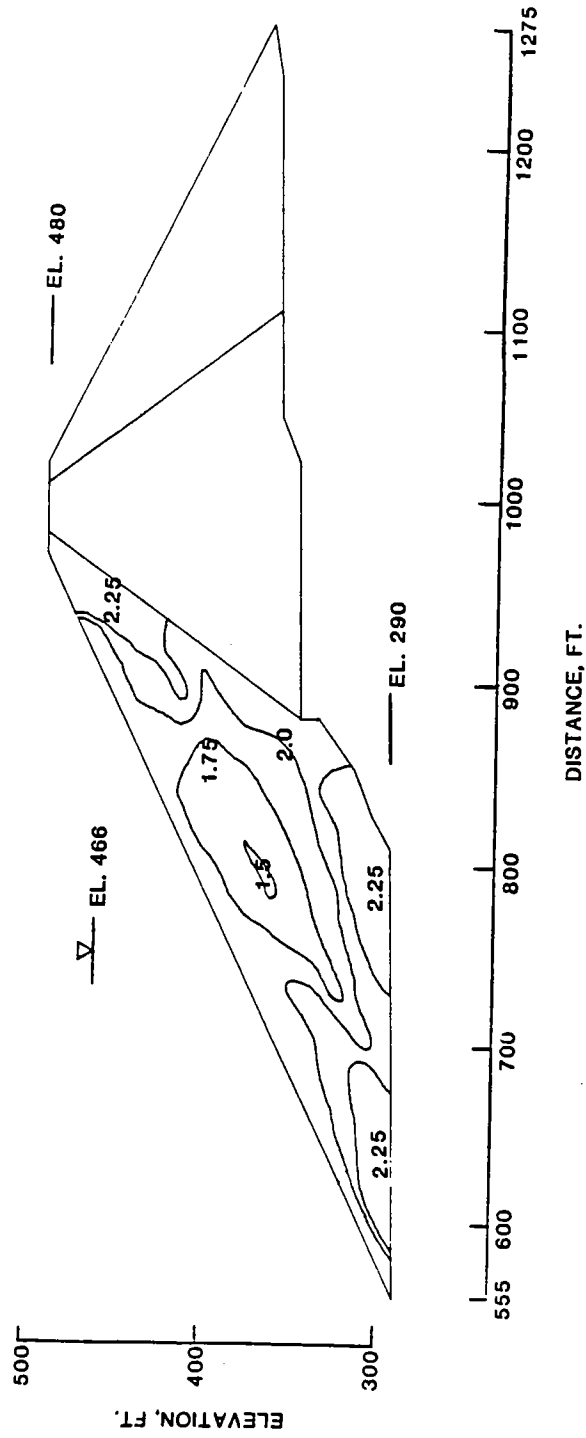


Figure 62. Factors of safety against liquefaction computed for Wing Dam analysis section.

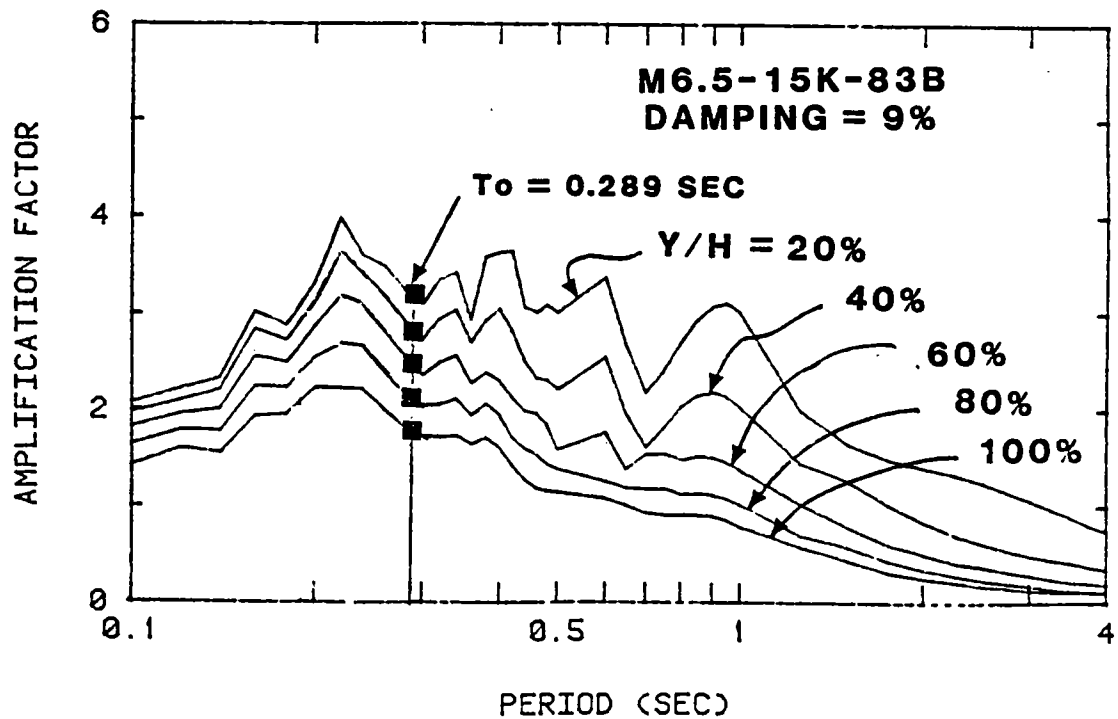
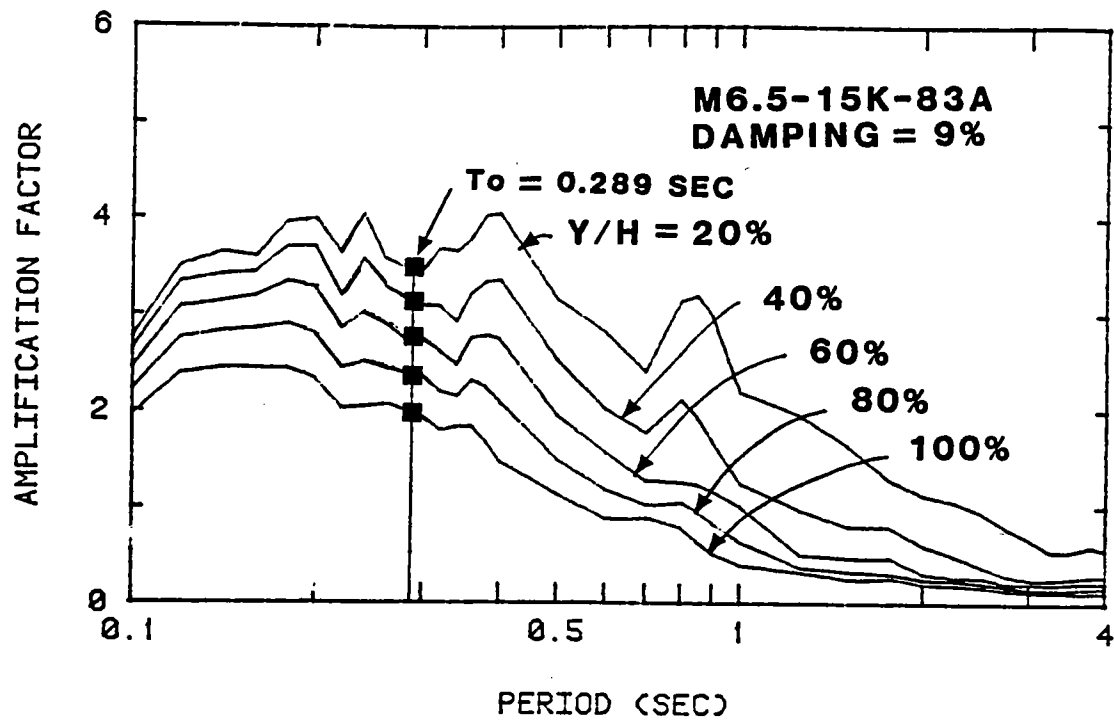


Figure 20. SEISCOE amplification factors from records A and B for embankments founded on rock

# RIGHT WING DAM -- DYNAMIC SHEAR STRESSES COMPUTED BY FLUSH

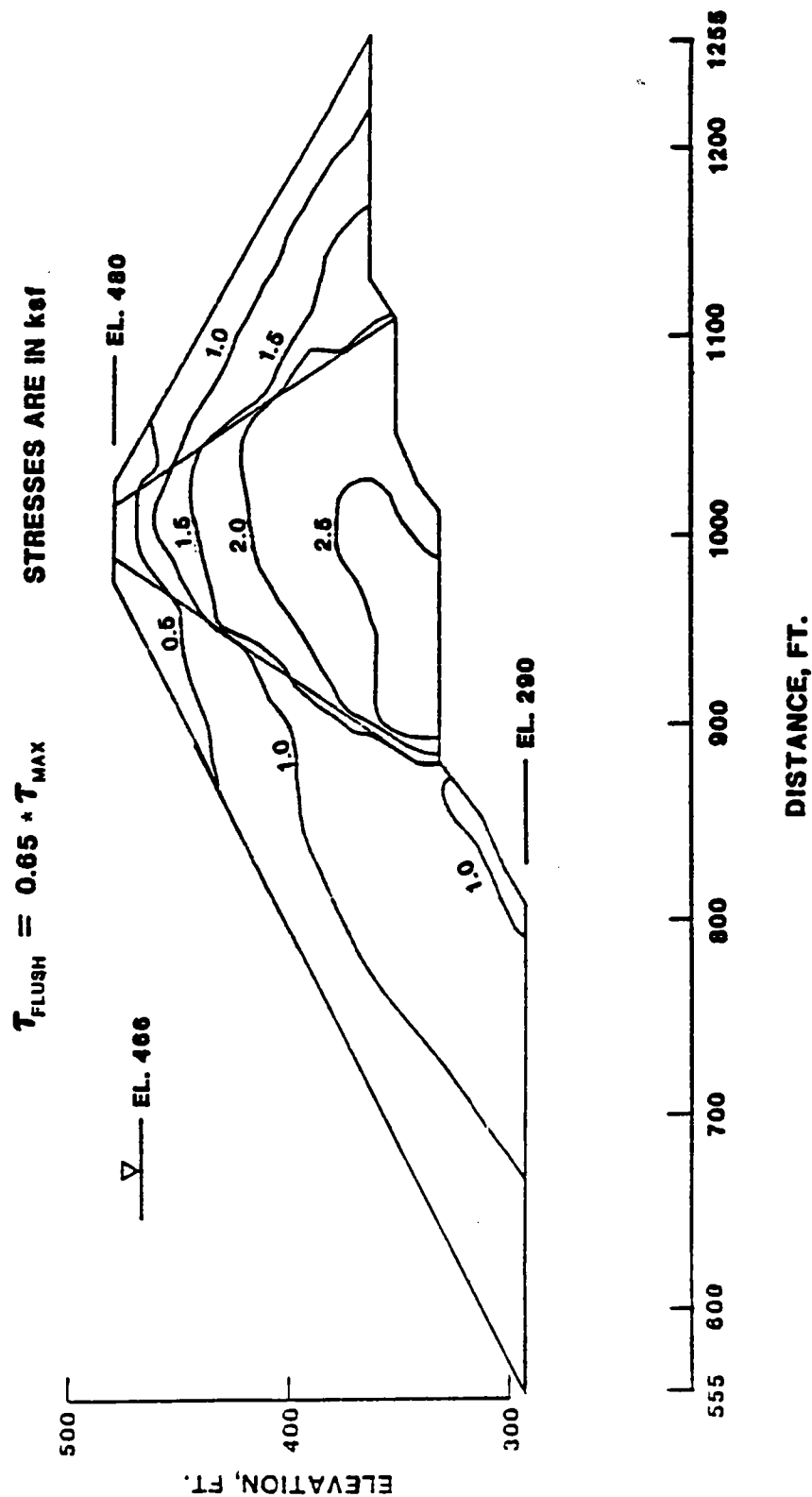


Figure 61. Average earthquake-induced shear stresses,  $\tau_{\text{FLUSH}}$ , computed by FLUSH with Accelerogram B in Wing Dam analysis section.

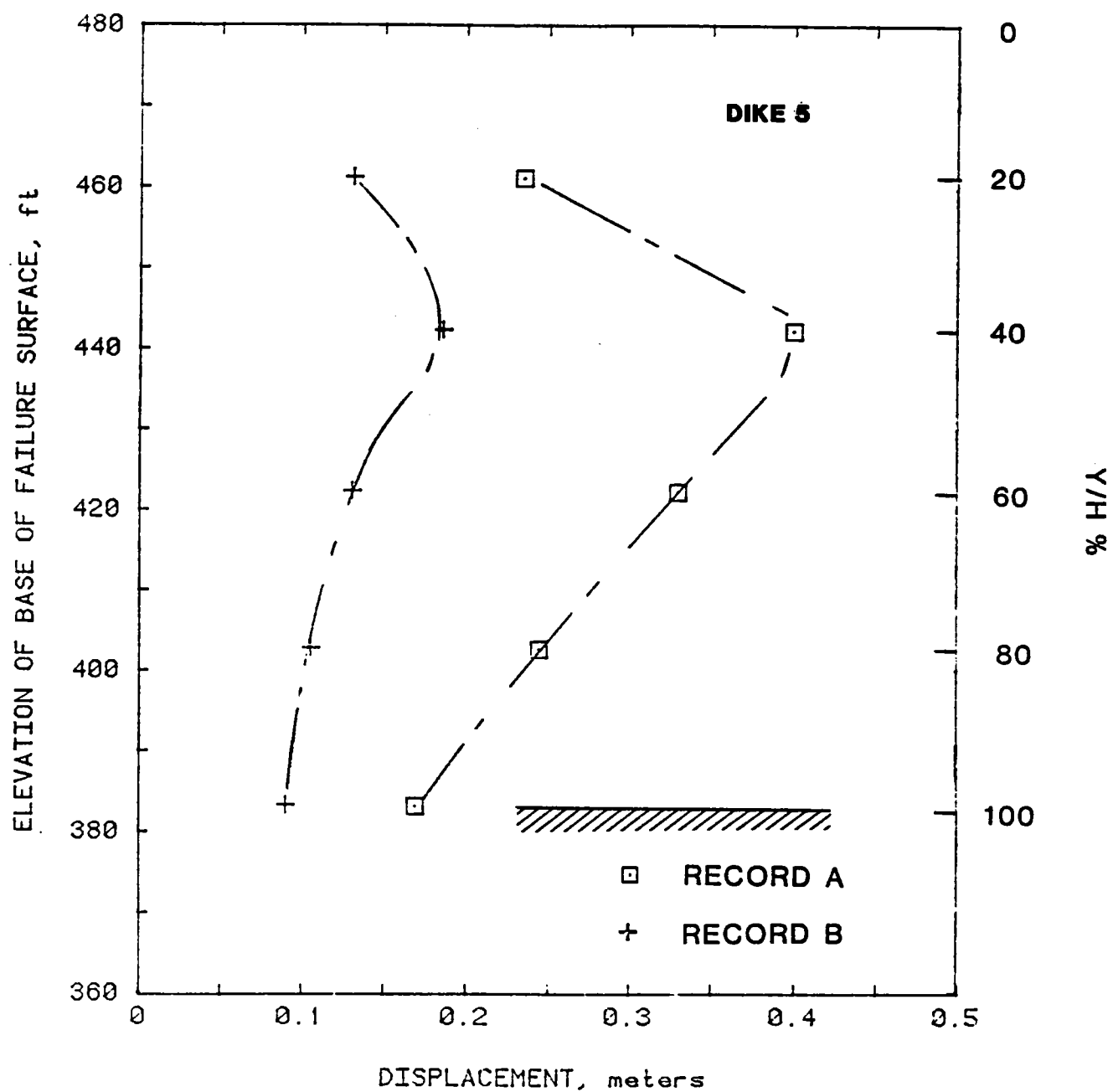


Figure 21. Permanent displacements of potential upstream sliding masses using the Sarma method, DIKE 5

# ACCELERATIONS COMPUTED BY FLUSH

ACCELERATIONS ARE IN g's

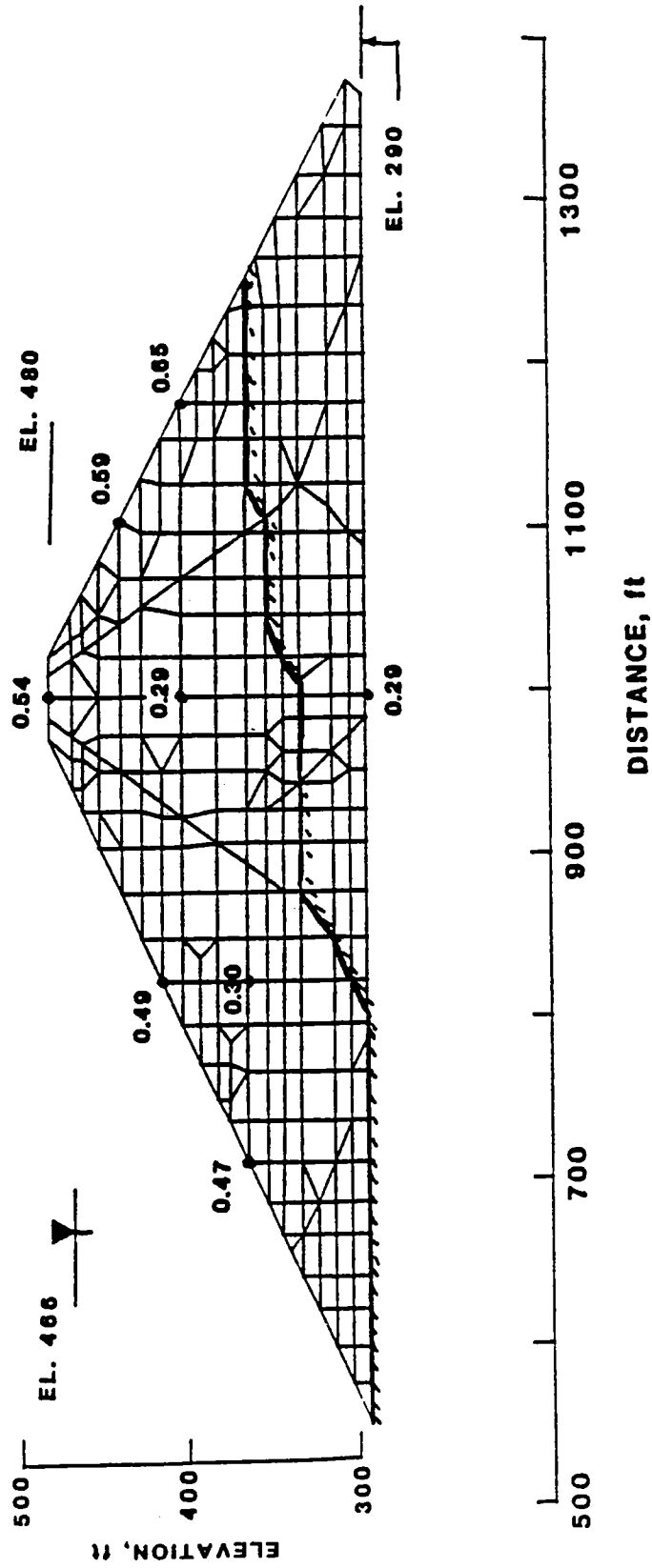


Figure 60. Peak accelerations computed by FLUSH with Accelerogram B in Wing Dam analysis section.

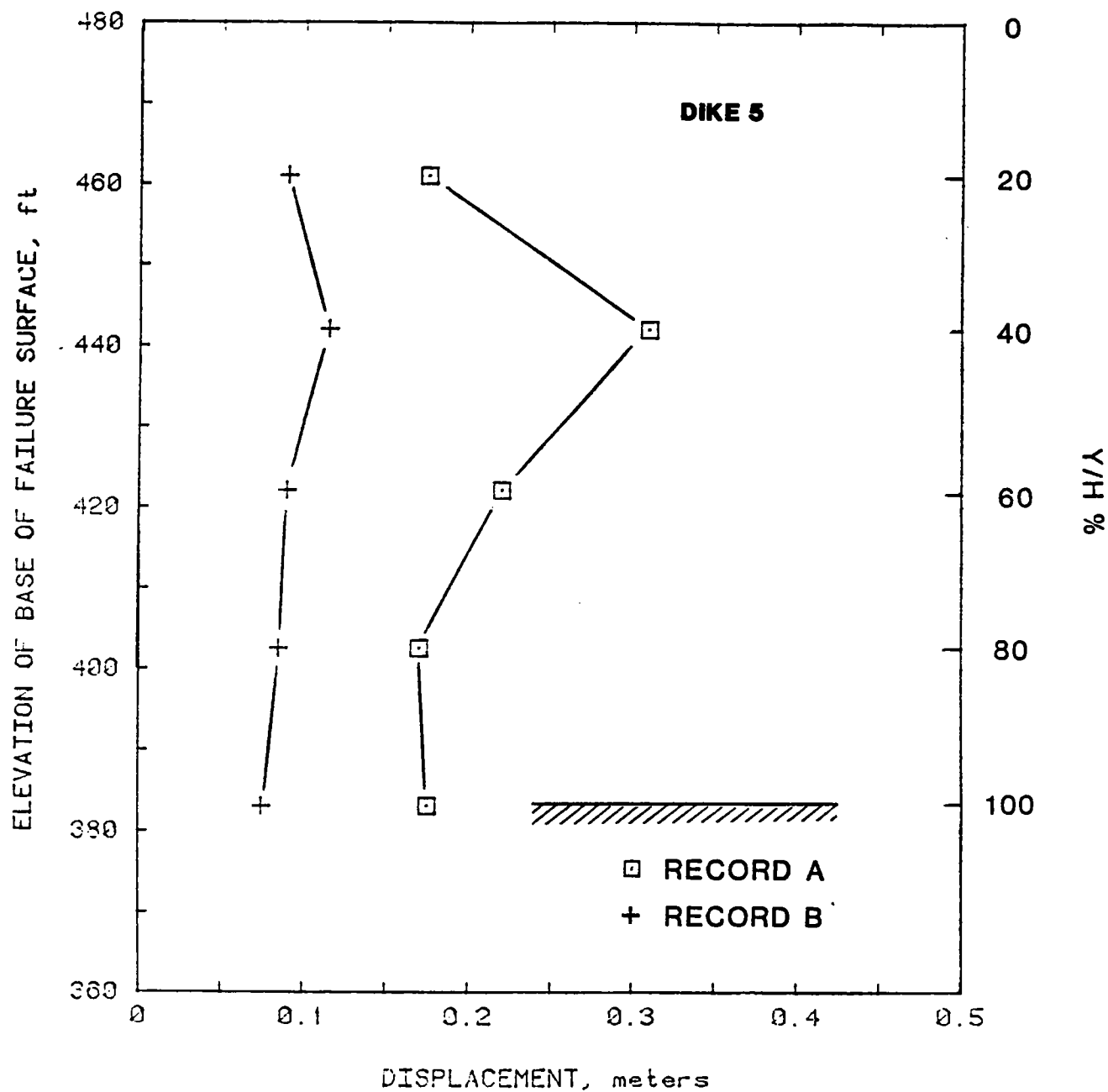
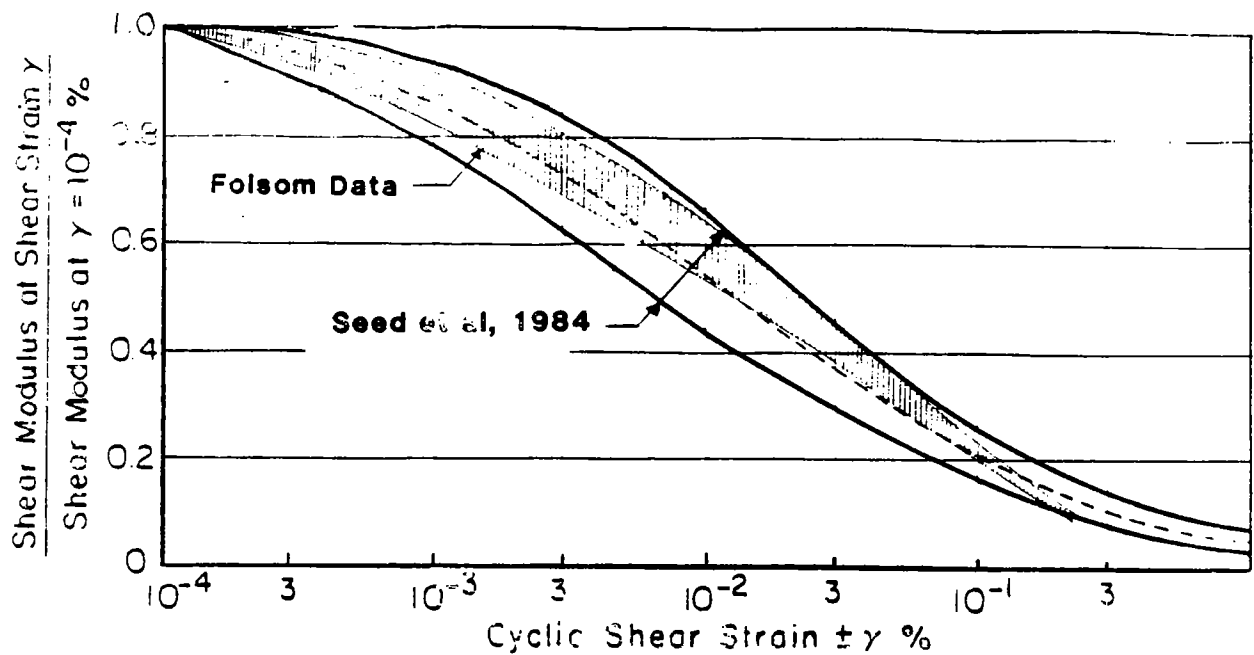
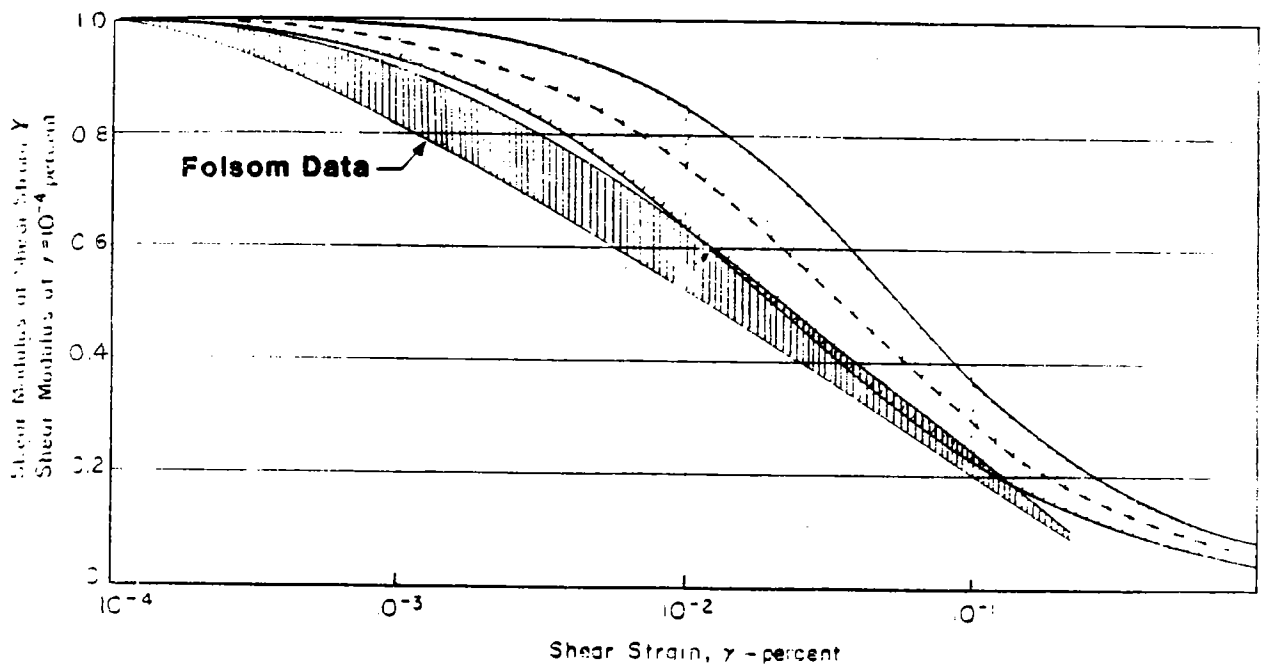


Figure 22. Permanent displacements of potential downstream sliding masses using the Sarma method, DIKE 5



a. Variation of shear modulus with shear strain for gravelly soils



b. Variation of shear modulus with shear strain for sands (after Seed and Idriss, 1970)

Figure 59. Comparison of shear modulus degradation curves from Seed et al. (1984) and Seed et al. (1970) with laboratory test data on Folsom gravels.

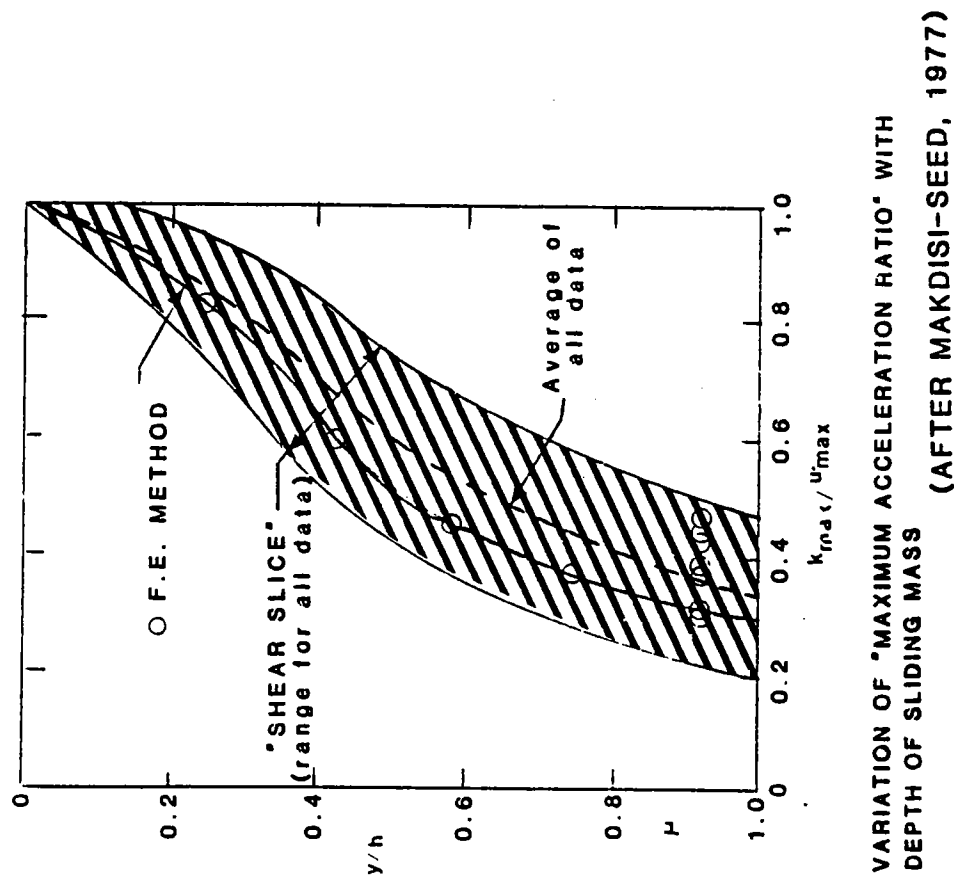
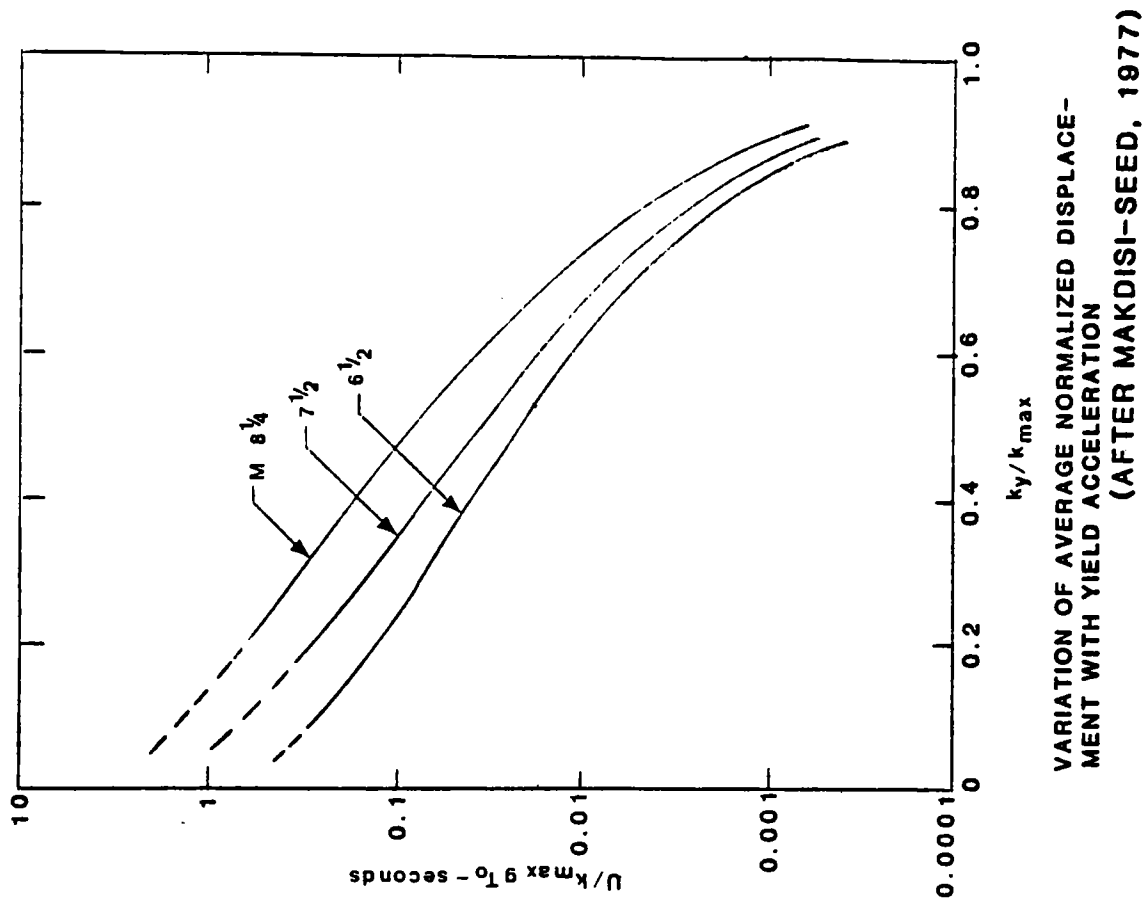


Figure 23. Normalized charts for computing permanent displacements using the Makdisi-Seed Technique

# **DYNAMIC MATERIAL PROPERTIES INPUT TO FLUSH**

**DENSITIES (pcf):**

SHELL (SUB) - 152  
 SHELL (DRY) - 139  
 CORE (SUB) - 142  
 ROCK - 150

**NOTE: ALL VELOCITIES ARE IN fps**

## **SHEAR WAVE VELOCITY DISTRIBUTION**

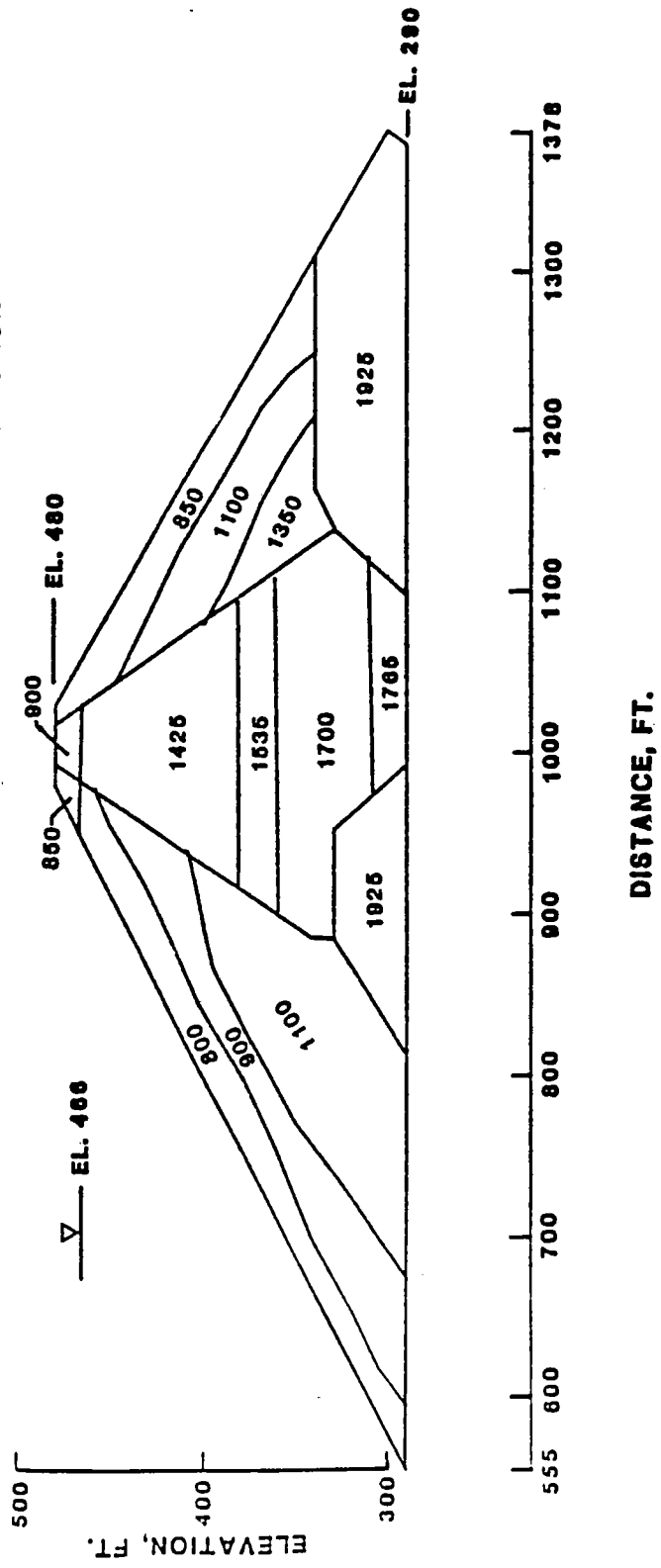


Figure 58. Shear wave velocity distribution in representative cross section, Wing Dam.

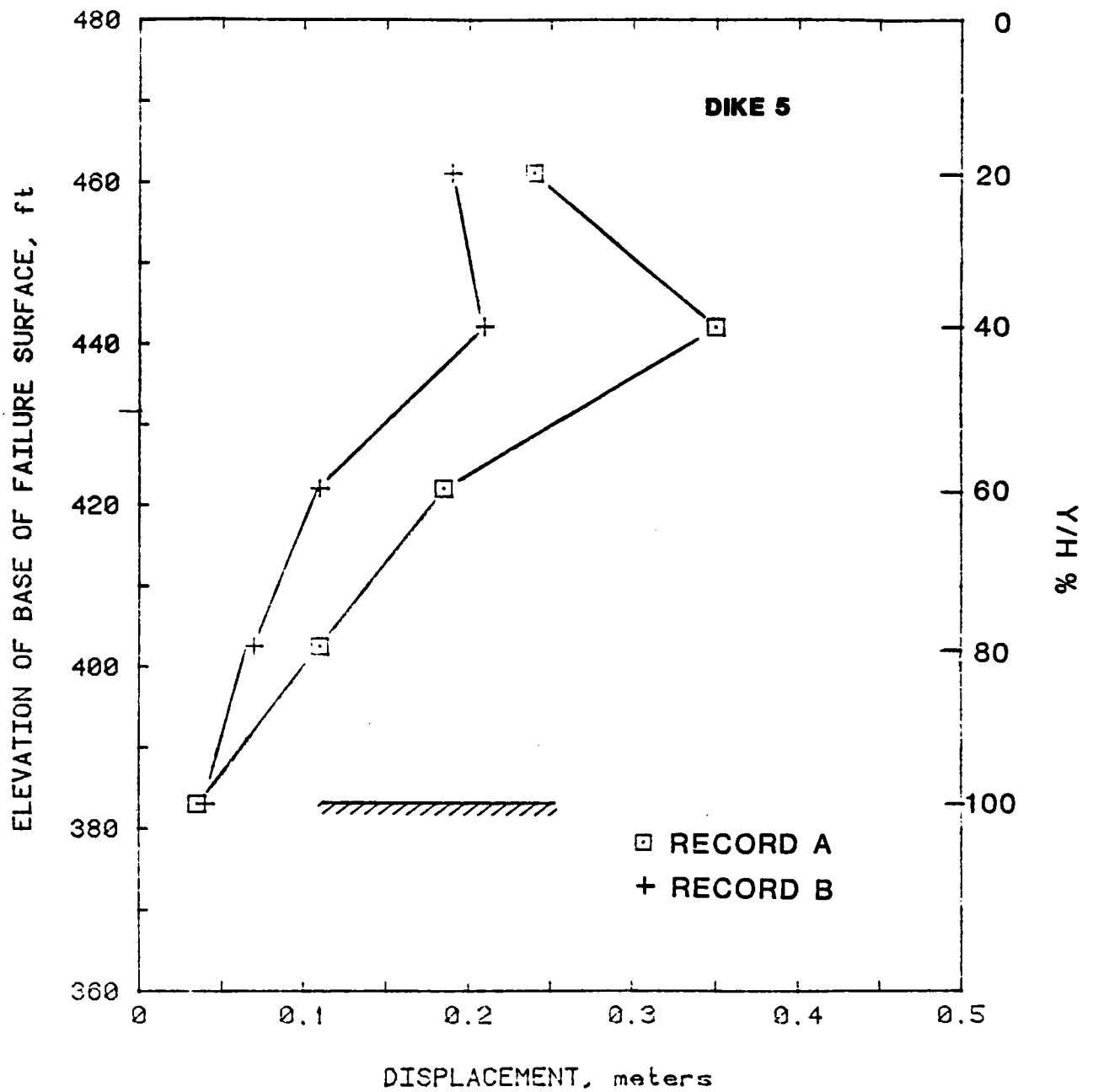


Figure 24. Permanent displacements computed for potential upstream failure masses using Makdisi-Seed Method, Dike 5

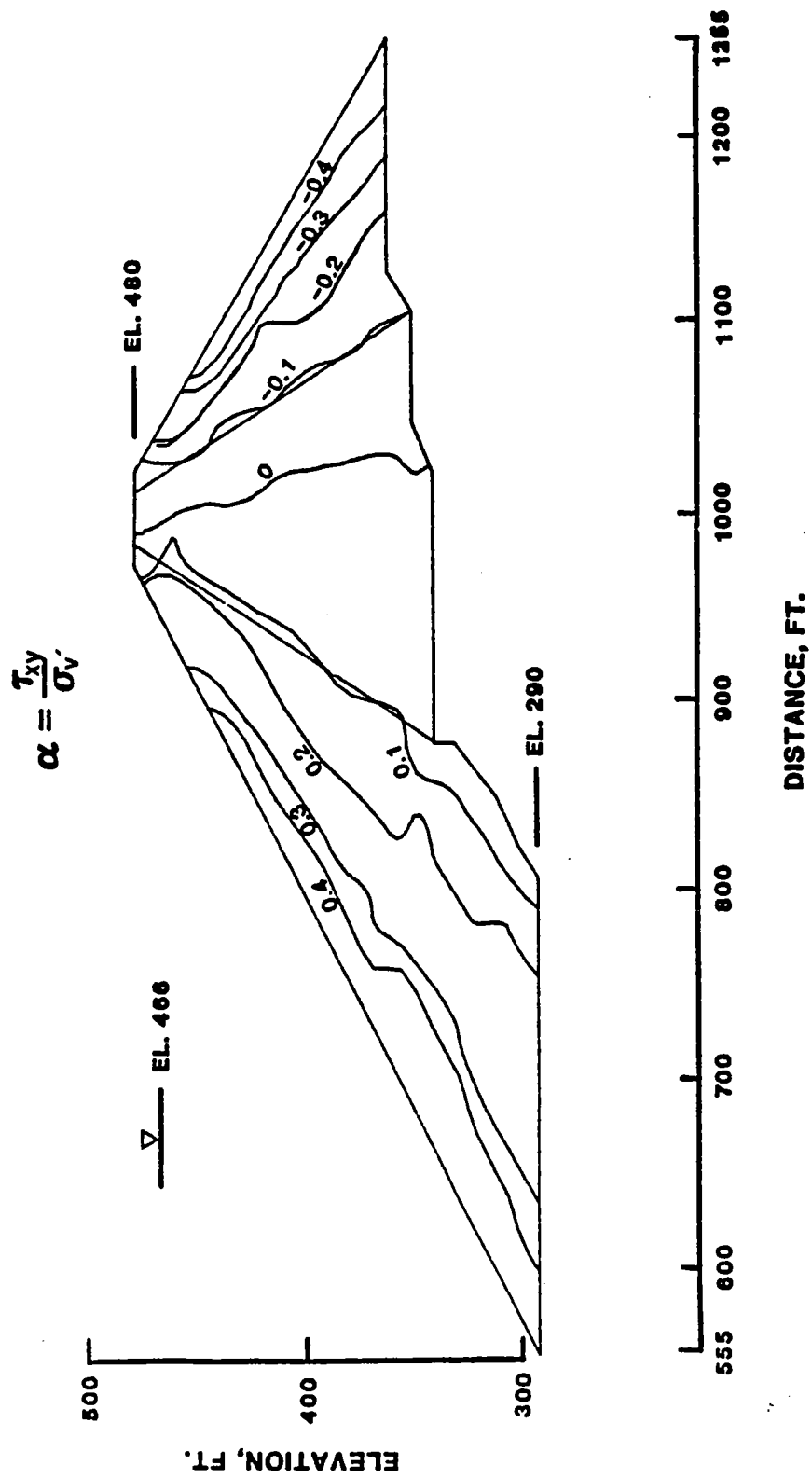


Figure 57. Contours of initial shear stress ratio,  $\alpha$ , for Wing Dam analysis section.

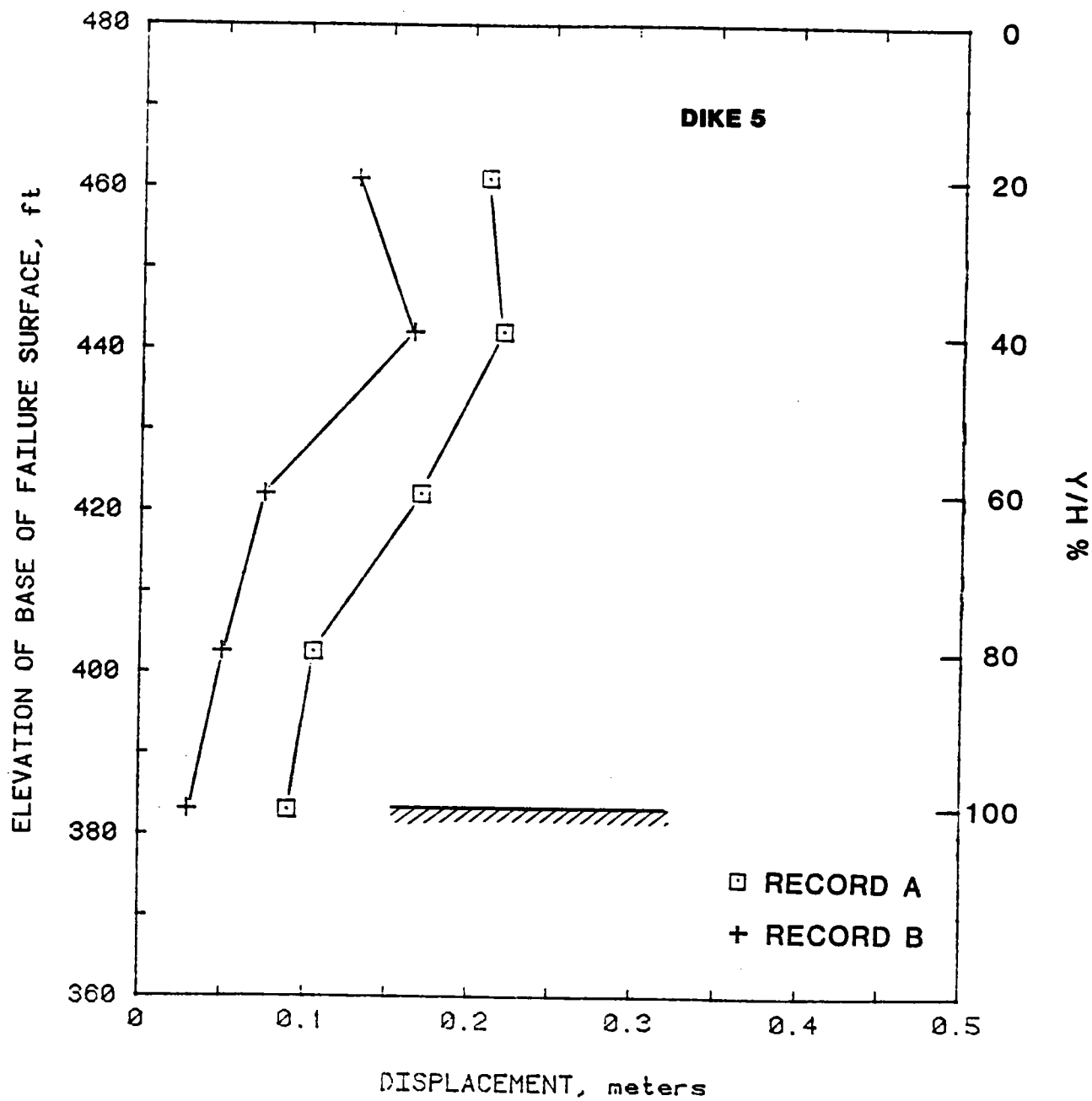


Figure 25. Permanent displacements computed for potential downstream failure masses using Makdisi-Seed Method, Dike 5

STRESSES ARE IN ksi

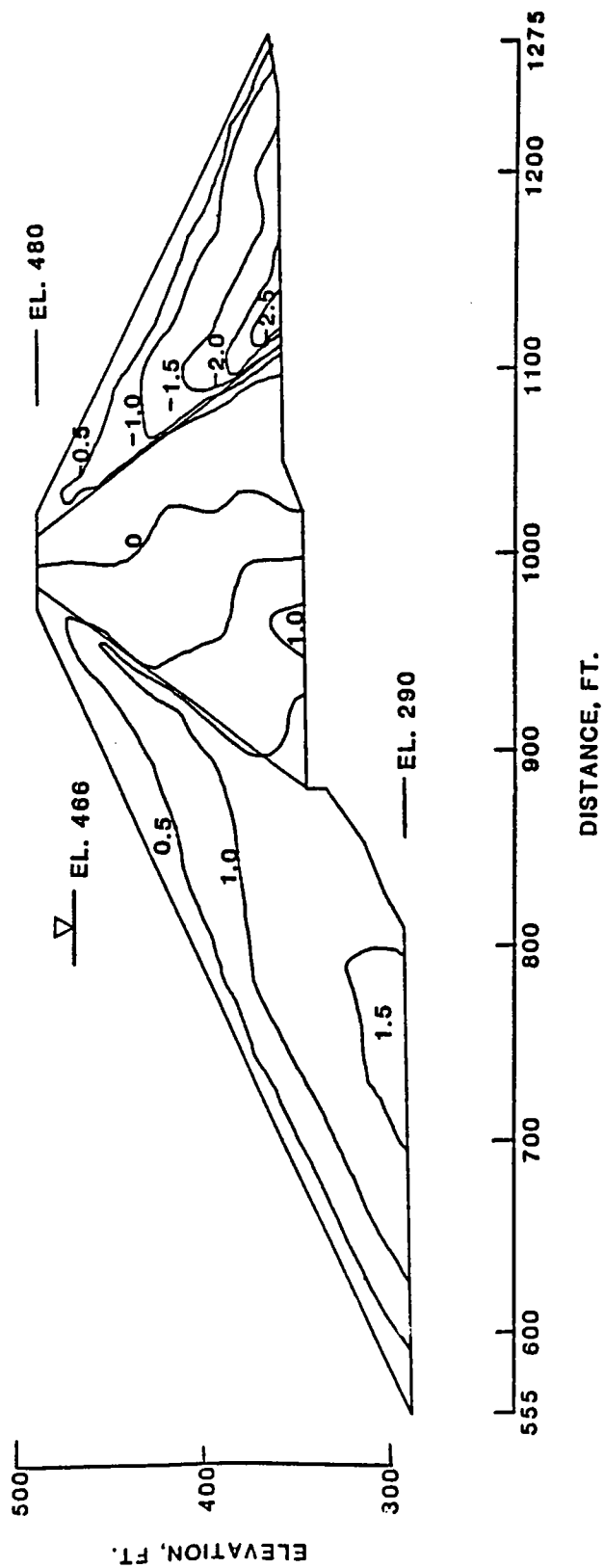


Figure 56. Contours of initial static shear stresses on horizontal planes for Wing Dam analysis section.

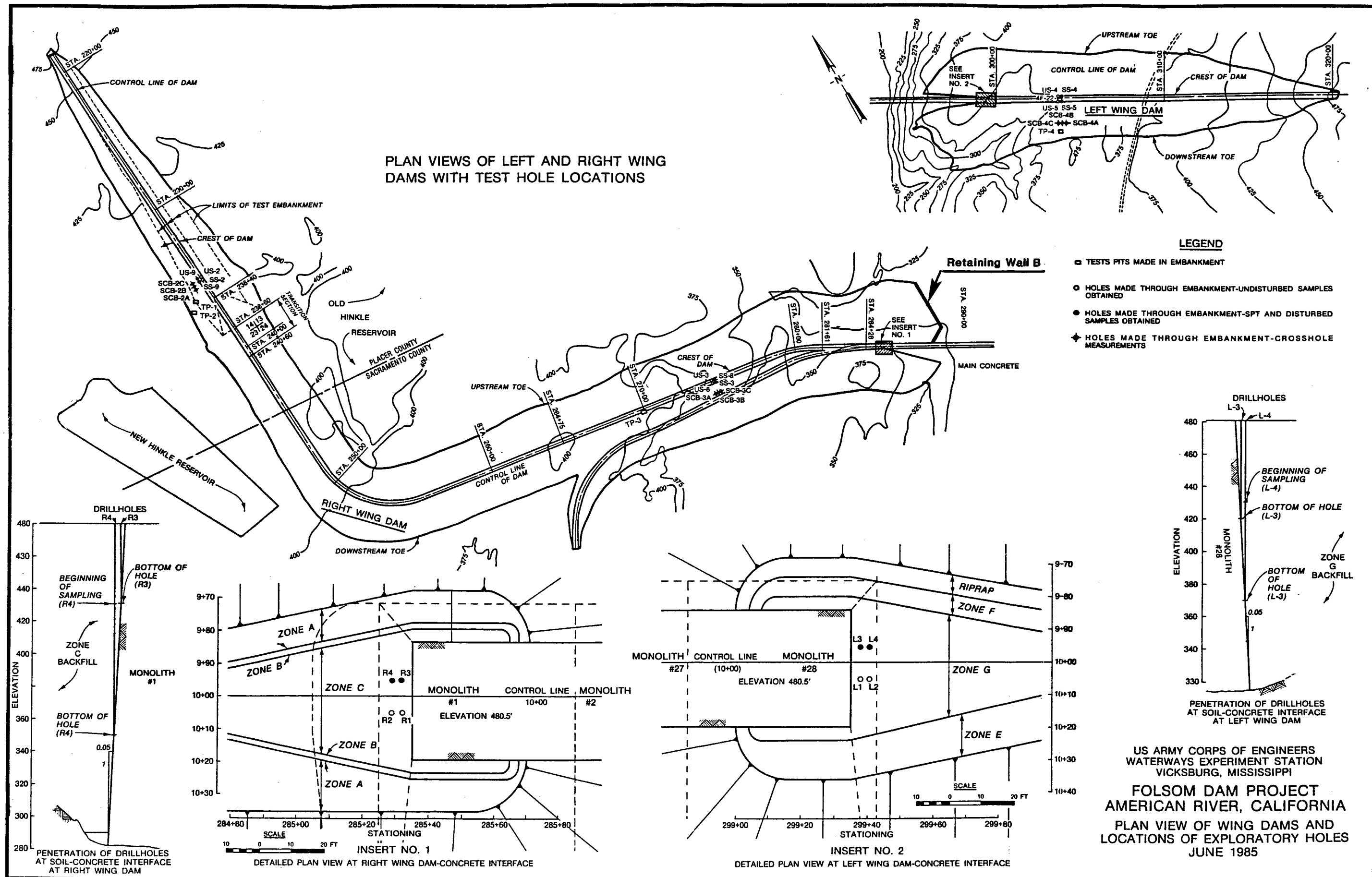


Figure 26. Plan view of Right and Left Wing Dams and detailed plan view of Interface areas.

STRESSES ARE IN  $\text{ksf}$

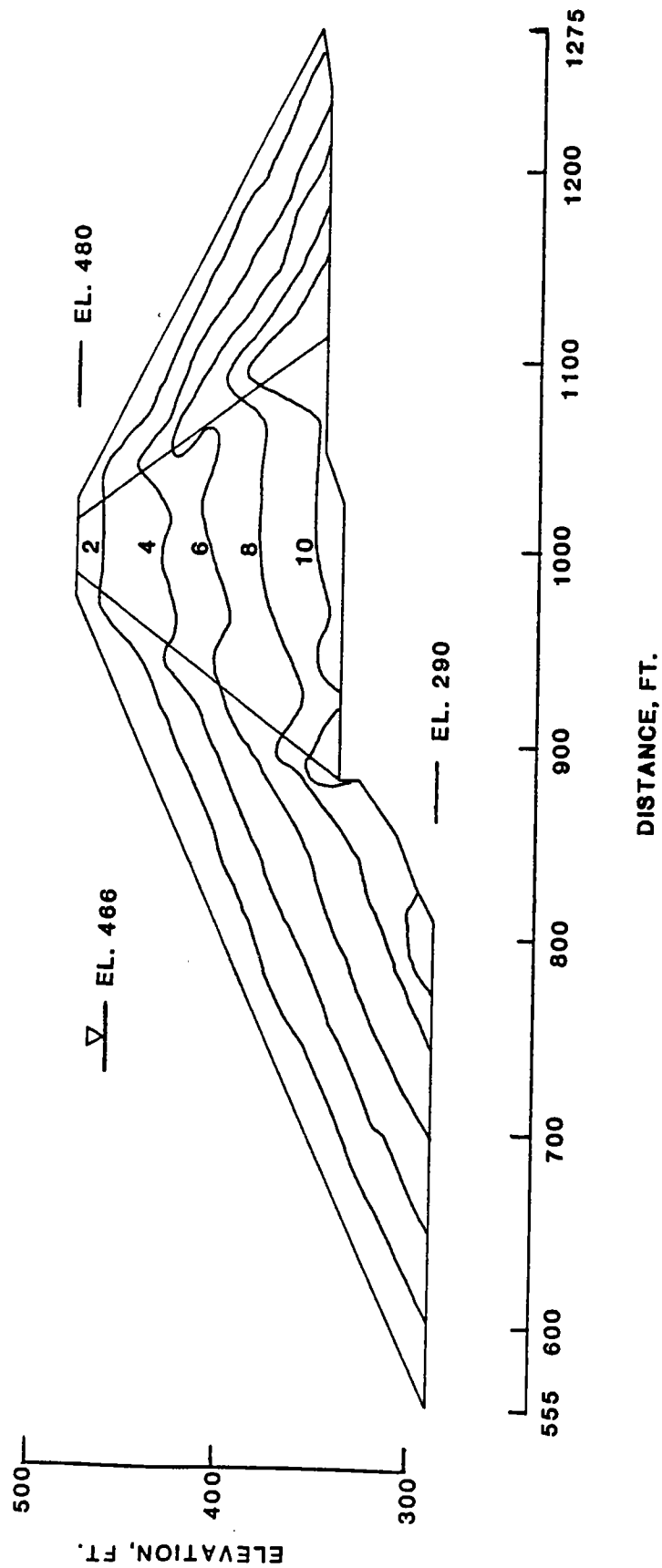


Figure 55. Vertical effective stress contours for Wing Dam analysis section.

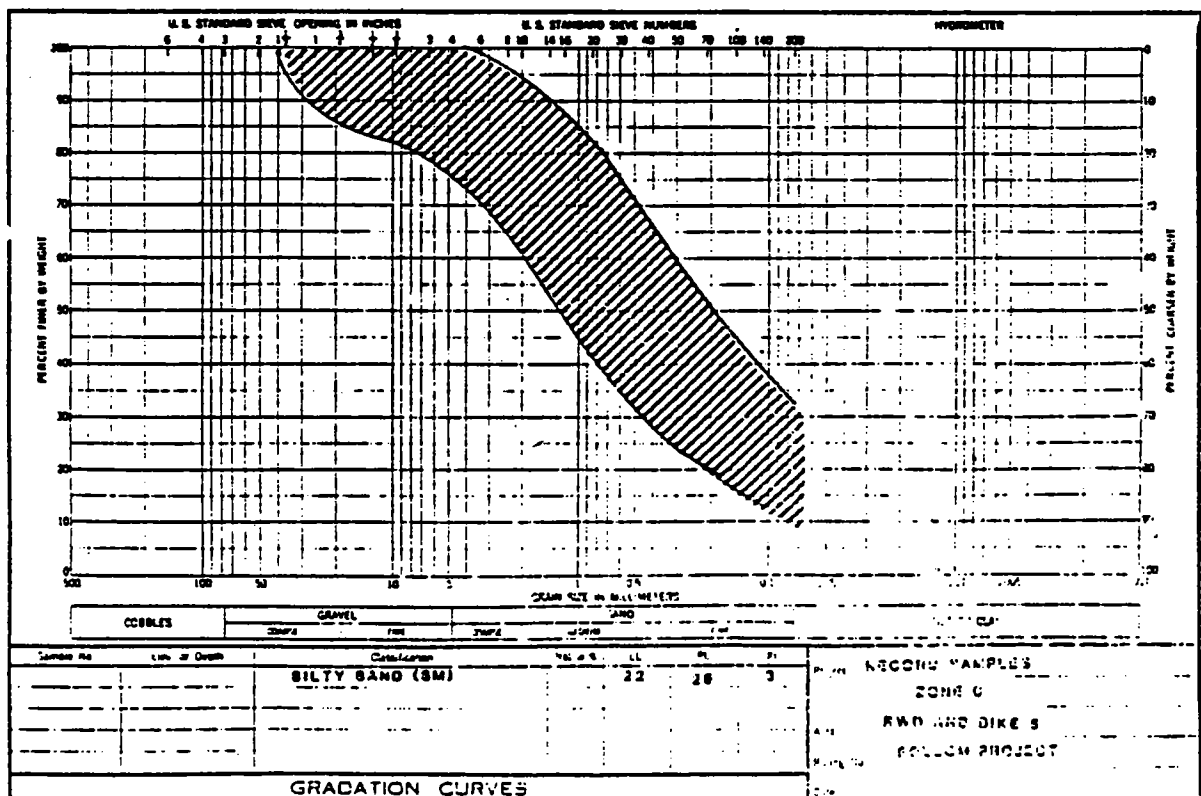
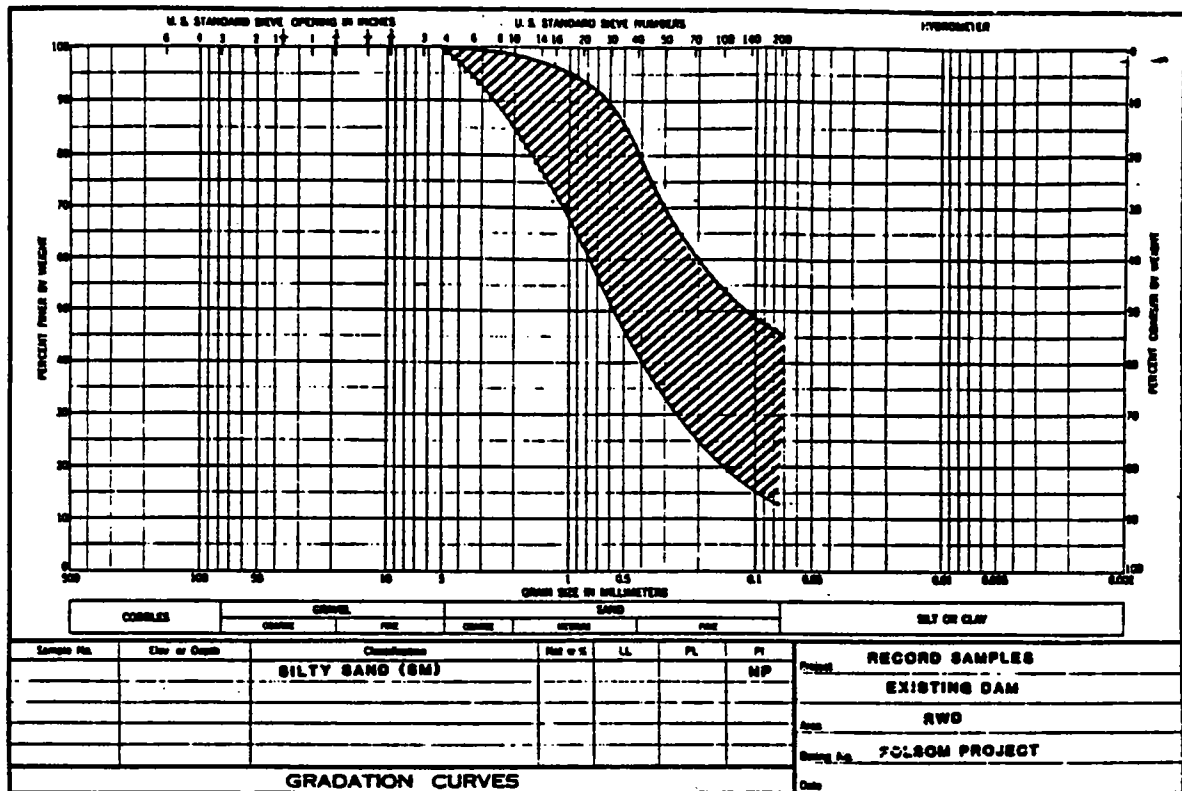


Figure 27. Grain size distribution for materials of Zone C and existing dam in Right Wing Dam.

# FINITE ELEMENT MESH FOR RIGHT WING DAM -

325 ELEMENTS  
343 NODAL POINTS

NOTE: ALL ELEMENTS BELOW LINE ARE SUBMERGED

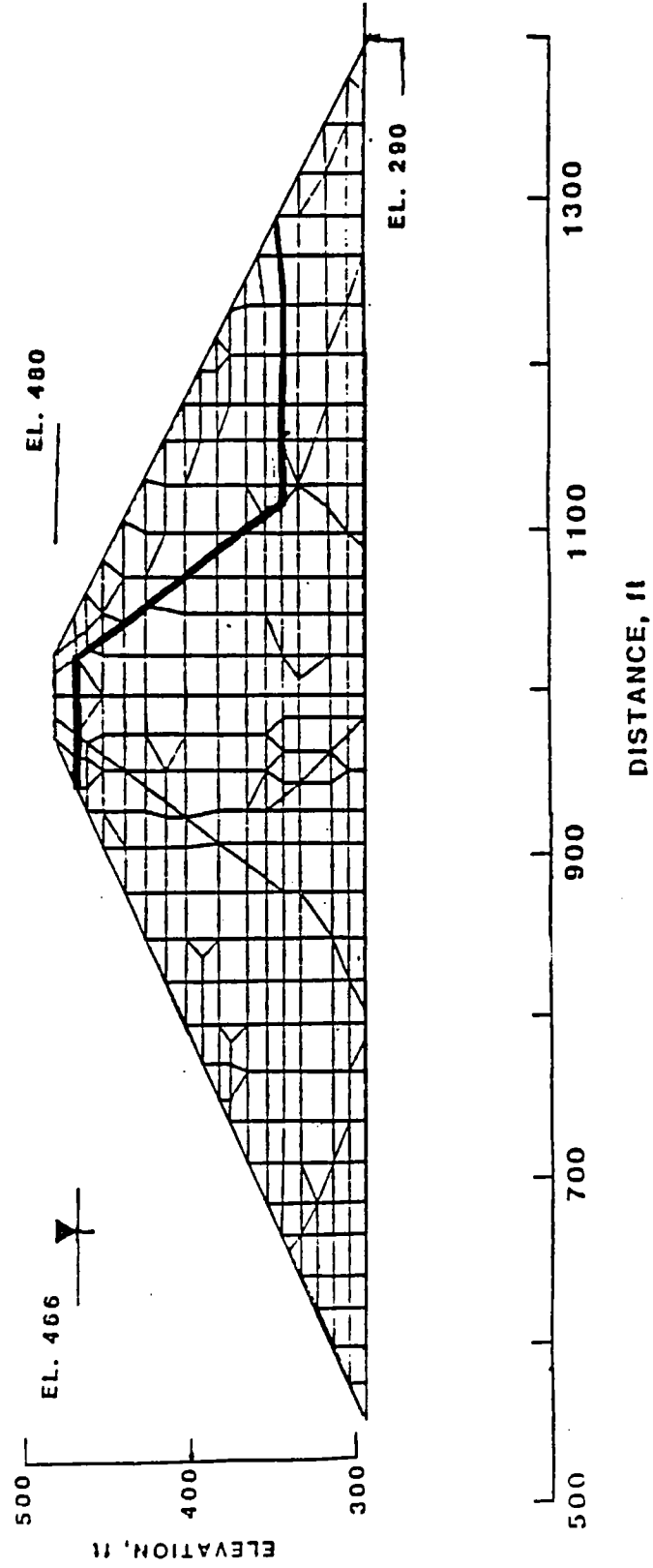
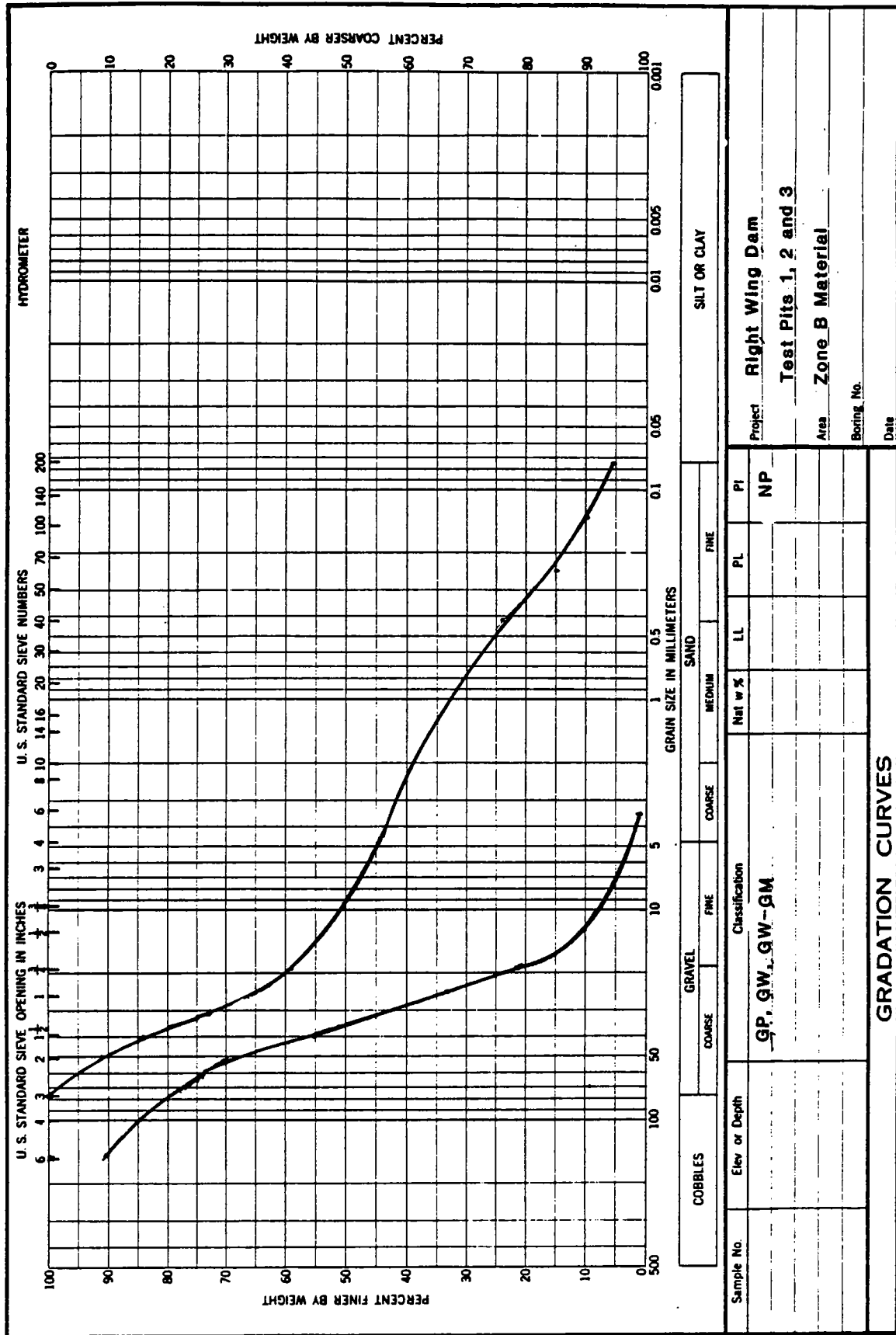
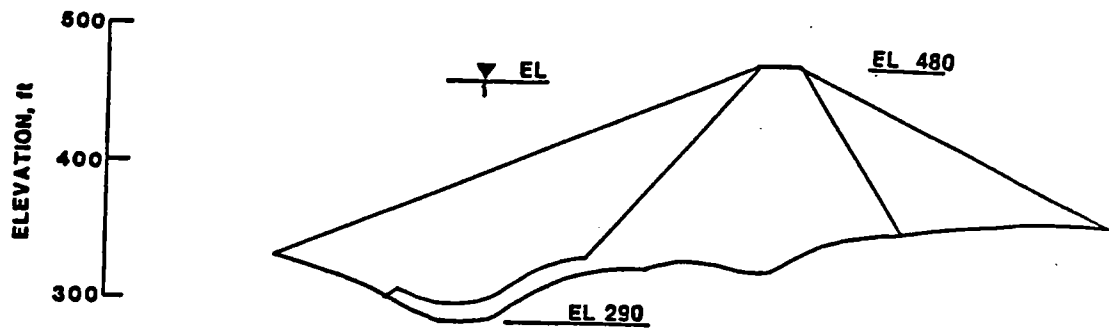


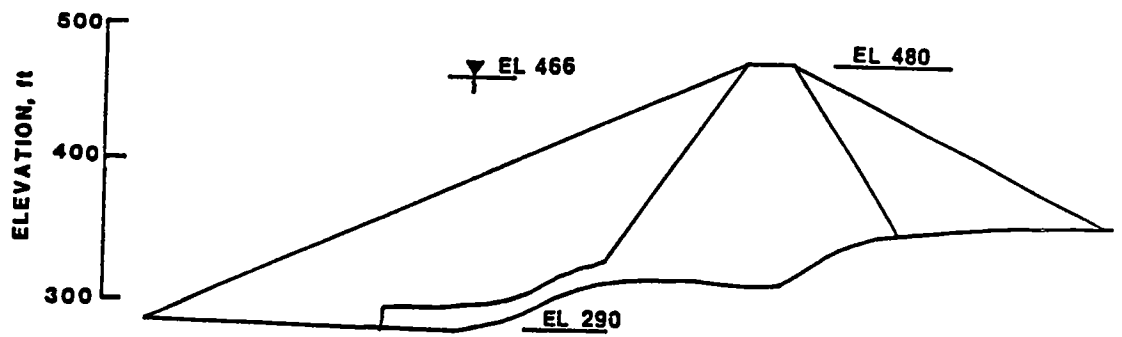
Figure 54. Finite element mesh of representative cross-section for Wing Dams.



ENG FORM 2087 1 MAY 83 Figure 28. Range of gradations observed in Test Pits 1,2 and 3 in Right Wing Dam.



ACTUAL SECTION -



LOCALIZED  
ANALYSIS SECTION - STA - 283 + 00

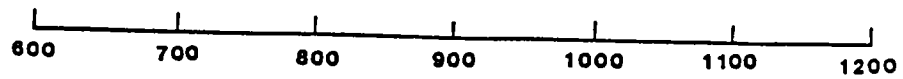


Figure 53. Cross section views of Right Wing Dam, STA 283.

[illegible]

Zone A - Rock From the American river channel

Zone B - Unprocessed sand, gravel, and cobbles from American river channel excavation

Zone C - Decomposed granite from Borrow Area No. 2 and suitable fine-grained river channel excavation

**Figure 29. Section of Right Wing Dam at Station 235+00.**

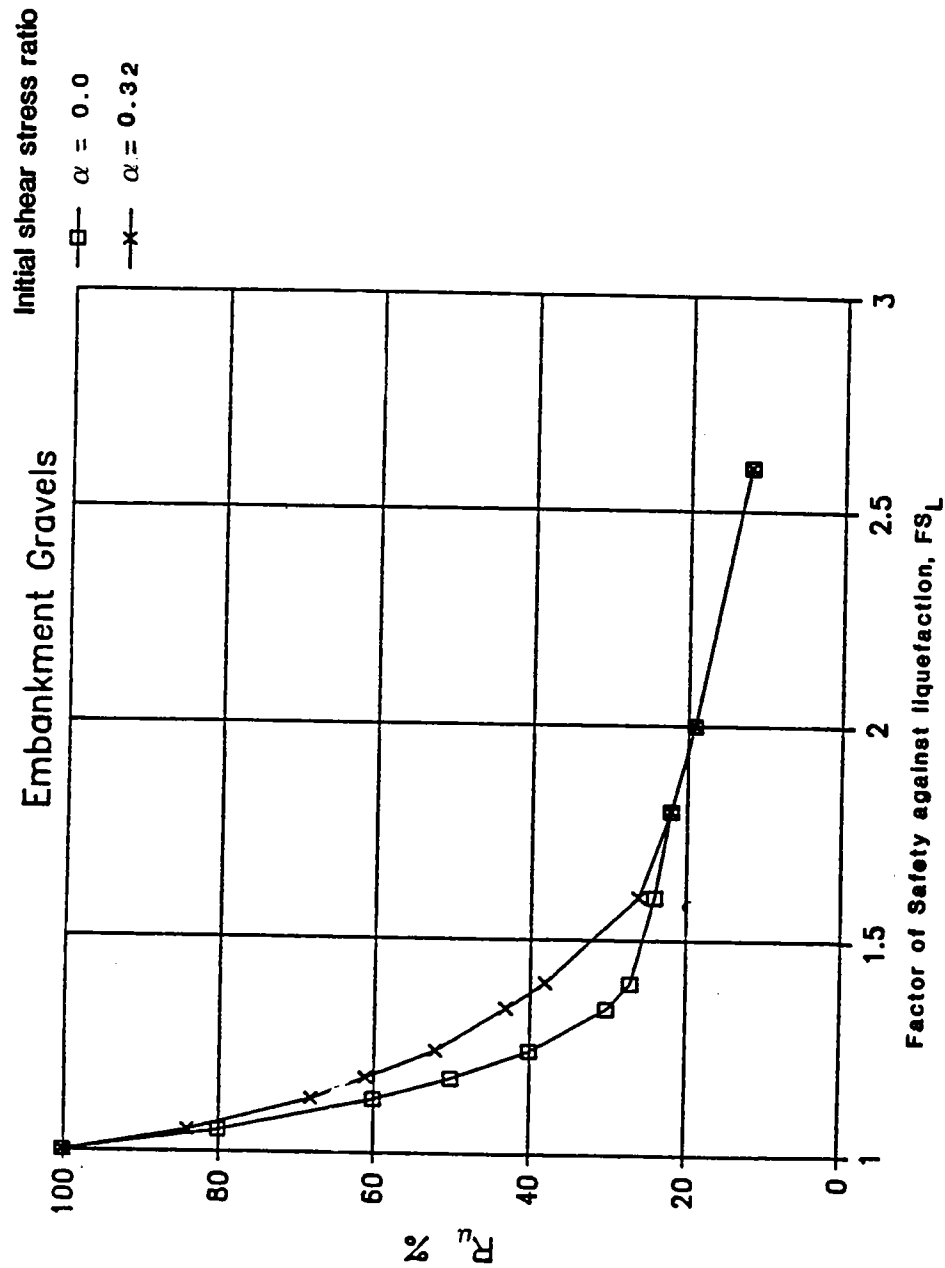
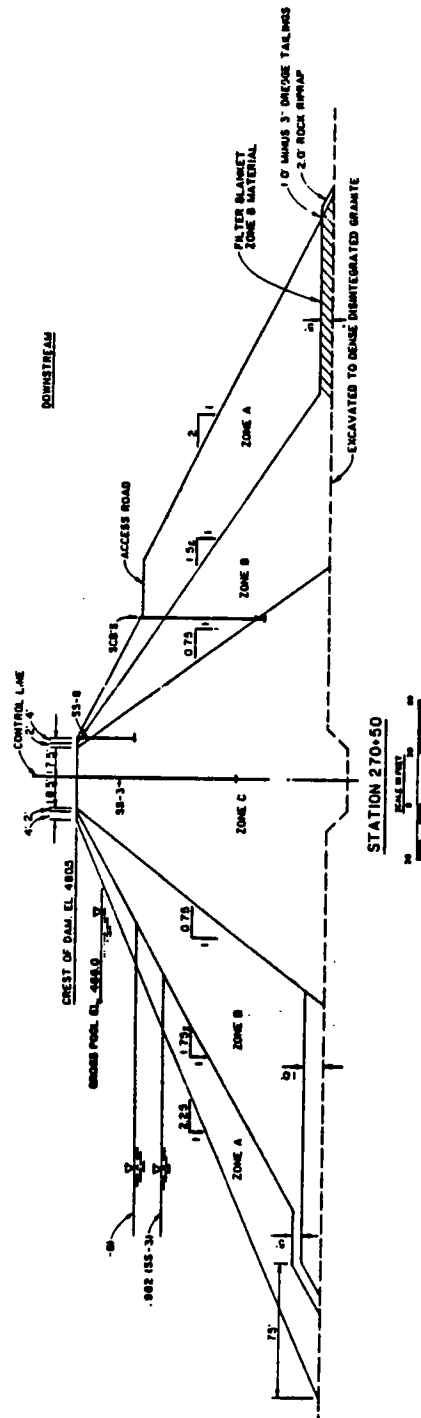


Figure 52. Residual excess pore pressure ratio,  $R_{U'}$ , and corresponding values of Factors of Safety against liquefaction,  $FS_L$ , estimated from laboratory tests on Folsom gravels, for initial shear stress ratios of  $\alpha=0.0$  and  $\alpha=0.32$ .



#### Material Descriptions

- Zone A - Rock From the American river channel
- Zone B - Unprocessed sand, gravel, and cobbles from American river channel excavation
- Zone C - Decomposed granite from Borrow Area No. 2 and suitable fine-grained river channel excavation

Figure 30. Section of Right Wing Dam through Station 270+50.

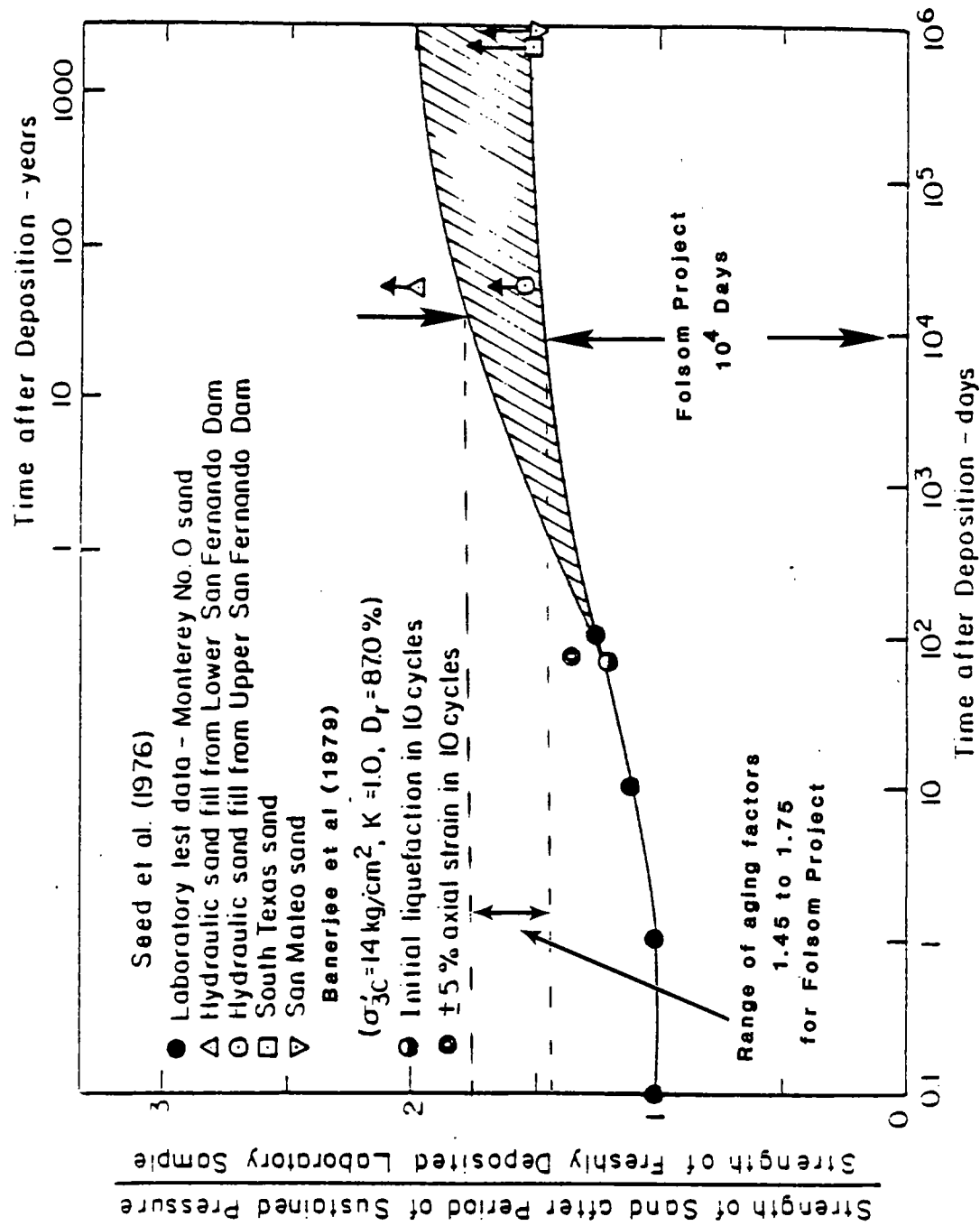
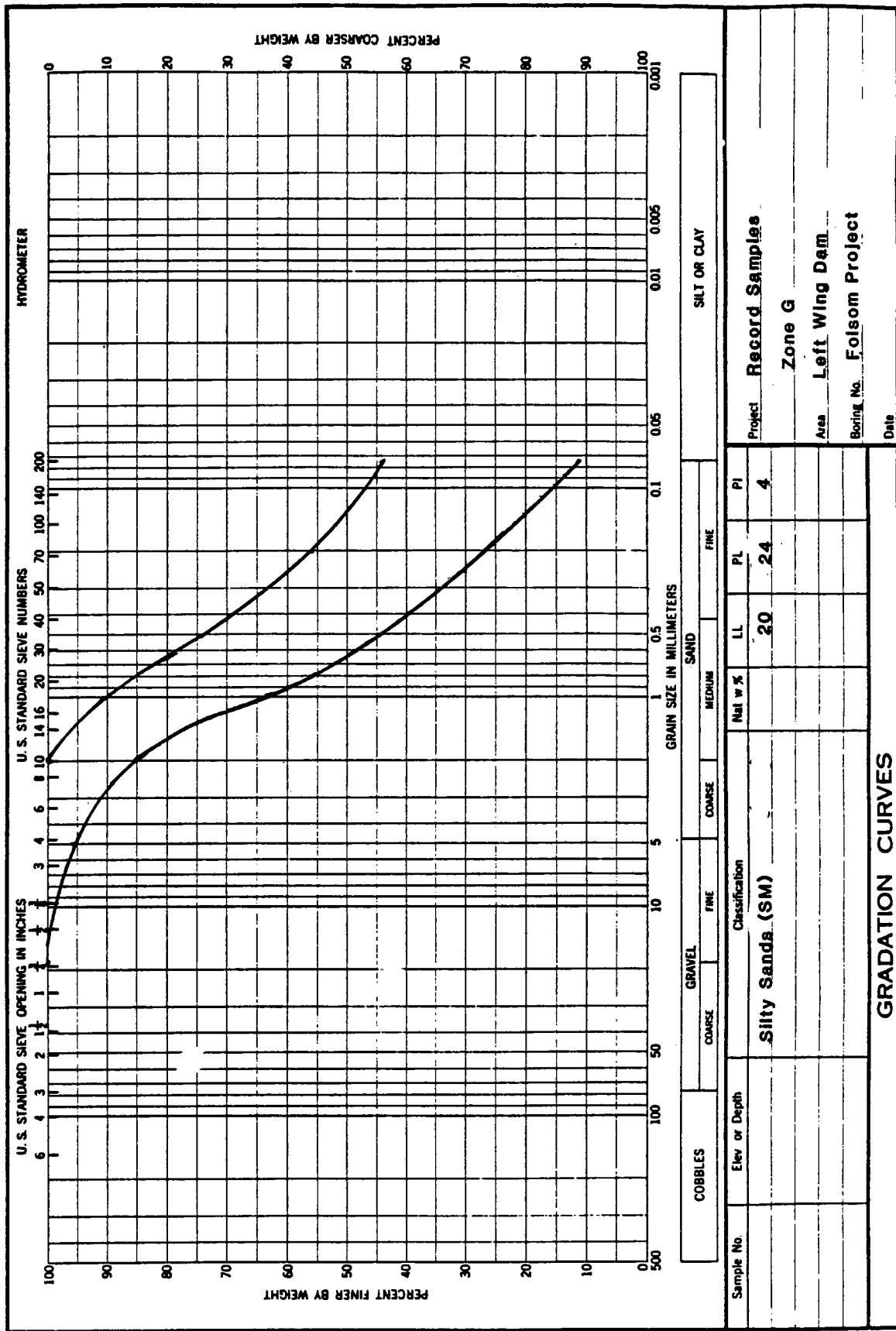


Figure 51. Influence of period of sustained pressure on stress ratio required to cause pore-water pressure of 100% or 2.5 to 5.0 strain in 10 cycles (from Banerjee, Seed, and Chan, 1979).



ENG FORM 2087 1 MAY 63 Figure 31. Range of gradations observed in record samples from Zone G, core of Left Wing Dam.

# ADJUSTMENT FACTOR

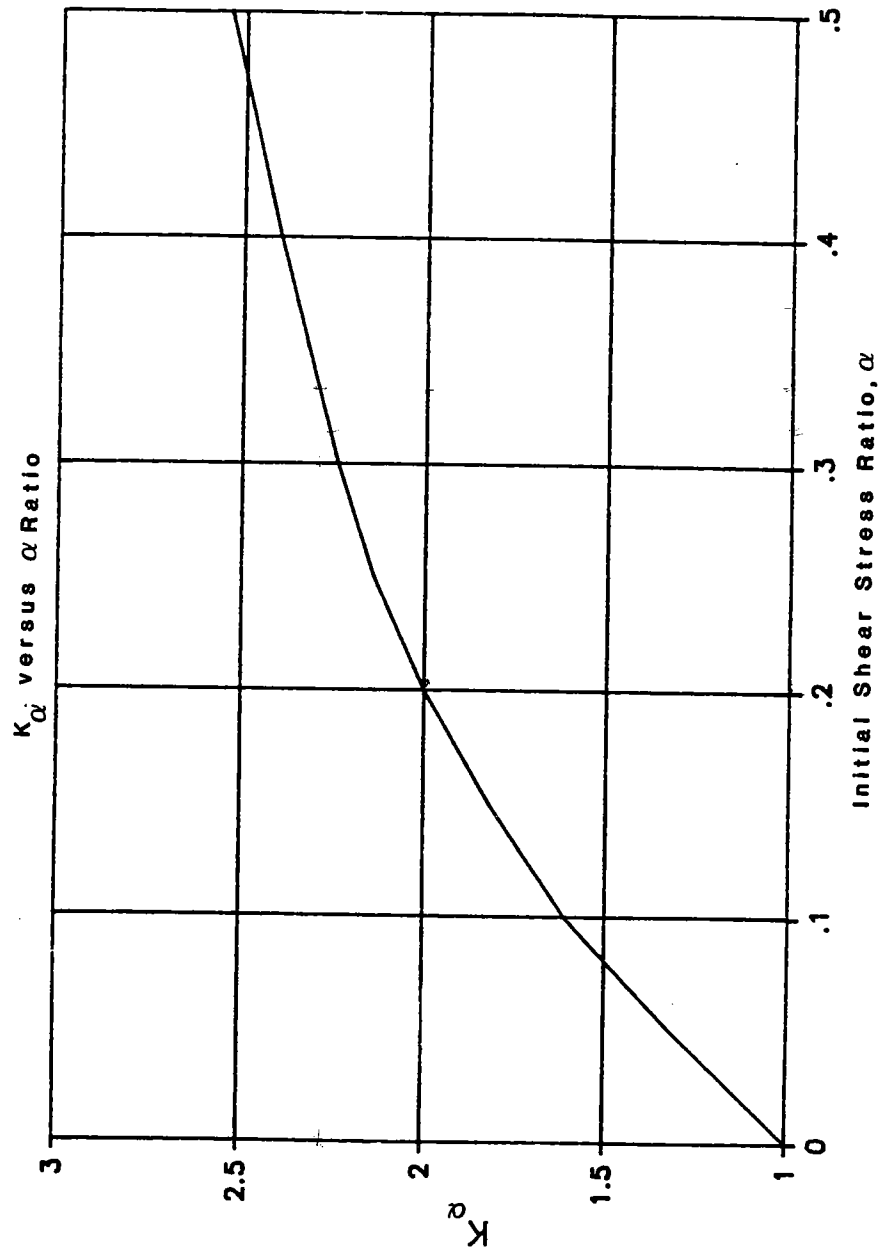
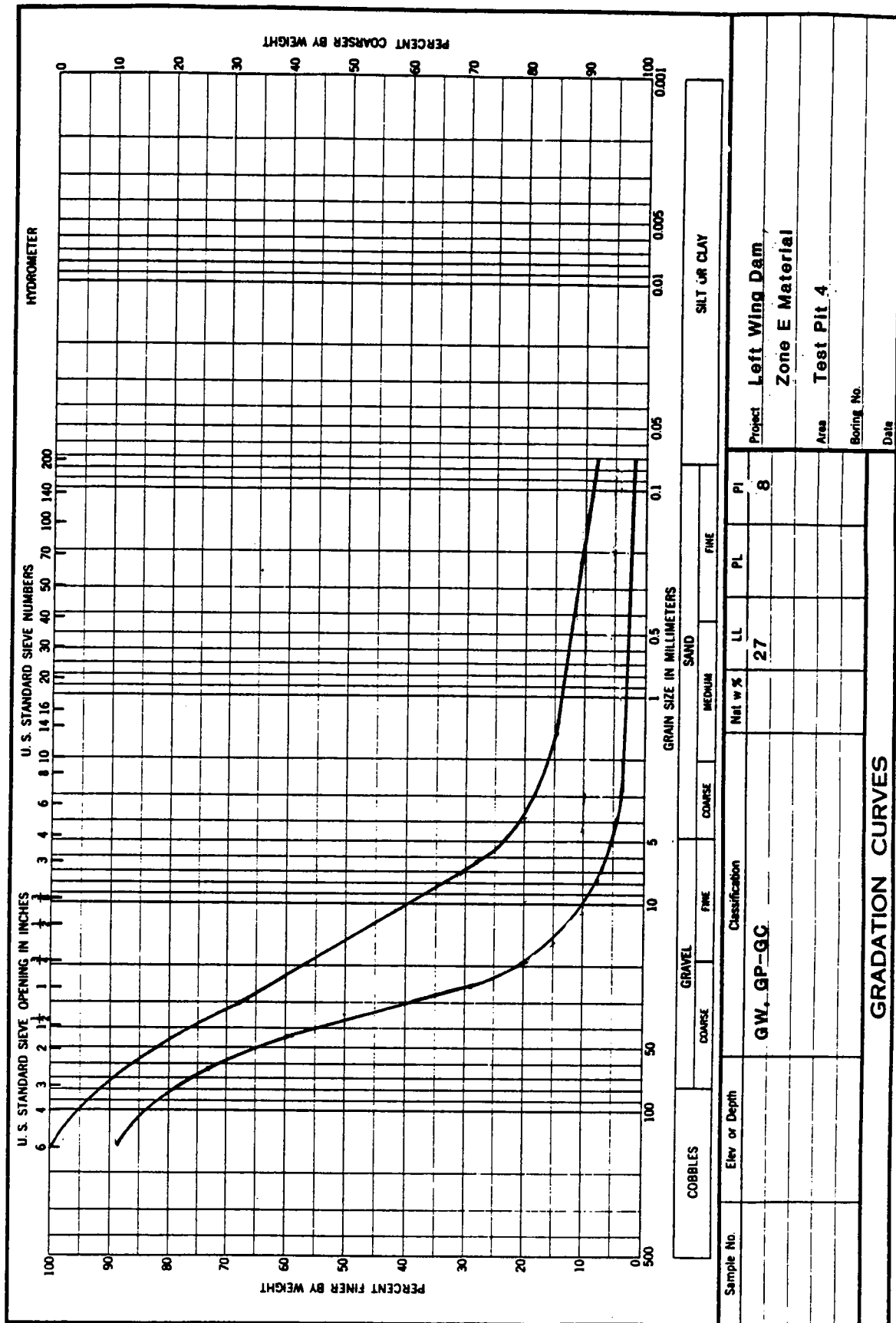


Figure 50. Adjustment factor,  $K_{\alpha}$ , for change in cyclic stress ratio required to cause  $R_u = 100$  with change in initial shear stress ratio,  $\alpha$ , determined from laboratory tests on Folsom gravels.



# ADJUSTMENT FACTOR

$K_G$  versus Vertical Effective Stress

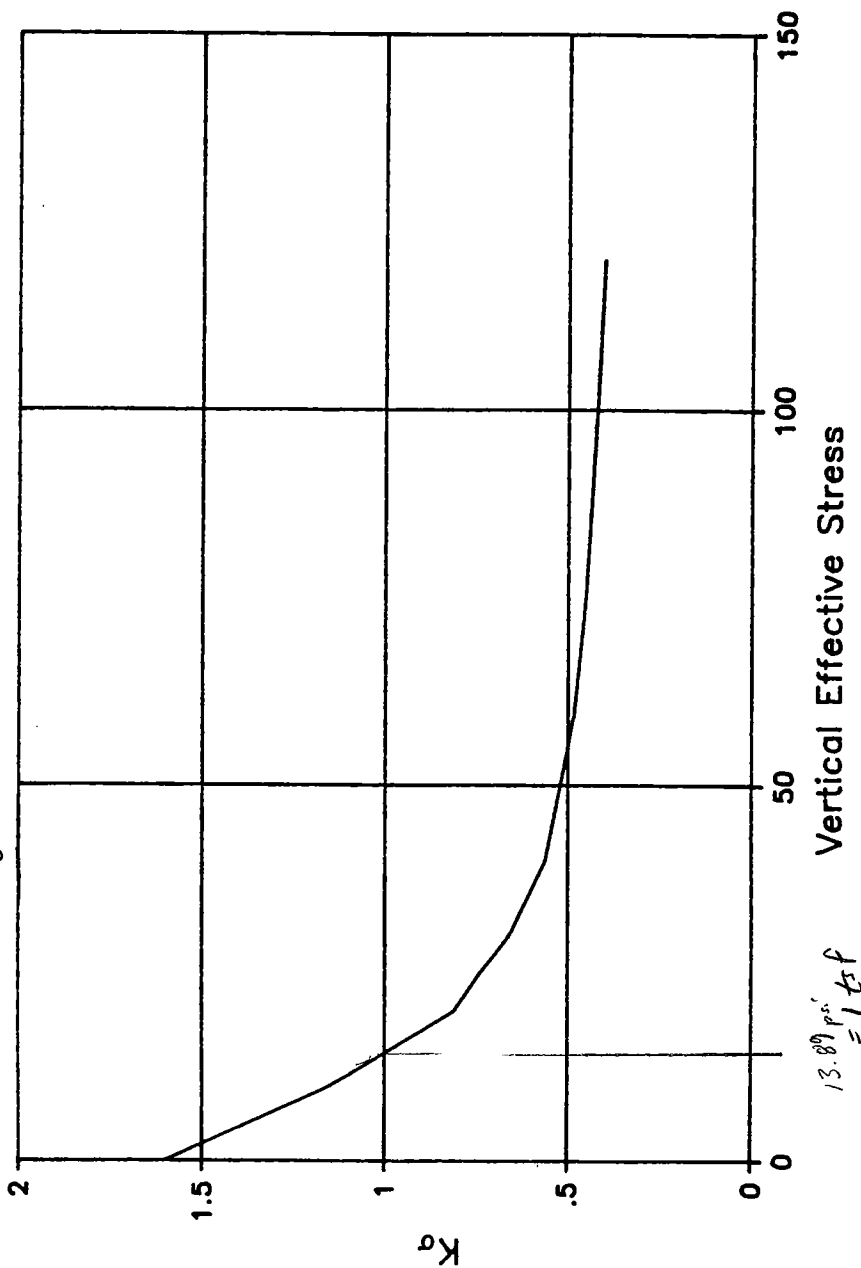
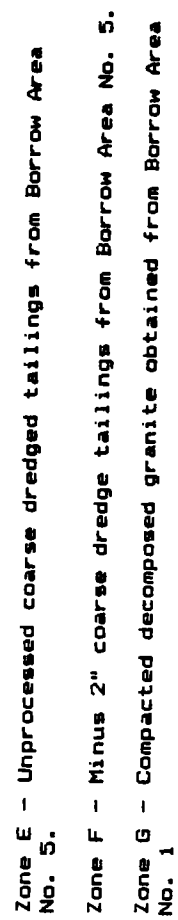
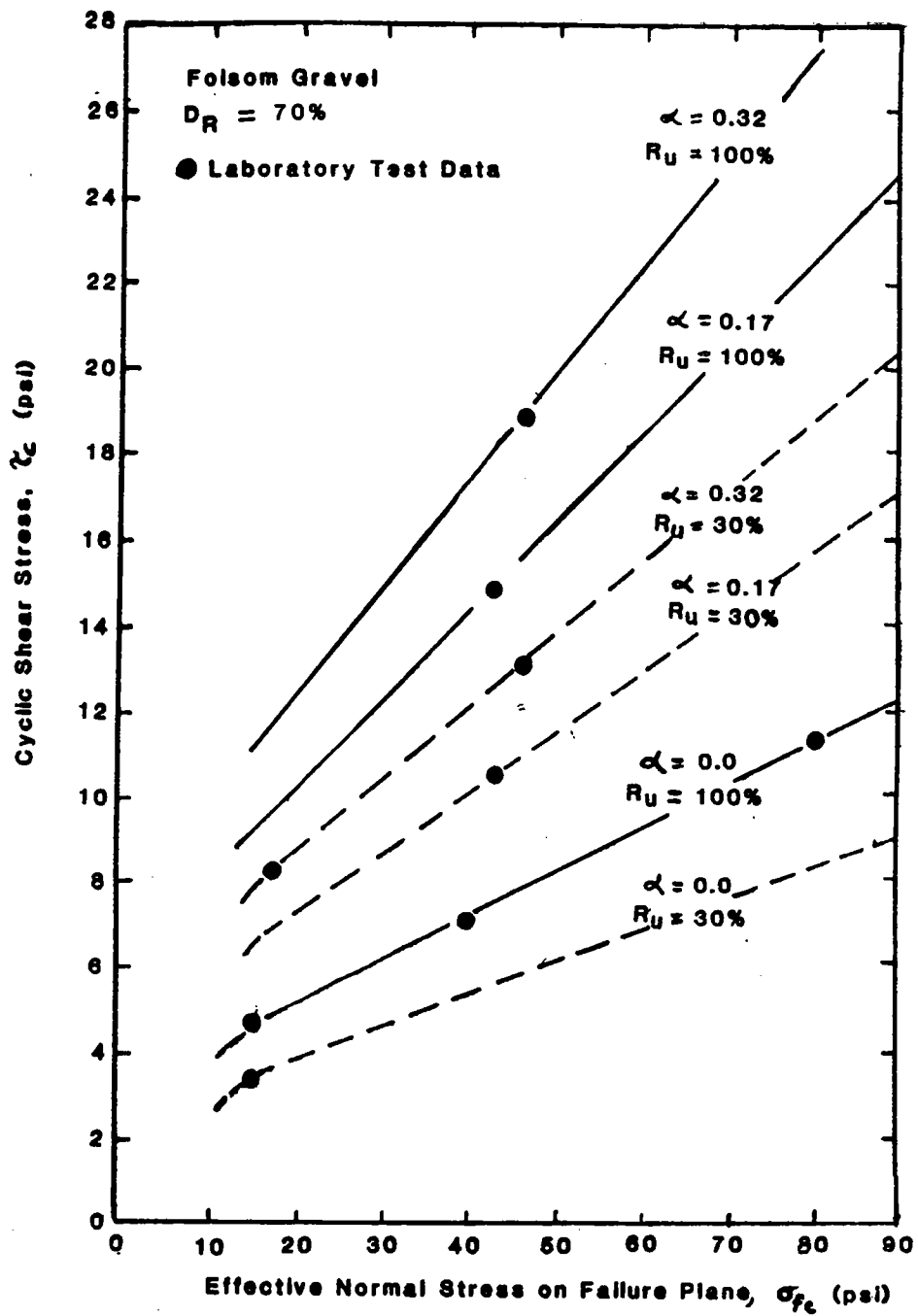


Figure 49. Adjustment factor,  $K_G$ , for change in cyclic stress ratio required to cause  $R_u = 100$  with change in effective normal stress, determined from laboratory tests on Folsom gravels.



**Figure 33. Left Wing Dam typical section through Station 303+75.**



**Figure 48. Cyclic strength envelopes for Folsom Dam.**  
 Shell gravels determined from cyclic triaxial laboratory tests.

# RIGHT WING DAM - STA 235 + 00 - CENTERLINE PROFILE

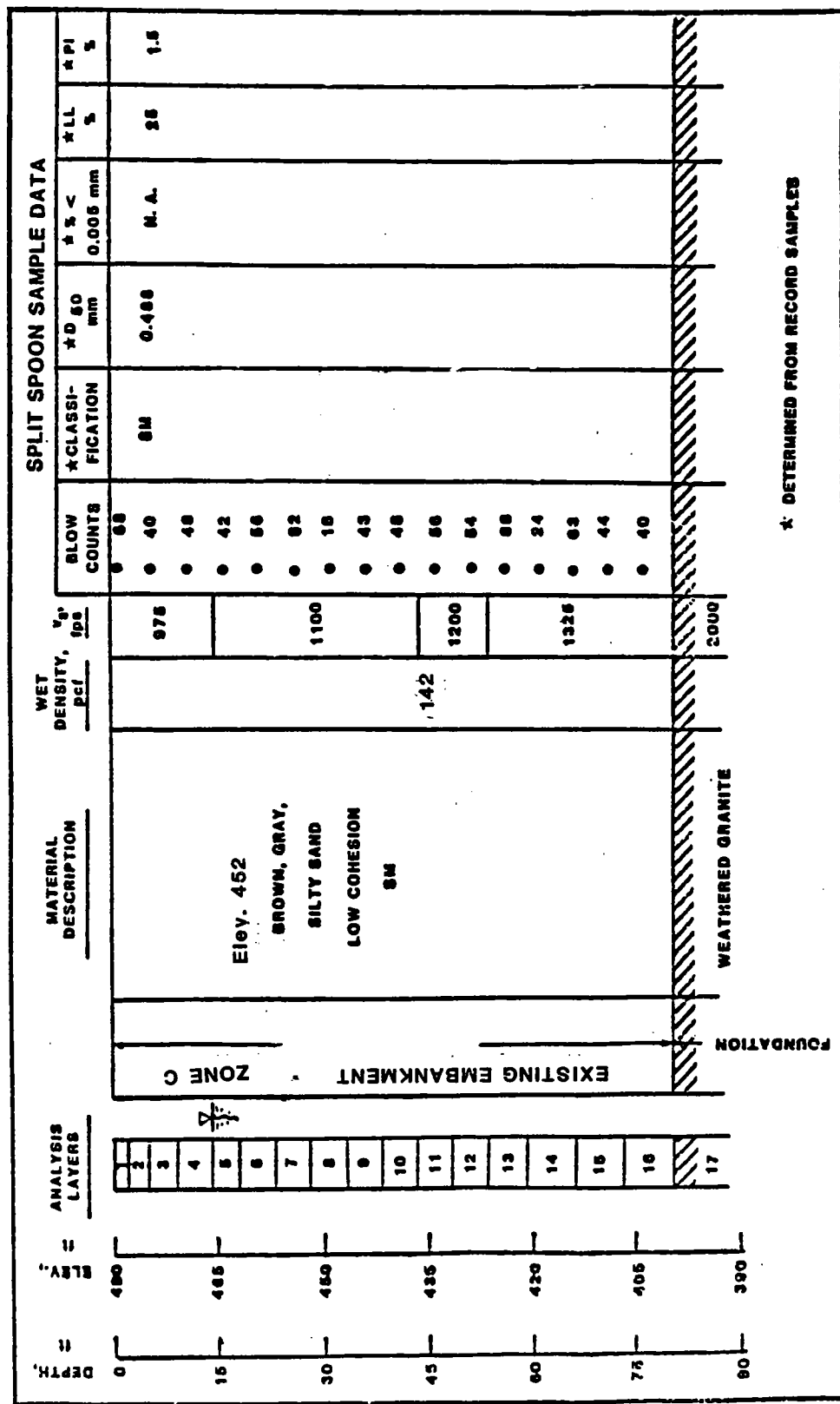


Figure 34. Summary of field data and input for SHAKE analyses, Right Wing Dam centerline profile, Station 235

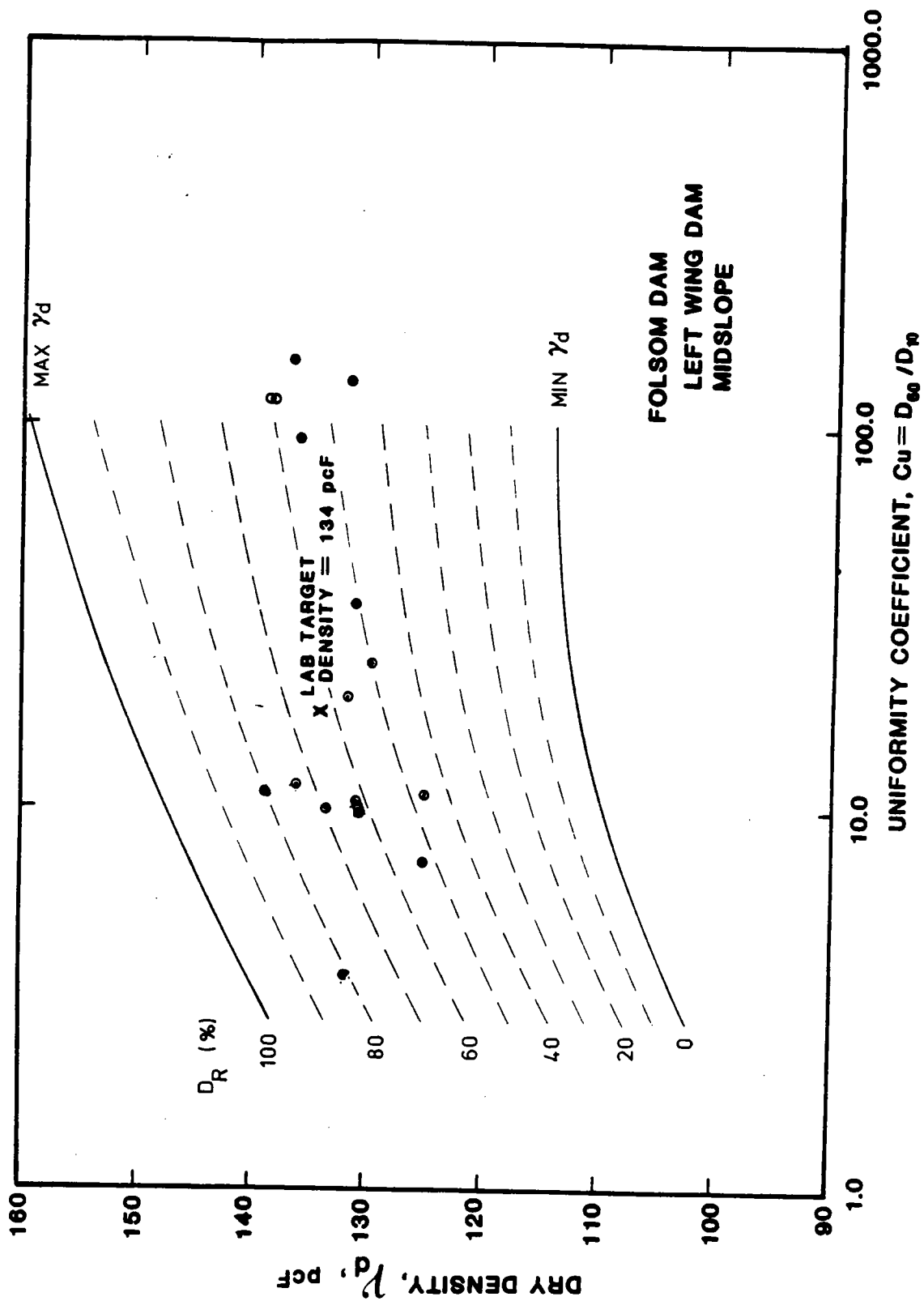


FIGURE 47. FIELD MEASURED DRY DENSITIES AND UNIFORMITY COEFFICIENTS FROM TEST PIT IN LEFT WING DAM EMBANKMENT GRAVEL

# RIGHT WING DAM - STA 270 + 00 - CENTERLINE PROFILE

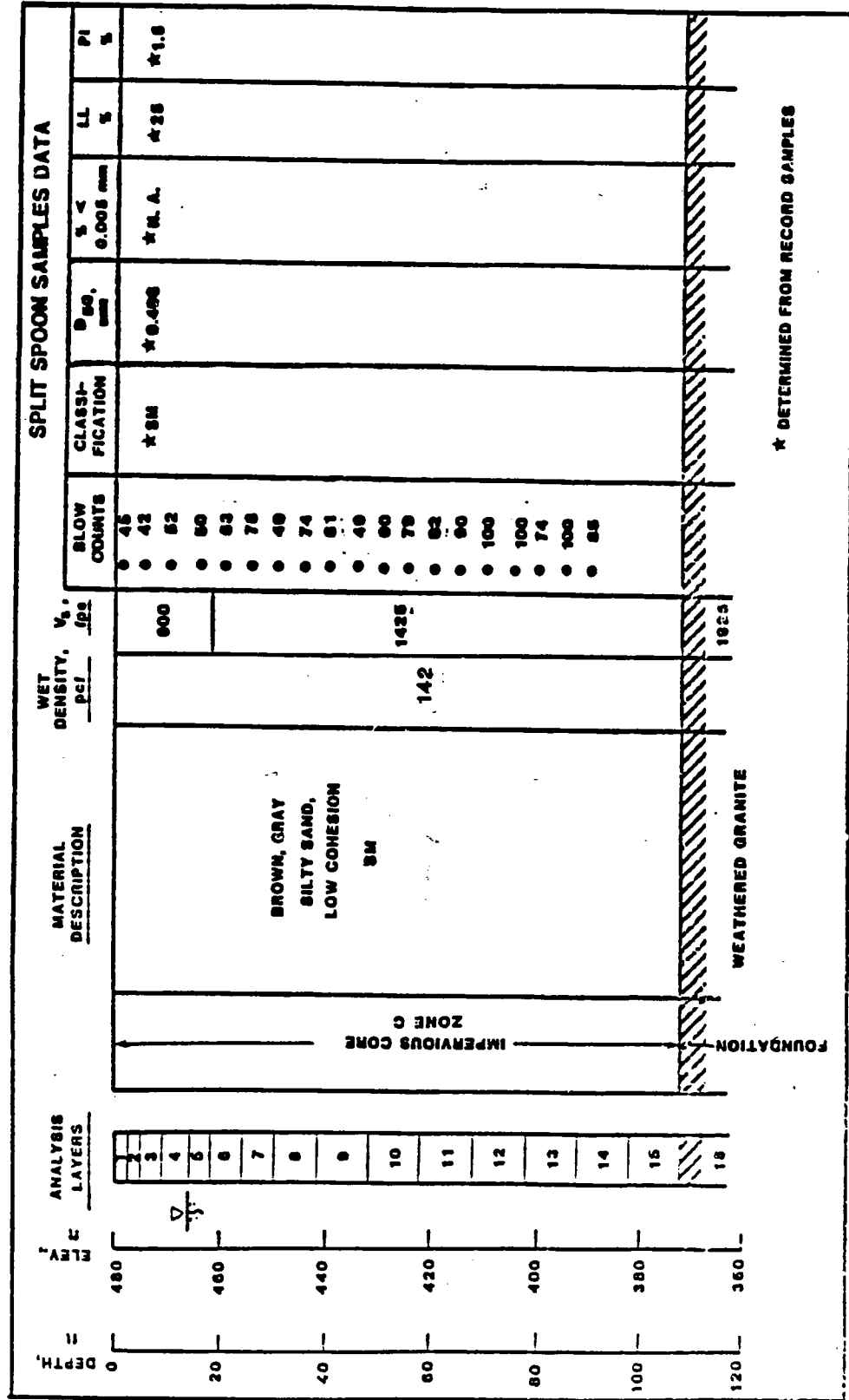


Figure 35. Summary of field data and input for SHAKE analyses, Right Wing Dam centerline profile, Station 270

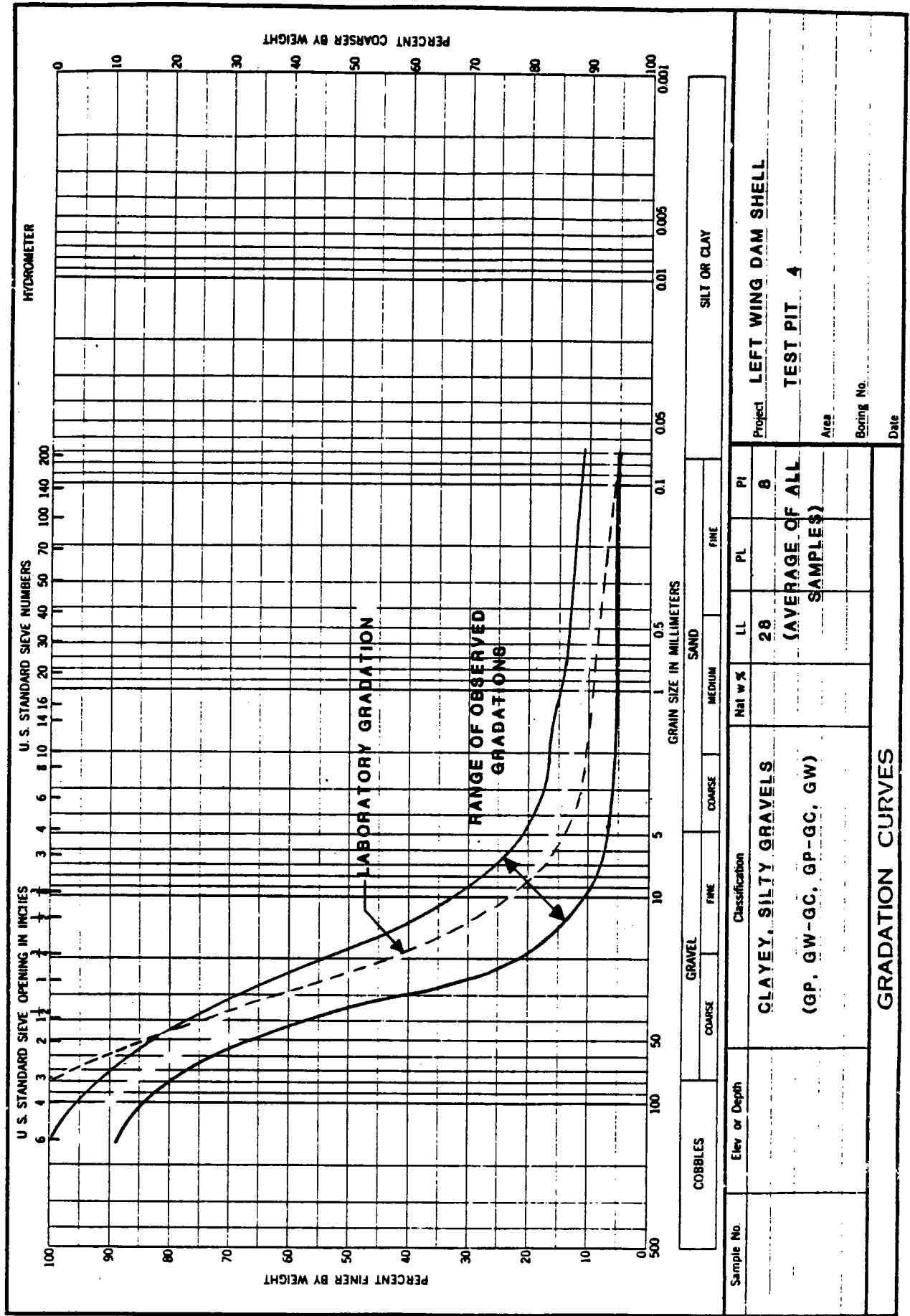


Figure 48. Range of gradations observed in Left Wing Dam shell compared with laboratory gradation

# LEFT WING DAM - STA 303 + 00 - CENTER LINE PROFILE

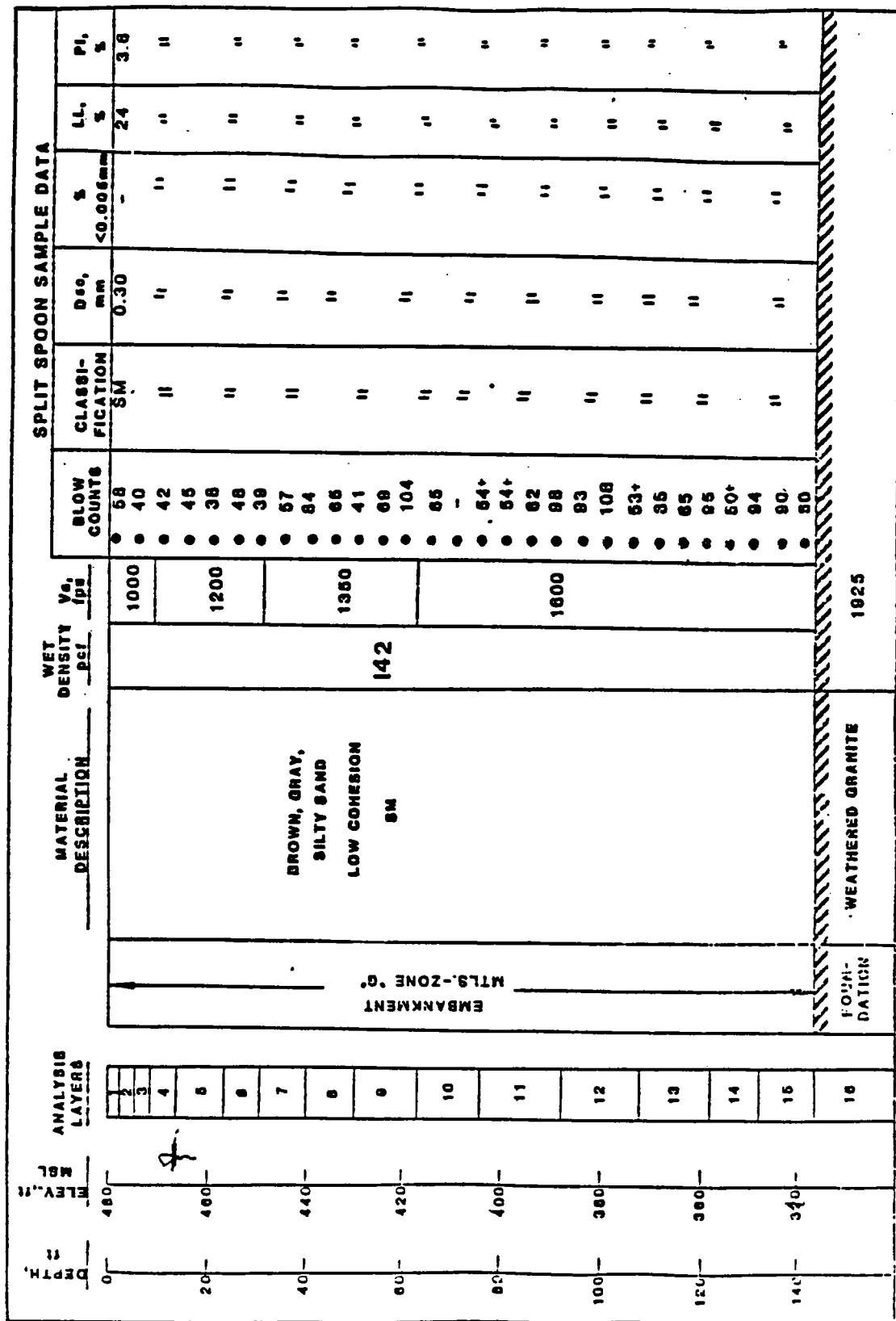


Figure 36. Summary of field data and input for SHAKE analyses, Left Wing Dam centerline profile, Station 303

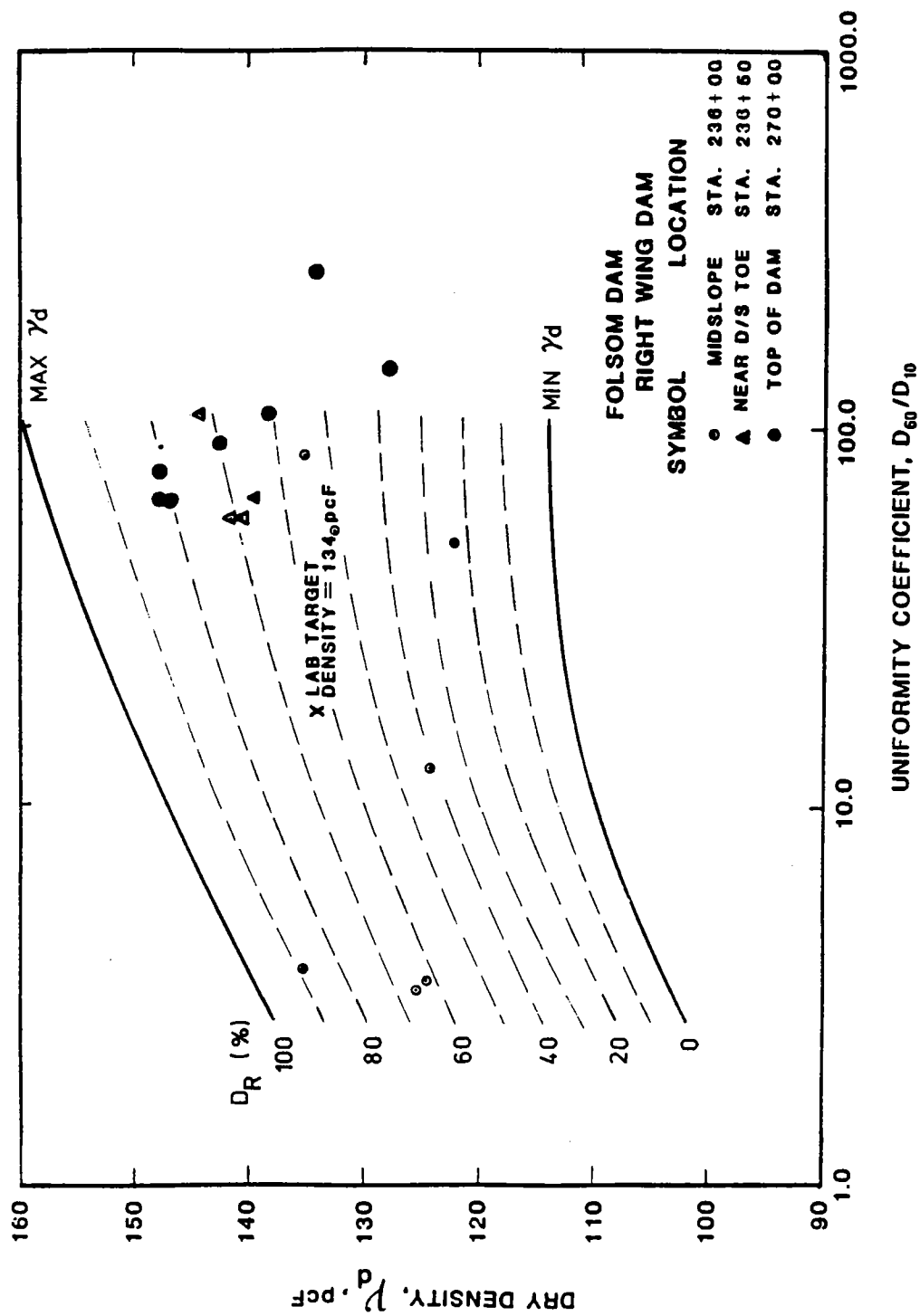
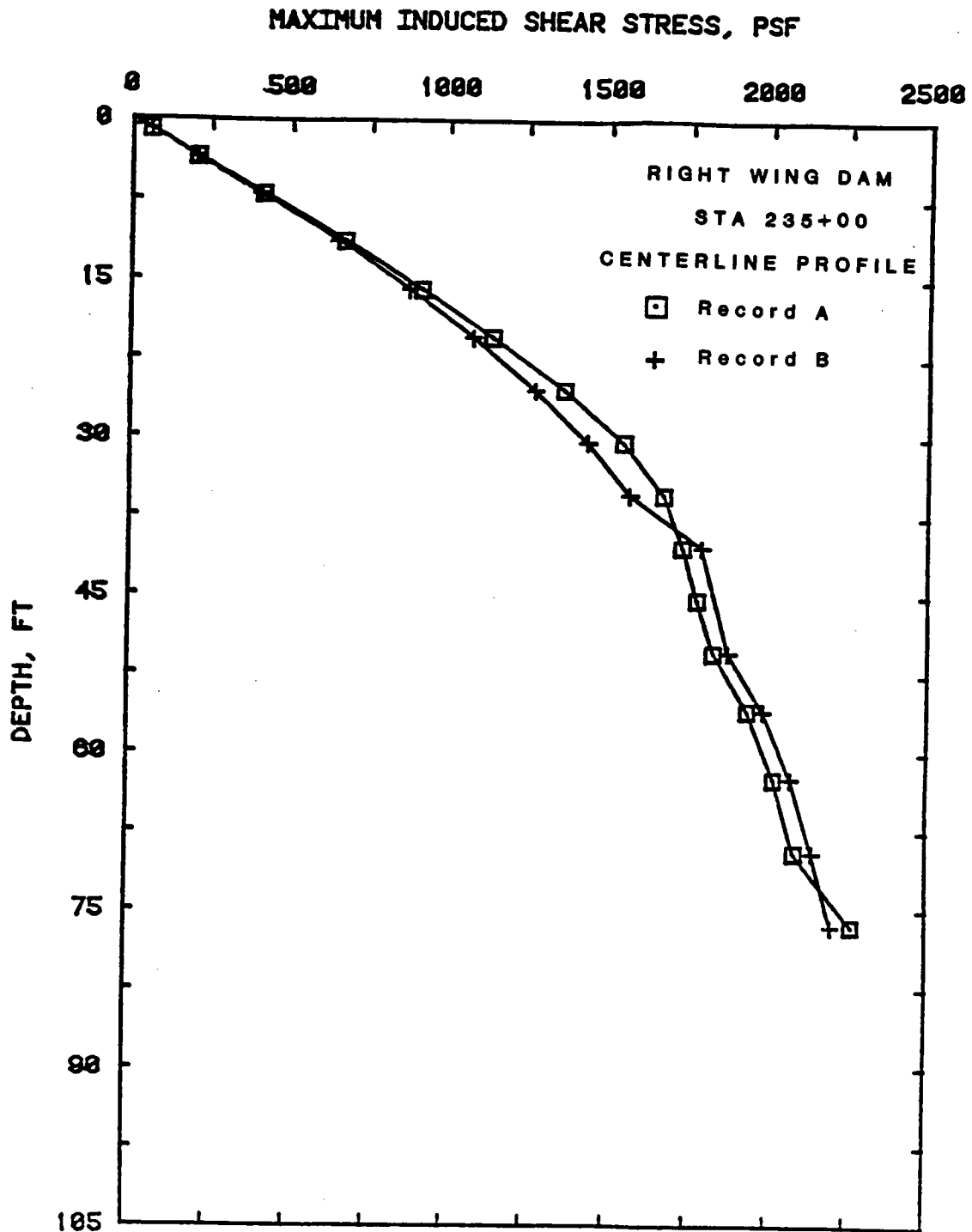
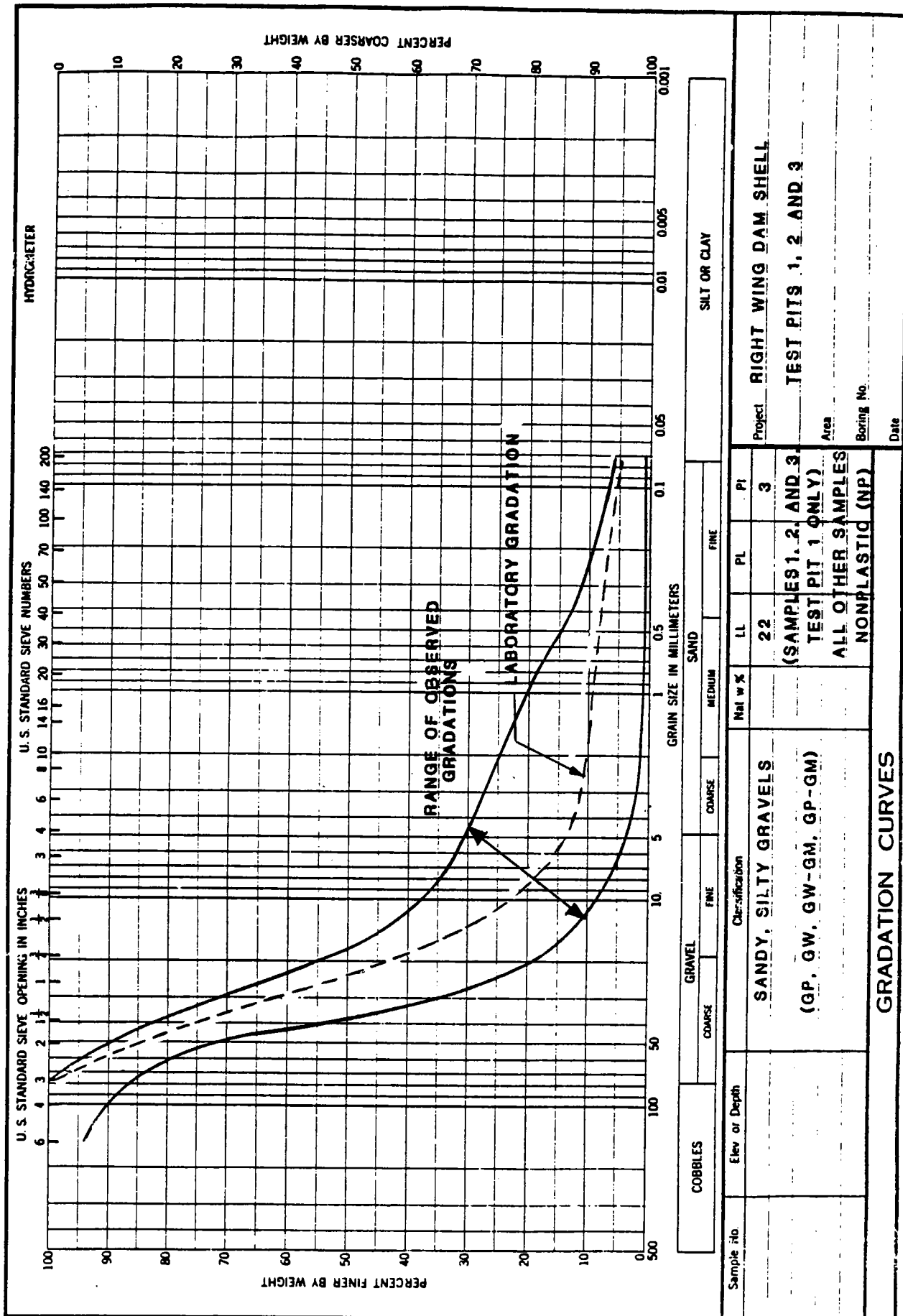


FIGURE 45. FIELD MEASURED DRY DENSITIES AND UNIFORMITY COEFFICIENTS FROM TEST PITS IN RIGHT WING DAM EMBANKMENT GRAVEL



**RIGHT WING DAM - STA 235 + 00 - CENTERLINE PROFILE**

Figure 37. Maximum earthquake-induced shear stresses in centerline profile of STA 235 of Right Wing Dam.



**Figure 44. Range of gradations observed in Right Wing Dam test pits compared with laboratory gradation**

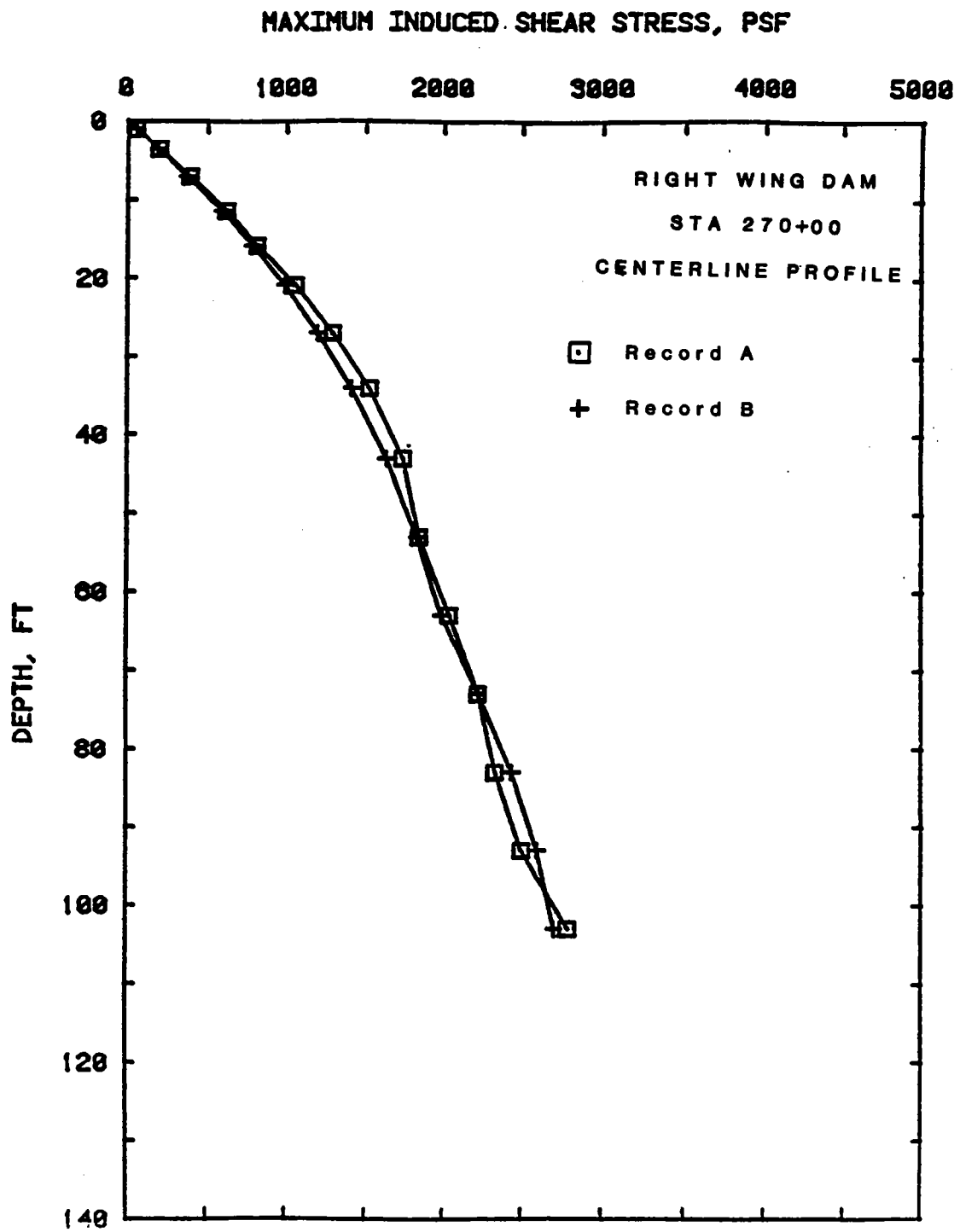


Figure 38. Maximum earthquake induced shear stresses in centerline profile at STA 270 of Right Wing Dam.

# SPT DATA FOR LEFT WING DAM

BORING SS-4 - STA 303

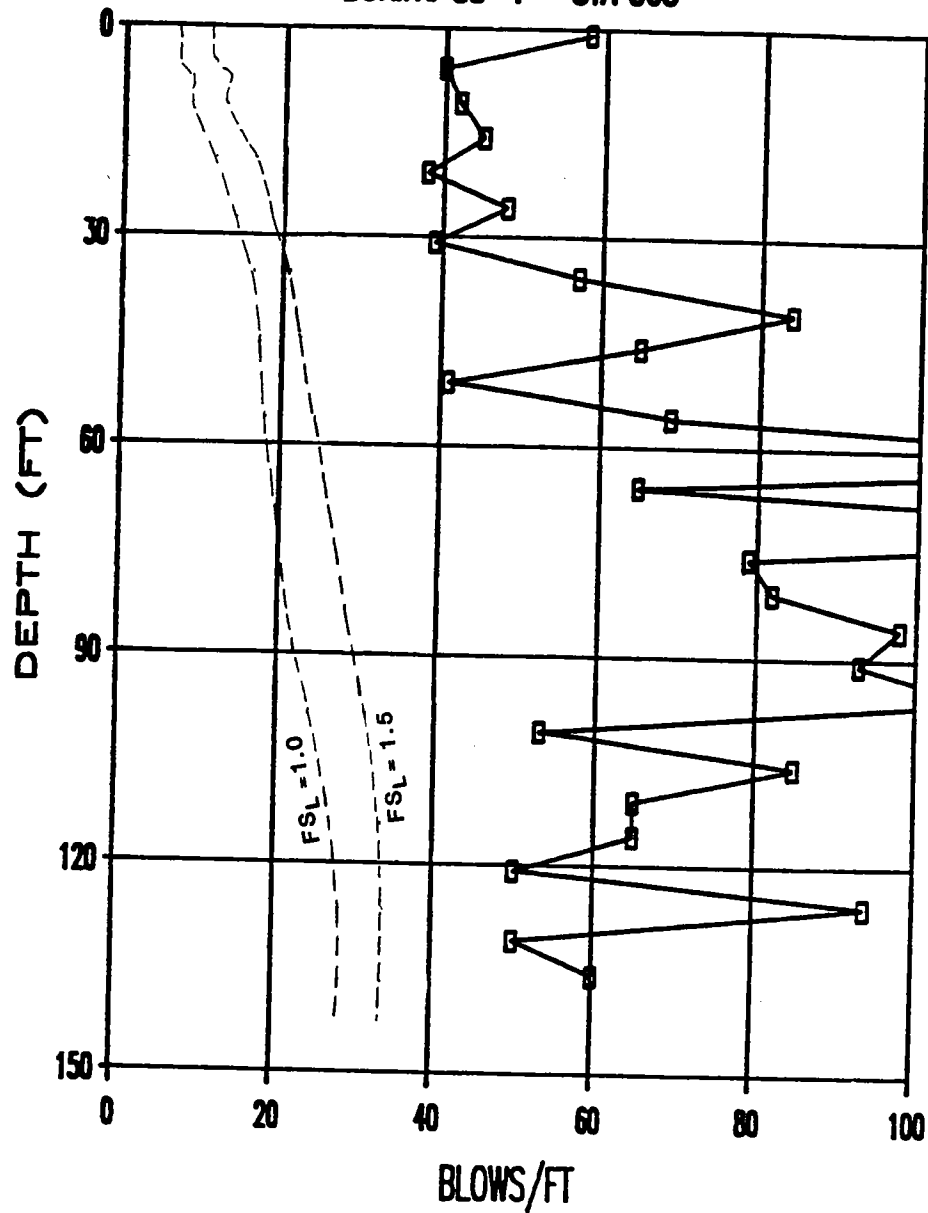


Figure 43. Field observed blowcounts from Boring SS-4 compared with contours of safety factor against liquefaction of 1.0 and 1.5.

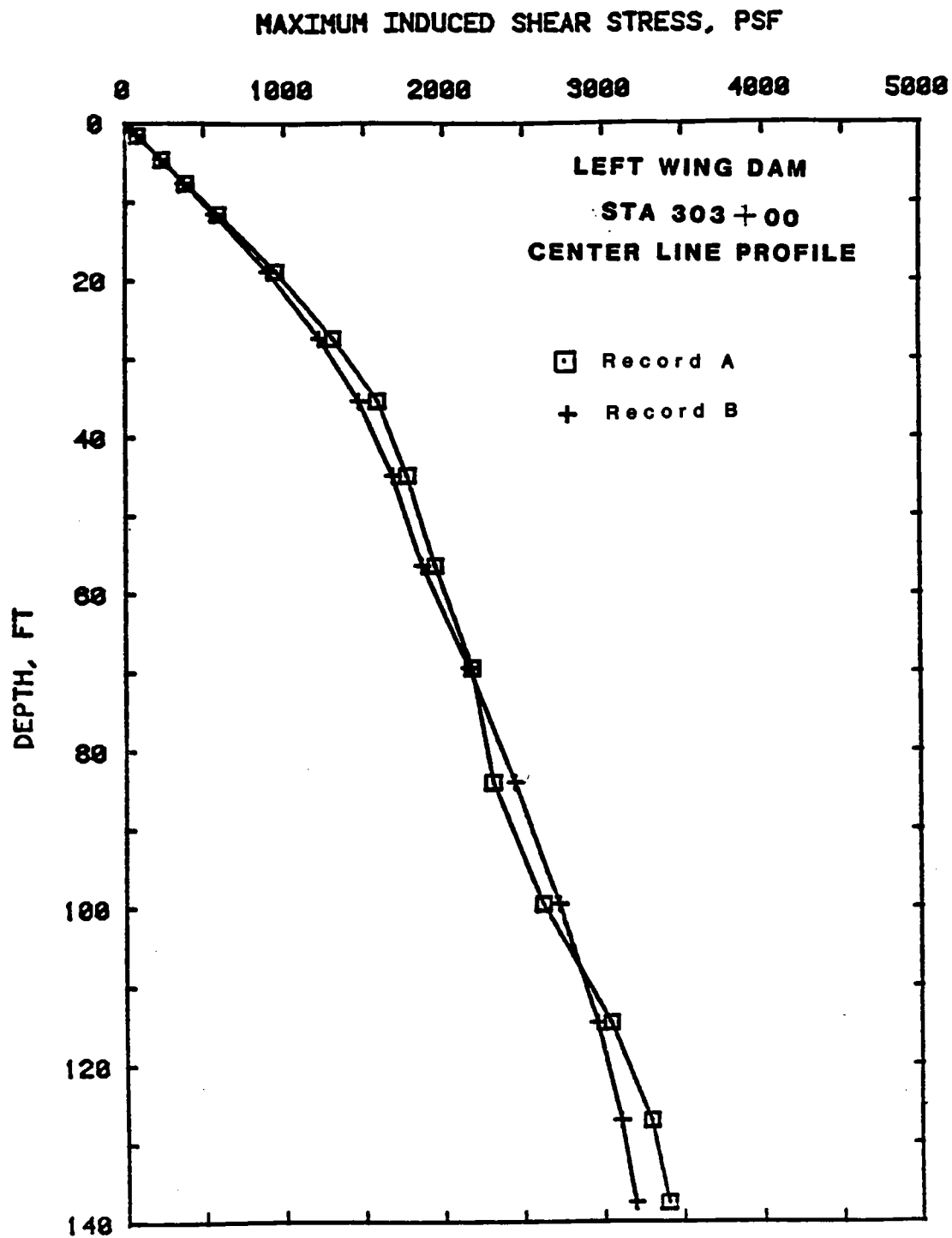


Figure 39. Maximum earthquake-induced shear stresses in centerline profile at STA 303 of Left Wing Dam.

# SPT DATA FOR RIGHT WING DAM

BORING SS-3 - STA 270

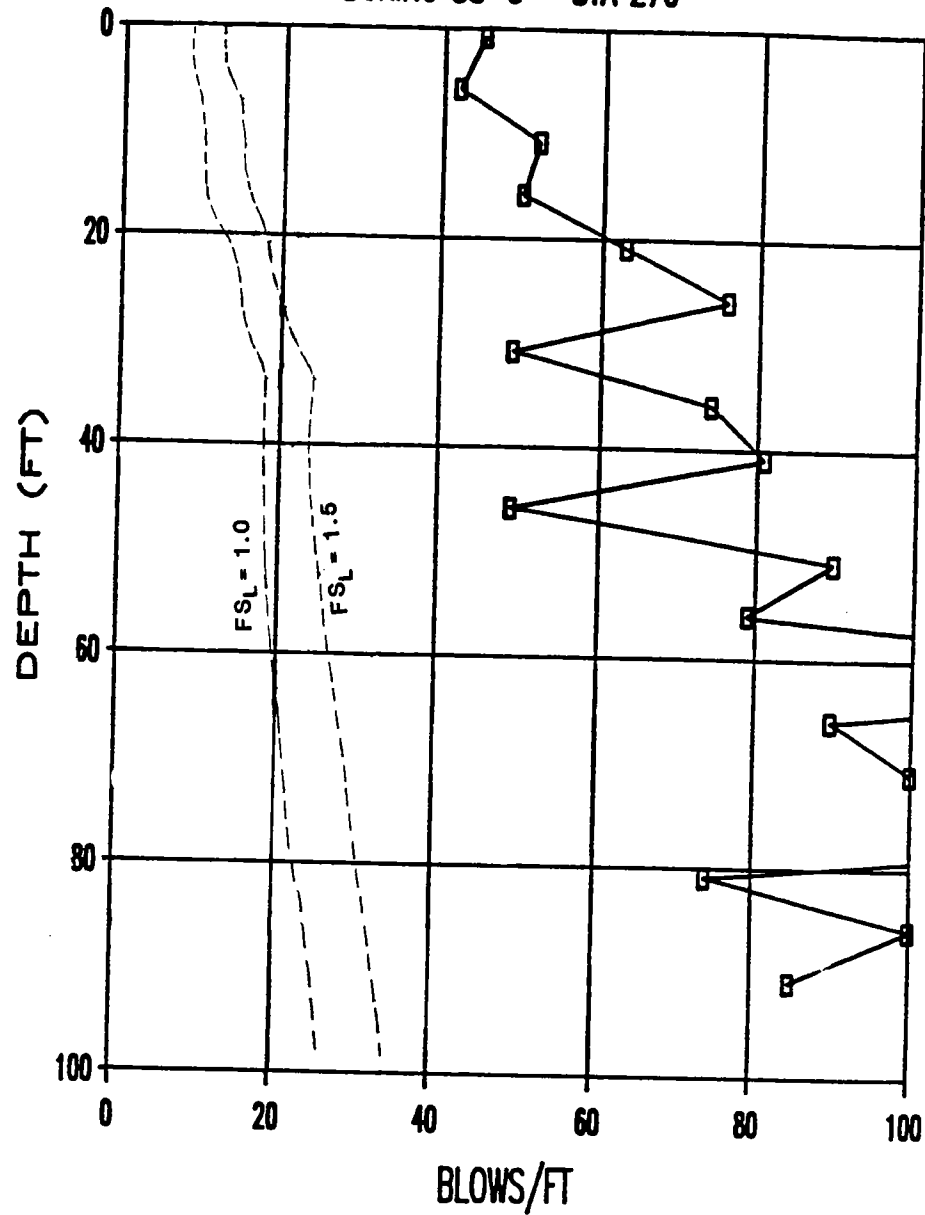


Figure 42. Field observed blowcounts from Boring SS-3 compared with contours of safety factor against liquefaction of 1.0 and 1.5.

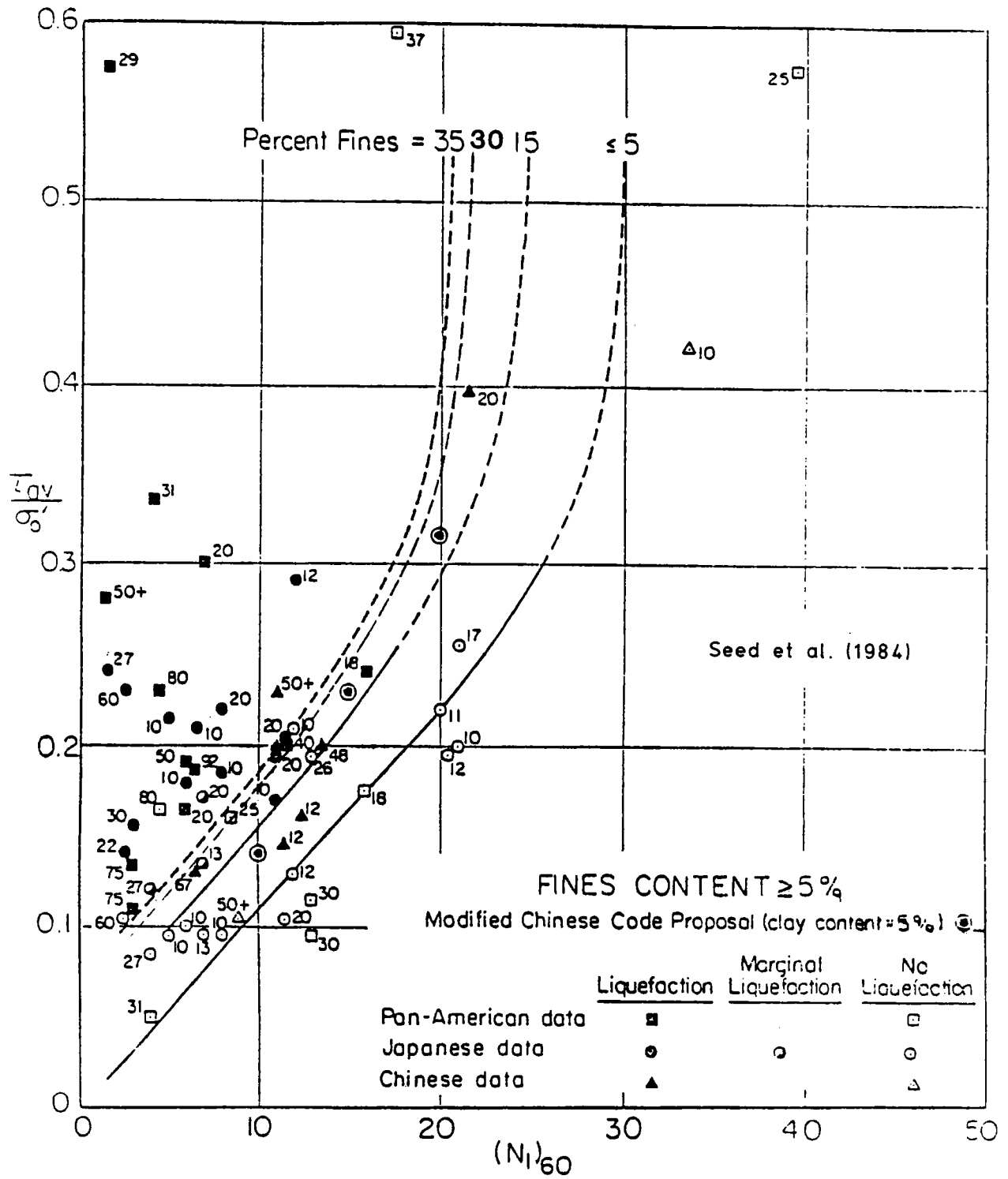


Figure 40. Relationships between stress ratio causing liquefaction and  $(N_1)_{60}$ -values for silty sands with  $M=7 \frac{1}{2}$  earthquakes (from Seed, Tokimatsu, Harder, and Chung, 1984).

# SPT DATA FOR RIGHT WING DAM

BORING SS-9 - STA 235

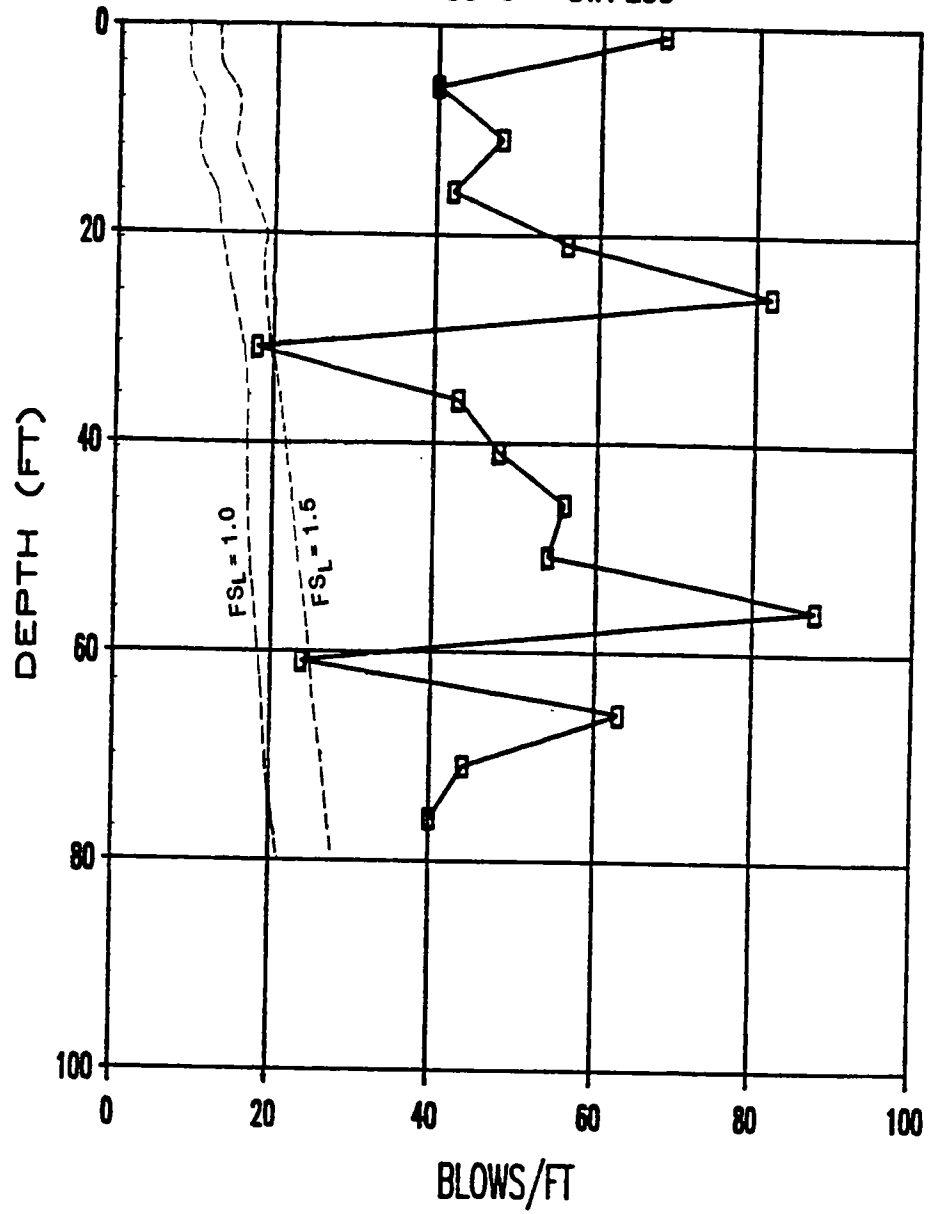


Figure 41. Field observed blowcounts from Boring SS-9 compared with contours of safety factors against liquefaction of 1.0 and 1.5.